UNIVERSITÉ D'ORLÉANS

ÉCOLE DOCTORALE ÉNERGIE, MATÉRIAUX, SCIENCES DE LA TERRE ET DE L'UNIVERS

Laboratoire de Physique et de Chimie de l'Environnement et de l'Espace (LPC2E)

THÈSE présentée par :

Clara Blanchard

soutenue le : 17 novembre 2025

pour obtenir le grade de : Docteur de l'Université d'Orléans

Discipline/ Spécialité : Astrophysique

Caractérisation détaillée des paramètres orbitaux et des éclipses des pulsars « veuves noires » par leur chronométrie radio et utilisation de cette nouvelle population de pulsars rapides pour la détection du fond d'ondes gravitationnelles

THÈSE dirigée par :

M. THEUREAU Gilles	Astronome CNAP, Université d'Orléans, Observatoire de Paris

THÈSE co-encadrée par :

M. GUILLEMOT Lucas	Astronome-adjoint CNAP, Université d'Orléans

RAPPORTEURS :

Mme JANSSEN Gemma	Professor, ASTRON Netherlands Institute for Radio Astronomy
M LINARES Manuel	Professor, Norwegian University of Science and Technology

JURY :

M KRETZSCHMAR Matthieu	Professeur, Univ. Orléans, **Président du jury**
Mme JANSSEN Gemma	Professor, ASTRON Netherlands Institute for Radio Astronomy
M LINARES Manuel	Professor, Norwegian University of Science and Technology
M CORBEL STÉPHANE	Professeur, Université Paris Cité et Université Paris Saclay
M DJANNATI-ATAÏ Arache	Directeur de recherches, Astroparticule et Cosmologie, CNRS
M THEUREAU Gilles	Astronome CNAP, Université d'Orléans, Observatoire de Paris

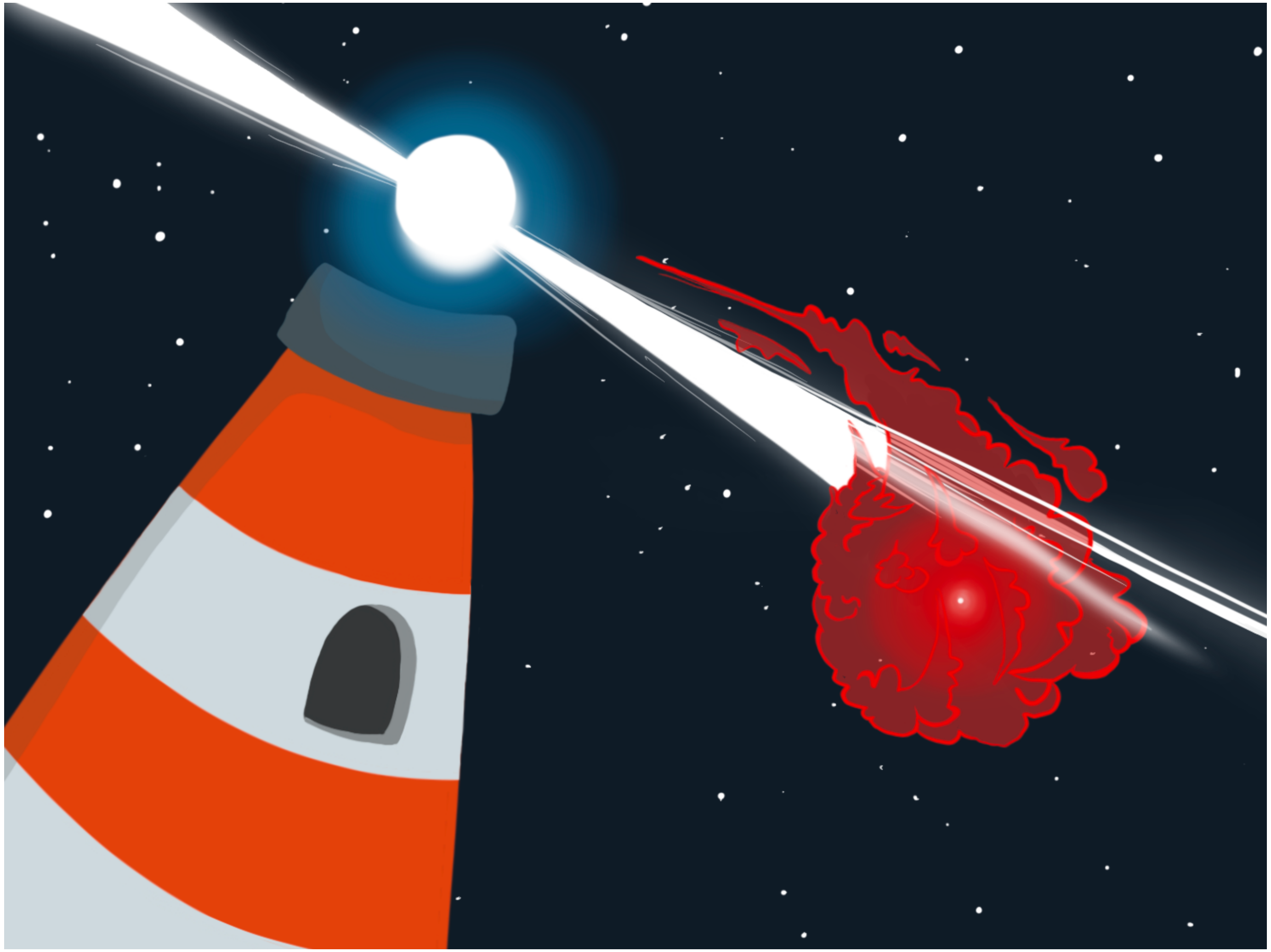

Artistic interpretation of a spider system. Illustration made by my brother Benjamin Blanchard, to which I am immensely grateful.

Remerciements

π À l'extrémité ouest, elle avait écrit «Extrême-Aval». Elle avait épaissi le trait qui matérialisait la falaise des Confins: la barrière aval de notre monde. Puis, juste devant: «Aberlaas.» À l'autre bout, elle avait inscrit «Extrême-Amont», suivi d'un gros point d'interrogation. Entre les deux, la plupart des grandes cités de la bande de Contre étaient indiquées. Jusqu'à Norska. Après régnait évidemment l'inconnu. À droite et à gauche de la bande, elle avait hachuré à la craie une surface blanche qui portait la légende: «Glaces.» Puis elle avait disposé une série de figurines aux deux tiers environ du trajet... Ça faisait toujours bizarre. Pourquoi pas au tiers ? Pourquoi pas à la moitié ou aux trois quarts de la bande ? Qu'est-ce qu'on savait de la distance qui restait à parcourir pour atteindre l'Extrême-Amont ? Si même cette distance n'était pas infinie...

Après trois ans de Contre, me voilà près d'arriver à Norska, la dernière étape connue d'un trajet commencé il y a longtemps. Le chemin n'a pas été aussi difficile que celui de la Horde évidemment (heureusement que personne n'est mort pour que cette thèse n'aboutisse) mais il aura tout de même fallu une certaine dose d'obstination. Je pars maintenant explorer d'autres chemins, admirer d'autres merveilles, et je regarde en arrière ces trois ans avec une gratitude infinie.

Merci infiniment à Gilles Theureau et Lucas Guillemot, mes directeurs de thèse, de m'avoir permis de faire cette thèse alors que j'avais un peu abandonné l'idée d'en trouver une, de m'avoir guidée et formée durant ces trois ans, merci pour votre bienveillance. Merci Gilles, pour ton écoute et tes conseils, tes connaissances. Merci Lucas pour ta patience, ta rigueur, tes encouragements, pour cette montagne de choses que tu m'as apprises, et ta façon de les transmettre. Merci à Guillaume Voisin, pour ton aide précieuse, et pour toutes les discussions que nous avons pu avoir, à propos d'étoiles ou non. Vous avez tous les trois cette grâce et cette générosité des gens qui ne se rendent pas vraiment compte de l'étendue de leur brio. Si je suis aujourd'hui une chercheuse (semi) compétente, c'est que j'ai eu la meilleure supervision possible et imaginable. Vous êtes pour moi une intarissable source d'inspiration et de respect.

Merci à l'équipe que j'ai eu la chance de côtoyer durant toute ma thèse. Si c'était un plaisir de chaque jour de venir au labo, c'était aussi grâce à vous. Merci Jean-Matthias, petite pierre, Cherry, modèle de gentillesse et d'intelligence, Pauline, petite sœur de thèse que j'aurai aimé côtoyer durant les trois ans, Ismaël, Fabian, et merci à vous Anaïs, Mark, Xiao que j'ai croisé un peu moins longtemps.

Merci aux chercheurs rencontrés durant ces trois ans, trop nombreux pour être raisonnablement nommés et qui ne liront sûrement jamais ces mots. Merci aux collègues de l'EPTA, de Manchester, de Bonn, de Hannovre, ceux avec qui j'ai pu échanger longuement ou ceux avec qui je n'ai discuté qu'un instant. La communauté dans laquelle j'ai travaillé pour cette thèse a été adorable, et je sais qu'une des choses qui me manquera le plus dans la recherche, ce seront les chercheurs.

Merci à ceux rencontés sur le chemin, qui sont à cet endroit charmant entre collègues et amis. Merci à Sebastian, Yanis et Hakim, je vous envoie du courage en nous sachant tous les quatre rédigeants. Merci à Erwann, qui m'a ouvert les portes de sa radio, et merci à Quentin, de m'avoir appris à raconter ce que j'aime tant, merci pour tout ce qui est passé et à venir.

Merci enfin à Antoine, merci mille fois, d'être resté ici pendant trois ans, et d'avoir inlassablement levé les yeux, les mains dans la terre, quand je pointais du doigt les étoiles.

Thank you to Gemma Janssen and Manuel Linares, for accepting to examine my work, and to anyone who read this thesis, thank you too.

Abstract

This thesis presents different studies carried out using the rich dataset of observations conducted with the Nançay Radio Telescope (NRT). The NRT is a telescope located in central France, one of the few 100-m class telescopes in the world, and is celebrating its 60^{th} birthday at the year of writing. Its long and fruitful pulsar monitoring campaign started in 1988, and includes over a hundred pulsars. Amongst them are 19 *spider pulsar systems*, which are the main focus of the works presented here.

Spider pulsars are binary systems in which a millisecond pulsar and a low mass star tightly orbit each other, leading to the slow evaporation of the star by the pulsar wind, which creates a cloud of blown-away matter that can eclipse the pulsar beam. The eclipses of spiders are very interesting plasma physics laboratory, therefore most studies about these eclipses look at one or two systems to decipher the phenomena happening in specific cases. It is rare however, to see work searching for group properties of the eclipses, to point the underlying similarities or disparities between systems. The NRT dataset provides a unique opportunity to do just so.

After introducing the telescope, the spider systems monitored and the main properties of this sample, I will present the first work of my thesis: the phenomenological study of the eclipses of the 11 eclipsing systems, as well as an exploration of the potential links between eclipses parameters and the inclinations of the systems. The parametrisation of the shape of eclipses allowed us to measure the duration during which the beam is delayed and attenuated by the plasma cloud, or during which the beam is completely obscured and no longer detectable, as well as the ingress and egress characteristic times or slopes and the asymmetries of the eclipses, both in terms of durations and slopes. By comparing these parameters with the inclinations or the mass functions, used as proxies for the inclinations, we aimed to add to a discussion started two decades ago to explain the fact that not all spider systems display eclipses, and one of the propositions is that one key is the viewing angle, which would mean that all spiders could be seen to eclipse if looked from the edge of the orbital plane. We indeed found that systems with higher mass functions, *i.e.* likely higher inclinations, tend to have longer eclipses, which seems to confirm a link between the geometry and the presence of eclipses.

The second work presented is the search for planets orbiting around binaries, focusing on two spider systems and another binary located in a globular cluster. In all three cases the orbital period is very large, which does not allow for a traditional timing method. Two different methods were used: the first, a computation of the orbital parameters from the spin frequency derivatives, which did not yield satisfactory results, and the second is the direct timing using a extension of the regular timing software, which is still in progress but seems more promising. The spider systems seem to harbour planetary companions, and the other binary a sub-solar mass stellar companion. We present the current best solution as well as what we plan on doing next to better constrain the orbital parameters and understand the limitations of the timing of orbits with period longer than the total monitoring time.

Résumé de la thèse

Résumé général

Cette thèse présente différentes études réalisées avec des données d'observations du radiotélescope décimétrique de Nançay (NRT). Le NRT est un télescope situé en Sologne, à 60 km au sud d'Orléans, qui fait partie des plus grands télescopes du monde et qui célèbre son 60e anniversaire en 2025, année de cette rédaction. La longue et fructueuse campagne d'observations de pulsars avec le NRT a débuté en 1988 et concerne plus d'une centaine de pulsars. Parmi eux, 19 systèmes « araignées », qui constituent l'objet principal des travaux présentés ici.

Les araignées sont des systèmes binaires composés d'un pulsar milliseconde et d'une étoile de faible masse, qui gravitent en orbite serrée, ce qui entraîne la lente évaporation de l'étoile par le vent du pulsar, créant ainsi un nuage de matière emportée par le vent capable d'éclipser le faisceau du pulsar. Les éclipses d'araignées constituent des laboratoires de physique des plasmas importants, la plupart des études sur ces éclipses se concentrent donc sur un ou deux systèmes afin de décrypter les phénomènes se produisant dans des cas spécifiques. Les travaux s'intéressant aux propriétés de groupe des éclipses sont cependant rares, alors qu'ils permettraient de mettre en évidence les similitudes ou les disparités sous-jacentes entre les systèmes. Le riche jeu de données NRT offre une opportunité unique de le faire.

Après avoir présenté le télescope, les systèmes observés et leurs principales propriétés, je présenterai le premier travail de ma thèse : l'étude phénoménologique des éclipses des 11 « éclipseurs » observés, ainsi qu'une exploration des potentiels liens entre les paramètres des éclipses et l'inclinaison des systèmes. La paramétrisation de la forme des éclipses nous a permis de mesurer la durée durant laquelle le faisceau est retardé et atténué par le nuage de plasma, et celle durant laquelle il est complètement obscurci et n'est plus détectable, ainsi que les temps caractéristiques d'entrée et de sortie et les asymétries des éclipses. En comparant ces paramètres à l'inclinaison ou à la fonction de masse, utilisée comme indicateur pour l'inclinaison, nous avons cherché à continuer une discussion entamée il y a deux décennies pour expliquer pourquoi tous les systèmes araignées ne présentent pas d'éclipses. Une des propositions est qu'un élément clé est l'angle de vue, ce qui signifie que toutes les araignées pourraient éclipser si elles sont observées parallèlement au plan orbital. Nous avons en effet constaté que les systèmes ayant une fonction de masse élevée, c'est-à-dire une inclinaison probablement élevée, ont tendance à avoir des éclipses plus longues, ce qui semble confirmer un lien entre la géométrie et la présence d'éclipses.

Le deuxième travail présenté porte sur la recherche de planètes orbitant autour de binaires, en particulier deux systèmes araignées et une autre binaire situées dans un amas globulaire. Dans les trois cas, la période orbitale est trop grande pour permettre l'utilisation d'une méthode de chronométrage traditionnelle. Deux méthodes différentes ont été utilisées : la première est le calcul des paramètres orbitaux à partir des dérivées de fréquence de rotation, qui n'a pas donné de résultats satisfaisants. La seconde est la chronométrie directe utilisant une extension au logiciel standard, étude encore en cours mais qui semble plus prometteuse. Les systèmes araignées semblent abriter des compagnons planétaires, et l'autre binaire un compagnon stellaire de masse subsolaire. Nous présentons la solution actuelle ainsi que les prochaines étapes pour mieux contraindre les paramètres orbitaux et comprendre les limites de la chronométrie des orbites dont la période est supérieure à la durée totale d'observation.

1. Introduction aux pulsars

Les étoiles ne meurent pas, elles suivent différentes trajectoires d'évolution selon leur masse, et la plupart de ces trajectoires conduisent à des rémanents pratiquement éternels. Les pulsars en sont un exemple. Après la séquence principale (SP) de leur évolution, les étoiles de plus de 8 masses solaires ($M_\odot$) manquent de combustible pour la fusion nucléaire qui maintient la pression de radiation contre l'autogravitation. Le déséquilibre qui en résulte provoque l'effondrement de l'étoile sur elle-même et conduit à une explosion appelée supernova (SN). Si le rémanent de cette SN est plus léger que 3 $M_\odot$, il s'agit d'une étoile à neutrons. En 1967, les pulsars ont été découverts, à la fois théoriquement et observationnellement. En juillet, Jocelyn Bell, étudiante en thèse sous la direction d'Anthony Hewish, a découvert des pulsations radio qui ont été attribuées à une étoile à neutrons pulsante. En novembre, avant la publication de la découverte de Bell, Franco Pacini a montré qu'une étoile à neutrons fortement magnétisée et en rotation pourrait émettre des faisceaux radio à ses pôles magnétiques, à la manière d'un phare. Les pulsars sont des objets extrêmes, qui émettent sur l'ensemble du spectre électromagnétique. Au moment de la rédaction de cet article, 3 838 pulsars sont répertoriés dans le catalogue des pulsars de l'ATNF, que les astronomes ont classés en fonction de différentes propriétés observationnelles : les pulsars lents, ou jeunes, ont des périodes de rotation de l'ordre de la seconde et un spin down assez important, tandis que les pulsars millisecondes ont des périodes de rotation inférieures à 30 millisecondes et une rotation très stable, avec un ralentissement plus faible. Certains pulsars ont des compagnons, ce qui en fait des systèmes multiples. Ces compagnons peuvent être d'autres pulsars ou des étoiles à neutrons, mais ils peuvent aussi être des étoiles ordinaires. Le sujet de cette thèse est l'étude d'une sous-catégorie de pulsars binaires, les binaires araignées, systèmes dans lesquels le compagnon du pulsar est une étoile semi-dégénérée légère en orbite très serrée. Les deux objets sont si proches que le vent du pulsar arrache de la matière à son compagnon, matière qui peut éclipser le faisceau radio du pulsar lorsqu'il le traverse.

2. Astronomie des pulsars

Pour étudier les pulsars, la première étape est de les observer. Depuis l'émission du rayonnement brut aux données exploitables sur nos ordinateurs, le signal du pulsar subit de nombreux processus naturels et traitements informatiques. Après leur émission, les ondes radio se propagent dans le milieu interstellaire (MIS), le plasma froid qui remplit l'espace à l'intérieur de la galaxie. Ce plasma froid a trois effets principaux sur une onde électromagnétique : la dispersion, la rotation de Faraday et la diffusion. Ces effets dépendent de la fréquence de l'onde, et comme l'émission radio couvre naturellement une large bande de fréquences radio, les effets du MIS se manifestent dans les données par des retards relatifs entre les différentes fréquences. Une fois que le signal atteint l'observatoire, il est enregistré par le télescope, nettoyé des signaux indésirables qui ne viennent pas du pulsar, corrigé de la dispersion causée par le MIS et prêt à être transformé en la donnée fondamentale de la chronométrie des pulsars, le temps d'arrivée (ToA). Les pulsars sont des rotateurs très stables et peuvent donc être comparés à des horloges de référence pour surveiller toute variation de leurs ToAs. Si un pulsar est correctement modélisé, les résidus, c'est-à-dire les différences entre les temps d'arrivée modélisés et mesurés, doivent être les plus petits possibles. Les ToAs sont extraits de données repliées à la fréquence de rotation du pulsar afin d'améliorer le signal. Pour extraire un ToA, une observation repliée est comparée à un profil de référence, une «empreinte» stable du pulsar. Les ToAs sont ensuite comparés, dans un logiciel de chronométrage, à un modèle composé de tous les paramètres susceptibles d'influencer la cadence observée du pulsar : les paramètres astrométriques, de rotation et, le cas échéant, orbitaux. Dans le cas des araignées, certains modèles sont privilégiés, capables de gérer des orbites faiblement excentriques et présentant de fortes variations de la période orbitale. La chronométrie des pulsars est une technique fructueuse, non seulement pour étudier les pulsars, mais aussi pour les utiliser comme outils pour sonder d'autres phénomènes, tels que les ondes gravitationnelles nano-Hertz, les planètes extrasolaires, la cartographie galactique ou la gravitation dans le régime de champ fort.

3. Les araignées du NRT

Au milieu des années 1950, plusieurs grands radiotélescopes furent construits, et la France décida de lancer son propre projet. Au lieu du modèle plus courant à parabole unique, le télescope construit dans la nouvelle station de Nançay fut conçu sur le modèle de celui de l'Université d'État de l'Ohio, mais à une beaucoup plus grande échelle. Le radiotélescope de Nançay fut inauguré en 1965. Le modèle Ohio/Kraus est un télescope méridien, le NRT observe donc le ciel qui passe au-dessus de lui, mais peut pointer et suivre des sources dont la déclinaison est supérieure à -39° pendant environ une heure. La première véritable instrumentation pulsar du NRT fut mise en service en 1988, permettant l'observation régulière de deux sources. En 1996, un nouvel instrument fut installé, et le programme d'observations de pulsars fut étendu à 20 sources, dont une araignée, toujours observée à ce jour. Une nouvelle instrumentation appelée « BON » a été mise en service en 2004, puis « NUPPI » en 2011, qui est toujours en service en 2025. Le NRT observe désormais plus d'une centaine de pulsars, dont 19 araignées. Le NUPPI est capable d'enregistrer une bande passante de 512 MHz et observe généralement à une fréquence centrale de 1484 MHz.

Ce chapitre détaille la préparation des données, ainsi que le jeu de données final. Ce jeu de données est riche, tant en terme de cadence que de durée. Plus de la moitié de l'échantillon d'araignées est observée pendant plus de 15 ans, et nombre d'entre elles sont observées plus de deux fois par mois.

Les propriétés astrométriques, de spin, orbitales et polarimétriques des pulsars sont présentées. Afin de replacer ces paramètres dans un contexte plus large, les propriétés orbitales sont comparées à celles d'autres pulsars binaires du catalogue ATNF, et les propriétés polarimétriques à l'étude de Wang et al., 2023a.

Enfin, chaque pulsar est présenté individuellement, avec leurs propriétés générales et leurs spécificités. Ce travail bibliographique illustre la remarquable diversité des phénomènes observés chez les araignées de l'échantillon NRT.

4. Eclipses des systèmes araignées

Les éclipses sont l'une des caractéristiques majeures des systèmes araignées. Le lien entre l'inclinaison du système et les éclipses observées est une hypothèse récurrente depuis deux décennies, et le jeu de données NRT, riche et homogène, offre l'opportunité d'étudier les propriétés des éclipseurs en tant que groupe.

Dans ce chapitre, nous présentons une caractérisation des systèmes éclipseurs basée sur le rapport signal/bruit des ToAs autour de la conjonction supérieure, identifiant huit non-éclipseurs, deux éclipseurs « superficiels » (pulsars dont le faisceau est toujours détectable à la conjonction supérieure, mais avec un retard mesurable) et huit éclipseurs « totaux » (pulsars qui ne sont plus détectables pendant une fraction significative de l'orbite). L'inclinaison des systèmes araignées est difficile à mesurer et dépend généralement beaucoup du modèle utilisé pour la mesure. Cependant, en supposant que tous les pulsars et tous les compagnons ont une masse similaire (condition qui peut être considérée comme valable pour 17 systèmes de notre échantillon), la fonction de masse peut être utilisée comme indicateur de l'inclinaison. Nous constatons en effet que la fonction de masse des systèmes à éclipses et de ceux sans éclipses ne provient probablement pas de la même distribution parente.

Nous utilisons un modèle phénoménologique pour dériver plusieurs paramètres de la forme des éclipses moyennées, tels que leur durée et leurs asymétries d'entrée et de sortie. Ces paramètres nous permettent de distinguer deux catégories d'éclipseurs «totaux» : les «brusques» et les «progressifs». Nous constatons que la durée de l'éclipse (fixée à zéro pour les non-éclipseurs) est corrélée à la fonction de masse. En revanche, nous ne trouvons aucun lien évident entre cette même durée et les inclinaisons orbitales du système, d'après les mesures publiées. Néanmoins, le faible nombre d'inclinaisons disponibles, parfois contradictoires, entrave ces recherches de corrélations.

Nous présentons également des variations des éclipses de PSR J1705−1903, où le délai maximal près de la conjonction supérieure change sur plusieurs mois, ajoutant ainsi un autre exemple de la large gamme d'échelles de temps de variation dans les systèmes d'araignées.

5. Recherche de planètes autour des binaires

La toute première exoplanète découverte orbite autour d'un pulsar. Cependant, après près de 50 ans d'observations, seule une poignée de pulsars à planètes sont confirmés. Il existe cependant quelques candidats potentiels. Les planètes peuvent orbiter autour d'un pulsar isolé ou d'un pulsar en binaire avec une autre étoile, comme une araignée. Dans ce cas, le système triple est considéré hiérarchique, car l'orbite interne est plusieurs ordres de grandeur plus petite que l'orbite externe, ce qui signifie qu'aucune interaction ne devrait déstabiliser le système.

Dans ce chapitre, nous essayons de contraindre les paramètres orbitaux des planètes en orbite autour des pulsars B1620−26, J1745+1017 et J2115+5448, en utilisant deux méthodes différentes : la première est un calcul des paramètres orbitaux à partir des cinq premières dérivées de fréquence de spin, suivant les calculs de Joshi et Rasio (1997), la seconde est la chronométrie directe des pulsars avec des éphémérides à deux orbites indépendantes. La première méthode n'a pas abouti sur des résultats satisfaisants, mais la seconde est plus prometteuse. Globalement, nos solutions pour les deux systèmes d'araignées tendent à trouver des planètes de petite taille, potentiellement rocheuses, orbitant à quelques unités astronomiques de la binaire interne. La solution pour PSR B1620−26 est très mal contrainte et la meilleure solution actuelle indique une période orbitale de plusieurs siècles et une masse du compagnon externe légèrement inférieure à un dixième de celle du Soleil. La solution pour PSR J1745+1017 est la plus prometteuse. La meilleure solution est un compagnon planétaire de $0.13 M_\oplus$ (où $M_\oplus$ est la masse de la Terre) sur une orbite très excentrique ($e \sim 0,9$) de 5 200 jours. Ce résultat semble indiquer que la campagne d'observations du NRT couvre l'orbite complète ou presque, ce qui donne plus de crédibilité à cette solution. De plus, les éphémérides résultantes semblent replier correctement les données du *Fermi-LAT*, ce qui confirme l'analyse radio. Le résultat pour PSR J2115+5448 est très préliminaire, mais la meilleure solution actuelle indique qu'un compagnon de $8 M_\oplus$ orbite le pulsar sur une orbite plutôt excentrique ($e \sim 0,5$) de période > 8000 jours. Dans ce cas, la couverture NRT serait de $\lesssim 40\%$, ce qui pourrait ne pas être suffisant, car les éphémérides résultantes ne parviennent visiblement pas à replier correctement les données *Fermi-LAT*, qui sont environ deux fois plus longues que les données NRT pour ce pulsar.

6. Conclusions et perspectives

Le premier travail présenté, constistant en l'étude des 19 systèmes araignées et de leurs éclipses, peut être augmenté et amélioré de plusieurs façons. La première serait de faire la même analyse avec un plus grand échantillon, pour confirmer la corrélation trouvée entre la fonction de masse et la durée de l'éclipse et obtenir des mesures d'inclinaison pour les systèmes de notre échantillon qui n'en ont pas encore. Une autre extension intéressante à cette étude serait d'inclure des données radio prises à d'autres longueurs d'onde, afin d'étudier la dépendance en fréquence des paramètres des éclipse.

Le second travail présenté est la recherche de planètes autour de systèmes binaires. Pour les deux systèmes araignées, une amélioration possible serait d'obtenir des données provenant d'autres télescopes prises le plus proche possible du passage au périastre, car contraindre ce paramètre permettrait de contraindre mieux tous les autres paramètres de l'orbite. Un prochain projet sera d'appliquer la chronométrie directe à des données simulées, en créant de faux temps d'arrivée de sorte à simuler un système triple hiérarchique, et à tenter de retrouver les paramètres corrects tout en réduisant progressivement la couverture de l'orbite pour estimer la couverture nécessaire à l'obtention d'une solution crédible.

Contents

List of Figures

List of Tables

Chapter 1

Introduction to pulsars

¿' Notre univers, croyez-moi, n'existe qu'à force de lenteur, par la bonne grâce du lentevent... Mais pour que vous puissiez comprendre, il va falloir que je revienne à l'aube du temps...

Abstract

Stars do not die, they follow various evolution paths depending on their mass, and most of these paths lead to remnants that last virtually forever. Pulsars are one example of such remnants. After the *main sequence* (MS) stage of their evolution, stars heavier than 8 solar masses ($M_{\odot}$) run out of fuel for the nuclear fusion that sustain the radiation pressure counteracting self-gravitation. The resulting imbalance causes the collapse of the star on itself, and leads to an explosion called supernova (SN). If the remnant of this SN is lighter than 3 $M_{\odot}$, it is a neutron star (NS). In 1967 pulsars were discovered both theoretically and observationally. In July, Jocelyn Bell, under the supervision of Anthony Hewish, discovered radio pulsations that later were attributed to a pulsating neutron star. In November, before the publication of Bell's discovery, Franco Pacini inferred that a highly magnetised rotating NS could emit radio beams at its magnetic poles, in the fashion of a light-house beacon. Pulsars are extreme objects, and emit radiations across the whole electromagnetic spectrum. At the time of writing, there are 3838 pulsars listed in the ATNF pulsar catalogue, that astronomers have categorised based on different observational properties: slow or young pulsars have spin periods of the order of magnitude of the second and a rather large spin-down, while millisecond pulsars have spin periods shorter than 30 milliseconds and a very stable rotation, with smaller spin-down. Some pulsars have companions, making them multiple systems. These companions can be other pulsars or NS, but they can also be regular stars. The subject of this thesis is the study of a sub-category of binary pulsars, the *spider binaries*, systems in which the pulsar companion is a light semi-degenerated star orbiting very tightly. The two objects are so close that the pulsar wind strips matter from its companion, matter than can eclipse the pulsar radio beam when it crosses it.

1.1 History

1.1.1 Historical observations of transients

Information and references for this section are mainly taken from the book *Historical Supernovae and their Remnants* by Stephenson and Green, 2002, unless specified otherwise.

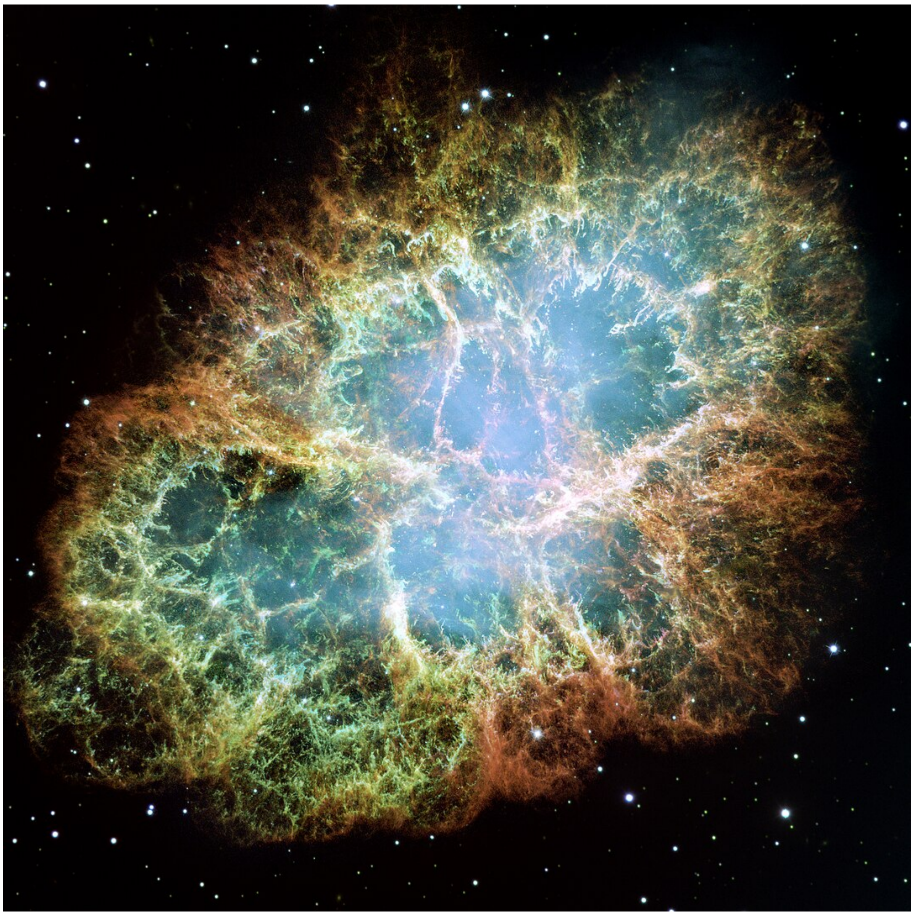

Figure 1.1: Picture of the Crab Nebula, the remnant of the 1054 SN recorded all around the world. The image has been taken by the Hubble Space Telescope, image credit NASA/ESA.

Stargazing is as old as humanity, or maybe even older. Stars and stories about them have been kept and used for calendars, navigation and spiritual practices. Pre-historical artifacts have been discovered around the world, but the first known written report of astronomical observation apart from that of the Sun and Moon[1] comes from Babylon and consists in a list of 36 stars and their localisations, generally considered to be written between 1800 and 1100 B.C. (Rochberg-Halton, 1983). The Babylonian also had the first known functional planetary theory, tracked Venus and understood the cyclical nature of its motion[2].

However, ancient astronomers were mostly interested in cyclical and permanent phenomena, and for time domain astronomy history had to wait for the very meticulous and exhaustive Chinese scientists, both astronomers and historians. The first recorded SN might be SN 185, in the

[1]It is difficult to date the beginning of Sun and Moon tracking, as this has been shown to predate the invention of writing.

[2]The Babylonian also invented the division of the sky in 360 degrees.

astronomical treatise of the Hòu hànshū (book of the later Han), which was reported to appear on AD 185 December 7th as a kè xīng "guest star". This guest star was visible in the night sky for 8 months or 1 year and 8 months. This identification is not certain however, as the SN remnant as not been confirmed yet, due to uncertainties on the position of this "guest star".

The first confirmed SN report is that of SN 1006, recorded in multiple sources from China, as well as from Japan, Korea, Egypt, Iraq, North-West Africa or Spain, Yemen, and possibly in Italy. Egyptian astronomer Ali ibn Ridwan stated that the "spectacle was a large circular body, $2\frac{1}{2}$ to 3 times as large as Venus. The sky was shining because of its light. The intensity of its light was a little more than a quarter that of Moon light". The remnant was identified by Gardner and Milne, 1965 in a radio sources catalogue from the Parkes telescope, cross-matching position limits from multiple historical sources. This supernova has been confirmed to be a type Ia SN, hence the remnant nebula is not expected to harbour a remnant star, as type Ia SN completely disrupt the progenitor star, or stars, SN 1006 being thought to be the result of a double white-dwarves merger.

The first confirmed historical supernova linked to a known neutron star is the famous SN 1054, also known as the Crab supernova. This bright supernova was reported by at least 6 independent Chinese records, two Japanese, an Egyptian astronomer based in Constantinople, with additional possible records from European, North American and Australian astronomers. According to Chinese sources, the "guest star" was visible from 1054 July 4th, and was visible in daylight for 23 days. After this period it was possibly as bright as a magnitude of ~ -3, brighter than Jupiter. It was some 40 degree west of the Sun and therefore well placed for observation by day. It disappeared from the night sky to the naked eye 642 days after its apparition.

The Crab Nebula was first identified by John Bevis in 1731, and then independently by Charles Messier in 1758, who first took it for a comet. Upon realizing his mistake, he created a catalogue of 110 celestial objects which might get mistaken for comets, and assigned the first entry "M1" to the Crab Nebula.

Radio emission from the nebula was first observed by Bolton, Stanley, and Slee, 1949 at the very beginning of radio astronomy. The Crab Nebula is a very bright X-ray source and was indeed the first extra-solar X-ray source detected (Bowyer et al., 1964). Pulsations from the Crab pulsar have been detected by Staelin and Reifenstein, 1968 a mere year after the discovery of the first pulsar (see Section 1.1.3). However the observational and theoretical evidences for a compact source lying in the centre of the nebula were presented as early as 1942, the Crab pulsar being also visible in the optical spectrum (Baade, 1942). This pulsar has a period of $P \simeq 33$ ms, and a spin down rate of $\dot{P} \simeq 4.2 \times 10^{-13}$ s/s, giving a characteristic age (see Section 1.3.2) of about ~ 1250 years, compatible with a birth (Earth) date of 1054 AD.

1.1.2 Neutron stars

The existence of a neutral nucleus, the neutron, was predicted in 1920 by Ernest Rutherford (Rutherford, 1920), but numerous experiments designed to find evidence for its existence failed during the following decade. In 1932, James Chadwick was the first to correctly infer that the results of bombardment of beryllium nuclei by alpha particles produced by a polonium source was neutrons (Chadwick, 1932), and not γ-rays as was thought by the Joliot-Curie, Bothe and Becker, or Webster, who conducted similar experiments at a similar time.

As soon as the next year, Walter Baade and Fritz Zwicky had the remarkable foresight of proposing a neutron star as a SN remnant, stating "with all reserve we advance the view that supernovae represent the transition from ordinary stars into neutron stars, which in their final stages consist of closely packed neutrons." (Baade and Zwicky, 1934a). They later expanded on this idea, "Such a star may possess a very small radius and an extremely high density. As neutrons can be packed much more closely than ordinary nuclei and electrons, the 'gravitational packing' energy in a cold neutron star may become very large, and, under certain circumstances far exceed the ordinary nuclear packing fractions. A neutron star would therefore represent the most stable configuration of matter as such." (Baade and Zwicky, 1934b).

Before the discovery of the neutron, Subrahmanyan Chandrasekhar presented a theory of stellar evolution, once radiative pressure could no longer counteract gravitational forces. Doing so, he derived the maximum mass for a stable WD, over which a star would undergo a collapse turning it into "something denser than a proton" (Chandrasekhar, 1931). Right after the discovery of the neutron, Lev Landau also discussed the evolution of stars denser than WDs (Landau, 1932), however his work became famous from 1938, when he showed that a stellar core only composed of neutrons could form and be stable (Landau, 1938). The next year, using the work of Richard Tolman, Robert Oppenheimer and Georges Volkoff simultaneously derived the maximum mass of a stable NS, similar to what Chandrasekhar did for WDs, a value which is now known as the Tolman-Oppenheimer-Volkoff (TOV) limit (Oppenheimer and Volkoff, 1939). In the original paper, they derived a mass of $0.75 M_{\odot}$ by neglecting nuclear interactions, however recent studies tend to put the limit around 2.2 $M_{\odot}$ (Rezzolla, Most, and Weih, 2018).

1.1.3 Discovery of pulsars

Around the same time as Chandrasekhar's and Landau's pioneering work, Karl Jansky, a radio engineer working on transatlantic radio communication systems, discovered that some of the extraterrestrial noise polluting the signals was coming from the Milky Way galaxy rather than from the Sun, as was first thought (Jansky, 1933). This dramatically changed our idea of the radio sky and led to more investigations in the subsequent years. The second world war put a hold on all research programs, but soon after radars and other military technologies were repurposed for radio astronomy, mainly the study of the Sun's emission and its interaction with the interplanetary medium. Quasars (for *quasi-stellar radio sources*) were discovered in the late 50s, as radio sources with no optical counterparts (Matthews and Sandage, 1963). In 1965, Anthony Hewish and his team from Cambridge University started to build an 81.5 MHz interferometer on the recently built Mullard Radio Astronomy Observatory site. The main goal of this instrument was to study the Solar system interplanetary medium by measuring variations in the radio emission from quasars. Jocelyn Bell was a graduate student who was part of Hewish's team that constructed the telescope. In July 1967, she was the first to notice regular flashes with a period of 1.3 seconds and a duration of 0.3 seconds. The source was located at a right ascension (RA) of 19:19 and a declination (DEC) of 21°0′ (Hewish et al., 1968). Bell was convinced of its extraterrestrial origin, but Hewish was sceptical and believed it to be radio frequency interference (RFI). By January 1968 Bell discovered 3 other sources. Pilkington later calculated the dispersion[3] of the sources, and concluded that they were outside the Solar system but within the Galaxy (Bell Burnell, 2017). In their article (Hewish et al., 1968), Hewish, Bell and co-authors correctly inferred that the likely source for the pulsations was a NS rather than a WD, but suggested that the pulsations were flares caused by radial pulsations (Meltzer and Thorne, 1966). This was not correct, however the idea was used for making the term pulsar that first appeared in *The Daily Telegraph*[4].

1.2 Fundamental properties of pulsars

1.2.1 Radio emission from pulsars

The same year as Bell's initial discovery, Franco Pacini suggested that a highly magnetized and rotating NS could produce beamed radio emission (Pacini, 1967), a process he linked in particular to the radio luminosity of the Crab Nebula. After the announcement of the discovery of radio pulsations, multiple explanations were proposed, and the NS origin quickly became clear. However parallel models were developed to explain the precise emission mechanism. In his 1968 article

[3]The dispersion is the frequency dependent delay caused by the matter that the photons travel through in the interstellar medium. This delay imprints a characteristic "sweep" in the data as for each flash low frequencies reach Earth later than high frequencies, see Section 2.1.1 for more details.

[4]*Pulsating Stars Traced*, by Dr. Anthony Michaelis, The Daily Telegraph, 5th March, 1968

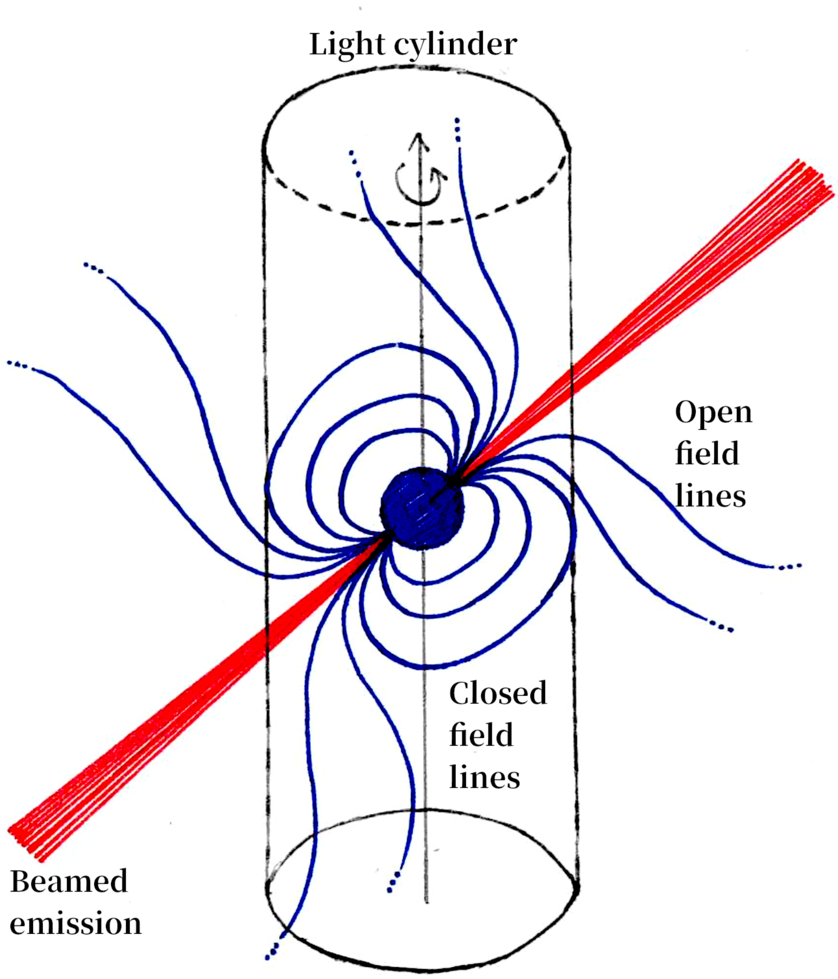

Figure 1.2: Sketch (not to scale) showing the primary features of the lighthouse model of the pulsar.

(Gold, 1968)[5], Thomas Gold inferred that in the vicinity of a rotating NS possessing a magnetosphere the plasma around the NS would co-rotate with it. However, in the case of an object with such a strong field and such a fast spin, at a certain distance of the NS the plasma might be enforced to co-rotate at a velocity exceeding that of light. This is the axisymmetric "velocity of light circle" (now called the *light cylinder*), a major consequence of this model. The relativistic plasma would radiate to lose energy before reaching the speed of light. At the radius where the co-rotation becomes impossible, charged particles from the plasma escape the magnetosphere, carrying away magnetic flux in the process, forming a *pulsar wind*. In parallel, Ostriker and Gunn, 1969 tried to explain the observed spin-down by modelling the NS as a magnetised body rotating in vacuum that loses rotational energy due to the time-variation of its magnetic dipole moment, which is not aligned with the rotation axis.

Goldreich and Julian, 1969 improved the Ostriker and Gunn, 1969 model by introducing plasma around the rotating NS, which is the starting point of our modern understanding of pulsar emission.

Ruderman and Sutherland (1975) improved upon the work of Sturrock (1971) to present a model of *polar cap* emission: charged particles, torn from the pulsar by the electric field, are accelerated along the curved magnetic field lines, and as such emit γ-rays via a curvature radiation mechanism. The photons produce electron-positron pairs, which are accelerated by the electric field. This is a recursive process, resulting in an accelerated secondary plasma emanating from the poles of the pulsar. This is called a *pair-cascade*, multiple photons emitted at different frequencies by a single seed electron. It is now commonly believed that it is from this secondary pair plasma that the observed radio emission originates, however it is possible that multiple mechanisms are at play throughout the process. The polar cap edge being defined by tangents to the last open field lines, the polar cap is assumed to be roughly conical. Through this mechanism it is thought that the high frequency photons would be emitted the closest to the pulsar, where the cone is the narrowest. Komesaroff, 1970 first argued that this was the reason why radio pulses were wider at lower frequencies, and narrower at higher frequencies, and called this effect the *radius-to-frequency mapping* (FRM).

Nowadays these simple models are quite challenged by the variety of behaviours displayed by the thousands of known pulsars. For example, millisecond pulsars (MSPs, see section 1.3) have pulse widths varying much less with frequency than expected by the traditional models, suggesting, if RFM still holds, that the emission of MSPs could originate from a smaller range of heights above the polar cap than in slow pulsars (Kramer et al., 1998). Moreover, the discovery of rotating radio transients (RRATs), objects with pulsar-like but sporadic emission (McLaughlin et al., 2009), or magnetars with no radio emission at all (Olausen and Kaspi, 2014), indicates that a single emission model might be insufficient.

A particularly mysterious property of pulsar emission is the polarisation of the radio pulses. Pulsars can be highly linearly polarised, which is thought to be caused by the propagation modes in the magnetosphere. The emergence of circular polarisation frequently observed, however, is still poorly understood and there is currently no generally accepted model that explains both circular and linear polarisation structures as seen in the observations.

1.2.2 Observational properties

The standard interpretation is that the pulses are not an intrinsic pulsation of the star but an observational effect, the radio beam sweeping across the Earth once per rotation. The rotation is extremely stable, largest variations being of the order of $\dot{P}/P \sim 10^{-12}$, which is a variation of one second over more than thirty thousand years. Figure 1.3 shows the first high time resolution of observations of PSR B1919+21, on which one can see two important features: the regularity of the pulses and the variability of their amplitude.

Generally speaking, pulsars are weak radio sources, and individual pulses such as shown in

[5] Article in which the image of a light-house beacon, very common nowadays as a mean to explain pulsars, is already brought up.

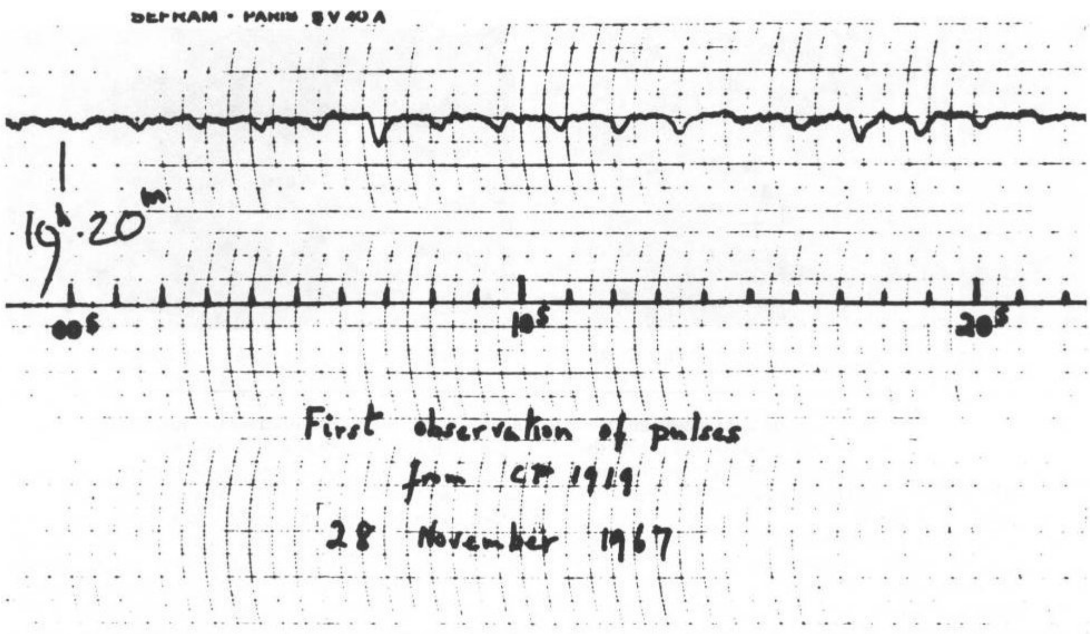

Figure 1.3: First high time-resolution recording of PSR B1919+21. The upper line is the pulsar signal, the lower line is a one Hertz reference clock.

Fig 1.3 are observable from the strongest sources. Weaker pulsars required the stacking of hundreds or thousands of single pulses to produce an *integrated profile*. Remarkably, these integrated profiles show little variation at a given observation frequency, even though the individual pulses have different shapes. However, integrated profiles vary with observing frequency, most of them displaying a broadening of the pulse when observed at lower frequencies. Observing frequency also influence the amount of radiation received, or *flux density*, from a given pulsar. For most pulsars, the dependence at mid to high frequencies ($\gtrsim 100$ MHz) can be approximated by a simple power law $S \propto f^{\xi}$ with $0 \gtrsim \xi \gtrsim -4$ with a mean around $\xi \simeq -1.4$ (Bates, Lorimer, and Verbiest, 2013).

1.2.3 Pulsars across the spectrum

While pulsars have been discovered in the radio domain, they emit over the entire electromagnetic spectrum. Historically they have been mostly observed at radio frequencies, leading to emission models focusing on this domain, as those discussed in the previous section. However, the modern multiwavelength approach is very fruitful and leads to a much more detailed understanding of these objects. In particular, searches for γ-ray pulsars with the *Fermi-Large Array Telescope* (*LAT*) expanded the number of known pulsars, and particularly millisecond pulsars (MSPs, see next section), by quite a lot. Figure 1.4 shows the number of radio MSPs discovered in the Fermi-LAT sources compared to all other surveys.

One reason behind the efficiency of γ-ray observations for discovering new pulsars is that at higher frequencies pulsars are among the brightest sources. The *Fermi-LAT* scans the entire sky in about 5 hours, and operates a continuous all-sky survey: over the past 17 years it created a single image of the whole sky by continuously recording photons, seeing deeper at every passage. A pulsar-like source in the *Fermi-LAT* map can be targetted by a radio telescope to search for pulsations. Because the location is known to within several arcminutes typically, the observing time is vastly decreased, compared to radio "blind" surveys where pulsations are searched for at all locations for a given region of the sky. This also allows for longer observations at the targeted points, which helps detecting faint pulsars or eclipsing systems that are only detectable for a fraction of the orbital period. Thanks to this, many radio surveys are targetting Fermi-LAT sources, finding

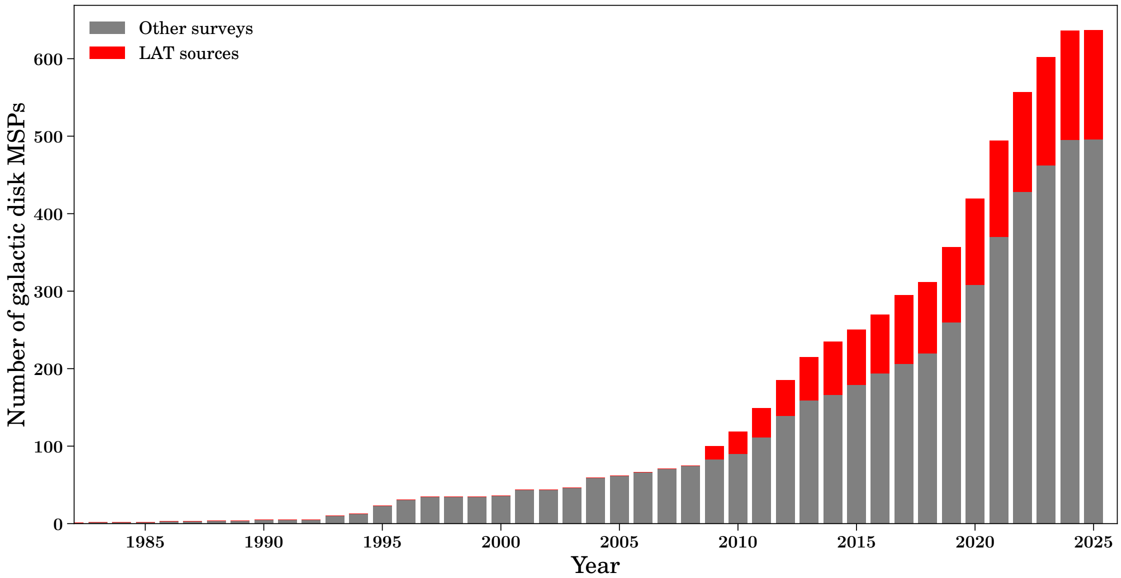

Figure 1.4: Histogram of the number of known galactic MSPs, the MSPs discovered by targeting pulsar-like sources from *Fermi-LAT* catalogues are highlighted in red. Data are taken from the Galactic Millisecond Pulsar Catalogue[6].

many new pulsars. Moreover some pulsars are visible at high energies, especially in γ-ray, but not at radio wavelengths, because of the geometry of the emission. Indeed, as the radio and γ-ray emissions do not originate from the same region, the beams are not necessarily pointing in the same direction.

High energy emission (from optical to γ-ray) has been detected from a significant fraction of the known pulsars. More than 300 pulsars have been detected in γ-rays (Smith et al., 2023), and more than two hundred pulsar counterparts are found in X-rays (Xu et al., 2025). The X-ray emission is observed to contain both thermal and non-thermal components. The thermal radiation is usually attributed to X-rays originating from the pulsar surface and makes up only a small fraction of the high energy emission. The majority is made up of non-thermal optical, X-ray and γ-ray radiation.

Many fields of pulsar studies are conducted based on high energy observations, such as for example:

- the high-energy emission properties, are naturally not accessible in radio.
- pulsar magnetosphere models can be constrained by high energy light curves or luminosity, which in turn deepens the theoretical understanding of the underlying magnetic fields.
- accreting binaries, sometimes composed of a pulsar and a regular star, are very bright in X-ray, and usually radio "quiet" (*i.e.* are not observed to emit). The stellar wind and possible accretion disk modulate the X-ray luminosity, allowing to probe components such as the magnetic field of the binary.
- γ-ray emission constitutes a significative fraction ($\gtrsim 10$ %) of the total spin-down energy of the pulsars, thus to constrain energy loss γ-ray light is the main indicator used.

Generally, the more interesting objects expand the neutron star "zoo", the more models and theories can advance to encompass every aspect of pulsar phenomena.

[6] https://www.astro.umd.edu/~eferrara/pulsars/GalacticMSPs.txt

1.3 The pulsar population

1.3.1 The $P - \dot{P}$ diagram

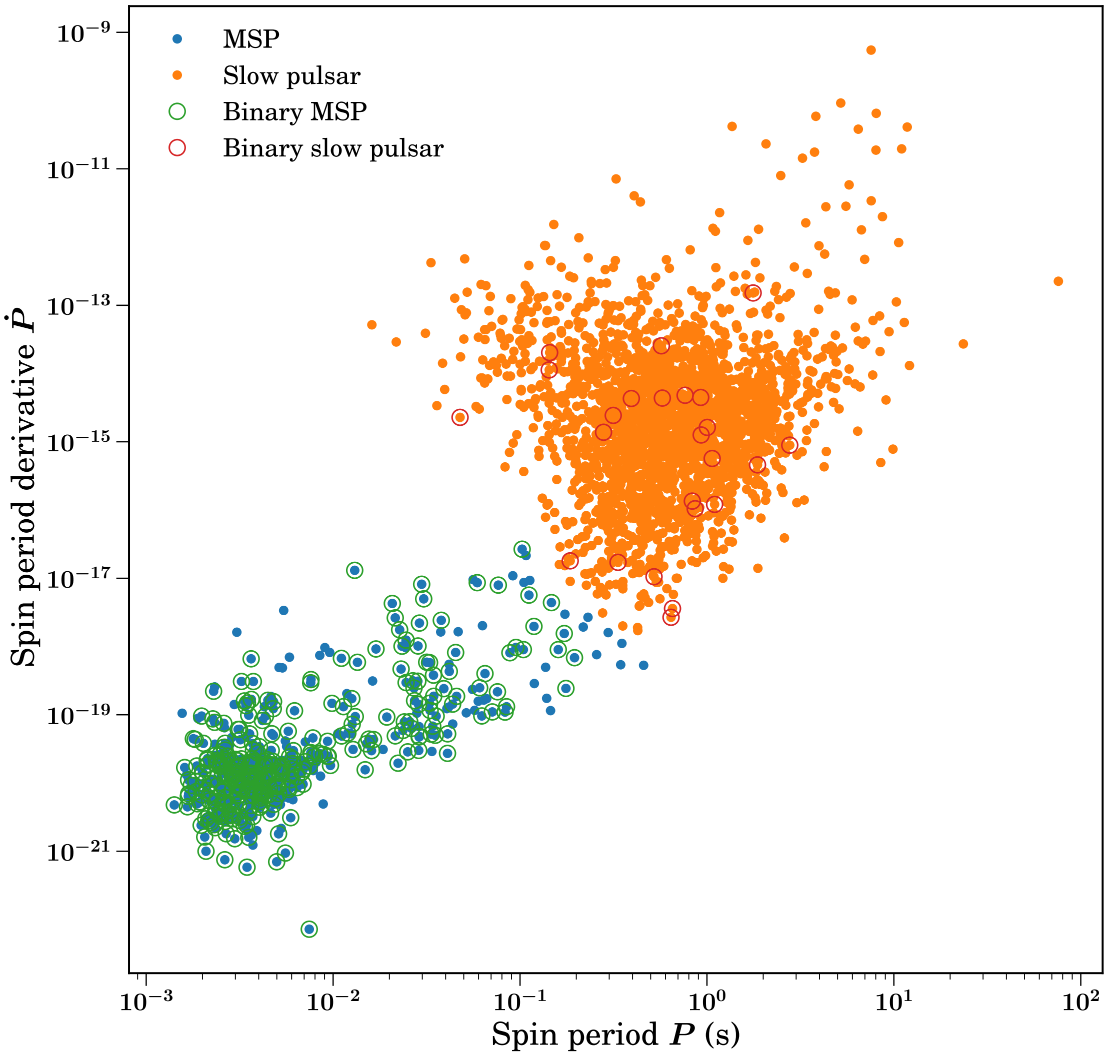

Figure 1.5: $P - \dot{P}$ diagram for all pulsars in the ATNF catalogue at the time of writing. We see the clear distinction between the central cluster of slow pulsars and the bottom left cluster of millisecond pulsars. Pulsars circled are in binary systems.

At the time of writing, there are 3838 pulsars listed in the *Australian Telescope National Facility* (ATNF) Pulsar Catalogue[7] (Manchester et al., 2005). Pulsars can be separated in multiple sub-populations depending on their properties. Figure 1.5 shows a plot of the first derivative of the spin periods as a function of the spin period, the so-called $P - \dot{P}$ diagram. Two main clusters can be identified in this parameter space: most of the pulsars dwell in the middle of the plot, with spin periods close to the second, while the millisecond pulsars (MSPs) form an island at the bottom left. The canonical threshold for MSPs is $P < 30$ ms, although this limit is not well defined, and in the ATNF catalogue 638 pulsars currently qualify. A distinction between MSPs and slow pulsars has been found by using machine learning techniques to classify pulsars in the

[7] https://www.atnf.csiro.au/research/pulsar/psrcat/

$P-\dot{P}$ diagram, resulting in an empirical definition of MSPs as pulsars with $\frac{\dot{P}}{10^{-17}} \leq 3.23\left(\frac{P}{100\text{ms}}\right)^{-2.34}$ (Lee et al., 2012). By definition MSPs have shorter periods, but they notably have smaller spin-down rates. Pulsars are born from rotating giant stars, hence as a consequence of the conservation of the angular momentum are to spin very rapidly after the gravitational collapse. A plausible evolution path for normal pulsars such as the Crab pulsar, would indeed be a birth with a short spin period, followed by a rapid spin down before becoming too faint to be detectable after 10^7 years. However MSPs must follow a different path to gather at the bottom left of the $P-\dot{P}$ diagram.

1.3.2 Characteristic age

If the radiation of the pulsar is assumed to be generated by the loss of kinetic energy of a rotator with the rotation frequency of $\Omega = 2\pi/P$, the dissipation of energy is (Lorimer and Kramer, 2004):

$$\dot{E}_{spin-down} = -\frac{dE_{rot}}{dt} = -\frac{d(I\Omega^2/2)}{dt} = 4\pi^2 I\frac{\dot{P}}{P^3} \quad (1.1)$$

where I is the moment of inertia. If this rotator has a purely dipolar magnetic field, according to classical electrodynamics, a rotating dipole of moment $\vec{\mu}$ radiates a power of:

$$\dot{E}_{dipole} = \frac{2}{3c^2}|\mu|^2\Omega^4\sin^2\alpha \quad (1.2)$$

where α is the angle between the magnetic moment and the rotation axis. By equating $\dot{E}_{spin-down}$ and $\dot{E}_{dipole}$ one can derive:

$$\dot{\Omega} = \frac{2}{3Ic^2}|\mu|^2\Omega^3\sin^2\alpha \quad (1.3)$$

Expressing this as a power law and in terms of rotational frequency $\nu = 1/P$ gives:

$$\dot{\nu} = -k\nu^n \quad (1.4)$$

where n is the *braking index* and $k = \frac{2}{3Ic^2}|\mu|^2\sin^2\alpha$. From eq.(1.3) we expect $n = 3$, corresponding to the braking index expecting in the case of a purely dipolar magnetic radiation, however other dissipation mechanisms exist, but they would lead to a similar scaling (Michel and Li, 1999; Spitkovsky, 2004). For the studies where the measurement of n have been possible, values are lower than 3:

Pulsar	Braking index	Reference
J0534+2200 (Crab)	2.52	Lyne et al., 2015
J0540−6919	2.13	Ferdman, Archibald, and Kaspi, 2015
J0835−4510 (Vela)	1.7	Espinoza, Lyne, and Stappers, 2016
J1119−6127	2.68	Weltevrede, Johnston, and Espinoza, 2011
J1208−6238	2.60	Clark et al., 2016
J1513−5908	2.83	Livingstone and Kaspi, 2011
J1826−1334	2.6	Espinoza, Lyne, and Stappers, 2016

Table 1.1: Braking indices for 7 pulsars

Expressing eq.(1.4) in terms of period instead of frequency:

$$\dot{P} = kP^{2-n} \quad (1.5)$$

Assuming a constant k and a braking index $n \neq 1$ one can integrate eq.(1.5) to derive the age of the pulsar:

$$T = \frac{P}{(n-1)\dot{P}}\left[1-\left(\frac{P_0}{P}\right)^{n-1}\right] \quad (1.6)$$

where P_0 is the spin period at birth. Under the assumption that $P_0 \ll P$ and $n = 3$ one can derive the *characteristic age*:

$$\tau_c = \frac{P}{2\dot{P}} \simeq 15.8\text{Myr}\left(\frac{P}{\text{s}}\right)\left(\frac{\dot{P}}{10^{-15}}\right)^{-1} \tag{1.7}$$

Because of the assumptions previously made, this does not gives a reliable age estimate. The estimated age for the Crab pulsar is ~ 1240 years, which is comparable to the known age of the pulsar of 970 years. An dramatic case of discrepancy can be found in PSR J0538+2817, for which the characteristic age is ~ 620 kyr, however its proper motion measurements indicate that this pulsar is linked to a nearby remnant, which is estimated to be ~ 30 kyr old (Kramer et al., 2003). In a few extreme cases the characteristic age can be larger than that of the Universe, for example J2019+2425 and J2322+2057 which have $\tau \simeq 27$ Gyr and $\tau \simeq 19$ Gyr, respectively (Nice and Taylor, 1995).

As the characteristic age scales with $P/\dot{P}$, MSPs are the oldest pulsars, and 'slow' pulsars are rather younger. However theoretical estimates of the spin period at birth suggest that for any given pulsar the value must lie between ~ 10 to 150 ms (Faucher-Giguère and Kaspi, 2006), but MSPs are known to spin faster. If the spin can only "naturally" decrease, the MSPs must undergo an additional process to *spin-up* up to the millisecond.

1.3.3 Isolated and binary pulsars

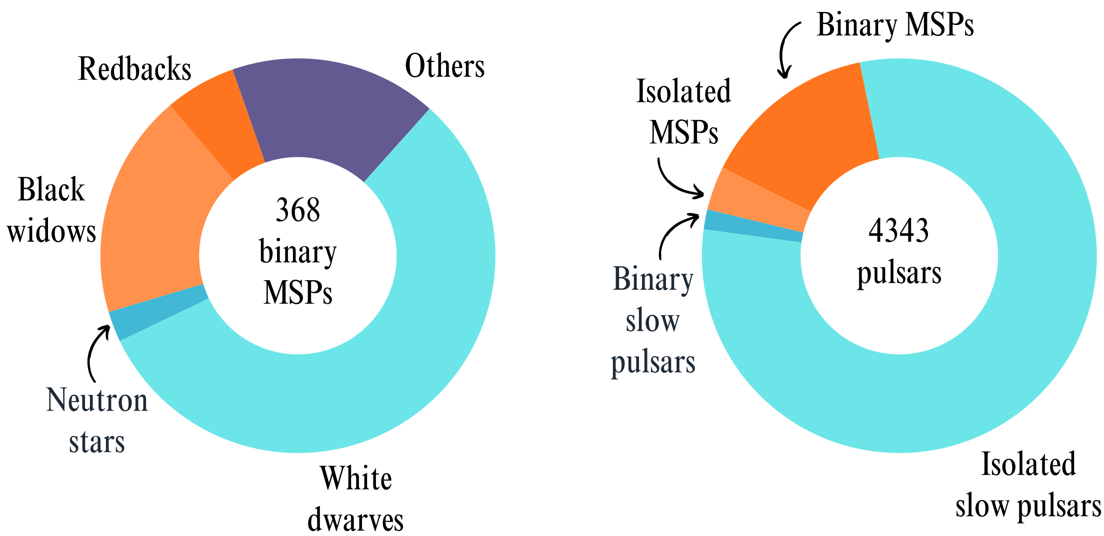

Figure 1.6: The pulsar population in the current version of the ATNF catalogue. The total number of pulsars (left chart) is currently 4343, composed of 82 % of slow pulsars ($P > 0.03$ s) and 18 % of MSPs. About 2 % of slow pulsars are in binary systems, whereas 46 % of MSPs are in binary systems. The companions of MSPs (right chart) are mostly WDs (56 %), but a large fraction (24 %) are spiders, with a total of 66 BWs and 21 RBs. Seven pulsars are in a system with another NS, and the remaining 17 % are wide binaries with stellar companion and companions of unknown nature.

Contrary to slow pulsars, it appears that most MSPs are in *binary systems*, being gravitationally bound to another object, called their *companion*. This companion can be a regular star, and will evolve as the pulsar did in its previous life stage. Because the evolution of each star depends on that of the other, the system has to be studied as a whole, hence the main evolution factor is the variation of total orbital and spin angular momentum, whether as an exchange within the system or a loss from the system. The system can lose orbital momentum via gravitational wave radiation, as detected very early by Taylor and Weisberg, 1982 in the first binary system discovered PSR J1915+1606, but also via magnetic braking (Verbunt and Zwaan, 1981), spin-orbit coupling (Witte and Savonije, 1999) and mass loss from the system.

Many different binaries can be found. Light stars, which make up for about 97 % of the stars of the Milky Way (Fontaine, Brassard, and Bergeron, 2001), become white dwarves at the end of their main sequence, hence most of the companions are white dwarves or regular stars, but in some cases both progenitor stars are heavy, resulting after both supernovæ in a double neutron star binary. The neutron star companion can be invisible in radio like that of the Hulse-Taylor pulsar (Hulse and Taylor, 1975), or can even be seen as a pulsar itself. A striking example of a double neutron star binary is PSR J0737+3039, a system composed of an MSP (pulsar A) and a slow pulsar(pulsar B), discovered in 2003 (Burgay et al., 2003). Since 2008, pulsar B is no longer visible in radio as it precessed out of sight, but is predicted to be observable again in 2035 (Perera et al., 2011). This object is a wonderful natural laboratory for general relativity, especially to study the loss of orbital energy via gravitational waves emission. It has been theorized that pulsar-black hole systems might exist but no example of such systems have been discovered at the moment of writing.

Many binary systems composed of regular stars are known, and evidences show that the binary developed during the star formation stage. A triple system could also arise, however the solution to the three-body problem predict that one of the three objects would be ejected if its mass is comparable to that of the two others, leaving a binary. A binary formed via gravitational capture could also exist, thought the odds are too low compared to the number of known binaries for this to be the main formation channel. It is believed that galactic pulsars in binary systems mainly stem from pre-supernova binaries which survived the explosion.

1.3.4 Recycled pulsars

Combining eq.(1.6) and eq.(1.7) gives the spin at birth:

$$P_0 = P\left[1 - \frac{n-1}{2}\frac{T}{\tau_c}\right]^{\frac{1}{n-1}} \tag{1.8}$$

For pulsars with known true ages and measured braking indices the spin period at birth can be derived. For example, for the Crab pulsar $P_0 \sim 19$ ms (the current spin period is $P \sim 33.5$ ms). Theoretical works suggest that P_0 should be about 11 ms to 150 ms for every pulsar (Faucher-Giguère and Kaspi, 2006). However plenty of faster pulsars are known, and so if the spin down is the natural evolution of pulsars, another mechanism has to be found to explain the older yet faster MSPs. If the angular momentum does not come from the progenitor star, it might come from another star.

As stated previously most of MSPs are in binary systems, compared to slow pulsars. The common explanation for spun up pulsars is that all MSP are formed in binary systems and that the pulsars has accreted matter (and with it angular momentum) post-supernovae. During the pulsar-MS star binary stage, the MS star will follow its own evolution path. Depending on its mass, this evolution can lead to the star bloating out of its Roche lobe, the volume around the star in which the matter stays gravitationally bounded to it. When the matter outflows the Roche lobe, it starts infalling onto the pulsar, transferring mass and angular momentum. This exchange of angular momentum spins up the pulsar, a process called *recycling*. These accreting binaries are extremely bright in X-rays, and therefore called X-ray binaries (XRB). During this phase the pulsar is *radio quiet* and therefore not observed as a pulsar. The accretion also reduces the magnetic field of the donor star (Bhattacharya, 2002), which can explain the relatively low magnetic fields of binary pulsars.

Isolated MSPs can be created by these XRB if the accretion consumes the companion entirely, or after the accretion has stopped, through several channels: if the companion is released in a exchange encounter, if the pulsar and the companion coalesced, if the companion undergoes a SN that disrupts the binary, or if the pulsar wind completely evaporates its companion. The latter explanation might be the creating channel of most of the isolated MSPs (Bhattacharya and van den Heuvel, 1991).

If the binary still exists once the accretion has stopped and is not disrupted in the following hundreds of millions of years, very old and stable binary MSPs remain. Once the accretion stops, the X-ray emission lowers a lot and the radio emission lights up. Because of the prevalence of light stars and the lifespan of such systems, most binary pulsars have white dwarf companions, however in some cases the star is still in the MS.

1.4 The spider binary subclass

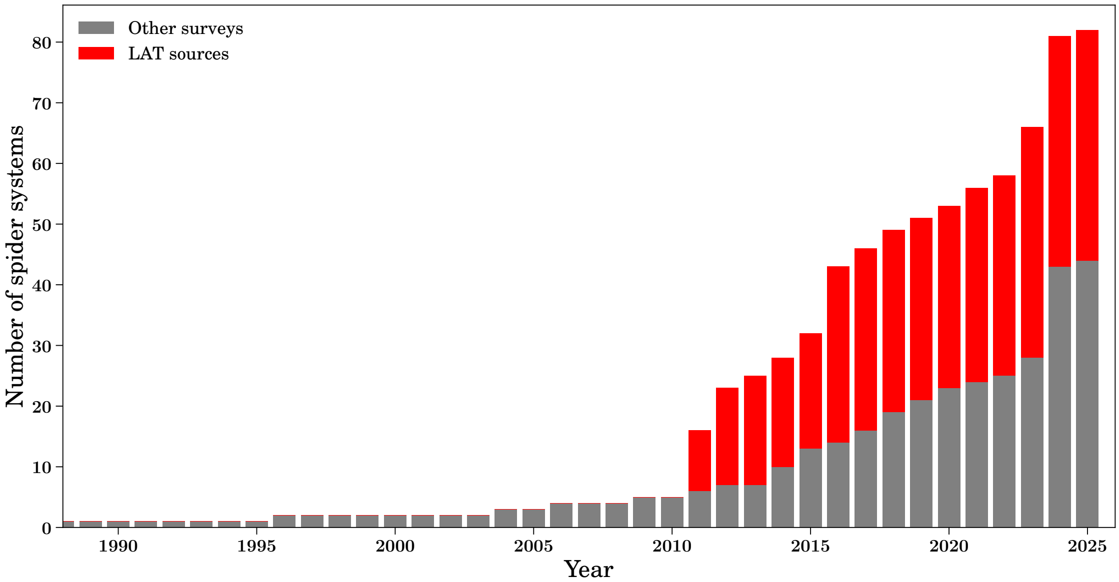

Figure 1.7: Histogram of spider systems known as a function of time, as catalogued in the SpiderCat catalogue[8] (Koljonen and Linares, 2025). Candidates systems that have no pulsations found as of 2025 are not plotted in this histogram. Systems found by targetting Fermi-LAT sources are highlighted in red.

The main works of this thesis focus on a peculiar sub-class of pulsar binaries: the *spider binaries*. Spiders are systems in which the pulsar companion is a light semi-degenerate star of mass $M_* \lesssim 0.5M_\odot \simeq 10^{30}$ kg, where $M_\odot$ is the mass of the Sun. These binaries orbit very closely, with orbital periods of typically $P_b \lesssim 1$ day. Spiders are usually divided into two sub-categories: the *black widows* (BWs) that have lighter companions ($M_* \lesssim 0.05M_\odot$)and the *redbacks* (RBs) that have heavier companions ($M_* \in [0.1, 0.5]M_\odot$) (Roberts, 2013). The names come from black widow and redback spiders, species that are thought to commonly practice mating cannibalism, although actual studies show that spider cannibalism is usually overestimated due to the 'cage bias' and that only about 65% of RBs males are actually eaten during mating (Andrade, 2003).

The first spider was discovered in 1988 (Fruchter, Stinebring, and Taylor, 1988), and before the *Fermi-LAT* only 5 spider systems have been found. Because of their radio eclipses that blur the flux for a significant fraction of the orbit, and their multiple orbital parameter to sample during a "blind" search, these pulsars are particularly easier to find by targetting *Fermi-LAT* sources. In the same manner as Figure 1.4, Figure 1.7 shows the number of spider systems discovered by searching for radio pulsations at the location of *Fermi-LAT* sources. The latest *Fermi-LAT* catalogue presented 12 additional spider candidates which might also expand the number of known spiders (Smith et al., 2023).

There are hints that pulsars of the spider class might be generally heavier than other classes of binary NS (Linares, 2020), and more recent and conservative results still find mass measurement above the traditional 1.4 $M_\odot$ value (Clark et al., 2023). Strader et al., 2019 found a median mass of 1.8 $M_\odot$ for RB pulsars.

1.4.1 Formation and evolution of spider systems

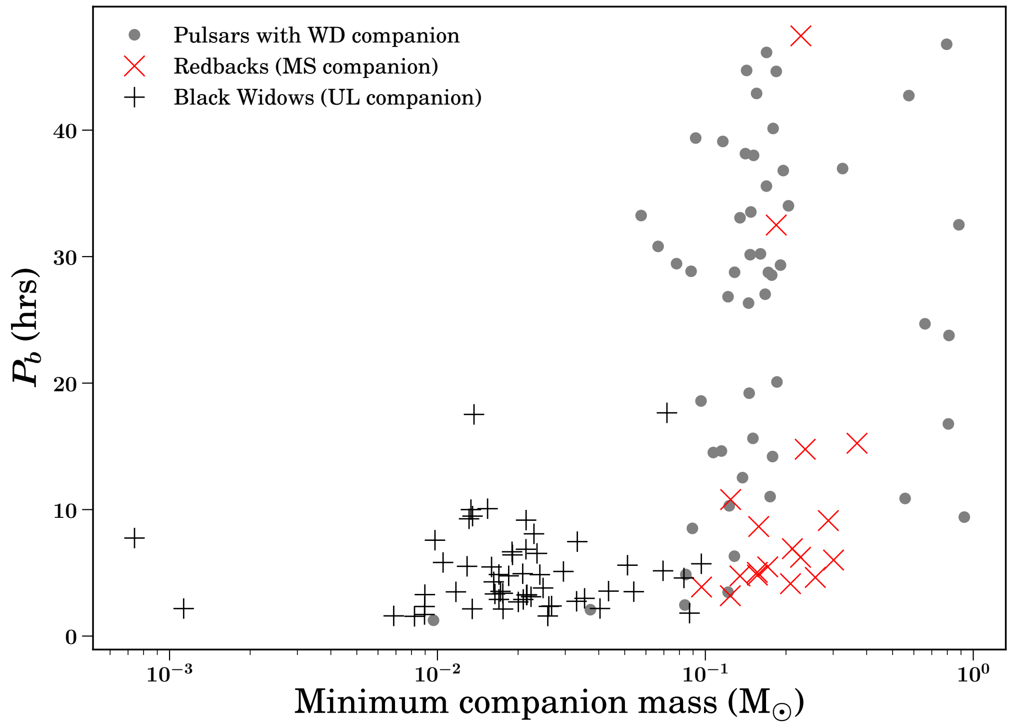

Figure 1.8: Orbital periods of known spider systems against minimum companion masses. In this figure, spider systems are categorised as BW or RB depending on the companion type listed in the ATNF catalogue: main sequence (MS) stars for RBs or ultra low-mass objects (ULs) in the case of BWs.

One of the possible outcomes of a recycling binary as described in section 1.3.4 is a spider system. X-ray binaries are separated into donor mass categories. The high-mass XRB have donors with masses > $10M_\odot$, and can form double NS binaries. The intermediate-mass XRB have donors with masses $1M_\odot < M_* < 10M_\odot$ and are often insufficient to completely spin-up the pulsar, ending in non- or partially-recycled pulsars with heavy white dwarves. A complete review of binary formation processes can be found in Tauris, 2015 and we will give here only a summary of spiders formation process.

Low-mass X-ray binaries (LMXBs), those whose donors have masses $\lesssim 1M_\odot$, tend to form accretion disks which is an accretion supposed to be more stable and longer lasting than that of high- or intermediate-mass XRBs, resulting in pulsars being spun-up to the fastest rotations. Depending on the initial orbital period, LMXRBs can lead to either a compact or a wide binary (Tutukov et al., 1985). Spider systems come from the most compact of these binaries. Their very close orbits of $P_b \lesssim 1$ day, submit the companion star to an extreme irradiation from the pulsar wind (Jia and Li, 2016), that can continue beyond the accreting X-ray binary phase into a spider system phase. The switching process between the XRB phase and the radio pulsar phase is still poorly understood, but has been observed in what is now called transitional pulsars, swinging between

[8] https://astro.phys.ntnu.no/SpiderCAT/

states on very short timescales of months or weeks (see e.g. Archibald et al., 2009; Papitto et al., 2013; Bassa et al., 2014). The accretion phase might also be a *propeller-mode accretion* (Archibald et al., 2009) where the matter might not even form a disk but be expelled out of the system if the accretion pressure is insufficient to counteract the outward radiation from the magnetic plasma and the pulsar wind. These transitional pulsars are all redbacks systems with companions masses $\gtrsim 0.1 M_\odot$, and have been suggested to represent the missing link between XRBs and stable spiders.

1.4.2 Nature of the companion

In spider systems, the very small orbital separation leads to tidal locking: the spin period of the companion equals the orbital period and the eccentricity tends to zero. Tidal locking comes from the vicious dissipation of the tidal deformation of the companion star, which is more efficient for stars with a deep convective envelope. BW companions are thought to be fully convective, but this is also the case of the lightest of RBs, as the upper limit for fully convective stars is expected around $0.3 M_\odot$ (Rappaport, Verbunt, and Joss, 1983). In the case of a fully convective star, the synchronisation timescale is:

$$\tau_s = 3\tau_{conv} \frac{I_c a^6}{m_c R_c^8} q^{-2} \tag{1.9}$$

where I_c, m_c, R_c are the moment of inertia, the mass and the radius of the companion star (assumed spherically symmetric), respectively, $q = m_c/m_p$ is the mass ratio and τ_{conv} is the convective time scale, that can be approximated as:

$$\tau_{conv} = 0.4311 \left(\frac{m_c R_c^2}{6 L_c} \right)^{1/3} \tag{1.10}$$

where $L_c = 4\pi R_c^2 \sigma T_{eff}^4$ is the luminosity of the star, related to its effective temperature (Hurley, Tout, and Pols, 2002).

τ_s is very dependent on the mass ratio q, and ranges from $\tau_s \sim 5 \cdot 10^3$ years for RBs ($q \sim 0.3, m_c \sim 0.1 M_\odot$) to $\tau_s \sim 6 \cdot 10^7$ years for BWs ($q \sim 0.02, m_c \sim 0.03 M_\odot$) (Voisin, Breton, and Summers, 2020). The upper limit values are still significantly less than the time spent as an XRB (Chen et al., 2013), therefore the system is tidally locked and circularised before entering the spider system phase.

In both BW and RB systems the companion star is strongly irradiated by the pulsar wind, although for RBs companions the irradiation is less visible due to the higher inner temperature of the larger star. The internal structure of the companion star is poorly known for the moment, and probing this structure would greatly help constraining the models of formation and evolution of such systems. One possible probe is the measurement of the orbital precession, which is caused by the variations of the gravitational quadrupole moment of the companion star. These variations are linked to the deformability of the star, and the tidal periastron precession depends on the companion star Roche-lobe radius ρ, its Roche-lobe filling factor f, the mass ratio between the pulsar and the companion q, the spin period of the pulsar P and the apsidal motion constant k_2 as (Voisin, Breton, and Summers, 2020):

$$\dot{\omega}_{tidal} = -10 \left(\frac{4\mathrm{h}}{P} \right) \left(\frac{k_2}{0.1} \right) \left(\frac{q}{1/16} \right)^{-1} f^5 \left(\frac{\rho(q)}{\rho(1/16)} \right)^5 \mathrm{cyc/yr} \tag{1.11}$$

The apsidal motion constant, or tidal Love number (Love, 1909), is a dimensionless number quantifying the deformability of a star in reaction to a centrifugal and tidal field perturbation. Companions of BWs are similar to hot Jupiters in mass and irradiation that have k_2 as large as ~ 0.2, for comparison Sun-like stars have $k_2 \sim 0.015$ (Ogilvie, 2014). But spiders are also similar to companions of cataclysmic-variable binaries, for which k_2 values as low as $k_2 \sim 10^{-4}$ have been measured (Warner, 1978). Such a low value is compatible with the companion being a stripped red-giant core (Cisneros-Parra, 1970), a mechanism compatible with the formation process of spiders.

The main explanation for the quadrupole distortions are magnetic cycles applying a strain that can distort the star (Applegate and Shaham, 1994), usually referred to as the Applegate mechanism. This mechanism is known to be present in cataclysmic variables (Applegate, 1992), and the application to pulsars has been studied in detail (see e.g. Lanza, 2006; Völschow, M. et al., 2016; Navarrete et al., 2019). The Applegate mechanism was at first proposed to explain the pseudo-periodic variations of orbital periods seen in close and tidally-locked binaries, however the Applegate mechanism alone could not be responsible for the magnitude of orbital variation seen in spider systems, as the energy necessary to produce the amplitudes of the variations via this mechanism exceeds the total available energy produced by the star, while it should represent only a minor fraction (Völschow, M. et al., 2016).

1.4.3 The eclipse phenomenon

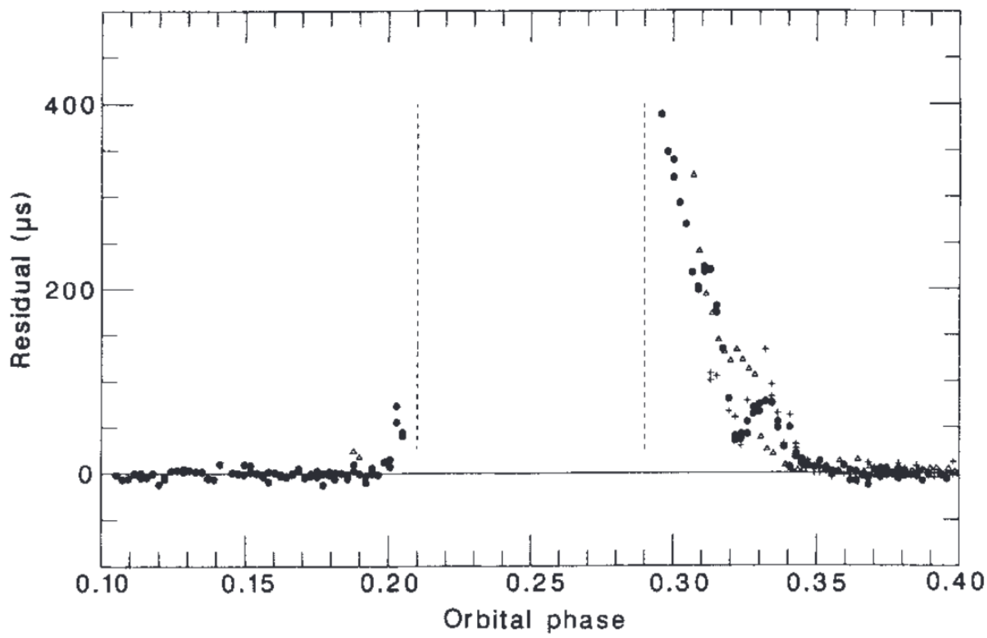

Figure 1.9: Figure 3 from Fruchter, Stinebring, and Taylor, 1988: residuals around the superior conjunction of spider system J1959+2048 observed at 430 MHz with the Arecibo telescope. The residuals are the excess delay measured in the pulsation times of arrival when compared to the modelling of the system. A positive residual indicates that the pulsation is delayed by additional plasma along the line-of sight. Orbital phase $\phi = 0.25$ is the superior conjunction, when the pulsar is the furthest from Earth along the line-of sight, and its companion the closest.

The first spider discovered was PSR J1959+2048, or B1957+20, sometimes called the "original black widow", reported by Fruchter, Stinebring, and Taylor, 1988 in an article titled *A millisecond pulsar in an eclipsing binary*. The most striking feature of this system, apart from its very short orbital period of 9.17 hours, was its 20 minutes long eclipses, during which the radio pulsations of the pulsar are no longer detectable, a phenomenon previously unknown in pulsar systems. The eclipses were observed to be happening at the same period as the orbital period of the binary. Observations were conducted with the Arecibo telescope, at 430 MHz as part of a general MSPs survey. It was noticed that the mass of the companion was surprisingly low, compared to the duration of the eclipse, and that before and after complete obscuration of the radio pulsations the beam was seen through additional ionised plasma surrounding the companion, and that delayed the pulses. Because this eclipsing phenomenon is tied to the orbital period, one can infer that this plasma belongs to the direct surroundings of the system, and is not the usual ISM delaying. Figure 1.9 shows the original plot in Fruchter, Stinebring, and Taylor, 1988 showing the recorded eclipses.

This delay appeared to vary from orbit to orbit, indicating a turbulent medium varying over a timescale of the order of a few hours. It was derived that the eclipsing region was $1.4R_{\odot}$ across, but the companion Roche lobe is only $0.3R_{\odot}$, indicating that most of the plasma was not gravitationally bound to the companion but rather flowing out of it, as a stellar wind powered by the radiation of the pulsar. This naturally explains the asymmetry of the residuals plotted in Figure 1.9 as a comet-like tail of escaping plasma. As we are witnessing the instantaneous evaporation of the companion star, the variation timescales are extremely short.

Since the discovery of PSR J1959+2048 many other eclipsing systems have been found. Giving a number of eclipsers is tricky, as the detection of eclipses depends on the observing frequency, as shown for example in Figure 13 of Polzin et al., 2019, figure reproduced in the following Figure 1.10. However at the time of writing, despite nearly 40 more years of data, a single mechanism model explaining the eclipses is still lacking. The variations of the eclipses in time and frequency, as well as the variations between the different spiders, have made the characterization of the exact mechanism difficult. As a result, most systems have been studied individually and over limited bandwidths.

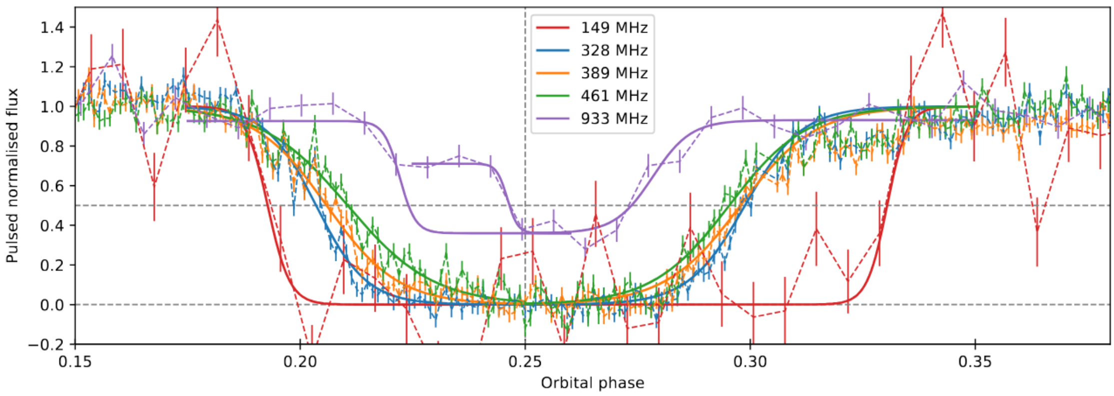

Figure 1.10: Upper panel of Figure 13 from Polzin et al., 2019: comparison of the pulsed flux densities (dashed lines) of an eclipse of PSR J2051−0827 observed at multiple wavelengths. The solid lines are the fitted curves. One can clearly notice that the eclipse gets shorter when observed at higher frequencies.

Thompson et al., 1994 investigated the interaction processes susceptible of causing eclipses and made specific diagnostic about the two eclipsing systems discovered at that time, PSRs J1959+2048 and J1748-2446A. A brief summary of the mechanisms proposed in this review is given here:

- **Refraction** of the radio beam out of the line-of-sight by the density gradients of the plasma was suggested at the discovery of the original BW by Fruchter, Stinebring, and Taylor, 1988. This mechanism was ruled out by Thompson et al., 1994, as the frequency dependence of the eclipses of J1959+2048 was largely different from that predicted by the model, and the observed plasma density around J1748-2446A was too low.

- **Scattering by plasma turbulence** in the ablated material, broadening the pulsar beam over more than the rotation period of the pulsar, thus making it undetectable. This was however not considered a convincing mechanism, as the smearing of the pulses would occur at frequencies much lower than the flux density reduction, which is not the case in observations.

- **Compton scattering** would alter the radiation spectrum and looking like absorption when observed over a finite bandwidth. Thompson et al., 1994 found that this effect could be part of the eclipse mechanism but alongside with something else, as the calculated effects did not have the same magnitude as the observed ones.

- **Stimulated Raman scattering** could induce turbulence in the plasma near the pulsar heated by the radio beam itself. Should the turbulence persist, the radio beam would be scattered away from the line-of-sight, without much smearing. Thompson et al., 1994 concluded that this mechanism could be responsible for the eclipses of the two systems should the plasma be hotter than a derived lower limit.

- **Free-free absorption** occurs in a relatively cold and low density wind, but this mechanism was quickly discarded by Thompson et al., 1994 as the predicted plasma temperature was too low to be that of a plasma that close to a pulsar.

- **Cyclotron/synchrotron absorption** requires a magnetic field in the vicinity of the companion, produced either by the pulsar wind or the magnetosphere of the companion star. Radio waves would be absorbed at the resonant frequency or one of its harmonics, and higher frequencies require stronger magnetic fields, hence are absorbed closer to the companion, reducing the size of the eclipsing region. This naturally explains why longer eclipses are observed at lower frequencies, and Thompson et al., 1994 showed that this mechanism does indeed reproduce the eclipse behaviour of the two pulsar studied.

The matter outflowing from the companion star forms a stellar wind that meets the pulsar wind between the two objects, creating a *intrabinary shock* on top of the relativistic shock of the *termination shock* of the pulsar wind on the circumbinary nebula (Arons and Tavani, 1993). In these shocks, highly accelerated particles produce synchrotron emission up to very high energies. The intrabinary shock is much closer to the pulsar than the termination shock of isolated pulsars, thus allowing to probe deeper into the pulsar wind and the magnetic intrabinary environment. Electrons in the intrabinary shock region are expected to be accelerated up to ~ 3 TeV (Arons and Tavani, 1993), producing a X-ray emission with orbital modulations, as X-rays are Doppler boosted along the curves of the shock.

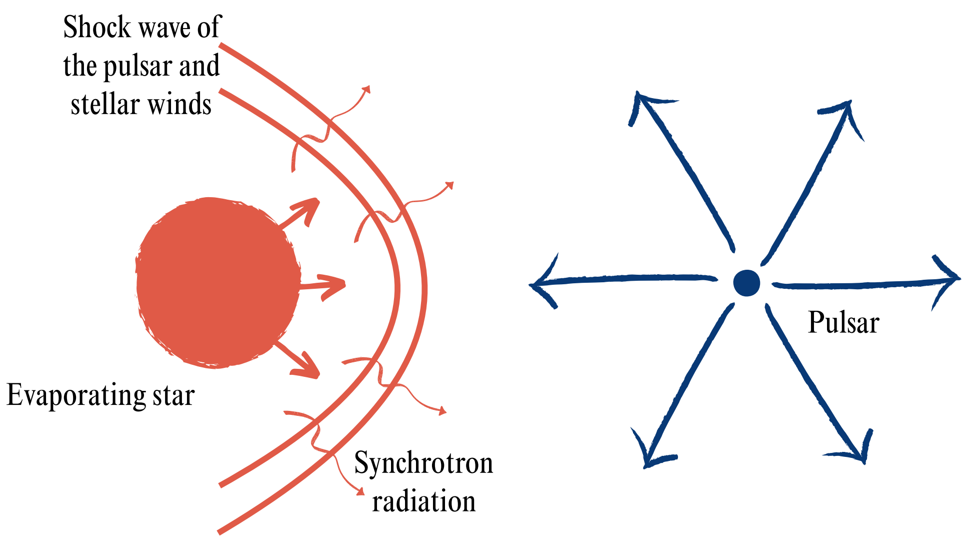

Figure 1.11: Sketch of an intrabinary shock formed close to the irradiated companion star. The shock forms where the pulsar wind pressure equalises with the pressure in material driven from the companion star surface. Figure following Arons and Tavani, 1993.

1.4.4 Pending questions

Many phenomena of pulsar science are still ongoing investigations, but some pending questions are specific to spider systems, or can be efficiently explored by studying spider systems. I present in this section some questions I did not work on, to illustrate the broad range of interesting spider studies.

Spider binaries evolution

One specific question about spider systems is the evolution of such systems. At the time of the discovery of the first BW, it was seen as a potential "missing link" for the formation of isolated MSPs, however in most known cases pulsars in spiders seem to evaporate their companion too slowly for isolated pulsars to be formed in less than the Hubble time, even though the precise mass loss from the companion is difficult to estimate. Because of its proximity to the pulsar, the companion is extremely irradiated, thus its evolution does not follow usual stellar models. Predicting the evolution of a star with a poorly known structure and subjected to extreme conditions is very challenging.

Distinction between BWs and RBs

At the time where the sub-categorisation between BWs and RBs was proposed, the bimodality of the companion mass distribution was very clear, but this might be less the case nowadays (see Figure 3.4). However, it has been recently proposed that they may display other differences, such as different X-ray luminosity (RBs being generally brighter in X-rays) or γ-ray to X-ray fluxes ratios (BWs generally having a higher ratio than RBs) (Koljonen and Linares, 2025). It was proposed that BWs and RBs form via different formation processes (Chen et al., 2013) or that BWs are all evolved from RBs (Benvenuto, De Vito, and Horvath, 2014), with the RB being a transition phase between XRBs and BWs (although not all RBs are expected to form BWs).

Transitional MSPs

As presented in Section 1.4.4, spiders are thought to come from accreting binaries. Finding the first *transitional* MSP (tMSP), J1023+0038 (Archibald et al., 2009) a pulsar switching between a radio pulsar state and an accreting binary state, was a key step in the understanding of binaries evolution. This pulsar was first detected in 2000 and 2001 as an accreting binary. Accretion stopped after 2002, and up until 2008. In 2007, observations conducted with the Green Bank telescope found pulsations at this location, and the timing revealed J1023+0038 to be in a RB system. This system and two others, both RBs, have been seen switching back and forth between states over timescales accessible to humans, much shorter than that predicted for recycling (Papitto et al., 2013; Stappers et al., 2014; Bassa et al., 2014). Additionally to the accreting XRB and the radio pulsar states, these tMSPs display an intermediate state, with an accretion disk but a lower X-ray luminosity than the first accretion state. A handful of candidates tMSPs are currently monitored, with hopes that they would switch state in a short amount of time. These candidates usually display characteristics similar to that of the intermediate state of the confirmed tMSPs (Papitto and de Martino, 2022). These systems, still rare, are incredible objects to confront theories to.

NS equation of state

One big theoretical question still unresolved is that of the NS equation of state (EoS). As the interior of a NS is not reproducible in a laboratory, constraints to discriminate between multiple models are difficult to obtain. One way to do so if by finding very massive NSs, pushing the maximum mass to eliminate certain theories. Figure 1.12 shows a selection of EoSs traces in the radius-mass parameter space, and the mass of the current heaviest NS known, that effectively rules out some of these models. Very recently, some RB systems have been suspected to harbour unusually massive pulsars, which could help constrain the EoS. At the time of writing, this is a very hot topic, energetically discussed in the community but with little publications out yet.

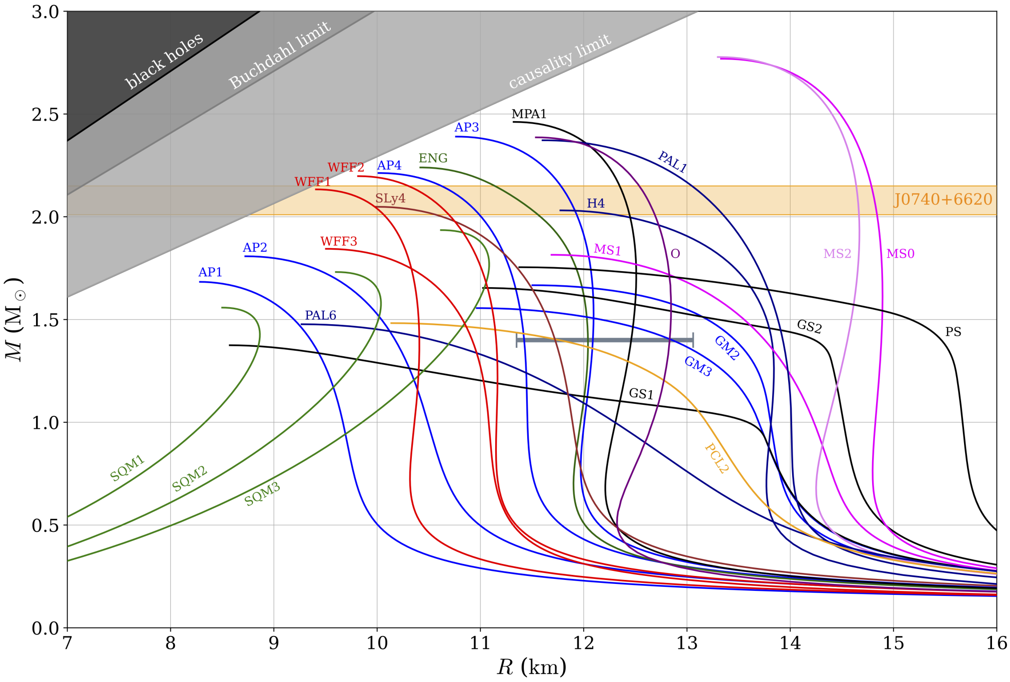

Figure 1.12: Figure from P. Freire's website[9]: a selection of EoS models are plotted in the radius-mass parameter space. The yellow band shows the mass of the heaviest known NS (Fonseca et al., 2021), that effectively rules out some of these models.

1.5 Thesis outline

In this introduction I reviewed the general properties of pulsars, and described their population. After introducing millisecond pulsars, I presented the sub-class of pulsars that this thesis is about, the spider systems. My work focused on 19 spiders, 18 black widows and one redback, all dwelling in the Galactic field.

As my work was entirely based on radio astronomy, I present in Chapter 2 some fundamental concepts in pulsar radio astronomy, specifically the effect of pulsar emission crossing the interstellar medium before being captured by the telescope, the *dispersion measure, rotation measure* and *scattering*. Then I present how to observe pulsars in the radio domain, the basis of the functioning of a radio telescope, the managing of radio emission coming from human activities. Finally I review the technique of pulsar *timing*, the concept and generation of the pulses *times of arrival*, the models used for binary pulsars and the software used to do the timing.

In Chapter 3 I present my data set, which is exclusively composed of observations conducted by the Nançay Radio Telescope (NRT). The data was taken as part of a 20-year long monitoring of several tens of pulsars by the NRT. I review the methods used for data preparation, before giving an overview of the properties of the 19 NRT galactic spiders, and a individual presentation for each system, providing a review of the phenomena observed as exhaustive as possible.

[9]https://www3.mpifr-bonn.mpg.de/staff/pfreire/NS_masses.html

In Chapter 4 I present the analysis of the eclipsing behaviour of the spider sample. Eclipsing systems are usually studied individually and often at lower frequencies. Taking advantage of the very long, dense and homogeneous dataset of the NRT archives, this analysis constitutes the first effort to systematically analyse the L-band data, providing an opportunity to look into their group properties. The morphological analysis of the eclipses and the relation between multiple relevant parameters allowed us to confront our sample of pulsars to existing theories about eclipses.

In Chapter 5 I present the search for planets around pulsar binaries, conducted on three systems: PSRs J1745+1017 and J2115+5448, two spider systems presented in Chapter 3, and PSR B1620−26, an MSP in a wide binary with a WD. Two methods have been tried for this project, the first was based on a theoretical computation of the orbital parameters which did not yield satisfactory results, and the second was direct pulsar timing, which gave slightly better results.

In Chapter 6 I summarise the main results presented and offer suggestions for future work.

Chapter 2

Pulsar astronomy

¿' Des parcoureurs, qui veulent tout voir, tout connaître, tout comprendre ! Des avaleurs d'espace, sans carte, qui azimutent au quadravent et aux étoiles, parce qu'ils naviguent aussi de nuit, à la fraîche !

Abstract

To study pulsars the first step is to observe them. On the path from the raw emission to being usable data on our computers, the pulsar signal undergoes many natural and computational processes. After their emission, the radio waves propagate through the interstellar medium (ISM), the cold plasma filling space inside the galaxy. This cold plasma has three main effects on an electromagnetic wave: the dispersion, the Faraday rotation and the scattering. These effects depend on the frequency of the wave, and as the radio emission naturally covers a large band of radio frequencies, the ISM effects show in the data as relative delays between different frequencies. Once the signal reaches the observatory, it is recorded by the telescope, cleaned from the unwanted non-pulsar signal, corrected from the dispersion cause by the ISM and ready to be transformed into the quantum of data used for the *pulsar timing* technique, the *time of arrival* (ToA). Pulsars are very stable rotators, and can therefore be compared to reference clocks to monitor any changes in their pulses ToAs. If a pulsar is correctly modelled, the *residuals*, the differences between the modelled and the measured ToAs, should be as small as possible. The ToAs are extracted from *folded* data, data that are integrated at the rate of the pulsar rotation, to enhance the available signal. To extract a ToA, a folded observation is matched to a reference profile, a stable "fingerprint" of the pulsar. The ToAs are then compared in a timing software to a timing model, composed of all parameters that would influence the pulsar observed cadence: the astrometric, spin, and when applicable, orbital parameters. In the case of spiders, some models are preferred, which can manage orbits with small eccentricities and large variations. Pulsar timing is a very fruitful technique, not only to study pulsars, but to use pulsars as tools to study other phenomena, such as nano-Hertz gravitational waves, extrasolar planets, galactic mapping or gravitation in the strong field regime.

2.1 Effects of the ISM

2.1.1 Dispersion

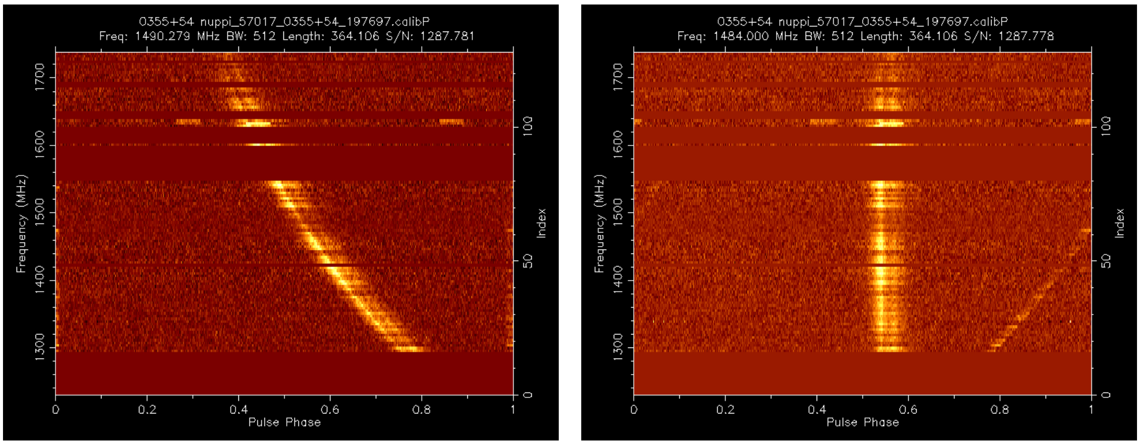

Figure 2.1: Example of the effect of dispersion on pulsar signal. When the observation is wrapped at the rotation period of the pulsar, the delay between higher and lower frequencies clearly shows (left panel). If the signal is de-dispersed the pulses are aligned (right panel).

Before reaching Earth, the pulsar emission has to go through the interstellar medium (ISM). It is a cold and ionised plasma, therefore the refraction index depends on the frequency. For a homogeneous plasma with no magnetic field, the refraction index is:

$$\mu = \sqrt{1 - \left(\frac{f_p}{f}\right)^2} \tag{2.1}$$

where f is the wave frequency and $f_p = \sqrt{e^2 n_e / \pi m_e}$ the plasma frequency. e is the electron charge, m_e the electron mass and n_e the electron number density, which depends on the location. We note from this equation that a wave will not propagate if $f < f_p$, and for the ISM $f_p \simeq 1.5$ kHz.

Since $\mu < 1$, the group velocity of the propagating wave is smaller than the speed of light c. The propagation of a signal will be delayed with respect to a signal of infinite frequency. For a path of length d, this delay is:

$$t = \left(\int_0^d \frac{\mathrm{d}l}{c\mu}\right) - \frac{d}{c} \tag{2.2}$$

In the (common) case where $f_p \ll f$, μ can be approximated by its Taylor expansion $\mu \sim 1 + (f_p/f)^2/2$, therefore:

$$t = \frac{1}{c}\int_0^d \left(1 + \frac{f_p^2}{2f^2}\right)\mathrm{d}l - \frac{d}{c} = \frac{e^2}{2\pi m_e c}\frac{\int_0^d n_e \mathrm{d}l}{f^2} = \frac{e^2}{2\pi m_e c}\frac{\mathrm{DM}}{f^2} \tag{2.3}$$

where the *dispersion measure*

$$\mathrm{DM} = \int_0^d n_e \mathrm{d}l \tag{2.4}$$

is usually expressed in $\mathrm{cm}^{-3}\mathrm{pc}$.

It comes that the delay between two waves of frequencies f_1 and f_2 is:

$$\Delta t = t_2 - t_1 = \frac{e^2}{2\pi m_e c}(f_1^{-2} - f_2^{-2}) \times \mathrm{DM} \tag{2.5}$$

A measurement of a delay between two known frequencies gives a value of DM *along the line of sight*. To counter this effect, observations have to be *de-dispersed*, based on a the measured value of DM.

In theory this effect would affect any astronomical signal, however most astronomical sources produce continuous emission, and the de-dispersion is therefore only relevant in time-domain astronomy, such as pulsar observations. This DM can then be used to derive a distance to the pulsar, assuming a model for the electron density. Corollarily, electron distribution models can be improved by using independent measurements of pulsar distances to calibrate the model. The most recent model, the YMW16 model from Yao, Manchester, and Wang, 2017 uses 189 pulsars and observations of more than 1800 HII regions. An accurate electron density model is crucial to correctly estimate pulsar distances, which for most pulsars we have no access to other than the DM measurement.

2.1.2 Faraday rotation

Dispersion appears in the case of a cold, homogeneous and non magnetised plasma. For a cold and magnetised plasma:

$$\mu = \sqrt{1 - \frac{f_p^2}{f^2} \pm \frac{f_p^2 f_B}{f^3}} \tag{2.6}$$

where f_B is the cyclotron frequency associated with the galactic magnetic field (along the line of sight) $B_{||}$:

$$f_B = \frac{eB_{||}}{2\pi m_e c} \tag{2.7}$$

for the Milky Way $B_{||} \simeq 1\ \mu$G, hence $f_B \simeq 3$ Hz. The two signs in eq.(2.6) reflect the different propagation speed of right ('+' sign) and left-hand ('−' sign) circularly polarised waves propagating through a magnetised medium. This effect is called Faraday rotation. The resulting phase shift between the two is:

$$\Delta\phi = \lambda^2 \times \mathrm{RM} \tag{2.8}$$

where λ is the wavelength and RM the rotation measure, defined as:

$$\mathrm{RM} = \frac{e^3}{2\pi m_e c^4} \int_0^d n_e B_{||} \mathrm{d}l \tag{2.9}$$

Combining the DM and RM gives the average magnetic field along the line of sight:

$$\langle B_{||} \rangle = \frac{\int_0^d n_e B_{||} \mathrm{d}l}{\int_0^d n_e \mathrm{d}l} = 1.23\mu\mathrm{G} \left(\frac{\mathrm{RM}}{\mathrm{rad\ m^{-2}}}\right) \left(\frac{\mathrm{DM}}{\mathrm{cm^{-3}\ pc}}\right)^{-1} \tag{2.10}$$

This average is weighted by the electron density, therefore regions of higher electron density along the line of sight contribute significantly more than regions of lower density. Moreover, $\langle B_{||} \rangle$ being an average, it is poorly representative of the variated media along the line of sight, and any change of sign in the magnetic field direction would lower the total magnetic field crossed during propagation.

2.1.3 Scattering

The actual ISM is not a homogeneous medium, but a turbulent and inhomogeneous one. This causes multipath propagation of the pulsar signal, and results in multiple delayed detection of the same pulse. Scattering typically shows as a convolution of the actual pulsar profile and an exponential 'tail', with a time constant called the *scattering timescale* τ_s. Figure 2.2 shows an example of such an exponential tail. This scattering timescale depends on the frequency, the broadening of the pulses being more pronounced at lower frequencies. Different models predict power-law dependency $\tau_s \propto f^{-\alpha}$, with $\alpha \sim 4$ in most cases (see e.g. Lee and Jokipii, 1976; Rickett, 1977, for theoretical works or Bhat et al., 2004 for observations review) .

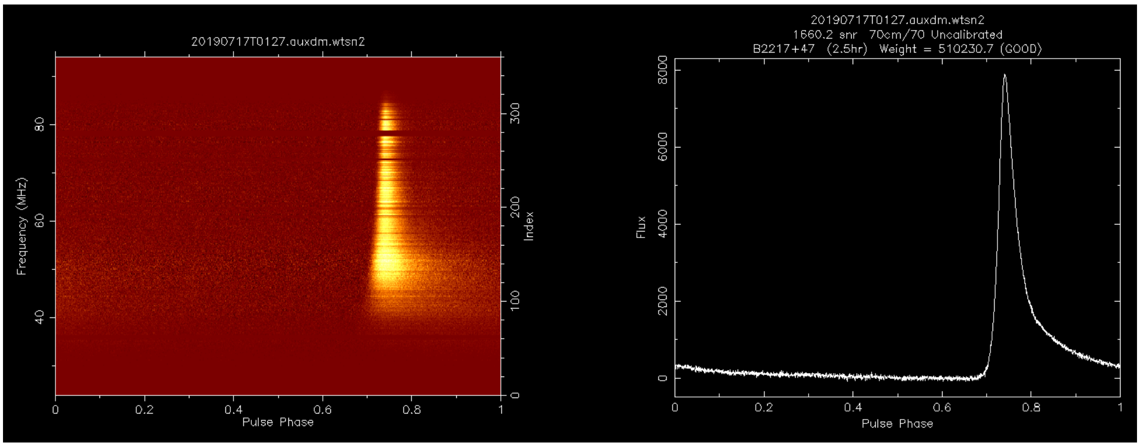

Figure 2.2: Example of the effect of scattering on signal from pulsar J2219+4754, observed below 100 MHz with the NenuFAR telescope. On the left the pulse is showing more pronounced broadening at lower frequencies, with the scattering delay broadening the profile asymmetrically, the tail being clearly visible at the right (i.e. after) the pulse. On the right is the resulting profile when integrated. The scattering tail is also clearly visible, skewing the profile to the right. Plot by courtesy of Pauline Noé.

Contrarily to dispersion and Faraday rotation, scattering cannot easily be corrected for, because of its random nature. Using a numerical deconvolution technique, Bhat et al., 2004 showed that the scattering timescale is strongly correlated with the DM.

2.2 Observing pulsars

2.2.1 Data acquisition

Pulsar observations are very demanding for data acquisition systems, as they require high time resolution, to obtain high-precision arrival times (see Section 2.3) or to resolve sub-millisecond structure in pulses, high frequency resolution, to correct for the effects of dispersion discussed in the previous section, and high sensitivity, as pulsars are generally weak sources. The main reference for this section is Section 5.1 of Lorimer and Kramer, 2004.

A telescope is generally composed of multiple reflectors concentrating radio waves in a horn, which resonate when coupling with the incident radio wave. At the bottom on the horn two receptors sample orthogonal senses of polarisation, usually called polarisation channels. The induced electric currents (or their corresponding voltages) are amplified and filtered of the unwanted signals like radio frequency interferences (RFI, see Sect. 2.2.2)

To correct for dispersion, two ways exist: the *coherent* and the *incoherent dedispersion*. The simplest way is the incoherent dedispersion, in which the frequency band is split into a number of channels on which are applied different time delays relative to a reference frequency, either the middle of the band or an infinite frequency, calculated by equation (2.5). The incoherent dedispersion process does not correct for the dispersion occurring inside the individual frequency channels. From equation (2.5) one can find the dispersive delay across a channel of width Δf centred around frequency f (when $f \gg \Delta f$)

$$t_{DM} \simeq 8.3 \times 10^6 \text{ ms} \times \text{DM} \times \Delta f \times f^{-3} \tag{2.11}$$

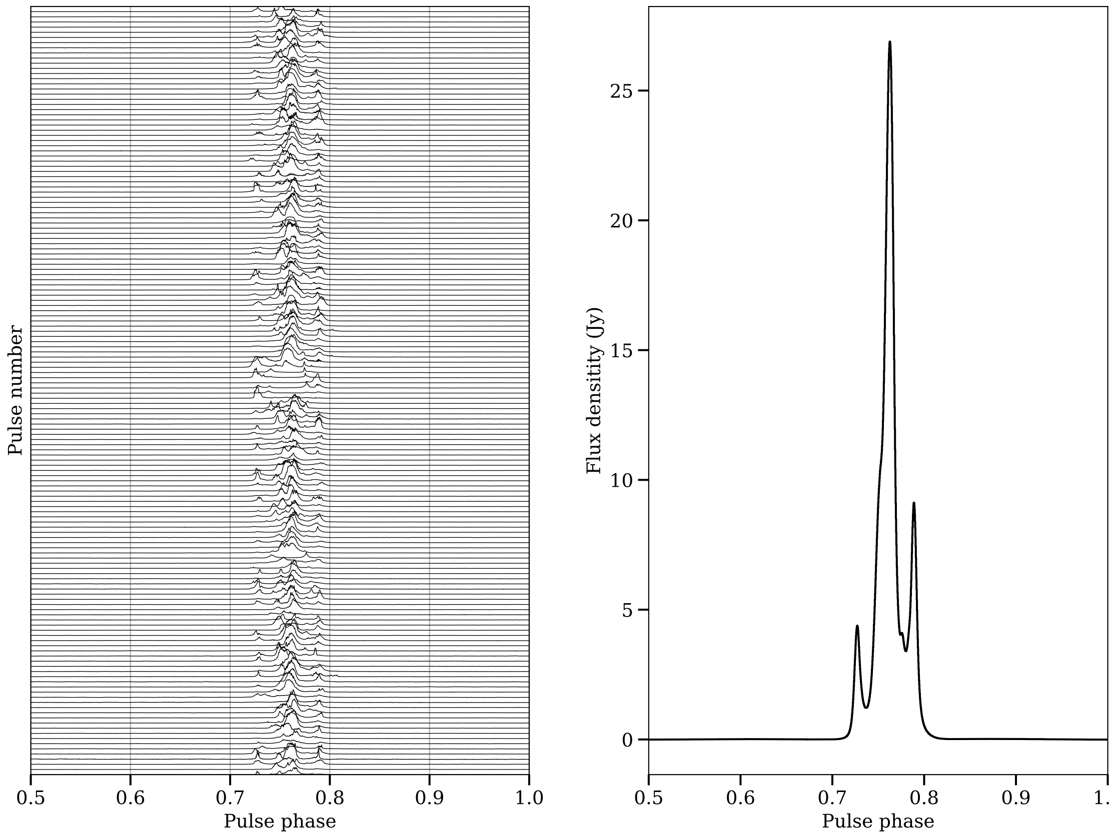

Figure 2.3: Example of an integrated pulse profile of PSR B0329+54, observed around 650 MHz with the uGMRT telescope (India). The left panel shows 150 individual pulses, which corresponds to 107.25 seconds over the whole observation. The right panel is the integrated profile of the whole observation. Every single pulse is different, in some rotations we see only one or two peaks, yet the integrated profile is very stable over many observations, and can be used as a "fingerprint" of the pulsar. Plot by courtesy of Fabian Jankowski.

with DM in cm^{-3} pc and f and Δf in MHz. t_{DM} should not be a significant fraction of the pulse period.

The coherent dedispersion makes use of the phases of the raw voltages. The modification of the signal by the ISM can be described as a "phase-only" filter. In the frequency domain, the Fourier transforms of the raw voltages of the received signal $V(f)$ and that of the pulsar original emission $V_{int}(f)$ are linked as such:

$$V(f_0 + f) = V_{ini}(f_0 + f)H(f_0 + f) \tag{2.12}$$

where H is the transfer function of the ISM "filter". As the delay can be represented as phase rotations $\Delta\Phi = -k(f_0 + f) \times d$ where $k(f)$ is the wavenumber and d is the distance to the pulsar. Therefore, the transfer function is:

$$H(f) = \exp(-ik(f)d) = \exp\left(+i\frac{2\pi\mathcal{D}f^2\mathrm{DM}}{(f_0 + f)f_0^2}\right) \tag{2.13}$$

when taking only the f-quadratic term into account. In this expression $\mathcal{D} = f_p^2/2cn_e$ is the dispersion constant. Applying the inverse function $H^{-1}(f)$ to the received voltage recovers the original signal. Moreover, some coherent dedispersion techniques allow all four Stokes parameters (see Section 2.2.3) to be readily accessible.

Pulsars generally being weak sources, the dedispersed data can now be *folded*[1]. Taking advantage of the fact that pulsars are stable rotators, one can create an array of n_{bins} elements equally spaced across the pulse period. The data is then split into chunks of the duration of the pulse period, and the chunks are stacked on the *phase bins* over a certain period of time, usually a few minutes (a 5-minute sub-integration of a pulsar with a period of 3 ms contains 100,000 individual pulses). This results in a bright and well-defined *time-integrated pulse profile*. Interestingly, despite the stochastic nature of the single pulses, the average profile virtually never changes. This results in a 4-dimensional profile, with spin phase, observation time, frequency and polarisation axis.

2.2.2 Radio frequency interferences management

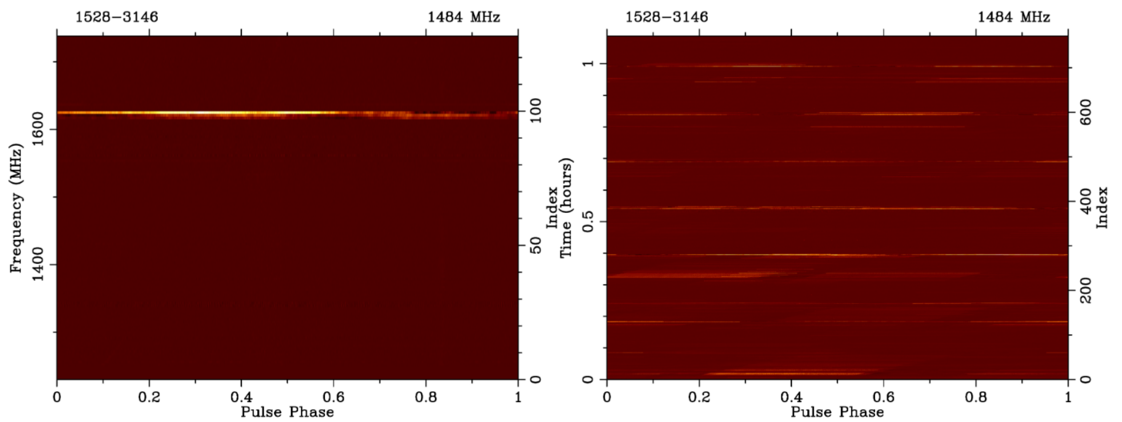

Figure 2.4: Figure 6.3 of Berthereau, 2023: pre-cleaning observation of PSR J1528−3146. In both frequency-phase (left) and time-phase (right) plots, the pulsar should appear as a straight vertical line. All horizontal signals are RFI.

Stargazing is becoming a luxury at every frequency. Radio frequency interferences (RFI), like visible light pollutions, are a growing concern for astronomy, among other things. The dramatic increase in the use of technologies such as TV, satellites, GPS, smartphones, wireless gadgets, etc.,

[1]Some high time resolution studies use individual pulses records, a method called *single-pulse observations*, but it is not the case for the works described in this thesis.

resulting in an extremely bright radio sky. Bands of a few mega Hertz are protected from non-scientific use[2], such as the 21 cm line of hydrogen, protected from 1400 to 1427 MHz. Fleeing the pollution, observatories are usually located in remote and/or protected areas. But finding quiet places is becoming impossible with more and more RFIs coming from space, and observatories that are already built are becoming obsolete due to the increase of RFIs in their environment, even while having a state-of-the-art maintenance. It is therefore of utmost importance to find efficient ways to manage the RFI present in every observations.

Figure 2.4 shows examples of RFI (horizontal lines) on a raw observation: the pulsar should appear as a straight vertical line (similar to the right panel of figure 2.1). Pulsars observed from Earth seem like pulsating sources and their pulsations can sometimes be similar to that of human technologies, such as radars. However, RFI from human origin are not dispersed by the ISM, which can be a way to discriminate between them. A first cleaning can be done by removing impulses that are too short and too bright, but that leaves quite a lot of unwanted signal.

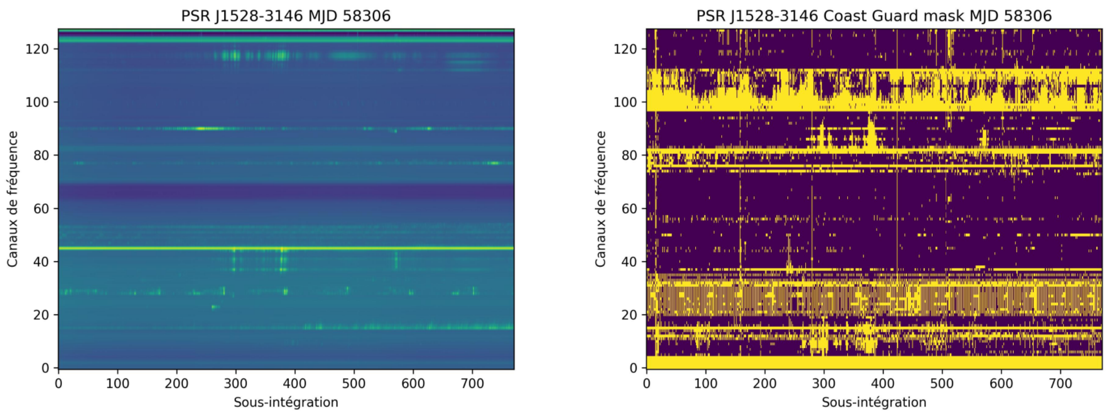

Figure 2.5: Figure 6.6 of Berthereau, 2023: the dynamic spectrum of an observation for an off pulse phase bin (left) and the corresponding COAST GUARD generated mask where signal pixels appear in purple and RFI pixels in yellow.

Multiple methods exist and are used by radioastronomers. Because this thesis focuses on data acquired with the Nançay Radio Telescope (see Section 3.1) I will only review the example of RFI management for this facility. At the NRT, the cleaning is done "offline", *i.e.* after the acquisition and part of the processing, and not "online", which would be nearly in real-time. The software used is COAST GUARD (Lazarus et al., 2016), which automatically analyses the dynamic spectrum of the observation to create a frequency-phase *mask* (see Figure 2.5 for an example) of pixels to remove or to which apply null weights in the subsequent analyses. In some cases where the cleaning needs to be more precise, the cleaning can be done manually in order to keep as much signal as possible or to excise RFI not cleaned by the automatic process.

2.3 Pulsar timing

Pulsars are very stable rotators, and therefore can be considered as natural clocks. By comparing these celestial clocks to reference terrestrial clocks, one can measure any deviation from the expected spin frequency and attempt to model it to uncover the physical phenomenon producing the deviation. This is the principle of *pulsar timing*.

[2]See for example page 2 of https://www.anfr.fr/fileadmin/medias/institutionnel/ANFR-spectre-frequences-juin-2020.pdf for the frequency distribution in France.

2.3.1 From topocentric to barycentric times of arrival

The "ticks" of the pulsar clock are recorded to extract the fundamental data of pulsar timing, the *times of arrival* (ToAs) of the pulses. Times are recorded on Earth, but extracted ToAs are converted to the Solar System barycentre (SSB), which is a good inertial reference frame (and a useful common frame for multiple telescope analyses). The transformation of a "topocentric" ToA t_{topo} measured with an observatory clock to a "barycentric" ToA t_{SSB} is as follows:

$$t_{SSB} = t_{topo} + t_{corr} - \Delta D/f^2 + \Delta_R + \Delta_S + \Delta_E \quad (2.14)$$

where:

- t_{corr} is the clock correction. The time stamp collected for a ToA in an observatory is first compared to the coordinated universal time (UTC) using GPS. UTC is defined on the international atomic time (TAI) and is never more than 0.9 seconds away from UT1, a time measure based on Earth rotation. Since this rotation is not uniform, the International Earth Rotation Service (IERS)[3] can decide to add or subtract a *leap second*, so that TAI = UTC + ΔT, where ΔT is the sum of leap seconds. Leap seconds need to be removed from the UTC time to obtain a ToA measured in the TAI timescale. The TAI is maintained by the Bureau International des Poids et Mesures (BIPM) by monitoring atomic clocks around the world. The BIPM also issues the Terrestrial Time (TT), defined as TT = TAI + 32.184 seconds, for historic reasons. The TT is intended as the idealised geocentric time and is the timescale t_{corr} is correcting for.
- $\Delta D/f^2$ is the frequency correction due to the dispersion. $\Delta D = \mathcal{D}/DM$ (see equation 2.13) has to be accounted for to take the ToA at an infinitely high frequency, thus removing the effects of the Solar System interplanetary medium and that of the ISM crossed before reaching the Solar System. It can vary with time, in which case one has to include the derivative terms $\dot{DM}$, $\ddot{DM}$ etc.
- Δ_R is the *Rømer delay*, the light travel time between the observatory and the barycentre of the Solar System. This delay obviously depends on the time of observation, computing this thus requires accurate knowledge of the locations of all major bodies in the Solar System. The ephemeris generally used is "DE440" (Park et al., 2021). To compute the precise location of the observatory, the non-uniformity of Earth's rotation needs to be taken into account, and is achieved using the UT1 corrections published by the IERS.
- Δ_S is the *Shapiro delay*, the relativistic delay due to the curvature of space-time caused by the presence of masses in the Solar System (Shapiro, 1964). The delays are largest for a signal passing the limb of the Sun (~ 120μs) while Jupiter can contribute as much as 200 ns.
- Δ_E is the *Einstein delay*, and combines two effects: the time dilation due to the motion of the Earth and the gravitational redshift caused by the other bodies in the Solar System.

2.3.2 Extraction of times of arrival

As stated previously, pulsars are weak sources, and ToAs have to be extracted from folded data. As shown in Figure 2.3, the way to elevate the significance of the signal is to fold, or integrate, or *scrunch* the observation along the time and/or frequency, to produce a phase profile. Profiles are quite stable from observation to observation, and usually over many years. One can therefore construct a profile with very high signal-to-noise ratio (SNR) as *template profile*, to compare individual folded profiles to. Assuming that the folded profile $P(t)$ is a rescaled and shifted version of the template $T(t)$ with added noise $N(t)$, one can write (Lorimer and Kramer, 2004):

$$P(t) = a + bT(t - \tau) + N(t) \quad (2.15)$$

[3] http://hpiers.obspm.fr

where a is the offset and b the scaling factor. The time shift τ is the phase offset between the template and the profile, and encodes the ToA relative to an arbitrary reference point of the template and the beginning of the observation. This cross-correlation can be done in the time domain, but preferably in the Fourier domain, in which case the precision is only limited by the profile SNR. The ToA uncertainty can be expressed as the ratio of the pulse width W to the profile SNR (Lorimer and Kramer, 2004):

$$\sigma_{ToA} \simeq \frac{W}{SNR} \sim \frac{S_{sys} W^{3/2}}{S_{mean}\sqrt{t_{obs} P \Delta f}} \tag{2.16}$$

where S_{sys} is the system equivalent flux density, Δf is the observing bandwidth, t_{obs} is the integration time, P is the pulse period and S_{mean} is the mean flux density of the pulsar. Optimal results are therefore obtained with sensitive wide-band systems (low S_{sys} and large Δf) for bright (high S_{mean}) pulsars with narrow pulses (*i.e.* low W).

In the projects presented in this thesis, two different template matching tools were used.

PSRCHIVE

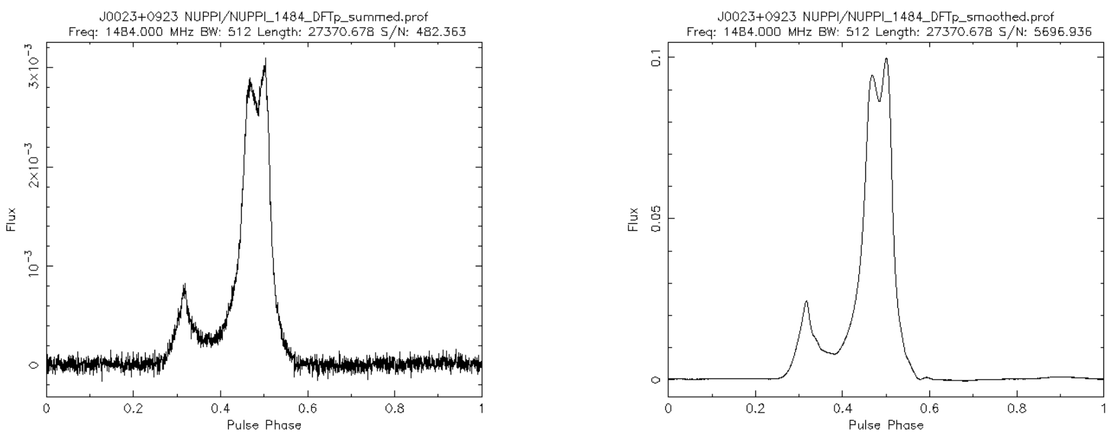

Figure 2.6: Summed (left) and smoothed (right) profiles of PSR J0023+0923 generated using PSRCHIVE on fully time and frequency integrated profiles.

The PSRCHIVE software library (Hotan, van Straten, and Manchester, 2004) is the most common pulsar toolbox. It includes routines for data preparation for timing, polarimetry studies, RFI mitigation, and pulse variability studies. To extract ToAs from a set of dedispersed and RFI-cleaned observation, our main steps and the routines used are:

1. Integrating in time and frequency to the required resolution with `pam`. The typical values we use are sub-bands of 64 MHz and sub-integrations of 5 minutes. This choice sets the number of ToAs we obtain, as we obtain a ToA per sub-band and per sub-integration. The longer the sub-integration or the wider the sub-band, the brighter the pulse profile, but at the expense of more limited resolution. In our case, spiders having very short orbital periods of a few hours, it is not relevant to make ToAs scrunched over a significative fraction of the orbit.

2. Constructing a reference profile by summing a certain number (typically eight)of high SNR observations using `psradd`.

3. Smoothing the reference profile into a noise-free profile with `psrsmooth`.

4. Estimating the ToAs using `pat`. The cross-correlation of the individual profiles and the smoothed reference is done in the Fourier domain.

This method is one we call 1-dimensional, as the profiles used are "only" functions of frequency versus pulse phase, as shown in Figure 2.6. Even in the case of profiles that are not fully scrunched in frequency, the template consists in multiple 1D profiles, one for each sub-band, generated independently.

This method is very widely used in the pulsar community, however NUPPI has a large bandwidth of 512 MHz (see section 3.1.3), and if the profiles of pulsars do not usually change over time, they do change with frequency.

PulsePortraiture

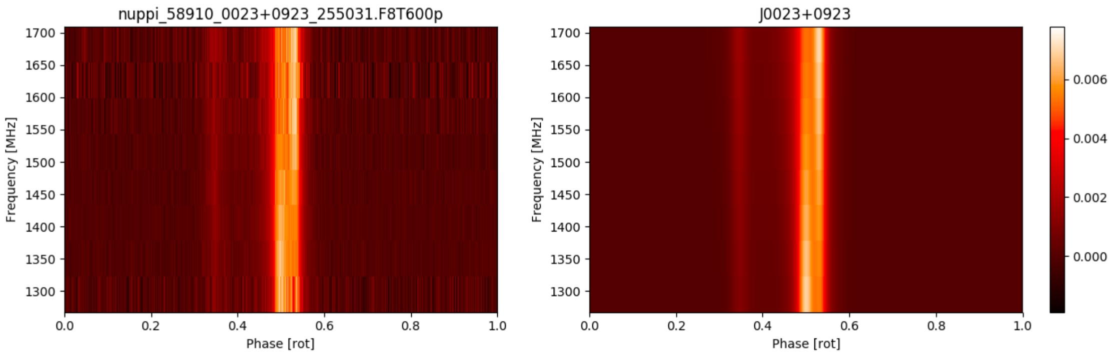

Figure 2.7: Summed (left) and smoothed (right) profiles of PSR J0023+0923 generated using `PulsePortraiture` as observed with NUPPUI on 64 MHz frequency integrated and fully time integrated profiles.

`PulsePortraiture` (Pennucci, Demorest, and Ransom, 2014) is a 2D template matching method as it keeps some frequency resolution. The method is quite similar to the PSRCHIVE method:

1. Integrating in time and frequency to the required resolution with `pam`.
2. Constructing a 2D (frequency and phase) reference profile using `psradd`.
3. Smoothing the reference profile into a Gaussian model of the profile with `PPgauss`.
4. Estimating the ToAs using `PPtoas`. The cross-correlation is also done in the Fourier domain.

One striking example of profile variation over the frequency bandwidth recorded by NUPPI (from 1.2 to 1.7 GHz) is PSR J0023+0923, the same pulsar shown in Figure 2.6. In this figure, we saw that the main pulse is composed of two peaks, however if we split the NUPPI into 8 sub-bands of 64 MHz, we can notice that the profile in the highest frequency sub-band and that in the lowest frequency sub-band are quite different: around 1300 MHz the first peak is quite higher than the second, around 1700 it is the contrary. Using PulsePortraiture allows for a reference template to have the same characteristic, limiting the bias during ToAs extraction originating from the differences between templates and profiles. Both the reference profile and the analytical model are shown in Figure 2.7.

Using `PulsePortraiture` reduces the number of extracted ToAs, as the full band is always used to produce only one single ToA per sub-integration, contrarily to the `pat` method, which extracts one ToA per sub-band (i.e. 8 ToAs per sub-integration in the case of a profile integrated over 8 sub-bands of 64 MHz). However, refining the profile templates also improves the quality of the ToAs, which is particularly interesting in the case of low SNR pulsars such as the NRT spiders (see Table 3.1). For observations near the detection limit, using the usual `pat` routine to determine one ToA per frequency-band of 64 MHz can result in a large number of outlier ToAs. In Table 2.1 we list the fraction of TOA outliers as obtained with the 1D and 2D TOA extraction methods. Extracting TOAs with the wideband-matching technique results in lower outlier rates in all cases.

Table 2.1: Fraction of outliers in the TOA datasets. For each pulsar we compared ToAs extracted from 8 frequency sub-bands of 64 MHz each using the standard `pat` method ("1D F8"), and ToAs extracted using the entire available bandwidth, with the wideband template-matching technique as implemented in the `PulsePortraiture` library ("2D"). For reference we also list the outlier rates as obtained when extracting TOAs from fully frequency-scrunched observations ("1D fscrunch"). Outliers are defined here are those with residuals (see Section 2.3.3) larger than 1% of P_{spin} considering the uncertainty.

Pulsar	1D F8	2D	1D fscrunch
J0023+0923	53.8%	5.3%	3.8%
J0610−2100	9.1%	2.1%	1.1%
J0636+5128	12.2%	3.4%	1.5%
J1124−3653	82.1%	60.3%	56.3%
J1513−2550	18.8%	5.4%	6.8%
J1544+4937	34.8%	2.9%	2.6%
J1555−2908	13.9%	6.4%	6.4%
J1705−1903	0.6%	0.0%	0.0%
J1719−1438	68.8%	2.0%	1.0%
J1731−1847	41.4%	28.1%	77.4%
J1745+1017	16.4%	1.2%	2.4%
J1959+2048	43.4%	6.6%	8.9%
J2051−0827	9.0%	3.1%	3.4%
J2055+3829	17.4%	11.5%	11.7%
J2115+5448	36.2%	23.5%	40.4%
J2214+3000	90.2%	5.3%	4.0%
J2234+0944	14.4%	6.5%	6.4%
J2256−1024	48.2%	5.4%	5.1%

2.3.3 Timing software

The proper *timing* of pulsars starts once the ToA extraction procedure is done. The principle of timing is to compute the difference between the modelled ToA and the measured ToA, difference being called a *residual*. The timing procedure generally consists in a least squares fit analysis of the ToAs, and can be done with the Tempo2 software (Hobbs, Edwards, and Manchester, 2006). This software takes as inputs a "parfile" that contains the model parameters, and a "timfile", that contains the ToAs. The fitting of the parameters is done once the data is loaded in the software, and can be done parameter by parameter. The residuals of a correctly modelled pulsar should have a Gaussian distribution centred around zero with a root mean square (RMS) comparable to the ToAs uncertainties. A misestimation of different parameters leads to different signatures in the residuals, as shown in Figure 2.8.

Tempo2

Tempo2 uses a linear fitting weighted least-squares algorithm, minimizing the expression:

$$\chi^2 = \sum_i \left(\frac{N(t_i) - n_i}{\sigma_i} \right)^2 \tag{2.17}$$

where $N(t_i)$ is the number of the pulse arriving at t_i, n_i is the nearest integer to $N(t_i)$ and σ_i the uncertainty of the ToA. The χ^2 is often used as an indicator of the goodness-of-fit. Tempo2 has a graphical interface that allows for a quick and easy handling, and is sufficient for most of the timing procedures needed. It shows in real time the pre-fit and post-fit residuals, and is made to allow iterated fitting, as the convergence is rarely obtained after only one fit. Tempo2 is the only timing software used for the analyses presented in Chapter 4.

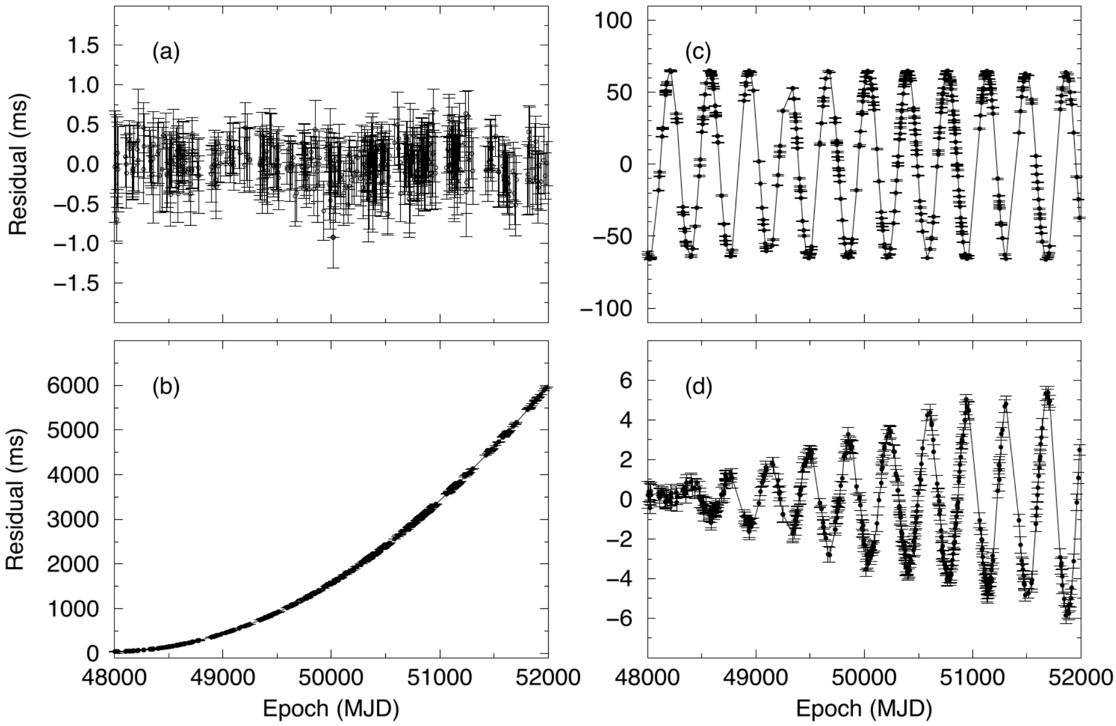

Figure 2.8: Figure 8.2 from Lorimer and Kramer, 2004: various effects of misestimated parameters. (a) Timing residuals for PSR B1133+16. A fit of a perfect timing model should result in normally distributed residuals. (b) an underestimation of $\dot{P}$ leads to a parabolic increase in the residuals. (c) An offset in position produces sinusoidal residuals with a period of 1 yr. (d) The effect of neglecting the pulsar's proper motion. In all plots the reference epochs is set at MJD 48000 to show the development of the amplitude of the various effects. Note the different scales on each of the vertical axes.

MCMC4T2

Tempo2 using a linear fitting algorithm, it can struggle to fit data for which the model parameters are too covariant, or when the effects of certain parameters are too faint. Voisin et al., 2020b presented an affine-invariant MCMC for Tempo2, called MCMC4T2[4]. This helps fitting for covariant parameters, but is more computationally expensive. MCMC4T2 is more robust and can more easily discard local minima than Tempo2, as the latter uses a local algorithm. Moreover, for error computing it has the benefits of an MCMC method: it samples the posterior distribution of the parameters, providing a confidence interval rather than a estimate based on an approximation of the χ^2. Nevertheless, Tempo2 works perfectly in most situations, and the computing time required to run MCMC4T2 confines it to be used in very specific cases, such as those discussed in Chapter 5.

2.3.4 Timing models used for spider systems

The model fitted to the data includes every parameter describing the observed spin frequency of a given pulsar over time. This model includes barycentric corrections described in Section 2.3.1, the proper motion of the pulsar relative to the SSB, the plasma effects from the ISM, and when applicable, the parallax (for nearby pulsars) and the orbital parameters (for pulsars in multiple systems). To construct a timing model of a newly observed pulsar, one starts with a limited set of observations covering hours or days and fits for the first typically available parameters: the pulsar position, usually expressed in right ascension (RA) and declination (DEC), the spin period,

[4] https://bitbucket.org/astro_guillaume_voisin/mcmc4tempo2/

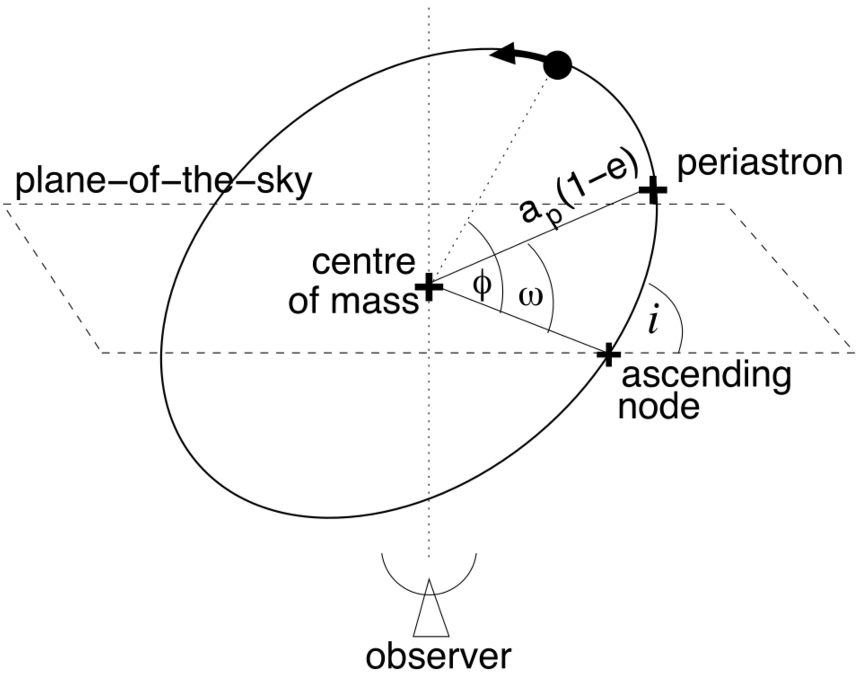

Figure 2.9: Figure 8.3 from Lorimer and Kramer, 2004: definition of orbital elements. ϕ is the phase measured from the ascending node, which is the crossing point between the orbit and the plane of the sky that the pulsar passes going away from the observer. Other parameters shown in this sketch are: the semi-major axis a_p, the eccentricity e, the orbital inclination i and the longitude of periastron ω.

possibly its first derivative and the DM (see Section 2.1.1). Longer time spans gradually require more and more parameters: the proper motion of the pulsar and its parallax, the time derivative(s) of the DM, and possibly multiple derivatives of the spin frequency. However, apart from very young pulsars, the intrinsic second spin frequency derivative is usually too small to be measured, thus the observed second (and subsequent) derivative(s) comes from timing noise mimicking such variation. Such noise can be produced by things such as: changes in the pulsar internal structure, changes in the radiation rate or the presence of one or several bodies orbiting the pulsar. As seen in Section 1.3.3, the presence of a stellar companion is seen around most MSPs, and it is the case of the spider systems that are the main topic of the following chapters.

For a pulsar in a binary, eq. (2.14) is extended by adding four additional parameters:

$$\begin{aligned} t_{SSB} = t_{topo} + t_{corr} - \Delta D/f^2 + \Delta_R + \Delta_S + \Delta_E \\ +\Delta_{RB} + \Delta_{SB} + \Delta_{EB} + \Delta_{AB} \end{aligned} \tag{2.18}$$

These new terms describe an additional Rømer delay due to the orbit, Shapiro and Einstein delays due to the companion mass, and an *aberration delay* Δ_{AB} caused by the beam rotation. With spider systems, the relativistic Shapiro and Einstein delays are not measurable (which is not the case of other binaries), and the pulsar orbit can be described using *Keplerian parameters*. These parameters, for the pulsar orbit, are:

- the *orbital period* P_b. To this can be added the post-keplerian parameters $\dot{P}_b$ and $\ddot{P}_b$, the time derivatives of the orbital period.
- the *projected semi-major axis* $x = a_p \sin i$, where a_p is the semi-major axis of the pulsar orbit and i the inclination of the orbit, *i.e.* the angle between the orbital plane and the plane of the sky. $i = 0°$ means that the orbit is seen completely face-on, and $i = 90°$ means that the orbit is seen completely edge-on.

- the orbital *eccentricity* e.
- the *longitude of periastron* ω, distant from the centre of mass by $a_p(1-e)$. The time derivative of this position $\dot{\omega}$ is a post-keplerian parameter that is sometimes measurable (see Section 1.4.2).
- the *epoch of periastron passage* T_0. This is a reference epoch, taken at an arbitrary orbit.

Using these five parameters one can write the Rømer delay (Blandford and Teukolsky, 1976):

$$\Delta_{RB} = x(\cos E - e)\sin\omega + x\sin E\sqrt{1-e^2}\cos\omega \tag{2.19}$$

where E is the *eccentric anomaly*, related to the five keplerian parameters at any given time t as:

$$E - e\sin E = \frac{2\pi}{P_b}\left((t-T_0) - \frac{1}{2}\frac{\dot{P}_b}{P_b}(t-T_0)^2\right) \tag{2.20}$$

These parameters are used in Tempo2 **T2** model (Damour and Deruelle, 1986). This model also manages multiple systems, by computing the effect of multiple independent keplerian orbits. However sometimes the orbital frequency $F_b = 1/P_b$ is used instead, alongside with its time derivatives $F_b^{(n)}$, which are not limited to the second, as spiders can have dramatic variations in their orbital frequency. In this case the orbital frequency varies as a Taylor expansion around T_0. This parametrisation is used in the **BTX** model (Nice, D., unpublished). In the case of spiders, the orbital eccentricity is usually very small, of the order of magnitude of 10^{-5} or 10^{-6}, and in this case the location of the periastron is not well defined. An alternative description of the keplerian parameters are implemented in the **ELL1** model (Lange et al., 2001) in which the epoch of ascending node T_{asc} and the Laplace-Lagrange parameters ϵ_1 and ϵ_2 are used, defined as:

$$T_{asc} = T_0 - \omega\frac{P_b}{2\pi} \tag{2.21}$$

$$\epsilon_1 = e\sin\omega \tag{2.22}$$

$$\epsilon_2 = e\cos\omega \tag{2.23}$$

In this case the Rømer delay approximated to the first order of eccentricity is:

$$\Delta_{RB} = x\left(\sin\phi + \frac{\epsilon_2}{2}\sin 2\phi - \frac{\epsilon_2}{2}\cos 2\phi\right) \tag{2.24}$$

These three models are far from being the only ones used for pulsar timing, however they are the only one we used for the timing of the NRT spiders, to account for small eccentricities and/or multiple orbital frequency derivatives. Combining the advantages of the three models, Voisin, Breton, and Summers, 2020 crafted a new model called **ELL1-Spider**[5]. A summary of the parameters used in these models can be found in Table 2.2.

The mass function

The *mass function* can be obtained by combining the projected semi-major axis and the orbital period in Kepler's third law:

$$m_f = \frac{4\pi^2}{G}\frac{(a_p\sin i)^3}{P_b^2} = \frac{(m_c\sin i)^3}{(m_p+m_c)^2} \tag{2.25}$$

where G is the gravitational constant, m_p the pulsar mass and m_c the companion mass. Assuming a pulsar mass (usually $1.4M_\odot$ or 1.5 $M_\odot$, see Section 1.4), one can derive the companion mass. In

[5]The timing model implementation is available at https://bitbucket.org/astro_guillaume_voisin/spider_timing_model/

Table 2.2: Summary of the main parameters used in T2, BTX, ELL1 and ELL1S models, as well as their names in TEMPO2. First time derivatives of the parameters ($\dot{x}, \dot{\omega}$ etc.) are usually also implemented.

Parameter	TEMPO2	T2	BTX	ELL1	ELL1S
x	A1	⋆	⋆	⋆	⋆
P_b	PB	⋆		⋆	
$\dot{P}_b$	PBDOT	⋆		⋆	
T_0	T0	⋆	⋆		
ω	OM	⋆	⋆		
e	ECC	⋆	⋆		
T_{asc}	TASC			⋆	⋆
ϵ_1	EPS1			⋆	⋆
ϵ_2	EPS2			⋆	⋆
F_b	FB0		⋆		⋆
$F_b^{(n)}$	FBN		⋆		⋆
Multiple keplerian orbits		⋆			⋆

practice however, the inclination of the system is rarely known, thus the values derived are usually lower limits, computed for $i = 90°$, and the median value, computed for $i = 60°$ For an upper limit, knowing that the probability of observing a binary system at an angle less than some value i_0 is $p(< i_0) = 1 - \cos(i_0)$, computing the companion mass for $i = 26°$ gives a constraint at the 90% confidence level.

With an estimation of the companion mass, and assuming a pulsar mass, once can derive the semi-major axis of the relative orbit or orbital separation, *i.e.* the distance between the two bodies:

$$a_R = a_p \frac{m_p + m_c}{m_c} \tag{2.26}$$

which is again known modulo the inclination of the system.

2.4 Pulsar as tools

Being such precise clocks, pulsars can be used as tools to study various physical phenomena. Here are a few examples of such phenomena explored with pulsar timing.

Pulsar timing arrays

During the collision of galaxies, the merging of the supermassive black holes dwelling in their centre creates gravitational waves (GW) that influence space and time as they propagate. That modification of space-time creates an extra delay in the pulsar ToAs, however contrary to other noises the GW noise comes from the same source, and therefore all pulsar GW noises are correlated. A pulsar timing array (PTA) is a set of pulsars with good timing precision that are monitored and correlated to extract the GW signal at nano-Hertz frequencies. The expected signature of this signal is the Hellings and Downs (HD) curve (Hellings and Downs, 1983), a certain shape of the function linking the expected correlation to angular separation of pairs of pulsars. This curve in shown in Figure 2.10. This signal can come from a single close-by merger, or from the GW stochastic "background" caused by many distant mergers. Evidences for this effects have recently been measured (see e.g. EPTA Collaboration, 2023; Reardon et al., 2023), and the ongoing efforts of multiple regional PTA collaborations and the International PTA (IPTA) will certainly lead to a proper detection in the next few years.

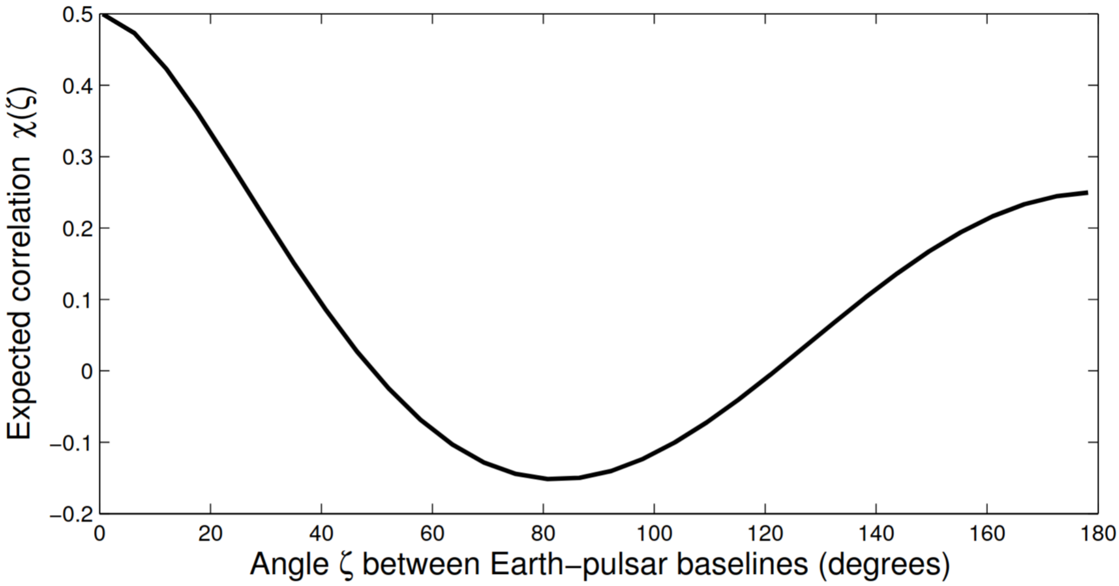

Figure 2.10: Figure 2 from Jenet and Romano, 2015: HD curve for the expected correlated response of a pair of Earth-pulsar baselines to an isotropic, unpolarized stochastic GW background, plotted as a function of the angle between the baselines.

Extrasolar planets

The first extrasolar planets ever discovered were those orbiting PSR J1300+1240. In 1992, Wolszczan and Frail announced the detection of two planets of mass ~ $3M_\oplus$ (where $M_\oplus$ is the terrestrial mass), orbiting 0.36 and 0.47 astronomical units (AU) away from the pulsar (Wolszczan and Frail, 1992). Two years later, a third planet was confirmed orbiting around the same pulsar (Wolszczan, 1994). Its mass is slightly larger than that of the Moon, which demonstrates the power of the timing technique, as this planet is still to this day the lightest ever discovered. Since then, a handful of planets orbiting pulsars have been discovered (Laycock and Christodoulou, 2025), however they can be quite smaller than the planets found with optical observations. The very existence of planets around pulsars was not considered possible and these discoveries challenge the pulsar evolution scenari. As will be discussed in Chapter 5, spider systems might be particularly susceptible to harbour such planets.

Tests of gravity

To test theories of gravity in the strong field regime, either General Relativity or any competing theory, one needs conditions that are not accessible on Earth, or even in the Solar System. Since neutron stars are compact objects, neutron star binaries which have orbital separations much larger than the size of the objects can be considered a pair of point masses. The first double neutron star binary, composed of a neutron star orbiting a pulsar (Hulse and Taylor, 1975), displays a decrease of the orbital period at a rate predicted by the general relativity due to the emission of gravitational waves. More recently, a new limit on the validity of the strong equivalence principle (SEP) was obtained by monitoring PSR J0337+1715 with the NRT (Voisin et al., 2020a). By developing a new timing model specifically designed for this study, they derived an SEP violation parameter $\Delta = (+0.5 \pm 1.8) \times 10^{-6}$ at 95 % confidence level, meaning that an alternative theory of gravity should comply with the SEP of the general relativity at least to that level.

Galactic maps

Through the measurement of DM and RM, pulsars can be probed to construct a map of the galactic ionised gas and magnetic field. If the galactic distribution of free electrons was known, the DM would provide the distance to the pulsar. However it is not the case, and more usually, pulsars with known distance estimates are used to constrain the electron distribution in order to map the galactic ionised gas distribution. Moreover, the observed proper motion of pulsars implies that they can exit the galactic plane where they are born, and should therefore be found in most regions of the Milky Way. A few ways of getting a distance to the pulsar independently to the DM exists such as the parallax for close-by pulsars, or neutral hydrogen absorption measurements (Weisberg et al., 2008). Similarly, the RM is used to map the large-scale structure of the galactic magnetic field by scanning the magnetic field along the line-of-sight. This has shown that the magnetic field of two neighbouring arms can have different signs, such as shown in Figure 2.11 (Han et al., 2018)

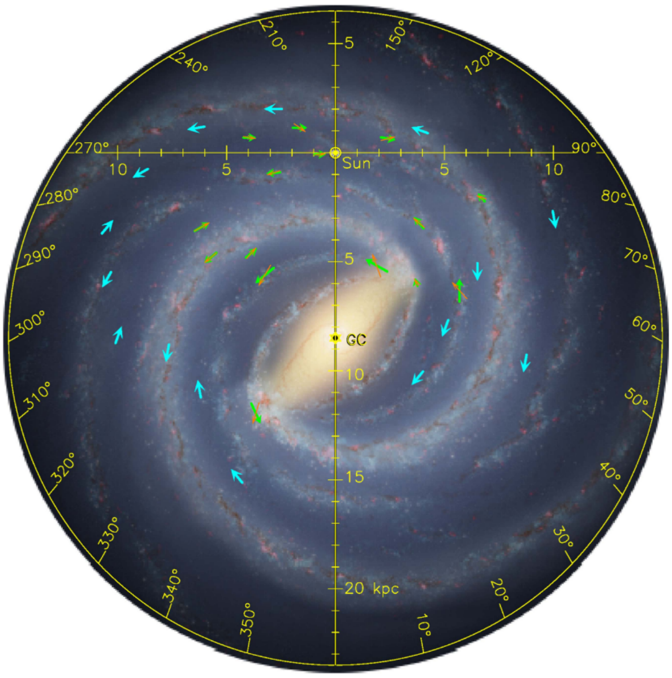

Figure 2.11: Figure 4 from Han et al., 2018: by fitting the gradient of pulsar RM values. The orange arrows give the derived line-of-sight magnetic field components and the green arrows show the inferred spiral field. The arrow length is proportional to the square root of the field strength. The blue arrows, which are all of the same length, give the inferred spiral field direction in places where the field strength is not well constrained.

After describing how to observe and process pulsars signals in the radio domain, I will in the next chapter present the telescope used to produce the data I used during my PhD, as well as the sample of spider systems monitored with it.

Chapter 3

The NRT spider dataset

π J'attachais une grande importance aux présentations. C'était souvent la seule image claire que nous laisserions aux gens : le Fer et le Pack, le Bloc ; nos différentes formations de contre, selon le vent ; la description des fonctions de chacun, où le troubadour en rajoutait des kilos.

Abstract

In the middle of the 1950s several radiotelescopes with large collecting area were built, and France decided to commission a large project for non-solar radioastronomy. Instead of the more common "single dish" design, the future telescope built in the newly founded Nançay station was decided to be modelled after the Ohio State University telescope, but on a much larger scale. The Nançay Radio Telescope was inaugurated in 1965. The Ohio/Kraus design is a meridian telescope, thus the NRT watches the sky passing over, but can point and track sources with a declination higher than -39° for about an hour. The first proper pulsar instrumentation for the NRT was implemented in 1988, and started the regular monitoring of two sources. In 1996 a new instrument was installed, and the pulsar monitoring is expanded to 20 sources, including one spider, still monitored to this day. A new instrumentation was commissioned in 2004, and in 2011 started operating the instrumentation still in use as of 2025. The NRT now monitors over a hundred pulsars, including 19 spiders. NUPPI is capable of recording 512 MHz of bandwidth, and most commonly observes at a central frequency of 1484 MHz.

In this chapter the data preparation is detailed, as well as the final dataset. This dataset is rich of its cadence and duration. More than half of the spider sample was monitored for more than 15 years, many of them observed more than twice a month. The astrometric, spin, orbital and polarimetric properties of the pulsars are presented. To put these parameters into a broader context, the orbital properties are compared to that of other short binaries of pulsars in the ATNF catalogue, and the polarimetric properties are compared to that of the study of Wang et al., 2023a.

Finally, each pulsar is presented individually, with both general information and specific peculiarities. This bibliography work shows the wonderful diversity of phenomena displayed by spiders in the NRT sample.

3.1 The Nançay Radio Telescope

The NRT is located in the Nançay Radio Observatory, in the Sologne region, 60 km south of Orléans.

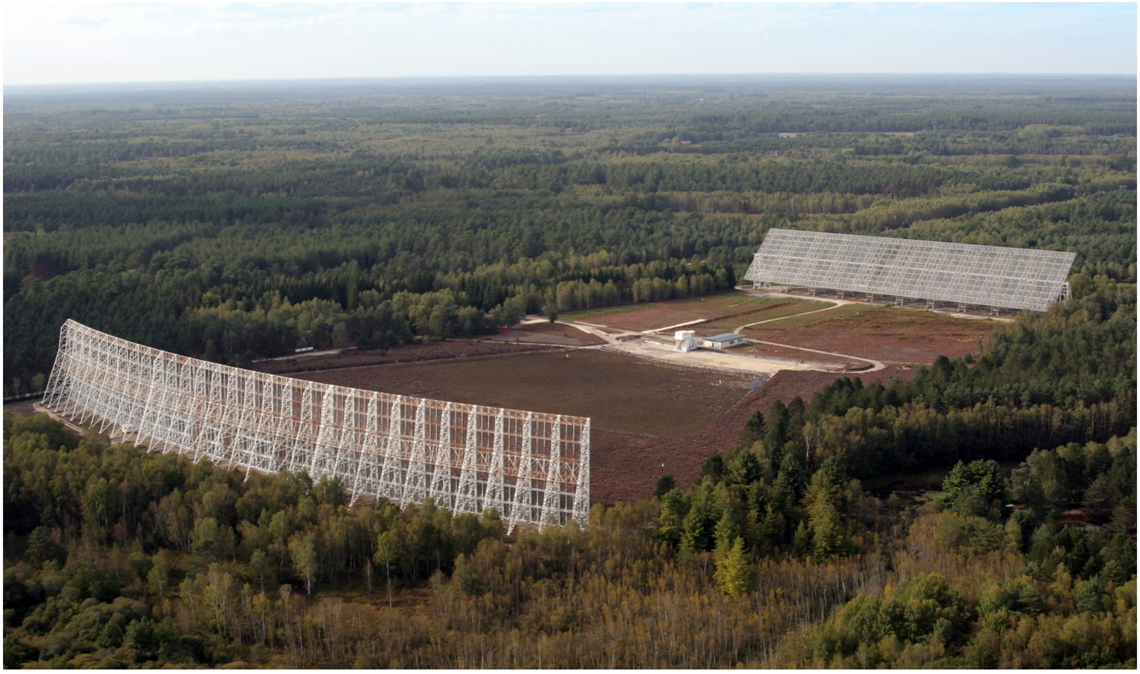

Figure 3.1: Picture of the Nançay Radio Telescope. The primary mirror (right) is facing south. It is a flat and tiltable surface of 200 × 40 m. The secondary mirror (left), 460 m away, is a section of a 560 m-radius sphere. It is 35 m high and 300 m long, and is fixed. The focal point is about 280 m north of the secondary. The movable focal cabin shelters two more mirrors and the receptors. Picture credit: Nançay observatory.

3.1.1 Genesis of the telescope

World wide interest for radio astronomy rose after the discovery by Jansky of the radio emission from the Milky Way. In France, the radio astronomy group of École Normale Supérieure (ENS), later relocated in the Meudon Observatory, took advantage of the two German Würzburg antennas left after WWII. The two antennas were transferred in 1955 from Marcoussis, south of Paris, to the Nançay field station founded by the ENS two years prior. The goal was to mount the Würzburg on carriages on N-S and E-W railways, to form a variable-baseline interferometer operating at 1420 MHz. This instrument was operational in 1959. On site, two solar interferometers were already implemented.

During the same period, single dish telescopes were constructed, notably the Jodrell Bank 76 m (completed in 1957), and the Parkes radiotelescope, now Murriyang (completed in 1961). Large interferometers were also constructed, notably the Cambridge University interferometer, which later discovered the first pulsar. As the context in France was favourable for such a large project, an instrument for non-solar radioastronomy was planned.

At that time, French radioastronomers mainly had experience in interferometry, from the major solar physics flavour that the community had. Therefore, an interferometer was naturally suggested for non-solar physics. However, the main science driver was the observation of the 21 cm atomic hydrogen line, to survey the distant universe. The need for a good sensitivity was stronger than the need for resoluting power, hence the rise of large collecting area single dish telescopes in the emerging non-solar astronomy. However, a fully-steerable paraboloïd in the same fashion as the Jodrell Bank or the Parkes telescopes was too expensive (and maybe not feasible or interesting for the French industry), and a different design had to be chosen.

It was decided that the NRT would be modelled on the Ohio State University telescope, built by Jonh D. Kraus and his team, but on a much larger scale. This design is much cheaper per collecting surface unit area, and has the secondary advantage of having a more accessible focal equipment, and less restricted in weight, than a dish of the same equivalent surface, but having the receptors that close to the ground makes the instrument more sensitive to thermal noise coming from the ground.

However, the main disadvantage is that the Kraus/Ohio State design is a meridian transit-type telescope. The integration time is therefore limited to about one hour around meridian crossing. Moreover, the rectangular beam shape makes the polarization calibration more difficult than that of a circular beam.

The building contract was signed with the Compagnie Française d'Entreprise (founded by G. Eiffel in the 1880s), and the construction started in May 1959. The complete instrument has been inaugurated on May 14^{th} 1965 (Lequeux, Steinberg, and Orchiston, 2010).

3.1.2 A brief history of pulsar observations with the NRT

Right after the announcement of the discovery of pulsars in 1968, first pulsar observations using the NRT were made. However, these were merely tests, and actual pulsar monitoring program started in 1988. Just before this campaign, a prototype of the first pulsar instrument was tested on the first discovered MSP, B1937+21. The first detection, that took place on March 13^{th} 1987, is shown in Figure 3.2. After the tests, the "pulsaroscope" started its first timing campaign over the summer of 1988, producing the first scientific ToAs (Fairhead, 1989). After that started the monitoring of B1937+21 and another MSP, B1821−24 (which is the first MSP discovered in a globular cluster). The pulsaroscope instrumentation was used until 2004.

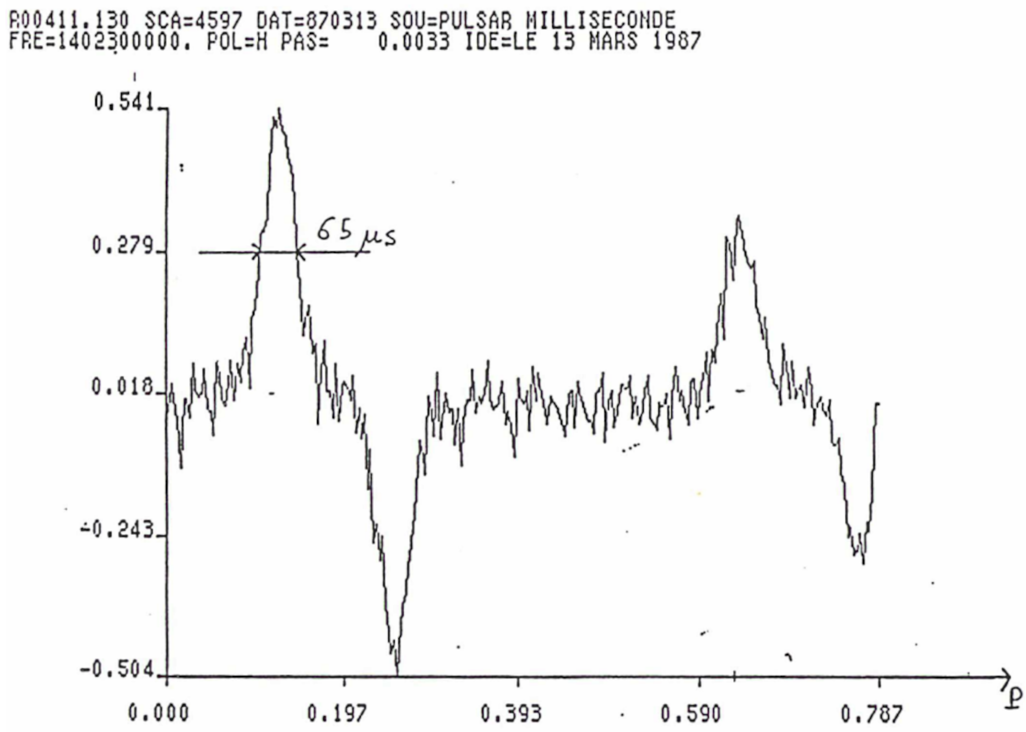

Figure 3.2: Figure VII.3 from Fairhead, 1989: profile of PSR B1937+21 (intensity as a function of pulse phase). Both main and secondary pulses are visible and also appear in negative.

In 1996, the Navy Berkeley Pulsar Processor (NBPP) was installed at Nançay, and late 1998 a new pulsar monitoring program was launched. In addition to the two pulsars previously mentioned, 18 pulsars were regularly observed with this new instrumentation, and one of the scientific goals was the search for gravitational waves (see Section 2.4). This new list included a spider system recently discovered, J2051−0827 (Stappers et al., 1996).

Since that, pulsars are regularly added to the list, with over a hundred pulsars regularly monitored by the NRT, nowadays making up for about 80 % of the observation time. The pulsaroscope and the NBPP were replaced in 2004 by the Berkeley-Orléans-Nançay (BON) backend, which was upgraded in 2008 by the introduction of GPUs. BON's successor, that is still in use as of 2025, is the Nançay Ultimate Pulsar Processing Instrument (NUPPI), started observations in 2011. The BON and NUPPI datasets are sometimes used together, when a longer time span is needed. Details about NUPPI are given in the next section. An upgrade for NUPPI, NUPPI 2GHz, is under development.

3.1.3 Characteristics

Telescope design

It is a meridian transit-type telescope of the Kraus/Ohio State design (Kraus, 1960). This very peculiar design is composed of 2 "external" mirrors and 2 "internal" mirrors, dwelling in the focal cabin with the receptors, as can bee seen in Figure 3.1. The primary, facing south, is composed of 10 independent panels. It is a flat and tiltable surface of 200×40 m. Four of those panels are steered and the other six are controlled by the steered panels, aligning with a precision of half an arcminute. Each panel weighs 40 tons and the structures on which those are fixated weighs 250 tons. The secondary mirror, 460 m away, is a section of a 560 m-radius sphere, and its shape does not deviate from that of a sphere by more than 5 mm. It is 35 m high and 300 m long, weighs 750 tons and is fixed. The focal point is about 280 m north of the secondary. The movable focal cabin shelters two more mirrors and the receptors, as shown in Figure 3.3. The collecting surface is equivalent to that of a 94-m dish.

This design makes the NRT a meridian telescope, meaning that the NRT basically watches the sky as its passes by. It cannot steer like a dish to point a source, but the tiltable deflector does allow for a certain amount of pointing. The deflector is perfectly facing south, thus the motion of the Earth translates into an observed motion of any given source from east to west. To counteract this motion, the focal cabin moves on a 80-m east-west railway to track the pointed source. Thanks to this, the NRT can observe a given object for up to ~90 minutes, but observations are usually more around 60 minutes long. Because of its position on the globe and the maximum tilt of the deflector, the NRT is restricted to sources with declinations higher that −39°, giving access to about 80 % of the sky.

The NRT is equipped with two receptors, one functioning between 1.0 and 1.8 GHz (L-band) and the other between 1.7 and 3.5 GHz (S-band). The first one includes both the 21-cm neutral hydrogen and the 18-cm OH lines and is the one more commonly used for observations, as the flux density received from pulsars generally decreases with frequency. They are helium cooled to 35 K to limit the noise intrinsic to the system temperature.

Backends

What was described in the previous section was the "frontend" of the telescope, which ultimately sends the raw electrical signals to the "backend", which in the case of the NRT is hosted a few dozens of meters away in a building protected by a Faraday cage. As briefly mentioned in Section 3.1.2, the NRT has seen four pulsar instrumentations as of 2025: the pulsaroscope, the NBPP, the BON and the NUPPI. Spiders have only been observed with the latter three, and NUPPI is the only backend used for the eclipses study of Chapter 4.

The Berkeley-Orléans-Nançay backend started operating in 2004. It was a member of the ASP-GASP coherent dedispersion backend family (Demorest, 2007). It was initially designed with

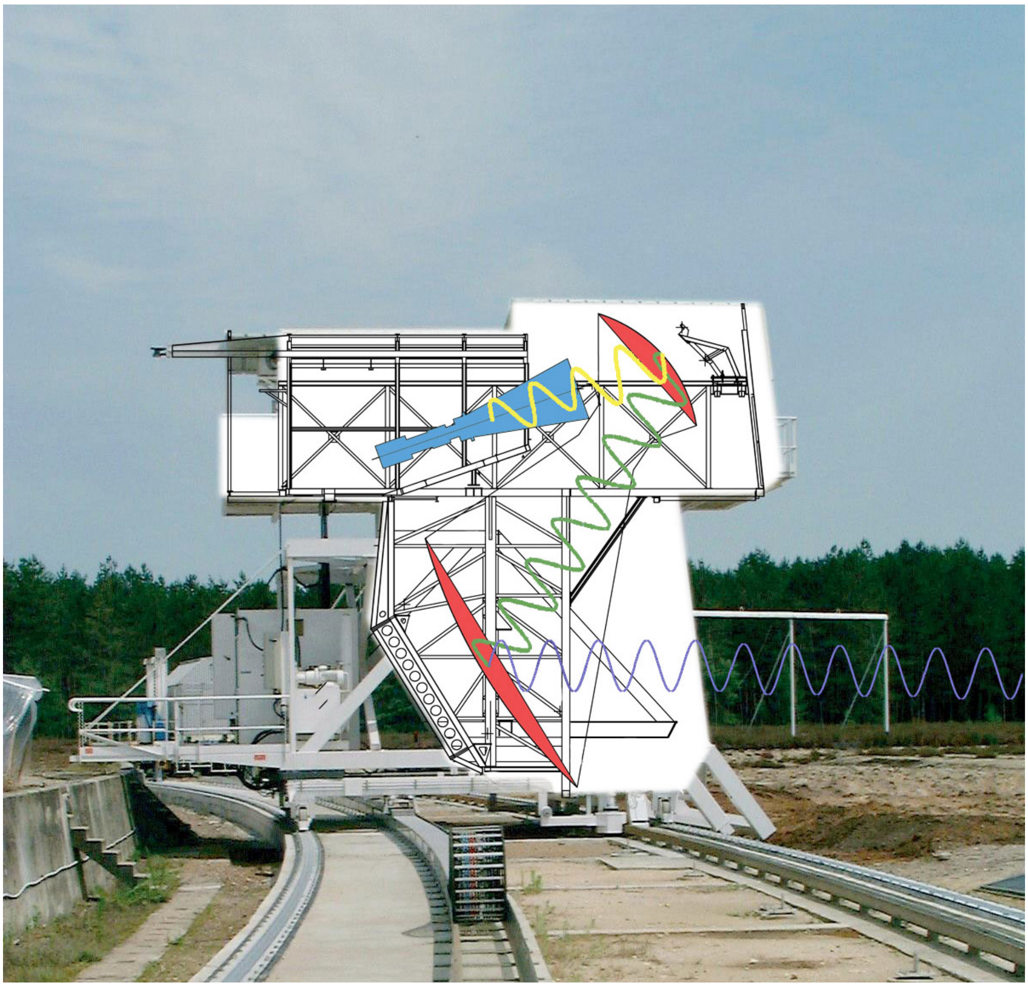

Figure 3.3: Schematic of the focal cabin of the NRT. The wave coming from the primary mirror reflects on two mirrors before entering the square base horn antenna, at the end of which lies the receptor. Image credit: Nançay observatory

CPUs and was at this time limited to a 64 MHz bandwidth, and got GPUs in 2008, upgrading to a 128 MHz bandwidth (composed of 32 channels of 4 MHz). After 2008, the NRT polarisation calibration method consisted of the observation of a pulsed diode prior to each observation, a calibration method that was vastly improved quite recently (see Guillemot et al., 2023 for more details).

Since August 2011, pulsar observations with the NRT have been conducted using the Nançay Ultimate Pulsar Processing Instrument, a backend based on the "GUPPI" used at the Green Bank telescope (DuPlain et al., 2008). NUPPI uses GPUs to coherently dedisperse and fold the data in real time (which corresponds to 16 Gb per second). In the normal pulsar observation mode, its total bandwidth of 512 MHz is split into 128 channels of 4 MHz each, with a central frequency of 1484 MHz, to exploit as much of the frequency interval covered by the L-band receiver as possible.

3.2 Data preparation

The general presentation of the data preparation procedure has been given in Chapter 2. All explanations of names and methods, as well as the relevant references, can be found in this previous chapter.

For the works presented in Chapters 4 and 5, we started by conducting timing analyses of all the selected pulsars, to construct timing solutions enabling us to determine pulsar orbital phases with good accuracy.

The NUPPI data on the selected pulsars were cleaned of RFI using the SURGICAL method of the COASTGUARD pulsar analysis library. The PSRCHIVE software library was used to calibrate the polarisation information, and to perform all subsequent data reduction steps.

The timing analysis was done in two steps. We first constructed reference profiles for each of the considered pulsars by summing up eight time- and frequency-averaged observations with high SNR values, and smoothing the obtained integrated profiles. We then extracted TOAs using the `pat` routine. We generated one TOA per 64 MHz of frequency bandwidth in order to track time variations of the DM and one per 5 min for the TOAs to cover less than a few percents of the pulsar's orbital period. The TOA data were analysed using the TEMPO2 pulsar timing suite. We discarded TOAs around superior conjunction in the case of pulsars observed to display eclipses in the NRT data (see Section 4.1.2). We then obtained timing solutions for each pulsar by fitting the timing residuals for their spin, astrometric, DM and orbital parameters. DM variations were modelled by fitting for up to two time derivatives, and similarly variations of the orbital period, which are commonly observed in these systems, were fitted for by including up to 17 derivatives (in the case of PSR J2051−0827).

In the second step of the timing analysis, we used the timing solutions obtained from the previous analysis step to refold all individual observations, and formed 2D template profiles from archives with 8 frequency sub-bands of 64 MHz each for each pulsar. For pulsars with observations that have SNR values larger than 100, we used the highest-SNR observation as 2D template. For the other pulsars we summed up the three highest-SNR observations to form the 2D template. With these standard profiles with frequency resolution we could follow the same analysis procedure as in Guillemot et al. (2019) and use the `PulsePortraiture` library to extract one TOA per 10 min of observation for the entire bandwidth.

After the latter analysis step, we obtained TOA datasets for each pulsar in the sample, with one measurement per 10 min of observation. This dataset timing solutions are the ones presented in the next section.

The PULSEPORTRAITURE ToA extraction procedure described in Section 2.3.2 estimates simultaneously a ToA and a DM for each individual profile, however spider systems are quite faint, and the precision of the measured instantaneous DM was to low to be used in our study.

3.3 Overview of the spider sample

As of 2025, the NRT monitors 19 spider systems. The sample includes 18 BWs and only one RB. Figure 3.5 shows every observation conducted with BON or NUPPI. The cadence of the observations is particularly high: some pulsars are observed on average once a week or so, as summarised in Table 3.1. This density of the sampling is one of the biggest asset of the NRT spider sample. The dataset presented here is that presented in Blanchard et al., 2025.

This rich dataset, prepared in a consistent manner, is a gold mine for whoever wishes to study the group properties of any behaviour of spiders. Spiders are widely studied, as they display many interesting particularities (see Section 1.4.4), however they are usually studied individually. Compared to the new radio facilities, such as MeerKAT or FAST, the NRT might not be the most sensitive instrument available, but its long lasting pulsar monitoring program offers opportunities that state-of-the-art but recent programs cannot. In the next Chapters 4 and 5, I will work with data composing this sample. This section will therefore be a presentation of the sample in terms of pulsar and binary parameters, and the next section will present every pulsar one by one, with what I wish to be a description as exhaustive as possible of their individual particularities discovered as of today.

3.3.1 General properties properties of the systems

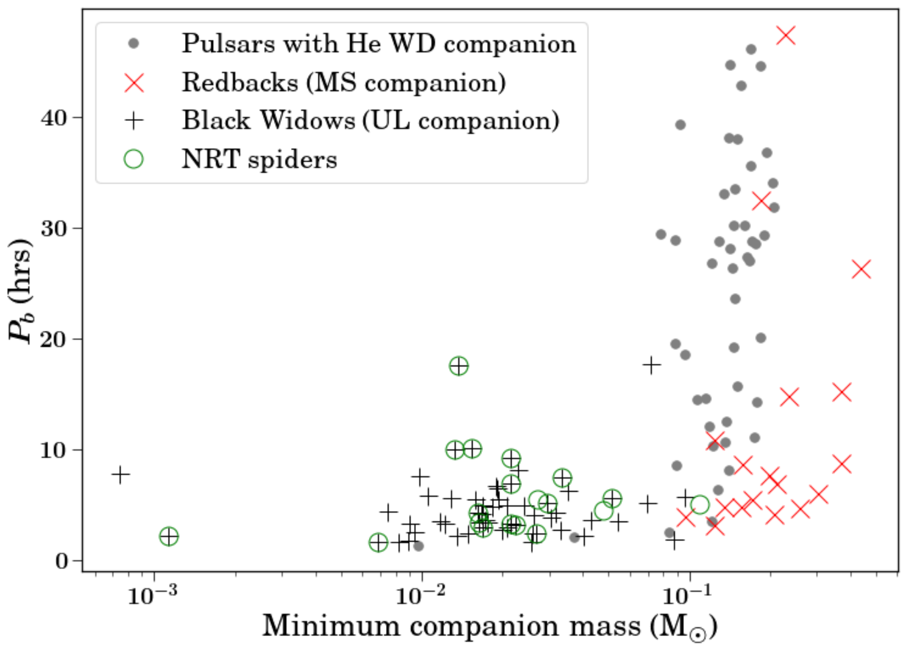

Figure 3.4: Same as Figure 1.8: orbital periods of known spider systems against minimum companion masses. In this figure, spider systems are categorised as BW or RB depending on the companion type listed in the ATNF catalogue: Main sequence (MS) stars for RBs or ultra low-mass objects (ULs) in the case of BWs. Some NRT spiders have no information about the companion type in the catalogue; hence, some circles have no cross inside.

Table 3.2 summarises the astrometric and spin properties of the pulsars in our sample, and Table 3.3 summaries their orbital properties. To put the latter into a broader perspective, Figure 3.4 shows the distribution of the NRT spiders in the context of all ATNF reported binaries, as previously shown in Figure 1.8. This shows that, in spite of the under-representation of RB-type objects in our sample, orbital periods and companion masses in our sample are fairly representative of those of the global, currently known spider population. The companion masses in Table 3.3 were

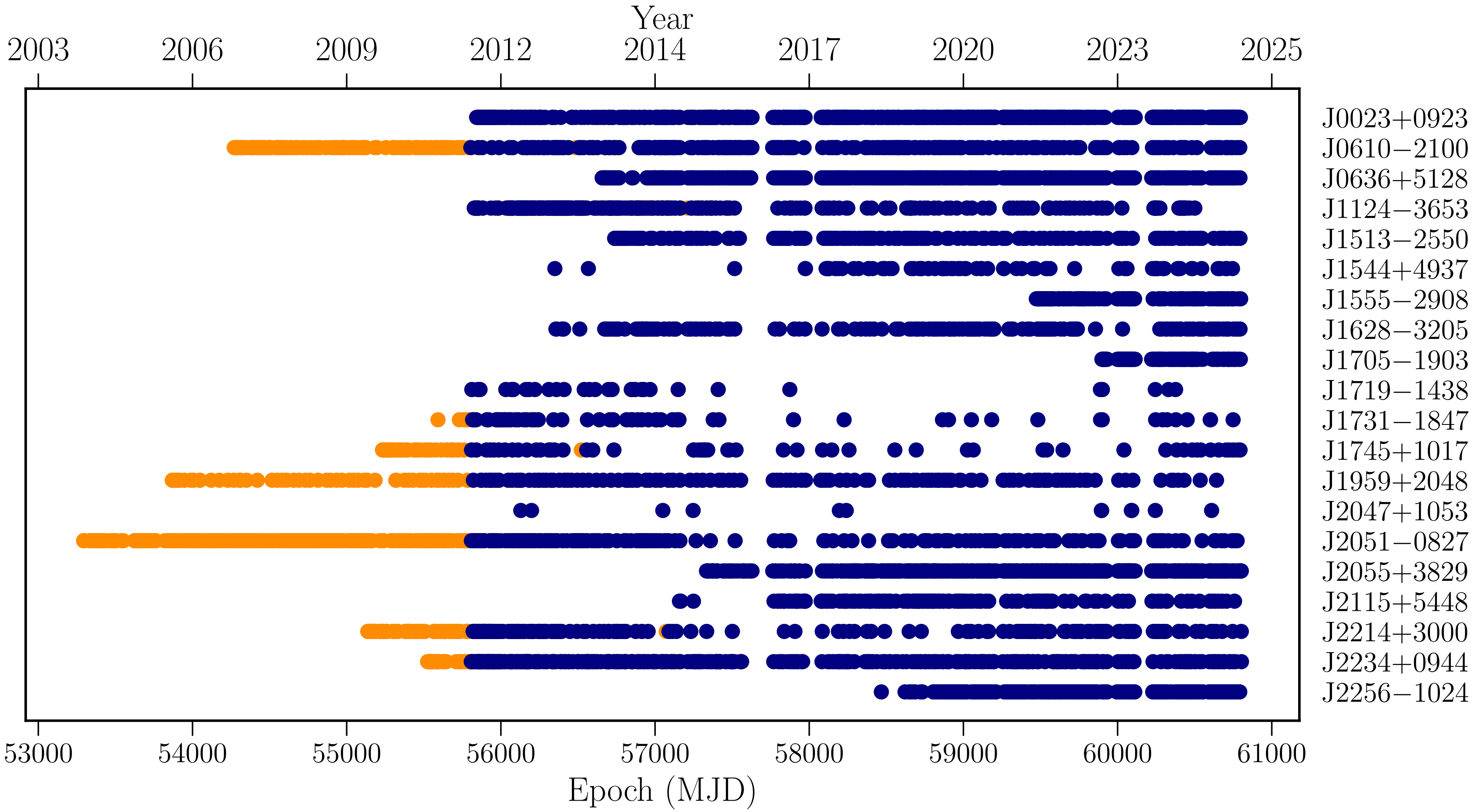

Figure 3.5: Time span of the NRT dataset considered in this study. Each blue (resp. orange) dot represents an observation made with the NUPPI (resp. BON) backend.

Table 3.1: Properties of the NRT dataset. For each pulsar, we list the total time span of the observations and the number of observations as of MJD 60935 (17 September 2025), as well as the median signal-to-noise ratio (SNR) of the frequency- and time-averaged observations, and the average number of days between two observations. In Chapter 4 we considered only NUPPI observations, for Chapter 5 NUPPI and BON observations when available.

Pulsar		BON			NUPPI		Total average cadence
	Time span (d)	N_{obs}	Median SNR	Time span (d)	N_{obs}	Median SNR	
J0023+0923	1784	196	11.5	4953	841	30.2	6.5
J0610−2100	3344	182	23.5	4987	230	42.4	20.2
J0636+5128	884	83	24.7	4137	466	66.0	9.1
J1124−3653	1657	253	6.5	4673	365	6.6	10.2
J1513−2550	809	52	9.0	4056	236	26.4	16.9
J1544+4937	/	/	/	4395	78	16.1	56.3
J1555−2908	/	/	/	1325	118	20.8	11.2
J1628−3205	578	30	13.5	4437	170	38.0	25.1
J1705−1903	/	/	/	898	134	178.6	6.7
J1719−1438	1598	25	14.9	4565	31	30.8	110.0
J1731−1847	1822	46	11.5	4933	57	28.7	65.6
J1745+1017	2293	71	15.8	4984	55	50.1	57.8
J1959+2048	3686	109	8.6	4820	131	15.6	35.4
J2051−0827	4225	449	31.6	4966	193	99.4	14.3
J2055+3829	278	22	10.1	3469	623	27.7	5.8
J2115+5448	/	/	/	3600	154	29.1	23.4
J2214+3000	2365	209	14.9	4982	180	21.9	18.9
J2234+0944	2036	189	23.7	4995	331	55.0	13.5
J2256−1024	/	/	/	2325	280	53.2	8.3

determined using eq.(2.25), assuming a pulsar mass of $1.8M_{\odot}$. In Blanchard et al., 2025, we used the default value of 1.5 $M_{\odot}$, however after more careful considerations decided on a heavier default mass, as explained in Section 1.4. This changes the values of the companions mass slightly but does not affect any other result, as the eclipse study was conducted using the mass function, which does not depend on the assumed pulsar mass. Minimum companion masses were determined using i = 90°, while median values were calculated assuming i = 60°. This table also includes a column indicating if the pulsar is seen to display eclipses at 1.4 GHz, which is relevant for Chapter 4.

3.3.2 Polarisation properties

In addition to the astrometric, spin and binary properties, we characterised the polarimetric properties. To construct polarimetric profiles for the 19 pulsars, we selected observations conducted after MJD 58800 (13 November 2019), which are observations that can be polarisation calibrated using the improved calibration scheme presented in Guillemot et al. (2023). For pulsars displaying eclipses (see Table 3.3 and Chapter 4) we only considered data with orbital phase >0.5. Individual observations, prepared with the same procedure as described in Section 3.2, were summed in time to form high SNR polarimetric profiles. For pulsars with RM information available in the ATNF pulsar catalogue, we corrected the polarimetric profiles from Faraday rotation of the polarisation position angle across the bandwidth (see Section 2.1.2). For the other five pulsars, no RM information was available in the ATNF catalogue at the time of writing. We attempted to determine RM values from the summed NUPPI polarimetric profiles, but the low degrees of linear polarisation in these pulsars and very low SNR values in some cases prevented us from determining the RMs. The summed observations were finally scrunched in frequency.

The resulting polarimetric profiles at 1.4 GHz for the 19 pulsars in our sample are shown in Figs. 6.1 to 6.3. Pulsar profiles that were not corrected for Faraday rotation are marked with a star. We note that the 1.4 GHz polarimetric profiles of PSRs J1124−3653, J1555−2908, J1628−3205, and J2115+5448 were unpublished before our article Blanchard et al., 2025, to the best of our knowledge. Polarimetric profiles for the other pulsars are consistent with the previously published ones. In Table 3.4 we list the pulsar RMs, and values of the polarised intensities and linear, circular and absolute circular intensities, as determined using the `psrstat` tool of PSRCHIVE (see Section 2.3.2). For pulsars for which we lacked an RM value and thus could not correct the data for Faraday rotation, we do not quote the polarised intensities and linear intensities. Polarisation fractions vary broadly across the sample, with values ranging from 13% to 66%.

In order to put our polarisation fraction measurements in a broader context, we plotted in Fig 3.6 the linear and absolute circular polarisation fractions listed in Table 3.4 along with the measurements for 682 pulsars published in Wang et al. (2023a), obtained using the Five-hundred-meter Aperture Spherical radio Telescope (FAST). One can see on this figure that most spider pulsars appear to have low degrees of polarisation, similarly to non-spider MSPs. It can also be noted that NRT measurements are complementary to those of Wang et al. (2023a) and display similar trends. We performed 2D Kolmogorov-Smirnov tests using the publicly available software NDTEST[1], to compare the polarisation fractions of spider pulsars with those of other MSPs and slow pulsars. For spider pulsars we combined NRT and FAST polarisation measurements, leading to a sample of 26 objects with linear and absolute circular polarisation fractions. The other samples included 66 non-spider MSPs, and 582 slow pulsars. We found a probability that polarisation data for spider MSPs and slow pulsars originate from the same parent distribution of approximately 8.5%, suggesting that the two populations have distinct polarisation properties. On the other hand, the test found a larger probability of ~ 20% that the data for spider and non-spider MSPs originate from the same parent distribution, thus preventing us from drawing any conclusions.

[1]Written by Zhaozhou Li, https://github.com/syrte/ndtest

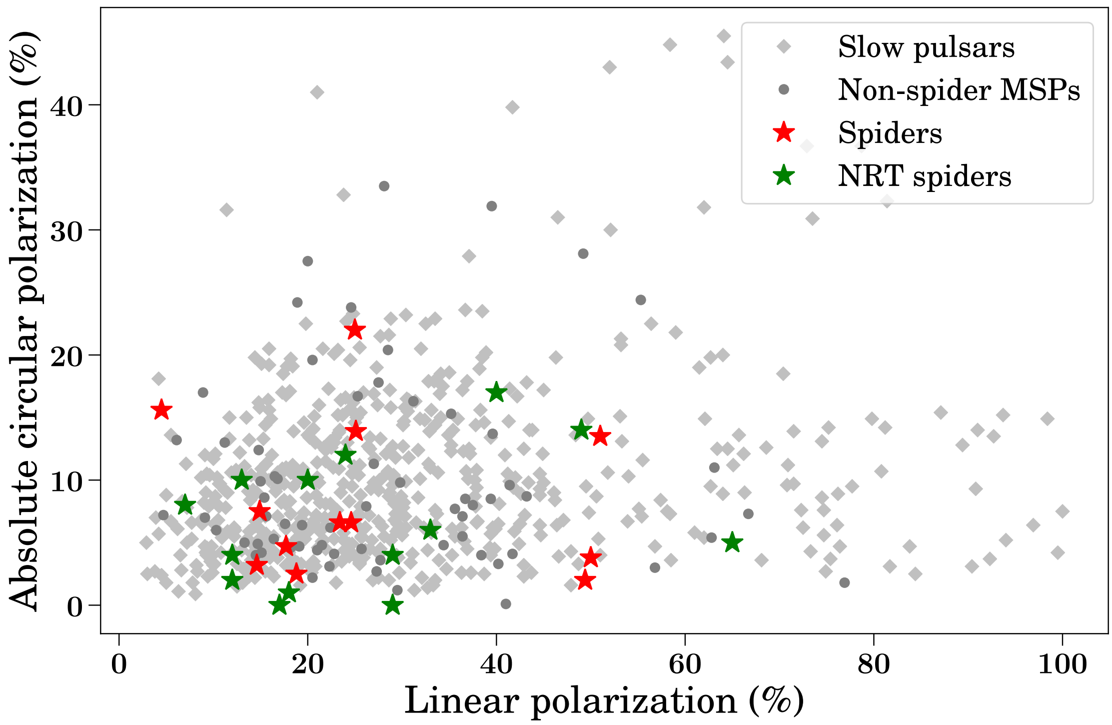

Figure 3.6: Linear polarisation fractions and absolute circular polarisation fractions for the 682 pulsars from Wang et al. (2023a). Grey diamonds are slow pulsars, and grey dots represent isolated MSPs or MSPs in non-spider systems (pulsars orbiting white dwarf companions or main sequence stars). Red stars are spiders that are not in the NRT sample, and green stars are the spiders analysed in this article. The values for the latter objects can be found in Table 3.4.

Table 3.2: Astrometric and spin properties of the 19 pulsars constituting our spider pulsar sample. For each pulsar we list the discovery article, the galactic coordinates, the spin period P, the dispersion measure DM, and the distance d. The latter distance values are based on the DMs and were estimated using the YMW16 model from Yao, Manchester, and Wang, 2017 (see Section 2.1.1).

Pulsar	Discovery article	Gal. lon. (J2000)	Gal. lat. (J2000)	P (ms)	DM ($pc\ cm^{-3}$)	d (kpc)
J0023+0923	Bangale et al. (2024)	111.38	–52.85	3.05	14.3	1.24
J0610–2100	Burgay et al. (2006)	227.75	–18.18	3.86	60.7	3.26
J0636+5128	Stovall et al. (2014)	163.91	18.64	2.87	11.1	0.21
J1124–3653	Bangale et al. (2024)	284.09	22.76	2.41	44.9	0.99
J1513–2550	Sanpa-Arsa (2016)	338.82	26.96	2.12	46.9	3.96
J1544+4937	Bhattacharyya et al. (2013)	79.17	50.17	2.16	23.2	2.98
J1555–2908	Ray et al. (2022)	344.48	18.50	1.79	75.9	7.55
J1628–3205	Ray et al. (2012)	347.43	11.48	3.21	42.1	1.22
J1705–1903	Morello et al. (2018)	3.25	13.03	2.48	57.5	2.34
J1719–1438	Bailes et al. (2011)	8.86	12.84	5.79	36.8	0.34
J1731–1847	Keith et al. (2010)	6.89	8.15	2.35	106.5	4.77
J1745+1017	Barr et al. (2013)	34.87	19.25	2.65	24.0	1.22
J1959+2048	Fruchter, Stinebring, and Taylor (1988)	59.20	-4.70	1.61	29.1	1.73
J2051–0827	Stappers et al. (1996)	39.19	–30.41	4.51	20.7	1.47
J2055+3829	Guillemot et al. (2019)	80.62	–4.26	2.09	91.8	4.59
J2115+5448	Sanpa-Arsa (2016)	95.04	4.11	2.60	77.4	3.11
J2214+3000	Ransom et al. (2011)	86.86	–21.67	3.12	22.6	1.68
J2234+0944	Ray et al. (2012)	76.28	–40.44	3.63	17.8	1.58
J2256–1024	Crowter et al. (2020)	59.23	–58.29	2.30	13.8	1.33

Table 3.3: Binary properties of the 19 pulsars constituting our spider pulsar sample. For each pulsar, we list the orbital period P_b, the projected semi-major axis of the pulsar orbit, $a_1 = a_p \sin(i)$, the mass function m_f and estimates of the minimum and median companion masses, $m_\mathrm{c,\,min}$ and $m_\mathrm{c,\,med}$. Companion masses were derived using Equation 2.25, assuming a pulsar mass $m_p = 1.8\ M_\odot$. Minimum and median masses were respectively derived assuming orbital inclinations i of 90° and 60°. In the last column we indicate whether the pulsar is seen to eclipse in the 1.4 GHz NRT data or not, with eclipsing pulsars defined as those displaying excess delays in their timing residuals around superior conjunction (see Section 4.1.3).

Pulsar	P_b (hrs)	a_1 (10^{-2} lt-s)	m_f ($10^{-6} M_\odot$)	$m_{c,\,\mathrm{min}}$ ($10^{-2} M_\odot$)	$m_{c,\,\mathrm{med}}$ ($10^{-2} M_\odot$)	Eclipsing at 1.4 GHz?
J0023+0923	3.33	3.48	2.34	1.98	2.29	-
J0610−2100	6.86	7.35	5.18	2.59	2.99	-
J0636+5128	1.60	0.90	0.175	0.83	0.96	-
J1124−3653	5.45	7.96	10.5	3.28	3.79	Yes
J1513−2550	4.29	4.08	2.27	1.96	2.27	Yes
J1544+4937	2.90	3.29	2.60	2.05	2.37	-
J1555−2908	5.60	15.14	68.0	6.18	7.16	Yes
J1628−3205	5.00	41.03	1.70e+03	18.88	22.03	Yes
J1705−1903	4.41	10.44	35.9	4.97	5.75	Yes
J1719−1438	2.18	0.18	7.85e-04	0.14	0.16	-
J1731−1847	7.47	12.02	19.1	4.02	4.65	Yes
J1745+1017	17.53	8.82	1.37	1.65	1.91	-
J1959+2048	9.17	8.92	5.20	2.59	2.99	Yes
J2051−0827	2.38	4.51	9.95	3.22	3.73	Yes
J2055+3829	3.11	4.53	5.89	2.70	3.12	Yes
J2115+5448	3.25	4.48	5.25	2.60	3.00	Yes
J2214+3000	10.00	5.91	1.27	1.61	1.86	-
J2234+0944	10.07	6.84	1.94	1.86	2.15	-
J2256−1024	5.11	8.30	13.5	3.57	4.13	Yes

Table 3.4: Polarisation parameters for the 19 pulsars in our sample. Rotation Measure (RM) values were taken from the articles listed in the "RM Reference" column. Polarised intensities (I_p), linear ($\langle L \rangle$), circular ($\langle V \rangle$) and absolute circular ($\langle \|V\| \rangle$) intensities are quoted in percentages of the total intensity (I).

Pulsar	RM (rad m^{-2})	RM Reference	I_p/I (%)	$\langle L \rangle/I$ (%)	$\langle V \rangle/I$ (%)	$\langle \|V\| \rangle/I$ (%)
J0023+0923	−6	Wang et al. (2023a)	30	29	3	4
J0610−2100	33.7	Spiewak et al. (2022)	66	65	−6	5
J0636+5128	−7.0	Wahl et al. (2022)	35	33	−5	6
J1124−3653	/	/	/	/	3	8
J1513−2550	/	/	/	/	−8	2
J1544+4937	10.3	Wang et al. (2023a)	15	12	1	2
J1555−2908	/	/	/	/	5	4
J1628−3205	/	/	/	/	−2	3
J1705−1903	−5.6	Spiewak et al. (2022)	19	18	1	1
J1719−1438	17.3	Spiewak et al. (2022)	38	24	−27	12
J1731−1847	21.5	Spiewak et al. (2022)	51	47	−20	17
J1745+1017	24.2	Wang et al. (2023a)	48	40	−23	17
J1959+2048	−70.1	Wang et al. (2023a)	27	20	15	10
J2051−0827	−46	Han et al. (2018)	13	7	−1	8
J2055+3829	−65.8	Wang et al. (2023a)	17	17	> 0.1	> 0.1
J2115+5448	/	/	/	/	−3	4
J2214+3000	−44.5	O'Sullivan et al. (2023)	29	29	> 0.1	> 0.1
J2234+0944	−10.4	Wang et al. (2023a)	15	12	4	4
J2256−1024	15.0	Crowter et al. (2020)	18	13	2	10

3.4 Individual presentations of the pulsars

PSR J0023+0923

PSR J0023+0923 was discovered as part of a survey of unassociated *Fermi* Large Area Telescope (LAT) sources with the Green Bank Telescope (GBT) at 350 MHz (Bangale et al., 2024). It has a period of 3.05 ms, and a DM of 14.32 pc cm^{-3} putting it at a distance of 1.24 kpc according to the YMW16 model for the distribution of free electrons in the Milky Way (Yao, Manchester, and Wang, 2017). It has been observed in X-rays (Gentile et al., 2014), and has been detected with the LAT as a pulsed source of γ-ray emission (see e.g. Smith et al., 2023).

It is classified as a BW due to its very typical $0.016\ M_{\odot}$ minimum companion mass, and short orbital period of 3.3 hrs. The companion has been observed at optical wavelengths with multiple instruments (Breton et al., 2013; Draghis et al., 2019; Mata Sánchez et al., 2023). The system is not displaying eclipses in the L-band, and is not reported to display eclipses at 350 MHz or 2 GHz (Bangale et al., 2024).

PSR J0610−2100

PSR J0610−2100 was discovered during the Parkes High-Latitude pulsar survey (Burgay et al., 2006). It has a period of 3.86 ms and a DM of 60.7 pc cm^{-3} placing it at a distance of 3.26 kpc according to the YMW16 model. It was first reported to emit pulsed γ rays by Espinoza et al. (2013).

It is classified as a BW due to its $0.021\ M_{\odot}$ minimum companion mass, and short orbital period of 6.9 hrs. The companion has been detected at optical wavelengths in archival observations obtained with FORS2 (Pallanca et al., 2012). This system is not known to display eclipses.

PSR J0636+5128

PSR J0636+5128 was found in the Green Bank Northern Celestial Cap Pulsar Survey (Stovall et al., 2014). It has a period of 2.87 ms, and a DM of 11.1 pc cm^{-3}. The YMW16 model predicts a very small distance of 0.21 kpc for this DM and set of sky coordinates. Pulsed γ-ray emission was first detected and reported by Smith et al. (2019). With its ultra-light companion (minimum mass of $0.007\ M_{\odot} \simeq 7.3 M_J$) and short orbital period of 1.6 hrs, it is classified as a BW pulsar. Its orbital period is among of shortest currently known among the binary pulsar population.

The companion has been detected in 2014 Gemini archival data (Draghis and Romani, 2018). This system is not known to display eclipses.

Unlike PSRs J0023+0923 and J0610−2100 that have been observed with NUPPI soon after it was installed in August 2011, NRT observations of J0636+5128 began in late 2013.

PSR J1124−3653

PSR J1124−3653 was found during a 350 MHz survey of unassociated *Fermi* LAT sources with the GBT (Bangale et al., 2024). It has a period of 2.41 ms, and a DM of 44.9 pc cm^{-3} putting it at a distance of 0.99 kpc according to the YMW16 model. It has been observed in X-rays (Gentile et al., 2014), and is detected to emit pulsed γ-ray emission (Smith et al., 2023).

With its low minimum companion mass of $0.027\ M_{\odot}$ and short orbital period of 5.4 hrs, it is a BW pulsar. It is extremely faint in 1.4 GHz NRT observations: as can be seen from Table 3.1 the median SNR of our observations of this one is only 6.5. Although the pulsar is seen to display eclipses at 1.4 GHz in the NRT data, the very low SNR values prevented us from obtaining satisfactory results for the eclipse analysis using the same analysis method as for the others.

PSR J1513−2550

PSR J1513−2550 was found in a survey for new pulsars at the locations of *Fermi* LAT unassociated sources at 800 MHz with the GBT(Sanpa-Arsa, 2016). It has a period of 2.12 ms, and a DM of 46.9 pc cm^{-3}. The YMW16 model of free electrons in the Galaxy places the pulsar at a distance of 3.96 kpc. It has been detected as a pulsed source of γ rays with the LAT (Smith et al., 2023).

It is classified as a BW due to its $0.016\ M_{\odot}$ minimum companion mass and short orbital period of 4.3 hrs. At 1.4 GHz this system is observed to eclipse, with short-duration (duty cycles of less than 10% of the orbital period) total eclipses. NRT observations of J1513−2550 began in March 2014.

PSR J1544+4937

This 2.16 ms pulsar with a DM of 23.2 pc.cm^{-3} was discovered as part of a search for pulsars in LAT unassociated sources with the GMRT(Bhattacharyya et al., 2013). The YMW16-predicted distance for this DM value is 2.98 kpc. The low minimum companion mass ($0.017\ M_{\odot}$) and short orbital period (P_b ~ 2.9 hrs) make it a BW pulsar. The analysis of *Fermi* LAT data revealed that J1544+4937 emits pulsed γ-ray emission (Bhattacharyya et al., 2013; Smith et al., 2023).

The companion has been detected in optical (Tang et al., 2014) and is thought to be nearly Roche-lobe filling (Mata Sánchez et al., 2023). This system displays total eclipses at 322 MHz, and the TOAs present significant delays around superior conjunction at 607 MHz, with delays reaching more than 10% of the pulsar's spin period (Bhattacharyya et al., 2013). The 1.4 GHz NRT data do not appear to reveal any significant delays around superior conjunction.

NRT monitoring of this object began in early 2013, *i.e.*, soon after the discovery of this pulsar.

PSR J1555−2908

PSR J1555−2908 was found in a search of *Fermi* LAT unassociated sources with the GBT at 800 MHz (Ray et al., 2022). LAT data analysis revealed that the pulsar also emits pulsed γ-ray emission. This pulsar has a period of 1.79 ms, and a DM of 75.9 pc cm^{-3}. For this DM and line-of-sight the YMW16 model predicts a distance of 7.55 kpc, making this pulsar the most distant in our sample.

The minimum companion mass of $0.051\ M_{\odot}$ and orbital period of 5.6 hrs make PSR J1555−2908 a BW pulsar. Optical observations constrained the minimum companion mass to be $0.060 \pm 0.005\ M_{\odot}$, placing the system at the upper limit of what is considered a BW (Kennedy et al., 2022). The companion is severely bloated, with a Roche-lobe filling factor ("measured as the ratio of the stars radius to the L1 point along the line joining both") of $f = 0.98 \pm 0.02$. At 1.4 GHz, this system consistently display eclipses.

Clark et al. (2023) showed by analyzing *Fermi* LAT data that PSR J1555−2908 displays eclipses in γ rays. Eclipses at such short wavelengths indicate that the system is seen nearly edge-on, the derived orbital inclination is greater than 83°. Moreover, analysis of the γ-ray eclipses enabled model-independent constraints on the pulsar mass, estimated to be $m_p = 1.645 \pm 0.065 M_{\odot}$.

NRT monitoring of PSR J1555−2908 began relatively recently, with first observations conducted in mid-2021.

PSR J1628−3205

PSR J1628−3205 was discovered in a survey of *Fermi* LAT unassociated sources at 350 MHz with the GBT (Ray et al., 2012). Pulsations were later detected in the γ-ray data recorded by the LAT, and reported in Smith et al. (2023). This pulsar has a rotational period of 3.21 ms, and a DM of 42.1 pc cm^{-3}, placing the pulsar at a distance of 1.22 kpc according to the YMW16 model.

Its comparatively larger minimum companion mass of $0.109\ M_{\odot}$ and short orbital period of 5 hrs make it a RB pulsar. It is the only RB in our sample. In fact, optical observations by Li, Halpern, and Thorstensen (2014) constrained the companion mass to be larger than $0.161 M_{\odot}$. Contrary to what we wrote in Blanchard et al., 2025, PSR J1628−3205 does display significant eclipses at 1.4 GHz.

Routine monitoring of this pulsar with the NRT began in early 2013.

PSR J1705−1903

PSR J1705−1903 was discovered with the Parkes radio telescope as part of the HTRU survey (Morello et al., 2018). It has a period of 2.48 ms, and a DM of 57.5 pc.cm^{-3}. The YMW16 distance for this DM and line-of-sight is 2.34 kpc. This pulsar is one of the few in this sample that are not detected in γ rays yet. It also does not appear to have any γ-ray counterpart: the nearest source from the *Fermi* LAT 14-Year Point Source Catalog (hereafter 4FGL; Ballet et al., 2023) is 11′ away, and is associated with PSR J1705−1906 (Smith et al., 2023).

It is classified as a BW due to its low minimum companion mass of $0.047 M_{\odot}$ and short orbital period of 4.4 hrs. This system does not display total eclipses in the NRT data at 1.4 GHz, but does display significant delays at superior conjunction. We therefore categorize it as an eclipser.

NRT monitoring on this one started in November 2022. The NRT dataset on this pulsar has the shortest time span among the datasets considered in this study.

PSR J1719−1438

PSR J1719−1438 was discovered with the Parkes radio telescope as part of the HTRU survey (Bailes et al., 2011). It has a period of 5.79 ms, and a DM of 36.8 pc cm^{-3}, placing it at a very close distance of 0.34 kpc according to the YMW16 model. Like PSR J1705−1903, it is currently undetected in γ rays, and there are no 4FGL sources within $1°$ of the pulsar position.

This system has a peculiar status: it is classified as a BW by default, but has an extremely light companion, with a minimum companion mass of $0.001\ M_{\odot}$. The companion is believed to be Jupiter-sized but up to 10 times more dense, around 23 g cm^{-3}. As the companion is likely closer to a planet than it is to a star, it has been suggested that the system could be part of a sub-class of BWs that have a different evolutionary path (Guo, Wang, and Han, 2022), or that it is not a BW at all, but could be the missing link between X-ray binaries and isolated pulsars (van Haaften et al., 2013). It has been searched for in optical (Bailes et al., 2011) but was not detected at the expected magnitude and location.

Computational evolutionary models constrain the companion to be Helium or Carbon rich (Bailes et al., 2011). The exact nature of the companion is yet unknown, but potential progenitors could be a He or C white dwarf (Bailes et al., 2011) or a He star (Guo, Wang, and Han, 2022). This could make PSR J1719−1438 a member of a separate category, different from BWs, in which the companions are usually considered non-degenerate. This system is not known to display eclipses.

PSR J1731−1847

PSR J1731−1847 was discovered with the Parkes radio telescope during the HTRU survey (Bates et al., 2011). It has a spin period of 2.34 ms, and a DM of 106.6 pc cm^{-3}, the largest in our pulsar sample. The YMW16 distance for this object is 4.77 kpc. Interestingly, the pulsar is located only 6.5′ away from a 4FGL source, 4FGL J1731.7−1850, with no known association. Nevertheless, no γ-ray pulsations have been reported from PSR J1731−1847 yet.

The orbital period is 7.5 hrs, and the minimum companion mass is $0.033\ M_{\odot}$, making this object a BW. This system displays eclipses from 1.4 GHz down to at least 700 MHz (Bates et al., 2011).

PSR J1745+1017

PSR J1745+1017 was discovered with the Effelsberg radio telescope in a search for pulsars at the locations of unassociated *Fermi* LAT sources (Barr et al., 2013). It has a rotational period of 2.65 ms and a DM of 24.0 pc cm^{-3}. The YMW16 model places this pulsar at a distance of 1.22 kpc. Unsurprisingly, given the fact that the pulsar was discovered within the confidence region of a LAT source with no known counterpart, the pulsar was detected to emit pulsed γ-ray emission soon after it was discovered (Barr et al., 2013).

With an orbital period of 17.5 hrs and a minimum companion mass of $0.014\ M_{\odot}$, it is classified as a BW pulsar. This system is not known to display eclipses.

PSR J1959+2048

The discovery of the so-called original BW PSR J1959+2048 (also known as B1957+20), was reported in Fruchter, Stinebring, and Taylor (1988) after a detection with the Arecibo telescope in a survey for millisecond pulsars. It has a period of 1.61 ms, and a DM of 21.9 pc cm^{-3}. The YMW16 distance for this pulsar is 1.73 kpc. Pulsed γ rays from this pulsar were detected using LAT data (Guillemot et al., 2012). The latter study also reported on the detection of pulsed X-ray emission using XMM-Newton data, at the 4-σ confidence level. However, new pulsation searches in X-rays using NICER data did not confirm this detection (Ng et al., 2022).

It is classified as a BW, with its $0.022\ M_{\odot}$ minimum companion mass and 9.2 hr orbital period. This system displays eclipses from 430 MHz (Fruchter, Stinebring, and Taylor, 1988) up to the L-band frequency range. The detection of eclipses shed new light upon the mechanism spinning up young pulsars to millisecond rotation periods. While radio eclipses of J1959+2048 have been studied thoroughly (see Main et al., 2018; Lin et al., 2023), the pulsar was also observed to eclipse in γ rays (Clark et al., 2023), indicating that the system is seen nearly edge-on: $i > 84.1°$. Clark et al. (2023) were also able to put constraints on the mass of the pulsar, finding $m_p = 1.805 \pm 0.135\ M_{\odot}$, a higher value than the canonical $1.4\ M_{\odot}$, as for J1555+2908, albeit much lower that the initially inferred 2.4 $M_{\odot}$ (van Kerkwijk, Breton, and Kulkarni, 2011).

PSR J2051−0827

PSR J2051−0827 was the second spider discovered. It was reported in Stappers et al. (1996) after a detection with the Parkes telescope during a survey of the southern sky. It has a spin period of 4.51 ms, and a DM of 20.7 pc cm^{-3} placing it at a distance of 1.47 kpc according to the YMW16 model.

It is classified as a BW, with its minimum companion mass of $0.027\ M_{\odot}$ and 2.4 hr orbital period. This system displays eclipses from 436 MHz (Stappers et al., 1996) up to the L-band. Polzin et al. (2019) showed that the eclipses are not seen at every orbit, and are variable, in duration and in occurrence. Additionally, the centroid of the eclipse is seen to vary in orbital phase over a year-long period (see Fig. 4 of Polzin et al., 2019, for a comprehensive plot of Effelsberg observations of J2051−0827 eclipses). Although these properties are unique among spider pulsars, this uniqueness is to be taken with caution, given the fact that PSR J2051−0827 has been studied much more extensively than most other spider pulsars. PSR J2051−0827 is also known to display rapid variations of its orbital properties (Shaifullah et al., 2016) that might be linked to the above-mentioned variability of the eclipses. Changes in rotation measure during the eclipse (Wang et al., 2023b) and intra-system plasma lensing (Lin et al., 2021) have also been reported for this pulsar. This is also the first (and to this date only) system for which the quadrupole moment of the companion has been measured (Voisin et al., 2020b).

PSR J2051−0827 has been detected to emit pulsed γ-ray emission (Wu et al., 2012; Smith et al., 2023), and its companion has been detected at optical wavelengths (Dhillon et al., 2022).

PSR J2055+3829

PSR J2055+3829 was discovered at 1.4 GHz as part of the SPAN512 survey conducted with the NRT (Guillemot et al., 2019). It has a spin period of 2.09 ms, and a DM of 91.9 pc cm^{-3}. The YMW16 distance for this DM and line-of-sight is 4.59 kpc. The pulsar has not been detected as a pulsed source of γ-ray emission, and there are no γ-ray sources within 1° of the pulsar position in the 4FGL catalog.

It is classified as a BW, with a minimum companion mass of $0.027\ M_{\odot}$ and an orbital period of 2.4 hrs. As can be seen from Fig. 4 of Guillemot et al. (2019), PSR J2055+3829 is observed to display total eclipses at 1.4 GHz.

It has been observed with the NRT since late-2015 with an average observation cadence of one observation every 5.5 days.

PSR J2115+5448

PSR J2115+5448 was discovered with the GBT at the location of a *Fermi* LAT unassociated source (Sanpa-Arsa, 2016). It has a spin period of 2.60 ms, and a DM of 77.4 pc cm^{-3}, for which the YMW16 model predicts a distance of 3.11 kpc. The pulsar was detected to produce pulsed γ-ray emission by analyzing LAT photons (Smith et al., 2023).

It is classified as a BW, with its minimum companion mass of $0.022\ M_{\odot}$ and short orbital period of 3.2 hrs. Analysis of the NRT data reveals that the pulsar displays variable eclipses around superior conjunction, with the radio signal being totally eclipsed during some orbits, and only delayed during others.

Routine monitoring of this pulsar with the NRT began in mid-2015.

PSR J2214+3000

This pulsar was discovered by Ransom et al. (2011) at the location of a *Fermi* LAT source with no known counterparts. It was quickly detected as a pulsed source of γ-ray emission, confirming that it was indeed powering the LAT unassociated source. It has a spin period of 3.12 ms, and a DM of 22.6 pc cm^{-3} placing the system at a distance of 1.68 kpc according to the YMW16 model.

Its orbital period of 10 hrs and minimum companion mass of $0.007 M_{\odot}$ make it a BW system. First detection of the companion has been reported by Schroeder and Halpern (2014). It has not been reported to display eclipses, and the analysis of the 1.4 GHz NRT indeed did not yield any eclipse detection.

PSR J2234+0944

PSR J2234+0944 was discovered at the location of a *Fermi* LAT unassociated source with the Parkes radio telescope (Ray et al., 2012). It was later confirmed to emit pulsed γ-ray emission (see e.g. Smith et al., 2023).

It has a spin period of 3.63 ms, a DM of 17.8 pc cm^{-3}, an orbital period of 10 hrs and a minimum companion mass of $0.008 M_{\odot}$. The YMW16 model places this pulsar at a distance of 1.58 kpc. This pulsar's orbital properties make it a BW-type object.

Investigation of the 1.4 GHz NRT data did not reveal the presence of eclipses, and the pulsar has not yet been reported to display eclipses at other frequencies.

PSR J2256−1024

PSR J2256−1024 was discovered with the GBT as part of a drift scan survey at 350 MHz (Crowter et al., 2020). It has a spin period of 2.30 ms, and a DM of 13.8 pc cm^{-3}. The YMW16 model of free electrons in the Galaxy predicts a distance of 1.33 kpc for this direction and DM value.

The pulsar has been observed in X-rays (Gentile et al., 2014) and has been detected to emit pulsed γ-ray emission (Smith et al., 2023). Optical observations of the system yielded a detection of the companion object (Breton et al., 2013). The pulsar is seen to exhibit total eclipses in the 1.4 GHz NRT data.

PSR J2256−1024 is monitored at the NRT since late-2018.

After presenting the telescope and the spiders that are monitored with it, I will in the next chapter present a first project conducted as part of my thesis: the study of the eclipses of the observed spiders, and their potential links to the geometry of these systems.

Chapter 4

Eclipses of spider systems

∫ Eux, les muages, ils créent à partir de rien, de vent pur, d'un peu d'air et d'eau (de lumière), ils façonnent des étoiles, des lunes planquées dans la voûte, ils t'inventent le temps qu'il fera, ils font pousser des forêts sur des couches de brume.

Abstract

Eclipses are one of the main features of spider systems. The link between the inclination of the system and the observed eclipses has been an ongoing question for two decades now, and the homogeneous and rich NRT dataset provides an opportunity to look at eclipses group properties.

We introduce in this chapter a characterisation based on the ToAs SNR around superior conjunction, finding 8 non-eclipsers, two "shallow" eclipsers (pulsars for which the beam is still detectable at superior conjunction but with a measurable delay), and 8 "total" eclipsers (pulsars that are not detected for a significant fraction of the orbit). The inclination of spider systems is not easy to measure, and is usually quite model-dependent. However, assuming a similar pulsar and companion mass (condition that can be assumed for 17 BWs of our sample), the mass function can be used as a proxy for the inclination. We find that the mass function of eclipsing and non-eclipsing systems are not likely to originate from the same parent distribution. We use a phenomenological model to derive several parameters of the shapes of average eclipses, such as their durations and ingress/egress asymmetries. These parameters allow us to distinguish two categories of "total" eclipsers, the "abrupt" and "progressive". We find evidence showing that the duration of the eclipse (set to zero for non eclipsers) is correlated to the mass function. On the contrary, we find no obvious link between the same duration and orbital inclinations for the system with published measurements. Nevertheless, the small number of available inclinations, which contradict each other in some cases, hinders such searches for correlations.

We also present variations of the eclipses of PSR J1705−1903, where the maximum delay near superior conjunction changes on the timescale of months, adding yet another example of the wide range of variation timescales in spider systems.

4.1 Introduction

This chapter presents the results published in Blanchard et al., 2025, enhanced with further introduction to the project context and stakes.

4.1.1 Motivations and goals for this study

Most spider studies dive deep into the physical phenomena happening during eclipses, but as previously explained in Section 1.4.3, these phenomena vary from one pulsar to the other. However, the NRT sample presented in the previous chapter gives the opportunity of comparing 19 spiders, thanks to the fact that the dataset is very homogeneous. At the central observing frequency of NUPPI, 11 out of the 19 spiders presented in the previous chapter show eclipsing behaviour, however some aspects of the study include non-eclipsers as well.

One important question that this study aims at exploring was the possibility that the observation of eclipses is merely a geometrical feature, rather than a characteristic intrinsic to the systems. This matter was raised by Freire, 2005, who noticed in a sample of spiders that the smallest mass functions belonged to non-eclipsing systems. As given in eq.(2.25):

$$m_f = \frac{4\pi^2}{G}\frac{(a_p \sin i)^3}{P_b^2} = \frac{(m_c \sin i)^3}{(m_p + m_c)^2} \tag{4.1}$$

thus if one assumes a narrow distribution of masses, the mass function is mostly determined by the inclination via the term $\sin^3 i$. This would imply that the non-eclipsers are seen with smaller inclinations, *i.e.* more face-on, than the eclipsing systems. This interpretation is completely compatible with the very first explanation of the eclipse phenomenon given by Fruchter, Stinebring, and Taylor, 1988: if the eclipsing material is blown away from the stellar companion by the pulsar, it should mostly surround the system around the orbital plane and therefore the higher the inclination the more plasma crosses the line-of-sight.

After the numerous discoveries of new BW systems over the last 15 years, Guillemot et al., 2019 re-investigated the mass functions of these systems, finding that the mass function distributions of eclipsing and non-eclipsing objects only have ~ 0.007% probability of originating from the same parent distributions. Figure 4.1 is the Figure 6 of this article, and clearly show the difference in distributions.

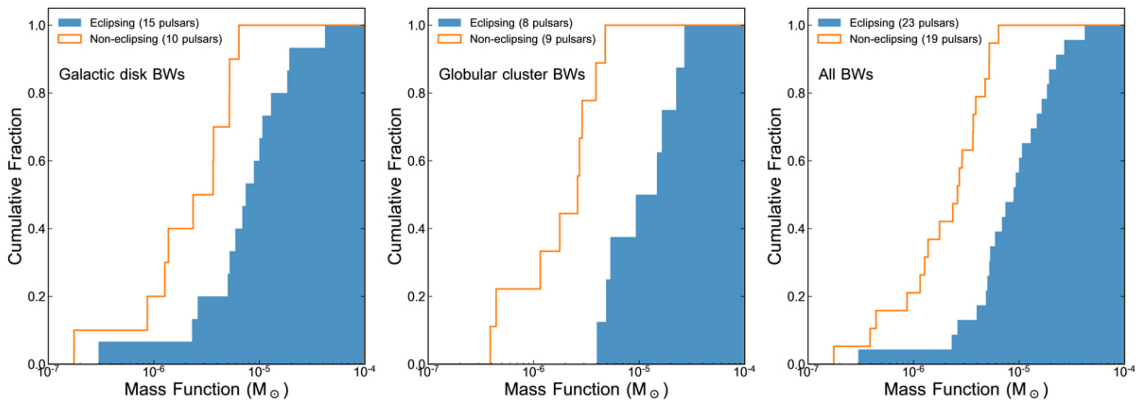

Figure 4.1: Figure 6 of Guillemot et al., 2019: Cumulative histograms of the mass functions of known eclipsing and non-eclipsing pulsars in the Galactic disk (left panel), in globular clusters (middle panel) and for the total population of BW pulsars (right panel).

This work aims at investigating whether the same trend holds for the pulsars in our sample, as well as exploring the possible link between the mass function and the eclipse parameters.

4.1.2 Eclipse characterisation

Depending on the precise geometry of the systems, the radio signal from eclipsing spider pulsars can disappear or get attenuated over a certain phase interval around superior conjunction. The ToA extraction procedure described in Section 3.2 determined ToAs in every 10-min sample of the pulsar observations, independently of whether the pulsar is detected or not. The procedure also determines a SNR associated which each ToA, therefore providing a way of discriminating eclipsing and non-eclipsing spiders: around superior conjunction, pulsars exhibiting eclipses are expected to be detected with lower SNR values than well away from superior conjunction, whereas pulsars that do not have eclipses should be detected with similar SNR values throughout their orbit. Figure 4.2 shows timing residuals and SNR values as a function of orbital phase for PSR J2055+3829.

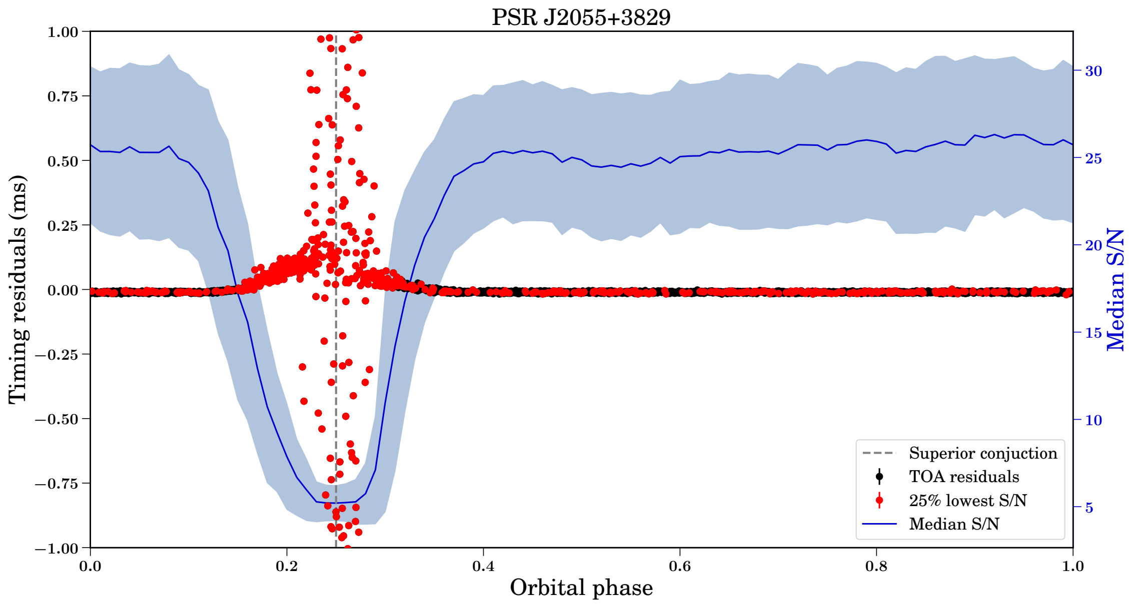

Figure 4.2: Timing residuals and median SNR values as a function of orbital phase for PSR J2055+3829. The ToA residuals are shown as red and black dots, with red dots corresponding to observations with SNR values among the 25% lowest. Error bars, which are much smaller than the vertical scale, are not visible in this figure. The blue curve is the median SNR of the ToAs computed over sliding windows of width 0.1 in orbital phase, and the blue zone shows the median absolute deviation around the median values. The dashed vertical line corresponds to superior conjunction, at orbital phase 0.25.

It should be noted that the data points shown in Figure 4.2 were recorded over more than 23 thousands of pulsar orbits, Figure 4.2 therefore shows the "average" eclipse properties of PSR J2055+3829 in our dataset. Nevertheless, median SNR values for this pulsar are clearly seen to drop around superior conjunction. We thus define PSR J2055+3829 as being an eclipsing pulsar in the 1.4 GHz NRT data, and generally define eclipsing pulsars as those displaying SNR drops around superior conjunction. In Figures 6.4 to 6.6 we show plots of the SNR values as a function of orbital phase for all the pulsars in our sample.

From these plots we classify eclipsers and non-eclipsers as follows: a pulsar is considered an eclipser when the median SNR at superior conjunction is lower than the median SNR away from the eclipse ($\phi > 0.5$) minus the median absolute deviation. With this definition, eight out of 19 spiders of the sample are found to be eclipsers. Those eight pulsars display what we call "total" eclipses, during which the beam is not detectable for a few sub-integrations, leading to very low SNR ToAs. In addition, around superior conjunction the residuals of the eclipsers display a significant delay. These ToAs are usually associated with SNR values lower than those of ToAs well away from the eclipse region, but still higher than the threshold we defined to determine non detections. The additional delay in ToAs that correspond to detections is due to the additional plasma crossing the line of sight.

Nevertheless, three pulsars in our sample display eclipsing behaviour in our data, without strictly respecting the criteria mentioned above for defining eclipsing pulsars. PSR J1124−3653, whose ToA residuals around superior conjunction are not distributed around zero unlike in other orbital phase ranges, appears to display eclipses. However, it is too faint for our eclipse analysis to yield satisfactory results. PSR J1705−1903 displays "shallow" eclipses: the SNR drop for this pulsar is less pronounced than in other pulsars due to the fact that its radio beam is detectable throughout the orbit. Yet, residuals around superior conjunction clearly depart from zero up to approximately 0.5% of its spin period, albeit much less strongly than in other eclipsers. Because the beam is eclipsed by plasma, the eclipsing mechanisms are frequency dependent, and eclipses are more pronounced at lower frequencies than at higher frequencies. This also means that the frequency below which the pulsed signal disappears, called the cut-off frequency, varies from one pulsar to another (it can also vary with time, see e.g. Kumari et al., 2024 for a detailed study of the variation of the eclipse cut-off frequency in PSR J1544+4937). The cut-off frequency in PSR J1705−1903 appears to be lower than that of most known eclipsers, at a frequency below 1.2 GHz. No observations of this pulsar at these low frequencies have been reported, to the best of our knowledge. The third pulsar, PSR J2051−0827, does not display any drop in SNR around superior conjunction. However, its ToA residuals depart from zero, indicating that extra material is traversed by the radio beam. We classify this pulsar as a "shallow" eclipser, like PSR J1705−1903. PSR J2051−0827's eclipses also appear to have a cut-off frequency below 1.2 GHz. This pulsar has been observed thoroughly and displays total eclipses at 660 MHz (Stappers et al., 1996). In conclusion, PSRs J1124−3653, J1705−1903 and J2051−0827 are still considered eclipsers in the rest of the paper, and are flagged as such in Table 3.3.

The legitimacy of averaging eclipses is not a straightforward question. Highly sensitive observations have shown that the eclipse properties of PSR J2051−0827 vary with all sorts of timescales (Polzin et al., 2019): from variations occurring on timescales shorter than 2 days, the shortest time interval between observations, to timescales of years. This pulsar however, as stated previously, does not display "total" eclipses at our observing frequency, but that is to be expected considering its frequency cut-off lower than our observing frequency. However, other spiders in our sample are known to display eclipses at lower frequencies, without having additional delay around superior conjunction. PSR J2051−0827 therefore constitutes a very interesting case, where the pulsar beam is observed throughout the whole eclipse, albeit with an additional delay caused by the eclipsing material. This allows for a fine probing of the eclipsing material, exactly what was studied in Polzin et al., 2019. The second "shallow" eclipser of our sample, PSR J1705−1903, has not been studied as thoroughly as PSR J2051−0827, however during the 3 years of monitoring with the NRT, we noticed some variations in the maximum delay around superior conjunction. This is discussed in Section 4.4.

Due to the above-mentioned peculiarities, the phenomenological fits presented in Section 4.2 did not yield satisfactory results for the very faint pulsar J1124−3653 which is therefore not included in the following discussion, and did not produce optimal results for PSRs J1705−1903 and J2051−0827.

4.1.3 Inclinations of spider systems

In the previous section, the focus on the mass function rather than on the inclination is not innocent. Accessing the inclination directly from timing is not possible for spider systems, as the post-keplerian parameters (for example the Shapiro delay) necessary are not measurable, due to limited timing precision for these objects. The usual method to determine the inclination is the modelling of the companion optical light curve (Breton et al., 2013). Optical light from a spider system is dominated by the companion, the pulsar contributing a very negligible amount, and shows very strong variation correlation with the orbital motion. The luminosity mostly comes from the irradiated side of the companion, thus most of the variations trace the percentage of the visible irradiated side throughout the orbit, but part of the variability also arise from the tidal distortion of the companion. As the "nose" of the companion star is the most irradiated point, in low inclination systems the nose is visible longer hence are variations of the light curve are smaller.

However, these methods depend very much on the models used, and a different irradiation or heat propagation model can drastically change the computation, thus the resulting estimations of masses and inclination are vastly improved by additional independent constraints. This is still the method that gives most of the inclination measurements for spider systems to this day.

We conducted a comprehensive review of published orbital inclinations for the spiders of our sample. The results of this literature review can be found in Table 4.1. Optical modelling can infer multiple parameters, including the inclination of the system, and the Roche-lobe filling factor (denoted f in the Table) of the companion object. This f is generally defined as the ratio between the star radius in the direction of the pulsar and the radius of the Lagrange L1 point. More details are given in Appendix D. The other orbital inclination constraints listed in Table 4.1 were obtained by fitting the eclipses seen in γ rays (Clark et al., 2023) or radio (Du et al., 2023). No constraints on the Roche-lobe filling factor could be obtained from these methods. As can be seen from the table, for some pulsars multiple i and/or f measurements were available in the literature; measurements that are in some cases inconsistent. For four of the eclipsing pulsars in our sample (PSRs J1513−2550, J1705−1903, J1731−1847 and J2115+5448) no inclination or Roche-lobe filling factor constraints have been published, and for two objects (PSRs J2055+3829 and J2256−1024) we found inclination measurements, but no measurements of f.

4.1.4 Mass function distribution for eclipsers and non-eclipsers

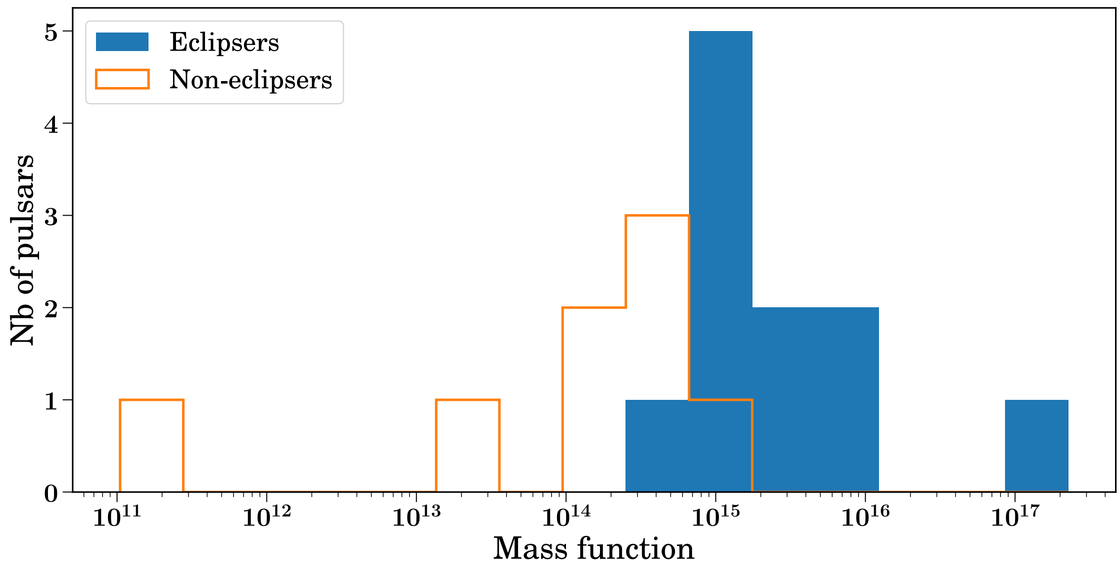

Figure 4.3: Mass function distributions for the pulsars in our sample. As stated in the text, the two extreme values are to be considered separately, however there is a clear distinction between the mass function of eclipsers and non-eclipsers.

Freire (2005) and Guillemot et al. (2019) focused on BW pulsars in their studies. Similarly, our pulsar sample comprises BW pulsars only, with two notable exceptions: first, PSR J1628−3205, which is a RB pulsar and therefore has the heaviest mass function among the sample (see Table 3.3). Given that the mass function scales as m_c^3, and since the masses of RB companions are roughly an order of magnitude larger than those of BW companion objects (by definition of the two categories, see Figure 3.4), the mass functions of RBs are roughly three orders of magnitude heavier than those of BWs. On the other hand, the median companion mass of PSR J1719−1438 is about an order of magnitude lighter than those of other BWs (see Table 3.3 and Sec 3.4 for more

Table 4.1: Published orbital inclinations and Roche-lobe filling factors for the pulsars in our sample. Two different definitions exist for the filling factor f in these articles. Most articles in this Table define f as the ratio of the companion radius at the nose to the L1 radius. These filling factors, whose values are underlined in the table, are denoted by $f_{\rm L1}$ and are those used in the rest of the paper. In certain cases f is defined as the ratio of the volume-averaged stellar radius to the volume-averaged Roche lobe radius. These values of f are denoted by $f_{\rm eff}$. To facilitate comparison we converted estimates when necessary. See Appendix D for details on the conversion. Pulsars marked with a star are those that display eclipses at 1.4 GHz

Pulsar	Inclination, i (°)	Roche-lobe filling factor, f	Reference	Note
J0023+0923	54 ± 14	0.3 ± 0.3	Breton et al. (2013)	$f = f_{\rm eff}$
		$\underline{0.2 \pm 0.2}$		conversion to $f_{\rm L1}$
	77 ± 13	$\underline{0.72 \pm 0.04}$	Draghis et al. (2019)	
	42 ± 4	$\underline{0.36 \pm 0.18}$	Mata Sánchez et al. (2023)	
J0610–2100	$73.2^{+15.6}_{-19.2}$	$\underline{0.86^{+0.08}_{-0.14}}$	van der Wateren et al. (2022)	
J0636+5128	24.3 ± 3.5	$\underline{0.75 \pm 0.20}$	Kaplan et al. (2018)	Values for $M_{\rm p}$ =1.4$M_\odot$
	23.3 ± 0.3	$\underline{0.98 \pm 0.02}$	Draghis et al. (2019)	
	24.0 ± 1.0	$\underline{f > 0.95}$	Mata Sánchez et al. (2023)	
J1124–3653	44.9 ± 0.4	$\underline{0.84 \pm 0.03}$	Draghis et al. (2019)	
*J1513–2550	/	/	/	
J1544+4937	47^{+7}_{-4}	$\underline{f > 0.96}$	Mata Sánchez et al. (2023)	
*J1555–2908	$i > 75$	$\underline{0.98 \pm 0.02}$	Kennedy et al. (2022)	
	$i > 83$	/	Clark et al. (2023)	γ-ray analysis
*J1628–3205	$i > 55$	$\underline{1}$	Li, Halpern, and Thorstensen (2014)	f is fixed and not fitted for
	$i < 82.2$	/	Clark et al. (2023)	γ-ray analysis
*J1705–1903	/	/	/	
J1719–1438	/	/	/	
*J1731–1847	/	/	/	
J1745+1017	/	/	/	
*J1959+2048	65 ± 2	$\underline{0.81 \leq f \leq 0.87}$	Reynolds et al. (2007)	
	62.5 ± 1.3	$\underline{0.90 \pm 0.01}$	Draghis et al. (2019)	
	$i > 84$	/	Clark et al. (2023)	γ-ray analysis
	85.1 ± 0.4	/	Du et al. (2023)	Radio analysis
*J2051–0827	$55.9^{+4.8}_{-4.1}$	$\underline{0.88 \pm 0.02}$	Dhillon et al. (2022)	
	59.5 ± 0.4	/	Du et al. (2023)	Radio analysis
*J2055+3829	46.8 ± 1.6	/	Du et al. (2023)	Radio analysis
*J2115+5448	/	/	/	
J2214+3000	/	/	/	
J2234+0944	/	/	/	
*J2256–1024	68 ± 11	0.4 ± 0.2	Breton et al. (2013)	$f = f_{\rm eff}$
		$\underline{0.3 \pm 0.1}$		conversion to $f_{\rm L1}$

details), so that this object has the lowest mass function among the pulsars in our sample, by two orders of magnitude.

With these caveats in mind, in Figure 4.3, we compare the mass functions of non-eclipsing pulsars with those of the eclipsing ones for the pulsars in our sample. PSRs J1719−1438 and J1628−3205 are located at the two extremes of the distribution plotted in Figure 4.3. The one-dimensional Kolmogorov-Smirnov (KS) test (Press et al., 1992) indicates a probability of ~0.08% for eclipsing and non-eclipsing pulsars, excluding PSRs J1719−1438 and J1628−3205, to originate from the same parent distributions. Our results are thus in agreement with the conclusions of Freire (2005) and Guillemot et al. (2019) for this pulsar sample.

4.2 Phenomenological study of eclipses

As mentioned above, the ToA extraction procedure determined ToAs for every 10 min sample, regardless of whether the observed pulsar is indeed detected in the considered time sample or not. The ToAs in these time samples corresponding to non-detections therefore needed to be discarded from our datasets. We made selections in our timing datasets based on the SNR values associated with the ToAs: as can be seen from Figure 4.2, ToAs with SNR values among the 25% lowest are mostly located in the orbital phase interval corresponding to the eclipse. Figure 4.4 shows the same pulsar residuals once cleaned of the 25% lowest SNR ToAs. For the 10 eclipsing pulsars we discarded ToAs associated with SNR values within the first quartile. This threshold of 25% was chosen as a compromise for the ten considered objects, between the need to eliminate data points corresponding to non-detections while keeping large enough numbers of data points. We also tried cleaning the data using thresholds ranging from 5% to 40%, and found that the resulting fit parameters (describe in the following section) did not vary significantly from about 15% to 35%, hence the decision to apply the same 25% threshold to every system.

We modelled the timing residuals of the pulsars in our sample to determine their average eclipse properties, following a phenomenological approach.

4.2.1 The phenomenological model

For each of the ten pulsars found to display eclipses in the NRT data, we fitted the timing residuals cleaned of the 25% lowest SNR detections to a symmetrical function over a background level:

$$F(\phi) = f_i(\phi)H(-(\phi - 0.25)) + f_e(\phi)H(\phi - 0.25) + b, \tag{4.2}$$

with

$$f_i(\phi) = \exp\left(\frac{\phi - \mu_i}{\tau_i}\right), f_e(\phi) = \exp\left(-\frac{\phi - \mu_e}{\tau_e}\right) \tag{4.3}$$

and H as the Heaviside step function: $H(x) = \begin{cases} 1, & x \geq 0 \\ 0, & x < 0 \end{cases}$.

In the above expressions, b is the background level, corresponding to the average timing residual value away from the eclipse, and the f_i and f_e are the functions used to fit the timing residuals in the ingress and egress phases. Each of the two functions has two parameters: a centroid μ and a characteristic phase τ. Five parameters were therefore fit for each pulsar: b and the μ and τ parameters. The function for the ingress part is fitted to timing residuals at orbital phases from 0 to 0.25, and that for the egress part is fitted to residuals at orbital phases from 0.25 to 0.5. The parameter space was explored using a parallelised affine-invariant Monte Carlo sampling algorithm implemented in the EMCEE library (Foreman-Mackey et al., 2013). Figure 4.4 shows an example of timing residuals as a function of orbital phase around superior conjunction for PSR J2055+3829, along with the best-fit function found from this analysis. Figures showing the fit results for the other analysed pulsars can be found in Appendix B. Results of the fits are summarised in Table 4.2.

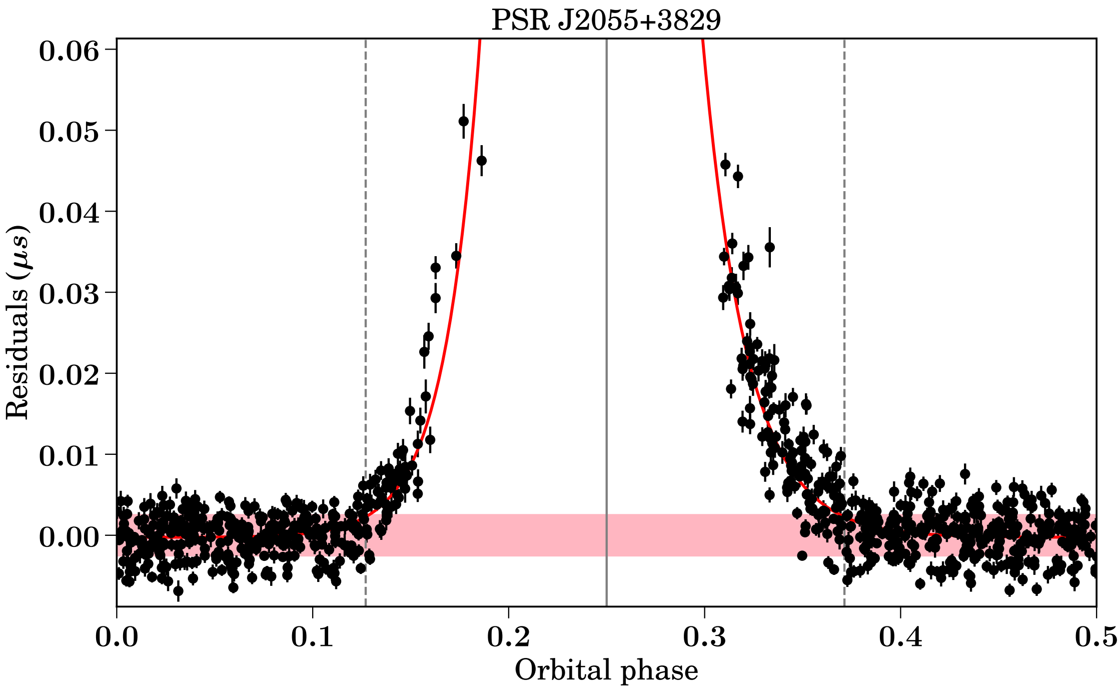

Figure 4.4: Timing residuals as a function of orbital phase around superior conjunction, indicated with a solid line for PSR J2055+3829. The best-fit function obtained from the analysis presented in Section 4.2.1 is shown in red. The light red zone shows the RMS of the timing residuals for orbital phases $\phi > 0.5$, and the dashed vertical lines correspond to the values of $\Phi_{\rm start}$ and $\Phi_{\rm end}$ as inferred from the fit.

Table 4.2: Parameters of the functions describing the eclipse ingress and egress phases. The terms μ and ϕ are orbital phases and therefore have no unit. The three 'abrupt' eclipsers (starred names) have no proper ingress phase; hence, the beginning of the eclipse is taken at the last ToA above the SNR threshold before the superior conjunction, and the τ_i is only an upper limit.

Pulsar	Ingress			Egress		
	μ_i	τ_i (ϕ^{-1})	Φ_{start}	μ_e	τ_e (ϕ^{-1})	Φ_{end}
*J1513−2550	0.37(9)	< 0.01	0.23	0.21(1)	0.019(2)	0.31(1)
*J1555−2908	0.37(9)	< 0.01	0.21	0.242(4)	0.0191(9)	0.37(2)
J1628−3205	0.224(8)	0.024(2)	0.102(4)	0.290(1)	0.0355(6)	0.471(2)
J1705−1903	0.440(3)	0.0461(7)	0.092(2)	0.072(6)	0.041(1)	0.381(3)
J1731−1847	0.20(7)	0.01(1)	0.134(7)	0.3430(5)	0.0123(2)	0.42(2)
J1959+2048	0.260(3)	0.0078(6)	0.21(1)	0.205(3)	0.0231(8)	0.345(7)
J2051−0827	0.346(1)	0.0356(3)	0.1509(7)	0.119(2)	0.0440(5)	0.361(1)
J2055+3829	0.2342(9)	0.0179(2)	0.127(2)	0.236(1)	0.0227(3)	0.3713(5)
*J2115+5448	0.36(9)	< 0.01	0.20	0.236(1)	0.0258(4)	0.352(1)
J2256−1024	0.273(3)	0.0114(6)	0.205(1)	0.211(1)	0.0200(2)	0.3297(5)

Table 4.3: Parameters derived from the results of the fit of pulsar eclipses. For each pulsar we list T_{delay}, the total duration of the eclipse, *i.e.*, the time over which the residuals display an excess delay, T_{obsc} ("obsc" for obscuration), the time over which the pulsar is completely eclipsed, the $T_{\mathrm{obsc}}/T_{\mathrm{delay}}$ ratio, and the ingress/egress slope ratio S and duration ratio D, as defined in Section 4.2.1. Values of T_{delay} and T_{obsc} are expressed in fraction of the orbital period and in minutes. Values of S and D were determined using the values of τ and Φ listed in Table 4.2. In the column category, A stands for 'abrupt', *i.e.*, eclipsers for which the SNR cut-off left no ToAs forming an ingress slope, P stands for 'progressive', meaning eclipsers that display a proper ingress phase, and S stands for 'shallow', meaning eclipsers for which the beam is detectable through the whole orbit.

Pulsar	T_{delay}		T_{obsc}		T_{obsc} / T_{delay}	S	D	Category
	(% P_B)	(min)	(% P_B)	(min)				
J1513−2550	8.3(5)	21(1)	6.4	16.6	0.78(2)	> 0.53	0.38(3)	A
J1555−2908	15.7(2)	52.7(7)	10.5	35.1	0.67(1)	> 0.52	0.331(6)	A
J1628−3205	37.0(4)	111(3)	16.8	50.5	0.456(5)	0.67(6)	0.67(3)	P
J1705−1903	28.9(3)	76.6(9)	0*	0.8	0*	1.13(3)	1.21(3)	S
J1731−1847	29(3)	1.3(1)e+02	21.5	96.4	0.75(2)	1(1)	0.7(2)	A/P
J1959+2048	13.1(2)	72(8)	4.6	25.5	0.353(5)	0.34(3)	0.39(6)	A/P
J2051−0827	21.0(1)	29.9(2)	0*	0.0	0*	0.81(1)	0.90(1)	S
J2055+3829	24.4(2)	45.6(3)	12.3	23.0	0.504(2)	0.79(1)	1.02(2)	P
J2115+5448	15.1(1)	29.5(2)	7.7	15.0	0.508(3)	> 0.39	0.485(5)	A
J2256−1024	12.5(1)	38.2(4)	3.2	9.8	0.258(4)	0.57(3)	0.56(1)	P

4.2.2 Additional fit parameters

From this fit we determined two additional parameters, the values of which are collected in Table 4.2: $\Phi_{\rm start}$, the orbital phase at which the ingress phase begins, and $\Phi_{\rm end}$, the orbital phase at which the egress phase ends. Between $\Phi_{\rm start}$ and $\Phi_{\rm end}$, the best-fit function is above $b + \sigma$, with σ denoting the standard deviation of the timing residuals away from the eclipse phase (in this case, we considered orbital phases larger than 0.5). For "abrupt" eclipses, no data points could be fit in the ingress phase. In these cases, $\Phi_{\rm start}$ was defined as the orbital phase of the last valid data point before superior conjunction.

Measuring $\Phi_{\rm start}$ and $\Phi_{\rm end}$ enabled us to determine eclipse duty cycles, $T_{\rm delay}$, as $T_{\rm delay} = \Phi_{\rm end} - \Phi_{\rm start}$. For each pulsar we also determined $T_{\rm obsc}$, corresponding to the phase interval over which the pulsar is completely eclipsed in our data, which is the duration between the leftmost point with $\phi > 0.25$ and the rightmost point with $\phi < 0.25$. Values of $T_{\rm eclipse}$ and $T_{\rm obsc}$ from our analysis are listed in Table 4.3. In this Table, the values of $T_{\rm delay}$ and $T_{\rm obsc}$ are expressed in fraction of the orbital period and in time. In Table 4.3 we also list slope ratios $S = \tau_i/\tau_e$, and ingress/egress duration ratios D, calculated as $D = (0.25 - \Phi_{\rm start})/(\Phi_{\rm end} - 0.25)$. The closer D is to 1, the more symmetric the eclipse is, and conversely.

The parameter $T_{\rm obsc}/T_{\rm delay}$ is the fraction of the eclipse phase over which the beam is not detectable. The closer to one this parameter is, the shorter the ingress and/or egress phases are before and/or after the flux drops below the detection level. Conversely, a value of zero indicates that the beam is detectable throughout the eclipse.

4.3 Analysis of eclipse properties

4.3.1 Correlations between eclipses parameters

Two categories of eclipsers can be distinguished in Figures 6.7 and 6.8, in addition to the "shallow" eclipsers PSRs J1705−1703 and J2051−0827. On the one hand, eclipsing pulsars displaying no ingress phases, for which the SNR cut-off left no ToAs forming an ingress slope outside the red zone (RMS of ToA residuals far from the eclipse), namely PSRs J1513−2550, J1555−2908 and J2115+5448, and on the other hand, pulsars with a progressive ingress phase, namely PSRs J1628−3205, J2055+3829 and J2256−1024. It is worth noting that two pulsars lie in a grey area between the earlier two categories: PSRs J1731−1847 and J1959+2048. PSR J1731−1847 is the least observed eclipser in our sample, and very few ToAs remained after data selection, making it difficult to probe the ingress region and search for a proper slope in that region. Unlike PSR J1731−1847, the data selection left numerous ToAs in the ingress phase of PSR J1959+2048. However, this one displays a very steep ingress and is seen to eclipse in gamma rays (Clark et al., 2023), similarly to PSR J1555−2908 which also displays an "abrupt" ingress phase. For these reasons, the two pulsars are represented with different colours than others in Figures 4.5 and 4.6.

Looking at Table 4.3, we can notice that eclipse durations ($T_{\rm delay}$) vary widely, ranging from 8.3% up to 37% of the respective orbital periods, as do the obscuration durations ($T_{\rm obsc}$), that range from 0% to 21.5% of the orbital period. These two parameters do not appear to be strongly correlated, as can be seen from Figure 4.5. Nevertheless, it appears from this figure that $T_{\rm obsc}$ seems to be closer to $T_{\rm delay}$ for "abrupt" eclipsers, represented as blue circles, than for those classified as being "progressive" eclipsers, shown with red diamonds. In this regard, PSR J1731−1847 bears resemblance to "abrupt" eclipsers, while PSR J1959+2048 shows similarities with "progressive" eclipsers.

In addition, it can be seen from Table 4.3 that most duration ratios D are found to be smaller than one for this pulsar sample, meaning that these objects have longer egress phases than ingress phases. This is not the case for PSRs J1705−1903 and J2055+3829, as can be seen from Fig 6.7: the eclipses of these pulsars are asymmetric but with longer ingress phases.

From the upper panel of Figure 4.6 we can notice a very rough trend of negative correlation between the symmetry parameter D and the fraction of the eclipse over which the beam is not detectable, $T_{\rm obsc}/T_{\rm delay}$, with abrupt eclipsers displaying larger $T_{\rm obsc}/T_{\rm delay}$ and lower D values,

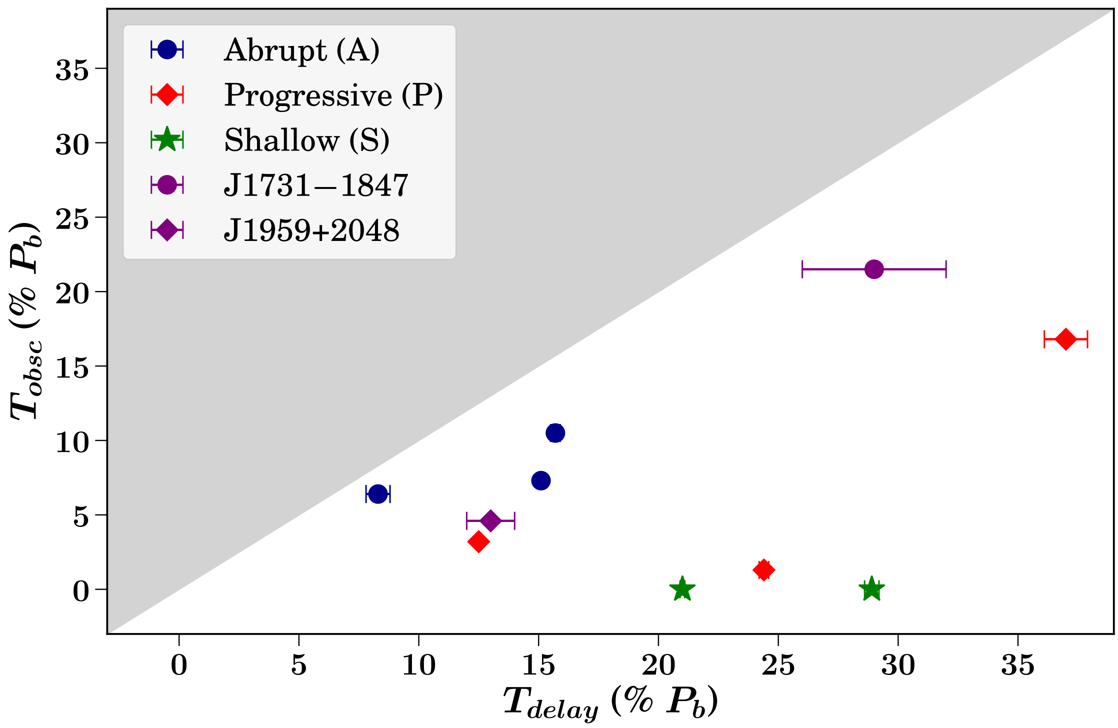

Figure 4.5: Obscuration duration ($T_{\rm obsc}$) against delay duration ($T_{\rm delay}$). The grey zone line is the 1:1 line. An eclipsing pulsar on this line would have no ingress and egress phases. The further a pulsar is from this line, the smaller is the fraction of the eclipse over which the beam is not detectable. Colours and shapes depend on the classifications, as given in Table 4.3: blue circles correspond to the "abrupt" eclipsers, PSRs J1513–2550, J1555–2908 and J2115+5448, red diamonds are the "progressive" eclipsers, PSRs J1628–3205, J2055+3829 and J2256-1024 and green stars are the "shallow" eclipsers, namely PSRs J1705–1903 and J2051–0827.

progressive eclipsers having intermediate $T_{\rm obsc}/T_{\rm delay}$ and D values, and shallow eclipsers having high D values and null $T_{\rm obsc}/T_{\rm delay}$ ratios. The difficulty to assign PSRs J1731–1847 and J1959+2048 one of the classifications given in Table 4.3 is clear from this figure, since PSR J1731–1847 has a high $T_{\rm obsc}/T_{\rm delay}$ value and an intermediate D value, while PSR J1959+2048 has an intermediate $T_{\rm obsc}/T_{\rm delay}$ value and a low D ratio. This porosity between the two categories is not surprising, because of the strong frequency dependence of eclipsing behaviour: for instance, some pulsars classified as "progressive" eclipsers at 1.4 GHz could appear as "abrupt" eclipsers at lower frequencies, where eclipses become more abrupt and obscuring phases become longer. It could be that the three categories we have distinguished in fact belong to a spectrum of eclipse behaviours.

Finally, slope ratios S are found to be smaller than 1 in almost all cases, corresponding to ingress phases that are generally steeper than the egress phases. In the case of the "abrupt" eclipses, values of the S parameter have large uncertainties. For these objects, the SNR cut left no ToAs in the ingress region, resulting in ingress slopes being difficult to measure accurately. The fit found slope values of 0.01 ± 0.01, leading to uncertain S parameter values. Otherwise, we note from the lower panel of Figure 4.6 that the ingress/egress slope ratio S shows, similarly to the D parameter, a trend of negative correlation with the fraction of the eclipse over which the beam is not detected, $T_{\rm obsc}/T_{\rm delay}$; however the sample is too limited to be conclusive.

4.3.2 Dependence of eclipse parameters on mass function

In Section 4.1.4 we showed that the non-eclipsing pulsars in our sample tend to have lower mass functions than the eclipsing ones, suggesting that eclipsing pulsars are indeed seen with higher

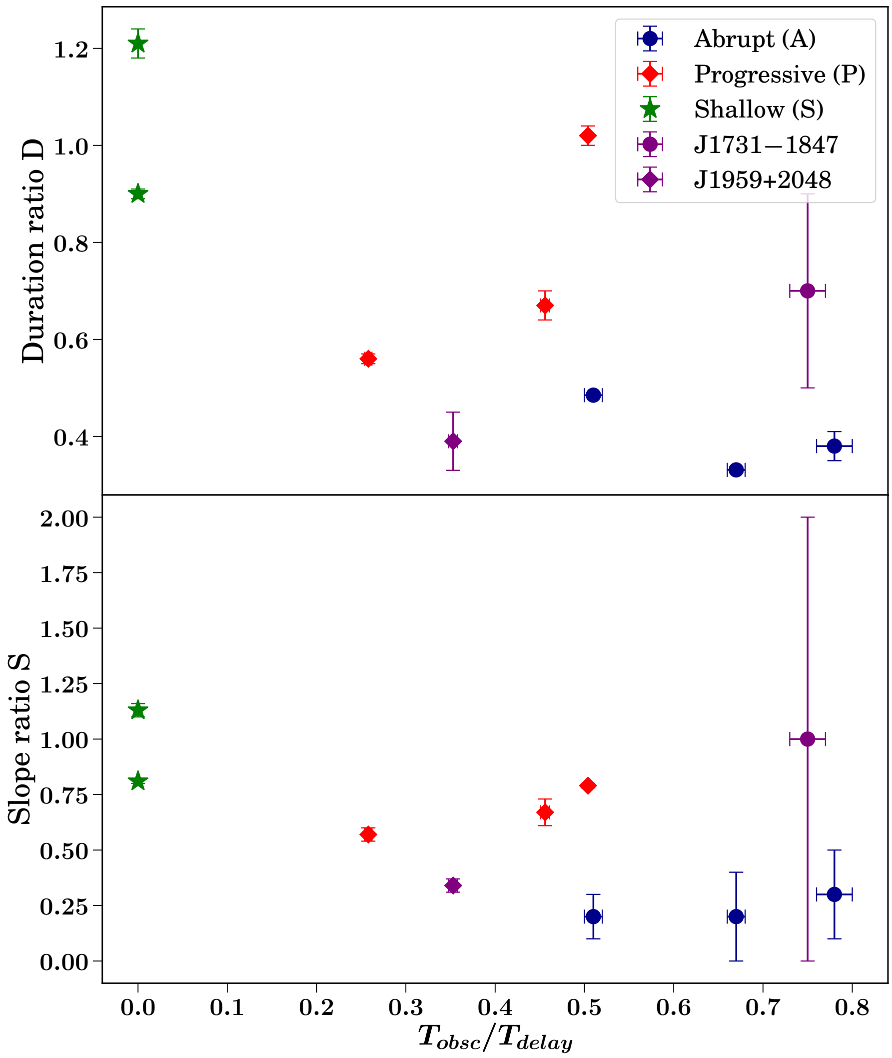

Figure 4.6: Ingress/egress duration ratio D and ingress/egress slope ratio S as a function of the $T_{\rm obsc}/T_{\rm delay}$ ratio. This ratio is the fraction of the orbit over which the radio beam of the pulsar is not detectable. Values of S and D can be found in Table 4.3. Colours and symbols are the same as in Figure 4.5.

inclinations. Beyond the detection or non-detection of radio eclipses at superior conjunction, the coherent analysis of the eclipse properties of the pulsars in our sample, as presented in Table 4.3, provides an opportunity to address the question of the dependence of eclipse parameters on viewing geometry. More specifically, lower inclinations should result in less eclipsing material crossing the line of sight, leading to shorter eclipses, if any.

In Figure 4.7 we plot a number of eclipse parameters determined from the analysis described in Section 4.2.1, against mass function. We observe no particular trends in the $T_{\rm obsc}$, $T_{\rm obsc}/T_{\rm delay}$, and duration ratio D parameters as a function of mass function. This is confirmed by the Spearman correlation coefficients (Spearman, 1904) of 0.5 found for these three panels, indicating a low to moderate (Hinkle, Wiersma, and Jurs, 1979) correlation. We also observe no particular differences in this figure between the three classes of eclipsing systems, other than those already mentioned in Section 4.2.1.

However, the top-left panel of Figure 4.7 hints at a linear correlation between $T_{\rm delay}$, the total duration of the eclipse, as a function of mass function. In this panel we included PSR J1124–3653, which is seen to eclipse but for which, as mentioned in Section 4.1.2, our phenomenological fits did

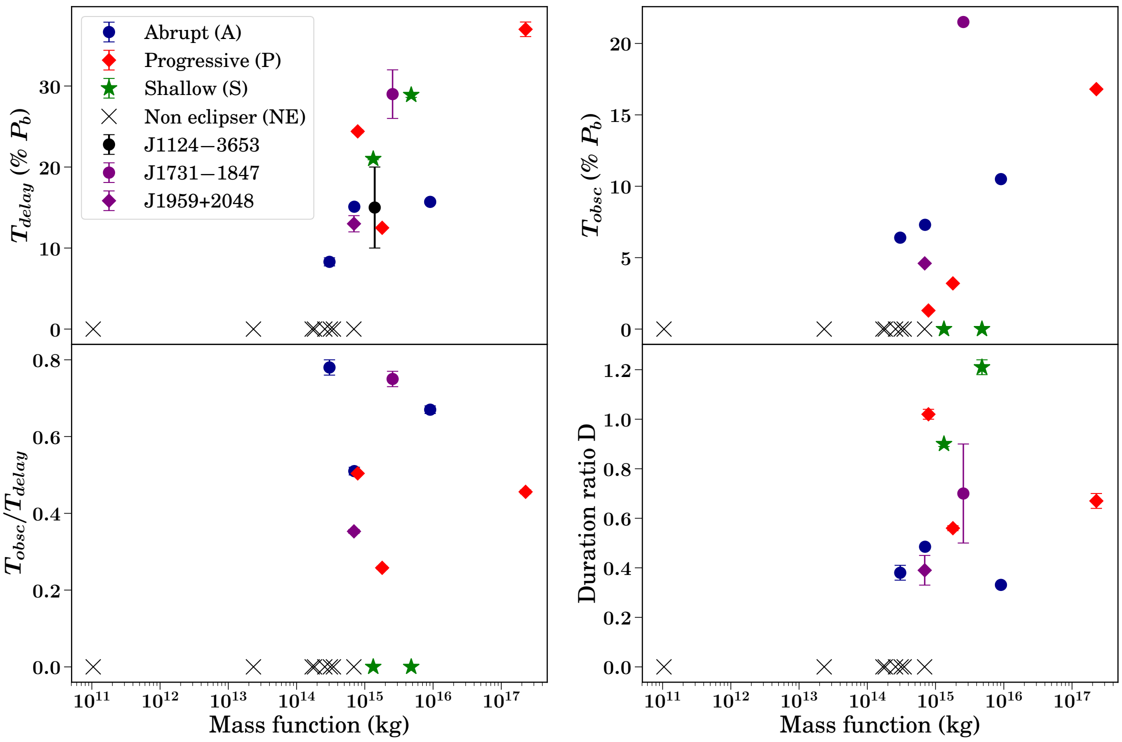

Figure 4.7: Eclipse parameters as determined from the phenomenological fits made in Section 4.2.1 as a function of mass function values. As in Figures 4.5 and 4.6, we respectively represent "abrupt", "progressive" and "shallow" eclipsers with circles, diamonds, and stars. Crosses represent non-eclipsing systems.

not yield satisfactory results. From a visual inspection of Figure 6.4 we conservatively estimated T_{delay} to be about $15 \pm 5\%$ of the orbital period. For the sub-sample of 10 eclipsing BWs (excluding the RB pulsar J1628−3205), we find a Spearman correlation coefficient (Spearman, 1904) of 0.6. This coefficient indicates a moderate correlation, with a p-value of ~10% , the p-value in this test being the probability of an uncorrelated system producing datasets that have a Spearman correlation at least as high. With the entire sample of 17 objects (10 eclipsers and 7 non-eclipsers, excluding PSRs J1719−1438 and J1628−3205), and setting T_{delay} to 0 for non-eclipsing systems, the coefficient becomes 0.8, with a p-value of ~0.04%. This high correlation coefficient seems to suggest that eclipsing pulsars with lower mass function values have shorter eclipses, and vice versa, as could be expected under the hypotheses mentioned above. A larger pulsar sample is required to confirm this possible trend.

4.3.3 Dependence of eclipse parameters on orbital inclination

In Sections 4.1.4 and 4.3.2 we searched for correlations between eclipse properties and mass function values, arguing that since the mass function scales as $\sin^3 i$, it can be used as a proxy for the orbital inclination. However, for some of the pulsars in our sample, actual orbital inclination measurements have been published, which allows us to test our hypothesis that the presence of eclipse is at least partially a question of system geometry more directly.

As explained in Section 4.1.3, we conducted a comprehensive review of published inclination measurements for our spider sample, which are listed in Table 4.1. In Figure 4.8 we plot the eclipse parameters presented in Table as a function of orbital inclinations i and Roche-lobe filling factors f found in the literature. Both eclipsers and non-eclipsers are shown in Figure 4.8, with fit parameters set to 0 in the case of non-eclipsers. In cases where multiple i and/or f constraints were available, we plotted each individual measurement. We note that the inclinations and Roche-lobe

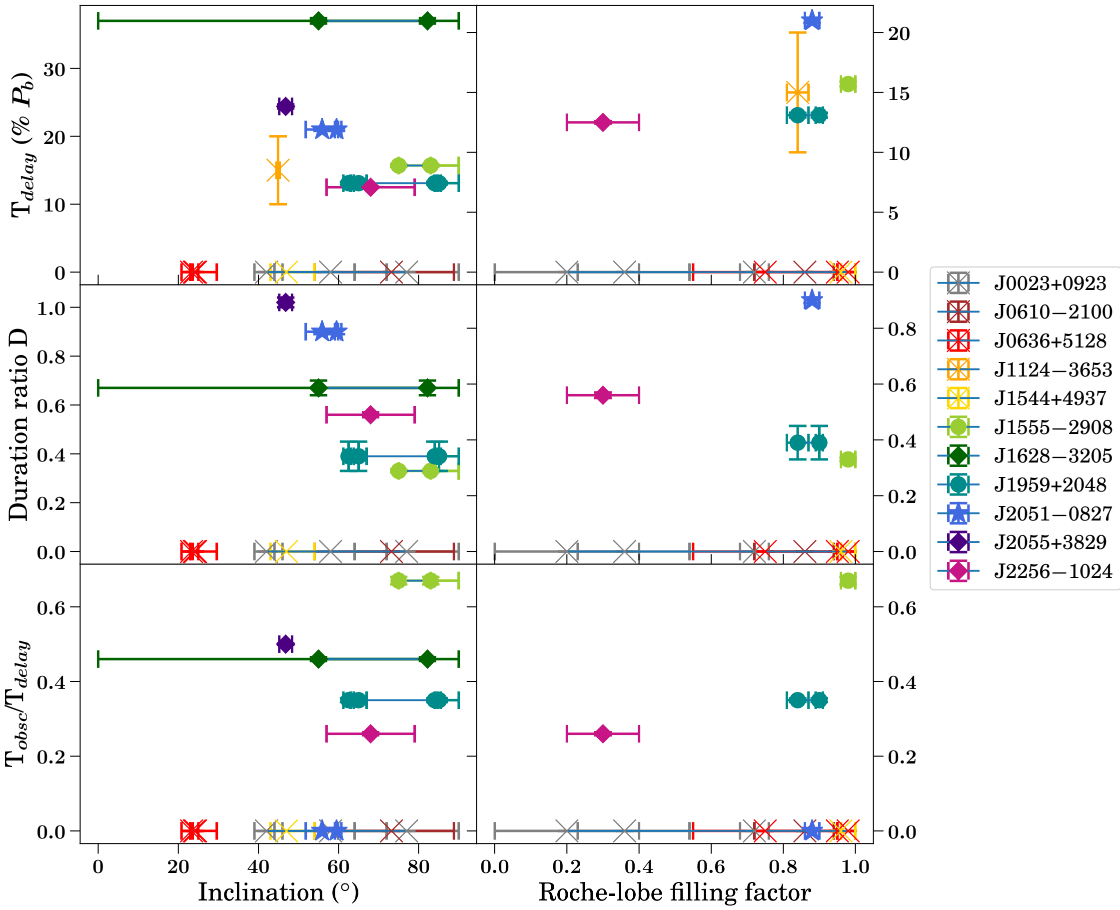

Figure 4.8: Comparison between the results of the phenomenological fits made in Section 4.2.1 and summarised in Table 4.3 and the published inclinations and Roche-filling factors listed in Table 4.1. The symbols are the same as in Fig 4.5 and Fig 4.6: circles correspond to the "abrupt" eclipsers, diamonds are the "progressive" eclipsers, and stars are the "shallow" eclipsers. Crosses are for non-eclipsing systems.

filling factors of non-eclipsing pulsars almost span the entire allowed ranges, albeit with large uncertainties. Especially, it seems to be the case for non-eclipsing pulsars, which could contradict our conclusions in the previous Section 4.1.4, however the discrepancies between different measurements for the same pulsar, the uncertainties, and all these measurements caveats explained in Section 4.1.3 undermine the credence of the conclusion drawn based on the inclination measurements. It could be interesting to note however that that all systems eclipsing at 1.4 GHz except for PSR J2256−1024 are nearly Roche-lobe filling, and it that no eclipsing pulsar has been measured at a inclination lower than 40°, except for PSR J1628−3205 for which the uncertainties actually span all possible values.

As for searching correlations, contrary to Figure 4.7, no obvious link can be found between the eclipse parameters we determined and the orbital inclinations and/or Roche-lobe filling factors, except for maybe a faint trend in the middle left panel that seems to indicate that the eclipses are more asymmetric when the system is seen at higher inclination. This is not seen when comparing the same duration ratio D with the mass function (bottom right panel of Figure 4.7) however, but could be interpreted as the evaporation cloud asymmetric tail/nose shape being more pronounced when observed more edge-on than from the top of the orbital plane. This lack of correlations is aggravated by the fact that few of the eclipsers in our sample have i and f measurements, with only seven of the eclipsers having measured orbital inclinations and five having Roche-lobe filling factor estimates. The sample of four objects with both i and f estimates is too small to draw any conclusions at present, but it can serve as a starting point for future studies, when more radio and/or optical studies of eclipsing spiders have been conducted.

4.4 Eclipse variation timescales: the case of PSR J1705−1903

Over the course of my PhD, the close monitoring of every system led to the discovery that one system displays interesting eclipse variations. We here describe these variations, not presented in Blanchard et al., 2025.

PSR J1705−1903, as stated previously, is a "shallow" eclipser, meaning that the pulsar beam crosses through the eclipsing material at every orbit. The resulting additional delay in the residuals is of the order less than 1% of the pulsar spin period, while non-"shallow" eclipsers tend to have additional delay of the same order of magnitude than the spin period. This small additional delay is not accompanied by a visible flux variation, contrarily to regular eclipses. This could suggest a very low density cloud, with very little matter crossing the line of sight. The "total" eclipses do not allow for a monitoring of the delay inside the eclipse, but the edges are seen to vary, although the variations are small enough in our dataset that we could determine J1705-1903's eclipse properties by analysing its average eclipse, as we did for other pulsars. However for the "shallow" eclipses of PSR J1705−1903, the very small delay allows a much finer monitoring of the plasma crossing the line-of-sight.

This pulsar is monitored by the NRT since October 2022, and for the first two months displayed the previously described shallow eclipses. From December 24$^{\text{th}}$ 2022, the NRT was inactive, which prevented us from observing over two months. Late March, when the telescope was operational again, the delay in the residuals was nearly zero, as if the pulsar no longer displayed eclipses.

The eclipsing turned on again in the following months, but until now the delays never reached the level of 2022 eclipses. This is visible in Figure 4.9, in which are plotted ToAs from 2022 and 2023.

This shows a variation timescale of months, similar to that found in the case of PSR J2051−0827, where "spikes" of DM are seen to last for several months (Polzin et al., 2019). This seems to be a similar event, maybe caused by an increase in the companion mass ablation. Figure 4.10 shows the evolution of the maximum delay of recorded eclipses.

Some investigations could be conducted in the future about these variations. One possibility would be to try to estimate a difference of plasma density between the "high" and "low" eclipses, as the additional delay can be converted into an additional DM along the line of sight. This could be tied under certain assumptions to the evaporation rate of the companion, in the same way as done

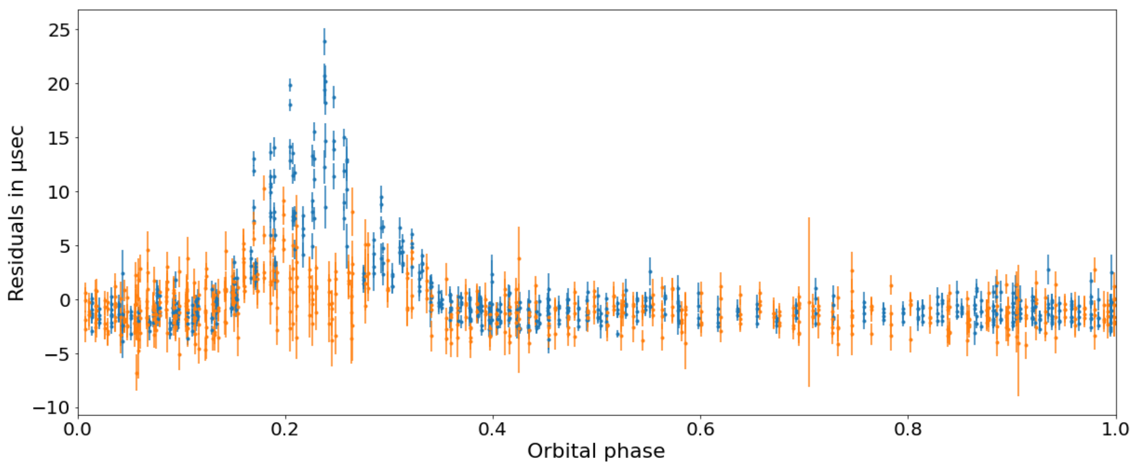

Figure 4.9: Timing residuals of PSR 1705–1903. The blue (resp. orange) residuals correspond to ToAs measured in 2022 (resp. 2023).

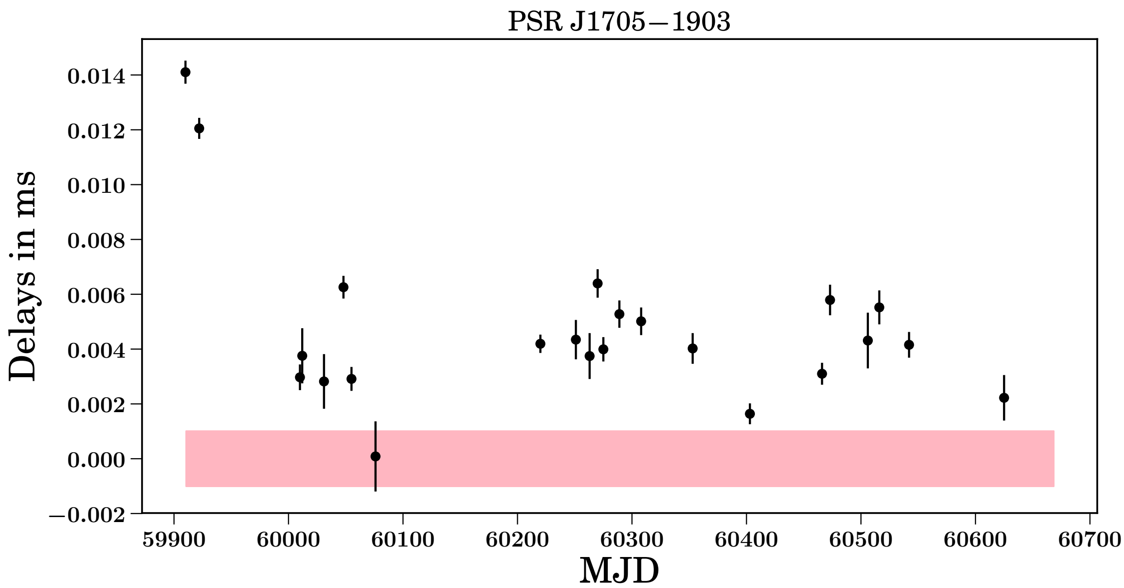

Figure 4.10: Evolution of the maximum delay measured during eclipses of PSR J1705–1903. The delays plotted correspond to those of the ToAs closest to the superior conjunction for each observation covering orbital phases $0.2 < \phi < 0.3$. The light red zone shows the RMS of the timing residuals for orbital phases $\phi > 0.5$.

in Polzin et al., 2018. Moreover, there seems to be a hint of periodicity in Figure 4.10, therefore another possible exploration, tied to the eclipse study presented in the previous sections, would be to compute the "instantaneous" mass function at each orbit, and to use this as a proxy for the inclination, to watch for signs of precession of the orbital plan, which can appear for non spherical objects. In this case the variations in the depth of the eclipse would be an effect of the variations in the width of the eclipsing cloud crossed by the line of sight. Another possibility might that the companion is nearly filling its Roche lobe, and some pseudo-periodic bloating of the companion star would overflow it, leading to more matter being blown away by the pulsar wind.

4.5 Conclusions and prospects

In the previous Sections 4.2 and 4.3, we presented a phenomenological fit of the ToA residuals around superior conjunction for all eclipsing pulsars in our sample except PSR J1124−3653, as mentioned above. Eclipse properties appear to vary widely, with eclipse duty cycles ranging from 8% to 37% of the orbit for the objects in our sample and intervals of complete obscuration ranging from 0% to 22%, with no apparent correlation between these two parameters. We further distinguished two categories of eclipsers in addition to the "shallow" eclipsers mentioned above. On the one hand, eclipsing pulsars display no ingress phases, namely, PSRs J1513−2550, J1555−2908, and J2115+5448; hence, we categorised them as 'abrupt' eclipsers. On the other hand, we categorised pulsars with more progressive ingress phases, namely, PSRs J1628−3205, J2055+3829, and J2256−1024, as "progressive". PSRs J1731−1847 and J1959+2048 are more difficult to firmly categorise with the present data, as they display characteristics seen in both the "progressive" and "abrupt" categories. We found that most ingress/egress slope ratios, S, and duration ratios, D, are smaller than one, meaning that eclipses generally have longer egress than ingress phases and that ingress phases are steeper than the egress phases. We found indications for a negative correlation between D (or S) and the fraction of the eclipse during which the beam is not detected; however, the pulsar sample is too small for the correlation to be firmly established.

The physical interpretation of the three categories is somewhat speculative, as the categories are based on the shape of the timing residuals. This shape, mainly the duration during which the residuals depart from the baseline, gives us information about the width of the plasma cloud perpendicular to the line-of-sight. The level of the residuals could under some assumption be converted to excess DM and excess electron column density, and therefore give information about the depth and/or the density of the cloud, i.e. information in the direction of line-of-sight. The shallow eclipses do not have duty cycles shorter than the other types, thus they could be caused by plasma clouds that are less dense or less deep but not necessarily smaller in width. The abrupt eclipsers have short excess delay duty cycles, but tend to have ratios of total obscuration and excess delay durations close to one (see Figure 4.5), which could indicate shorter but denser clouds.

As explained in this chapter's introduction, eclipse properties are likely to depend on viewing geometry. We searched for correlations between some of the eclipse properties determined from the phenomenological fits and the mass functions of the systems, assuming that the mass function can be used as a proxy for the inclination. We found that the mass function distributions of eclipsing and non-eclipsing systems have a low probability of originating from the same parent distributions, in accordance with previous studies. We also found marginally significant evidence for a positive correlation between eclipse durations and mass functions, suggesting that larger sections of the eclipsing material cross the line of sight in systems with high orbital inclinations.

To further the exploration of this correlation, we conducted a comprehensive review of published orbital inclinations and Roche-lobe filling factors for the pulsars in our sample, and searched for trends between these parameters and the eclipse parameters. Contrary to the previous comparison, no correlations were found. Nevertheless, the limited pulsar sample, the paucity of available orbital inclination and Roche-lobe filling factor measurements for these pulsars, and the fact that the results for a given pulsar often contradict each other hindered such correlation searches.

We argue that a systematic orbital inclination and Roche-lobe filling factor measurement campaign, with a common analysis methodology, would be highly beneficial. Analyses of large samples of pulsars similar to the systematic study presented in our article would also be beneficial. In the future, we will look into extending our study to include data taken with other telescopes using a similar methodology, with the goal of increasing the sample of pulsars with eclipse fits and comparing their properties with those determined at other wavelengths.

Moreover, the variability of the eclipses, as seen in the eclipses of PSR J2051−0827 studied by Polzin et al., 2019 and of PSR J1705−1903 presented in Section 4.4, could suggest that "total" eclipsing systems display variation of the edges of the eclipses, and that the phenomenological study could be applied to individual observations to track the variations of the shapes of ingress and egress phases, but this might be reserved to the brightest pulsars of our sample or observations conducted with more sensitive instruments.

Chapter 5

Searching for planets around binaries

∫ Orpailleur du ciel, braconnier des rues, pêcheur de nuage, chercheur, piégeur, les termes abondent.

Abstract

The very first exoplanet found was orbiting a pulsar, however after nearly 50 years of pulsar observations only a handful of pulsar planets have been confirmed. There are however, a few serious candidates of pulsars harbouring planets. These planets can orbit an isolated pulsar or a pulsar in a binary with another star, such as a spider. In this case, the triple system is considered hierarchical, as the inner orbit is orders of magnitudes smaller than the outer orbit, which means that no interactions are expected to destabilize the system.

We try in this chapter to constrain the orbital parameters of the planets orbiting PSRs B1620−26, J1745+1017 and J2115+5448, using two different methods: the first one is a computation of the orbital parameters from the five first spin frequency derivatives, following the calculations of Joshi and Rasio, 1997, the second is the direct pulsar timing using ephemerides with two independent orbits. The first method did not yield satisfactory results, but the second is more promising. Overall, our solutions for the two spider systems tend to find small, planet size objects, orbiting a few astronomical units away from the inner binary. The solution for PSR B1620−26 is very poorly constrained and the current best solution indicates an orbital period of several centuries, and an outer companion mass slightly below a tenth of that of the Sun. The solution for PSR J1745+1017 is more promising, the best solution being a $0.13 M_\oplus$ (where $M_\oplus$ is the Earth's mass) planetary companion in a very eccentric ($e \sim 0.9$) 5200-days orbit. This result means that the NRT monitoring campaign covers the full orbit or most of it, which gives more credence to this solution. Moreover the resulting ephemeris seems to fold the *Fermi-LAT* data correctly, which is a good confirmation of the radio analysis. The result for PSR J2115+5448 is very preliminary, but the current best solution indicates a $\sim 8 M_\oplus$ companion in a rather eccentric ($e \sim 0.5$) orbit of period > 8000 days. In this case the NRT coverage would be $\lesssim 40\%$, which might not be enough, as the resulting ephemeris clearly fails to fold the *Fermi-LAT* data correctly, which is about twice as long as the NRT data for this pulsar.

5.1 Introduction

5.1.1 Pulsar planets: a long history of hunting

A conference named *Planets around pulsars* was held at Caltech on April 30$^{\text{th}}$ and May 1$^{\text{st}}$ of 1992, only four months after the simultaneous announcement and publication of the discovery of the planetary system orbiting PSR J1300+1240 (or B1257+12) (Wolszczan and Frail, 1992). If this system has been remembered as the first pulsar with planets discovered, it is far from being the first pulsar with planets claimed. The discussion about pulsar planets started more than 20 years prior, with the report by Richards et al., 1970 of quasi-sinusoidal oscillations in the timing of the Crab Pulsar. The oscillations had a period of about 77 days, and were interpreted as an Earth-mass planet orbiting the pulsar in a ~ 0.4 astronomical units (AU) circular orbit. These oscillations were subsequently showed not to be periodic, and the putative planet was in fact *timing noise*. If this was less exciting from the perspective of system formation studies, it was a major discovery for pulsar astronomers and NS scientists. This planet false alarm however prompted other teams to inspect their own data for evidence of a planetary companion. In 1979, Demianski and Proszynski, 1979 reported that PSR B0329+54 displayed a timing signal corresponding to a ~ $0.1M_{\oplus}$ object in a 3-year orbit, which was proved to be timing noise later. Finally, Bailes, Lyne, and Shemar, 1991 proposed PSR B0329+54 as another candidate for a pulsar with a planet, but retracted their claim the following year, in the same conference and a few hours before the announcement by Wolszczan and Frail. The striking characteristics of this system was that not one but two planets of ~ $4M_{\oplus}$ were discovered, orbiting the pulsar in 66 and 98 days. This is also the first ever discovered exoplanet system, a tremendous milestone in modern astronomy. This highlights the sensitivity of the pulsar timing technique. Two years later, a third body as light as the Moon was discovered (Wolszczan, 1994). To this day, this system is the only pulsar with multiple planets confirmed.

This was the context of the conference *Planets around pulsars*, the proceedings of which (Phillips, Thorsett, and Kulkarni, 1993), is the main source for this section. Even is this conference happened very shortly after the discovery of this first planetary system, the number of formation models put forth during this meeting is not a surprise, considering the long history of researches for such systems.

There are two families of in-situ formations, either pre- or post-SN, and captures. The in-situ pre-SN formation scenario or "planet survival model" as called in Podsiadlowski, 1993, would favour long period orbits, so that the planet survives the bloating envelop stage of the progenitor star, and the SN blow in itself, which comes with several severe problems. Post-SN formation would involve a protoplanetary disk, which could come from the debris of the SN (Lin, Woosley, and Bodenheimer, 1991), the collision between the newly formed NS and a former stellar companion (Hirai and Podsiadlowski, 2022) or a disk that surrounded the XRB before the SN and that stayed bounded to the pulsar (Podsiadlowski, 1993). Overall, disk scenari give birth to planets with rather circular orbits. Capture processes conveniently avoid the problem of the SN survival. The capture can be that of a planet orbiting another star which has a decent probability of happening in a globular cluster but less so in the Galactic disk (Sigurdsson et al., 2003), or a free-floating planet (Miret-Roig et al., 2022). The capture would favour eccentric orbits.

As of 2025, the number of pulsar planets in itself is a debate. A recent meta review (Laycock and Christodoulou, 2025) found 4 planetary systems accepted by most, and an additional 16 claims. However in these 20 potential planetary systems many different configurations are seen, hence a single formation channel is unlikely to explain all findings. Moreover, due to one common planet definition of any body with a mass smaller than 10 Jovian masses, many (8 out of 20) are BW systems, in which the stellar companion is very light. Two of these BWs are included in the NRT spider sample (namely PSRs J0636+5128 and J1719−1438). Five out of the 20 are retracted or questioned claims, and 3 have a measured orbital period suspiciously close to the observation time. This leaves very few currently confirmed planets, the best claim still being those of the original system discovered by Wolszczan and Frail, 1992.

5.1.2 Motivations and goals for this study

The presence of a body orbiting a pulsar is detectable as the gravitational pull of said body induces a small motion of the pulsar around the common centre of mass. This motion is observed as a cyclic Doppler shift applied to the pulsar's spin frequency f. For most binaries these cycles are relatively short and over a few years can be clearly identified. Moreover, the vast majority of known pulsar companions are of stellar mass, which ensures that the amplitude of the motion is large enough not to be missed. In the case of planets however, the signal is much fainter, and should the orbit be much longer than the typical monitoring time, tracking the body can be a difficult exercise. In the specific case of planets orbiting spider binaries, an additional problem is the timing noise caused by instabilities of the internal orbit. However a recent paper proposed that a planet could orbit a BW, in a hierarchical triple system (HTS). Nieder et al., 2022 noted instabilities in the *Fermi-LAT* timing of PSR J1555−2908, and found that a Mercury-mass ($0.02 M_\oplus \lesssim M_o \lesssim 0.06 M_\oplus$) outer companion orbiting around the inner binary with an orbital period of ~ 4500 days could account for this noise. Moreover, two other systems, PSRs J1745+1017 and J2115+5448 are known to harbour planets in HTS but in the case of PSR J2115+5448 the orbit is poorly constrained. Both systems are observed by the *Fermi-LAT*, and therefore are also studied by the team that published the Nieder et al., 2022 article. Because the orbits of the planets are so wide, having a dataset as long as possible is key to constrain the parameters. The *Fermi-LAT* data span is of about 17 years at the time of writing, making this dataset very interesting for such searches. Because the *Fermi-LAT* is doing a continuous all-sky survey, when a pulsar is found at a location where the telescope sees a source, the finding of pulsations at this location retroactively gives access to the full *Fermi-LAT* data span.

It happens that these three systems are also part of the NRT spider sample, which also have a long data span. However, for PSR J1555−2908 the NRT dataset is less than 2000 days long, presumably too short for such searches. We therefore have focused on the two other pulsars J1745+1017 and J2115+5448, respectively observed over 5500 and 3500 days.

In this chapter we will try to constrain the outer orbit of PSRs J1745+1017, J2115+5448 and B1620-26 (or J1623-2631), a non-spider system that will be presented in the next section. We are conducting this work in parallel with Nieder et al., 2022, analysing entirely different datasets, and are in regular communication. Therefore, some of our results will be compared to their non published own findings, that we obtained by private communication.

All the work presented in the chapter is at the time of redaction still work in progress, and has not been published yet.

5.1.3 Examined systems

The following is a brief description of the systems examined and the information available to me about the outer orbit at the beginning of the project. All three sources were chosen because they display a level of timing noise that is far higher than that expected for MSPs and for which no satisfactory explanation has been proposed, other than the possible presence of a planetary companion.

PSR J1745+1017

PSR J1745+1017 is a non-eclipsing binary, sparsely observed with the NRT over more than 15 years or 5500 days, with an average cadence of one observation every 34 days. The monitoring of this pulsar started in May 2010 (on MJD 55232) with the BON backend. Before this project, a 3-body ephemeris was already implemented in the NRT pipeline, making PSR J1745+1017 a good candidate to test a new way of constraining orbital parameters. This ephemeris is preliminary but results in residuals good enough to serve as reference. The inner binary has a relatively simple timing solution, no particular orbital derivatives were needed. Moreover the fact that this system does not display eclipses allows us to use all of the data to search for a more precise timing solution.

PSR J2115+5448

PSR J2115+5448 has been monitored by the NRT since MJD 57158 thus over 3600 days or a little under 10 years. The average cadence is of one observation every 23 days. The system displays wide eclipses (see Chapter 4), thus we have to get rid of nearly 40 % of the data to conduct our planet searches. Similarly to PSR J1745+1017, no 3-body solution was previously published, but in this case we did not have a starting point ephemeris with approximate outer orbit parameters. Nevertheless, this pulsar has a level of timing noise that is very unusual for an MSP and any timing model needs a lot of spin derivatives to keep track of the pulsar's rotation, which led to the conclusion that PSR J2115+5448 likely has a second companion.

PSR B1620−26

PSR B1620−26 (or J1623−2631), is a 11-ms pulsar dwelling in the M4 globular cluster (GC). It has been discovered in 1988, and was the fifth MSP discovered, the second in a globular cluster (Lyne et al., 1988). It is in a 191-days binary with a light ($0.3M_{\odot}$) WD. Soon after its first report, it was clear that a binary model could not account for the pulsar timing noise and that its spin acceleration $\ddot{f}$ was too large (about seven orders of magnitude above the expected value) to be an intrinsic property (Thorsett, Arzoumanian, and Taylor, 1993). Some pulsars in GC display high $\ddot{f}$, because of the acceleration caused by the gravitational field of the cluster, but Phinney, 1993 ruled out this possibility by calculating the maximum expected $\ddot{f}$ and concluding that it would be too small to correspond to the measured $\ddot{f}$. Rasio, 1994 proposed that the inner binary eccentricity could even be explained by secular perturbations from a massive ($\lesssim M_{\odot}$) second companion in a wide (~ $10^2 - 10^3$ years) and eccentric ($e \gtrsim 0.5$) orbit. Evidence piled up in the following years, leading to a general agreement about the presence of a third body. Models of the formation of this system have been presented (see *e.g.* Sigurdsson et al., 2003), but no precise orbital parameters were measured, as the orbit seems to be very long. In 1997, Joshi and Rasio, 1997 presented a method to derive orbital parameters from spin frequency derivatives, and applied it to PSR B1620−26. This method will be presented in the next section, but their result was that the third body was of sub-stellar mass ($0.01 \pm 0.005 M_{\odot}$) and 38 ± 6 AU from the centre of mass of the inner binary (the errors correspond to the 80 % confidence interval). However at this time the timing precision on $f^{(3)}$ and $f^{(4)}$ were not what they are now, and the fifth derivative could not be measured. The latest published timing solution is now 10 years old (Fonseca et al., 2015) and proposed an orbital period of ~ 60 years.

The NRT monitoring of PSR B1620−26 covers more than 7000 days, or 19.5 years.

5.2 Computing orbital parameters

The Joshi and Rasio, 1997 method was developed with the case of PSR B1620−26 in mind, therefore is is particularly relevant for long orbital periods, as the timing can more precisely measure the spin derivatives than orbital parameters. This was the first method we tried for this project. Section 5.2.1 is a summary of this work and refers to it, unless specified otherwise.

5.2.1 Theoretical background

In pulsar timing, the spin frequency derivatives $\dot{f}, \ddot{f}, f^{(3)}$ etc., are basically the coefficients of the Taylor expansion of the spin frequency around a reference epoch. Assuming a value for the pulsar mass, five orbital parameters can be determined: the companion mass m_c, the projected semi-major axis of the companion's orbit a_c, the eccentricity e_c, the argument of the periastron ω_c (measured from the ascending node) and the longitude of the companion at a reference epoch λ_c (measured from periastron). In most Tempo2 timing models, λ_c is replaced by an epoch at which the companion passes at periastron, which is equivalent. In this chapter, the subscript "c" (resp. "p") will refer to the companion (resp. the pulsar), and all orbital elements correspond to the motion around the centre of mass. Similarly to timing, the inclination of the system cannot be derived directly. The biggest caveat of this method (see discussion is Section 5.2.5) is that the acceleration $\dot{f}$ and higher frequencies have to be assumed to be purely induced by the planet orbit, however the observed $\dot{f}$ is a combination of intrinsic spin-down and acceleration:

$$\dot{f}_{obs} = \dot{f}_{acc} + \dot{f}_{int} \tag{5.1}$$

and it is generally not possible to measure the two components separately. However in some cases, it is reasonable to assume $|\dot{f}_{int}| \ll |\dot{f}_{acc}|$, particularly if $|\dot{f}_{obs}|$ is large. Timing noise $\ddot{f}_{int}$ can also sometimes be estimated, but for millisecond pulsars higher derivatives are not supposed to be measurable, if not dynamically induced.

After subtraction of the intrinsic and other known kinematic contribution(s), we can write the derivatives of the pulse frequency as:

$$\dot{f} = -f\frac{\vec{a}\cdot\vec{n}}{c}, \quad \ddot{f} = -f\frac{\dot{\vec{a}}\cdot\vec{n}}{c} + \frac{\dot{f}^2}{f}, \quad \text{etc.} \tag{5.2}$$

where $\vec{a}$ is the acceleration of the pulsar caused by the pull of the second companion, $\vec{n}$ a unit vector in the direction of the line of sight and c the velocity of light. The second term of $\ddot{f}$ is smaller than the first by a factor of $\sim v/c$ where v is the orbital velocity of the pulsar, and can be neglected. We can therefore simplify the expressions as:

$$\dot{f} = -f\frac{\vec{a}\cdot\vec{n}}{c}, \quad \ddot{f} = -f\frac{\dot{\vec{a}}\cdot\vec{n}}{c} \quad \ldots \quad f^{(5)} = -f\frac{\vec{a}^{(4)}\cdot\vec{n}}{c}. \tag{5.3}$$

This forms a system of five non-linear equations with five unknowns (m_c, a_c, e_c, λ_c and ω_c), which needs to be solved numerically.

5.2.2 Method

The basic idea is the following: using more explicit expressions of the spin frequency derivatives we can explore the space parameters of (m_c, a_c, e_c, λ_c and ω_c) to compute the corresponding ($\dot{f}, \ddot{f}, f^{(3)}, f^{(4)}$ and $f^{(5)}$) and find the point in this space where the derivatives are the closest to the measured values. The measurement of the derivatives is easily done using Tempo2 on the dataset presented in Chapter 3.

Introducing additional parameters helps expressing the system of eq.(5.3) differently. The acceleration of the pulsar caused by its motion around the common centre of mass is of magnitude $a = k/r_p^2$ where r_p is the distance from the pulsar to the centre of mass and

$$k = G\frac{m_c^3}{(m_p + m_c)^2} \tag{5.4}$$

where G is the gravitation constant. This k is similar to the mass function (see Section 2.3.4). The distance r_p for an elliptic keplerian orbit of semi-major axis a_p and eccentricity $e_p = e_c$ is

$$r_p = \frac{a_p(1 - e_c^2)}{1 + e_c \cos\lambda_p} \equiv \frac{h}{A} \tag{5.5}$$

where we have defined $h = a_p(1 - e_c^2)$ and $A = 1 + e_c \cos\lambda_p$. The system of eq.(5.3) can be re-written as

$$\dot{f} = -f\frac{a}{c}\sin(\lambda_p + \omega_p)\sin i \tag{5.6}$$

$$= -f\frac{k}{c}\frac{A^2}{h^2}\sin(\lambda_p + \omega_p)\sin i \equiv -fKA^2\sin(\lambda_p + \omega_p) \tag{5.7}$$

$$\ddot{f} = -fKB\dot{\lambda}_p \tag{5.8}$$

$$f^{(3)} = -fKC\dot{\lambda}_p^2 \tag{5.9}$$

$$f^{(4)} = -fKD\dot{\lambda}_p^3 \tag{5.10}$$

$$f^{(5)} = -fKE\dot{\lambda}_p^4 \tag{5.11}$$

where

$$K = \frac{k\sin i}{h^2 c} \tag{5.12}$$

$$B = 2AA'\sin(\lambda_p + \omega_p) + A^2\cos(\lambda_p + \omega_p) \tag{5.13}$$

$$C = B' + \frac{2BA'}{A} \tag{5.14}$$

$$D = C' + \frac{4CA'}{A} \tag{5.15}$$

$$E = D' + \frac{6DA'}{A} \tag{5.16}$$

with the prime symbol indicating a derivative with respect to λ_p. We note here that the derivation of $f^{(5)}$ is not presented in Joshi and Rasio, 1997 but in Perera et al., 2017 where the method is applied to PSR B1820−30A.

Taking f from eq.(5.6), we can re-write eq.(5.8)-(5.11) as

$$\ddot{f} = \frac{B\dot{\lambda}_p\dot{f}}{A^2\sin(\lambda_p + \omega_p)} \tag{5.17}$$

$$f^{(3)} = \frac{C\dot{\lambda}_p^2\dot{f}}{A^2\sin(\lambda_p + \omega_p)} \tag{5.18}$$

$$f^{(4)} = \frac{D\dot{\lambda}_p^3\dot{f}}{A^2\sin(\lambda_p + \omega_p)} \tag{5.19}$$

$$f^{(5)} = \frac{E\dot{\lambda}_p^4\dot{f}}{A^2\sin(\lambda_p + \omega_p)} \tag{5.20}$$

which is a non-linear system of four equations and four unknowns: $e = e_p = e_c$, $\lambda = \lambda_p = \lambda_c$, $\omega_p = \omega_c + 180°$ and $\dot{\lambda}_p$. To reduce the number of unknown parameters, we can isolate $\dot{\lambda}$ in eq.(5.17) and inject it into eq.(5.18) to (5.20), as was done in Perera et al., 2017:

$$\dot{\lambda} = \frac{A^2\sin(\lambda + \omega_p)\ddot{f}}{B\dot{f}} \tag{5.21}$$

$$f^{(3)} = \frac{CA^2 2\sin(\lambda + \omega_p)\ddot{f}^2}{B^2\dot{f}} \tag{5.22}$$

$$f^{(4)} = \frac{D(A^2 2\sin(\lambda + \omega_p))^2\ddot{f}^3}{B^3\dot{f}^2} \tag{5.23}$$

$$f^{(5)} = \frac{E(A^2 2\sin(\lambda + \omega_p))^3\ddot{f}^4}{B^4\dot{f}^3} \tag{5.24}$$

Exploring the (e, λ, ω_p) parameter space gives at each point of the space a set of values for $(f^{(3)}, f^{(4)}$ and $f^{(5)})$ to compare to the measured values.

On each point, we compute the "distance" from the computed values to the measured values as:

$$d = \sqrt{\sum_{n=3}^{5} \left(\frac{f^{(n)}_{computed} - f^{(n)}_{measured}}{u\left(f^{(n)}_{measured}\right)} \right)^2} \tag{5.25}$$

The parameters can finally be combined to derive two useful orbital quantities, the inclination-independent mass function and the orbital size, as

$$a_p \sin i = -\frac{\dot{f} c A^2}{f(1-e^2)\sin(\lambda+\omega_p)\dot{\lambda}} \tag{5.26}$$

$$k = G\frac{m_c^3}{(m_p+m_c)^2} \tag{5.27}$$

$$= -\left(\frac{\dot{f}c}{f \sin i \sin\lambda}\right)^3 \left(\frac{A^2}{\dot{\lambda}^4}\right) \tag{5.28}$$

The parameter space can be constrained as $0 \le e < 1$ and both λ and ω_p (simply noted ω from now on) are angles, thus $\in [0, 360[°$. However, due to the symmetries of the problem, the same equations give four families of solutions. These four families are

$$(\omega_1, \lambda_1) \tag{5.29}$$

$$(\omega_2 = \pi - \omega_1, \lambda_2 = 2\pi - \lambda_1) \tag{5.30}$$

$$(\omega_3 = \omega_1 + \pi, \lambda_3 = \lambda_1) \tag{5.31}$$

$$(\omega_4 = \pi + \omega_2 = 2\pi - \omega_1, \lambda_4 = \lambda_2) \tag{5.32}$$

The recurring term with λ and ω is $\sin(\lambda+\omega)$, and the four families of solutions give

$$\sin(\omega_1+\lambda_1) = \sin(\omega_2+\lambda_2) = -\sin(\omega_3+\lambda_3) = -\sin(\omega_4+\lambda_4) \tag{5.33}$$

Because of eq.(5.26) we know that we need the sinus term to be negative, to obtain a positive semi-major axis, hence two families are *de facto* producing non-physical solutions. We therefore can reduce the parameter space to λ and $\omega \in [0, 180[°$ to select only one family, and then transform the solution using eq.(2.29) to (2.32) so that the obtained solution is physical.

To test our implementation of this computation we tried and successfully reproduced the results presented in Perera et al., 2017.

5.2.3 PSR J1745+1017

Table 5.1: Values of spin frequency derivatives used for the computation of PSR J1745+1017 outer orbital parameters.

	Value	Uncertainty
$\dot{f}$	-3.54×10^{-16}	1.56×10^{-17}
$\ddot{f}$	-8.94×10^{-23}	6.57×10^{-25}
$f^{(3)}$	2.92×10^{-31}	1.61×10^{-32}
$f^{(4)}$	-4.45×10^{-39}	2.20×10^{-40}
$f^{(5)}$	2.82×10^{-47}	1.34×10^{-48}

As already stated in Section 5.1.3, a timing solution with two orbits, with parameters awaiting confirmation, is already implemented in the NRT timing pipeline. This made PSR J1745+1017 a good candidate to test the method presented in Joshi and Rasio, 1997. In Table 5.1 are the spin derivatives values used for the computation, and the results are plotted in Figure 5.1. As explained in the previous section the "distance" as defined in eq.(5.25) should be as small as possible, hence the "best solution" is the point in the (e, ω, λ) space for which the value of d is minimum. The parameters derived from this best solution are given in Table 5.2. As can be seen in Figure 5.1 and Table 5.2, the best solution is very different from the parameters included in the NRT preliminary timing solution, as indicated with the example of the orbital period by the grey line. Potential explanations for these discrepancies are discussed in Section 5.2.5.

Table 5.2: Best solution for outer orbital parameters of PSR J1745+1017.

Parameter	Computed value	NRT ephemeris
P_b, in days	2474	4353
a_p, in lt-sec	1.92 $\times 10^{-3}$	1.19 $\times 10^{-3}$
M_c, in $M_\oplus$	0.47	0.20
e	0.106	0.957

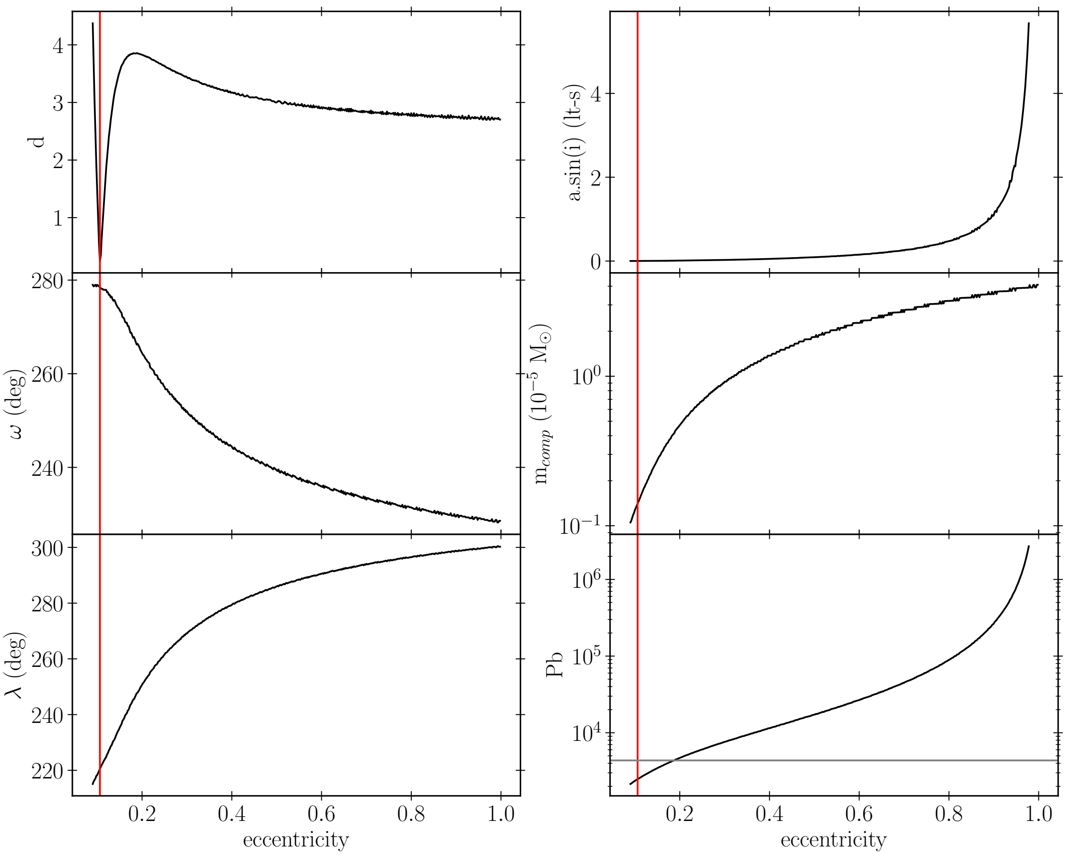

Figure 5.1: Results of the computation of orbital parameters using the Joshi and Rasio, 1997 method for PSR J1745+1017. The results are parametrised as function of the eccentricity for a better reading. The upper left panel shows the distance as defined in eq.(5.25), the middle and bottom left panels the two angles introduced in the previous section, the top and middle right panels the projected semi-major axis and companion mass, respectively computed from eq.(5.26) and (5.27) assuming a pulsar mass of $1.5 M_\odot$ and the lower right panel the orbital period derived from Kepler's third equation using the two previous parameters. The grey line in this panel indicates the value in the NRT timing solution. The red line indicates the best solution, *i.e.* the solution for which d is minimum.

5.2.4 PSR B1620−26

Using the same algorithm on PSR B1620−26 did not yield good results either. The results are plotted in Figure 5.2.

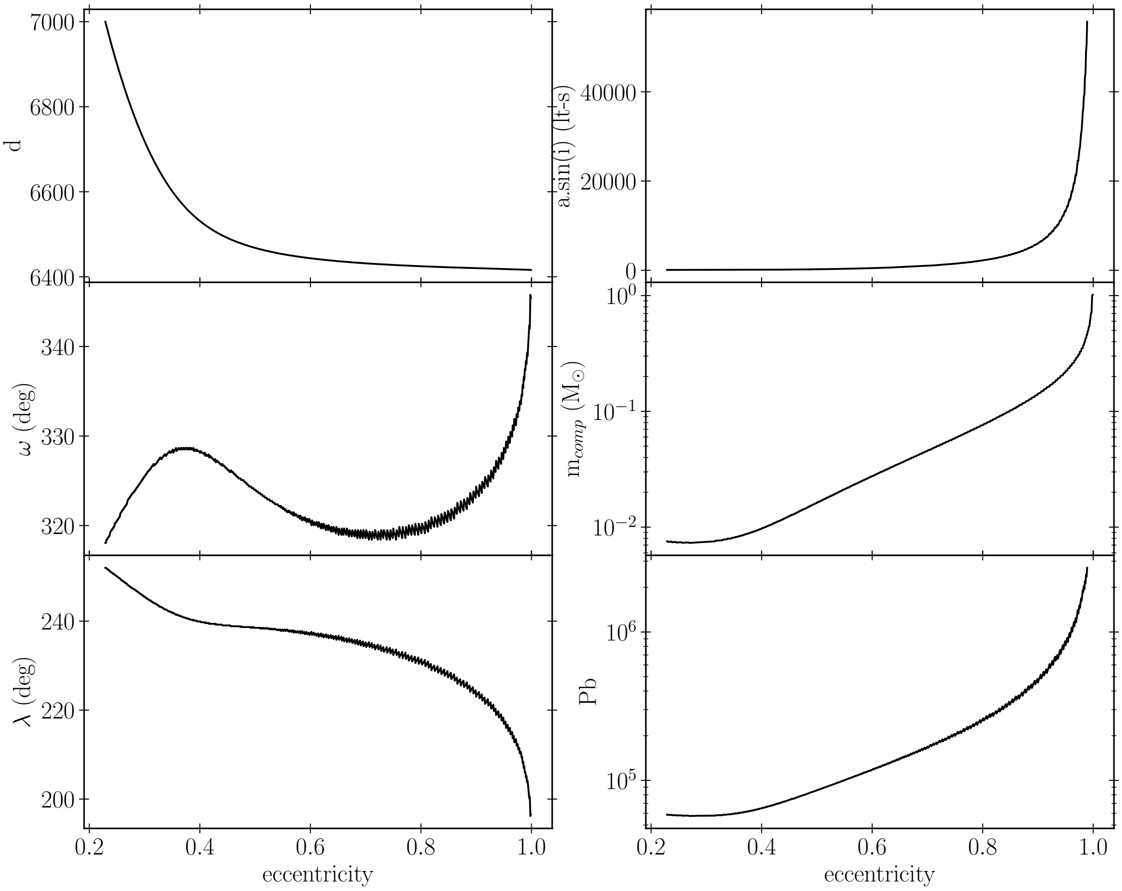

Figure 5.2: Same as Figure 5.1 but for PSR B1620−26.

Trying to update the results published in Joshi and Rasio, 1997, we ran the algorithm using updated spin derivatives measurements. We note that we did not obtain a curve similar to that of the original study, nor a similar range of parameters. The main issue with this computation is the fact that the "best" solution has the highest allowed eccentricity, which could indicate that the perturbation comes from a body flying by, resulting in a parabolic or hyperbolic orbit, however this feature has been recurrent in all computations that we ran, except for PSR J1745+1017. We tried on PSR J2115+5448 and got the same results, without finding a satisfactory explanation nor a way to fix it. We also noticed that other studies using this method seemed to favour very high eccentricity solutions. Perera et al., 2017 found for PSR B1820−30A an eccentricity of 0.993 and Dutta et al., 2025 could not rule out a hyperbolic encounter.

5.2.5 Discussion

The shortcomings of this method are still unclear. One main problem is the value of $\dot{f}$: it is used in every equations of the computation, and is naturally the largest of the derivatives, however it is not possible to distinguish the intrinsic $\dot{f}$ from the acceleration induced by the companion pull. As explained in Joshi and Rasio, 1997, the acceleration can be nearly the total observed $\dot{f}$ or 1 % of it, but by varying the $\dot{f}_{acc}$ value from $\dot{f}_{obs}$ to $0.01 \times \dot{f}_{obs}$ they did not find the range of result parameters values to change. In our case however, we do see a significant change in the resulting parameters caused by a variation in the input spin frequency derivatives. These variations are caused by a "problem" that the original study did not have: since the method was developed, larger datasets have enabled us to measure more frequency derivatives, and while Joshi and Rasio, 1997 had to change their equations to accommodate for the lack of a measurable $f^{(5)}$, the timing solution giving the best residuals for PSR J1745+1017 can go as far as $f^{(12)}$. Because the spin derivatives are very covariant, fitting up to $f^{(5)}$ or up to $f^{(12)}$ changes the values of the first five derivatives significantly. In Table 5.3 are the values of the five first derivatives for a timing solution with five or twelve spin frequency derivatives, and in Figure 5.3 are plotted both computation results for the orbital period.

Table 5.3: Comparison between the spin frequency derivatives found when using a model with five or twelve derivatives to fit PSR J1745+1017 data.

	F5 ephemeris	F12 ephemeris
$\dot{f}$	-3.54×10^{-16}	-5.96×10^{-16}
$\ddot{f}$	-8.94×10^{-23}	-1.86×10^{-23}
$f^{(3)}$	2.92×10^{-31}	1.17×10^{-29}
$f^{(4)}$	-4.45×10^{-39}	-1.97×10^{-36}
$f^{(5)}$	2.82×10^{-47}	1.96×10^{-43}

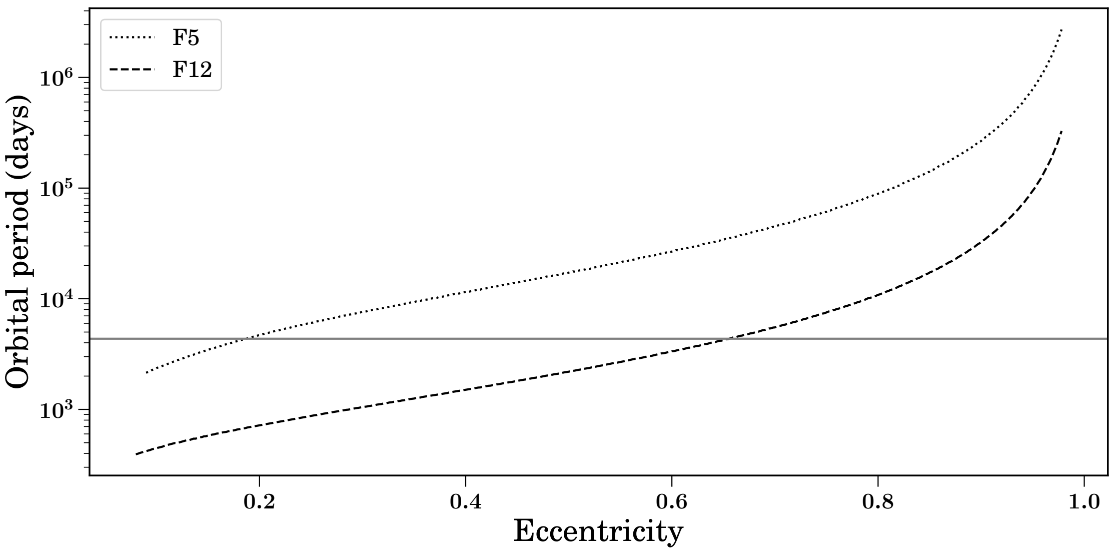

Figure 5.3: Comparison of the computation results for PSR J1745+1017 using an ephemeris fitted for up to $f^{(5)}$ and an ephemeris fitted for up to $f^{(12)}$. The grey line indicated the orbital period in the NRT's double orbit ephemeris presented in Table 5.2.

While the best solution was still around $e = 0.1$, every parameter of the $f^{(12)}$ solution was at least an order of magnitude different from those from the $f^{(5)}$ solution. A way of better understanding the limitations and establishing "best practices" when using this method could be to conduct simulations using fake ToAs to explore the impact of the number of spin frequency derivatives measured on the accuracy of the retrieved parameters.

5.3 Direct timing

After the rather unsuccessful attempt to compute the orbital parameters from the spin derivatives, we decided to try timing the two orbits directly. Because the timing is quite unstable, it cannot be done with Tempo2. We decided to try the MCMC4T2 algorithm developed by G. Voisin and presented in Voisin et al., 2020a. For more details on MCMC4T2 see Section 2.3.3. The fitting was done in two steps: first, the only parameters fitted for were the spin frequency and its derivatives alongside with the outer orbit parameters, then all the parameters of the ephemeris were fitted for. The results presented in the next sections might be more promising, but are preliminary.

5.3.1 J1745+1017

The current best solution for this pulsar is presented in Table 5.4, and the residuals are plotted in Figure 5.4. For this pulsar the solution is a improvement and a confirmation of the timing and parameters already implemented in the NRT timing solution.

Table 5.4: Current best solution from the fitting of the outer orbital parameters of PSR J1745+1017. The relevant values for the inner orbit are also in the table.

Parameter	Value	Uncertainty	Inner orbit
P_b, in days	5200	519	0.73
T_0, MJD	56892.5	8.9	
a_p, in lt-sec	8.7×10^{-4}	0.6×10^{-4}	0.088
ω, in degrees	326.8	1.3	
e	0.9058	0.0096	7.7×10^{-5}

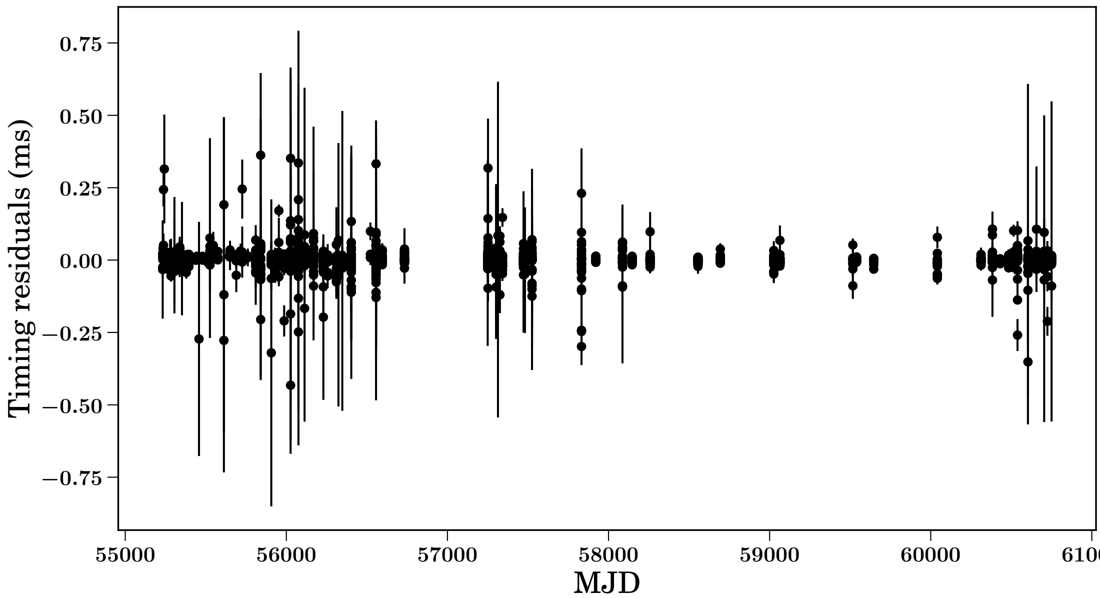

Figure 5.4: Timing residuals of PSR J1745+1017 with the best solution for the second orbit. The residuals have $\chi^2 = 2.14$.

The residuals are good, and the fact that the periastron is included in the dataset helps constraining the solution. Unfortunately the exact time of the periastron passage seems to happen during a period when the NRT planning did not include PSR J1745+1017 for a little while, therefore we do not have data around this point. Having a precise measurement of T_0 would be greatly

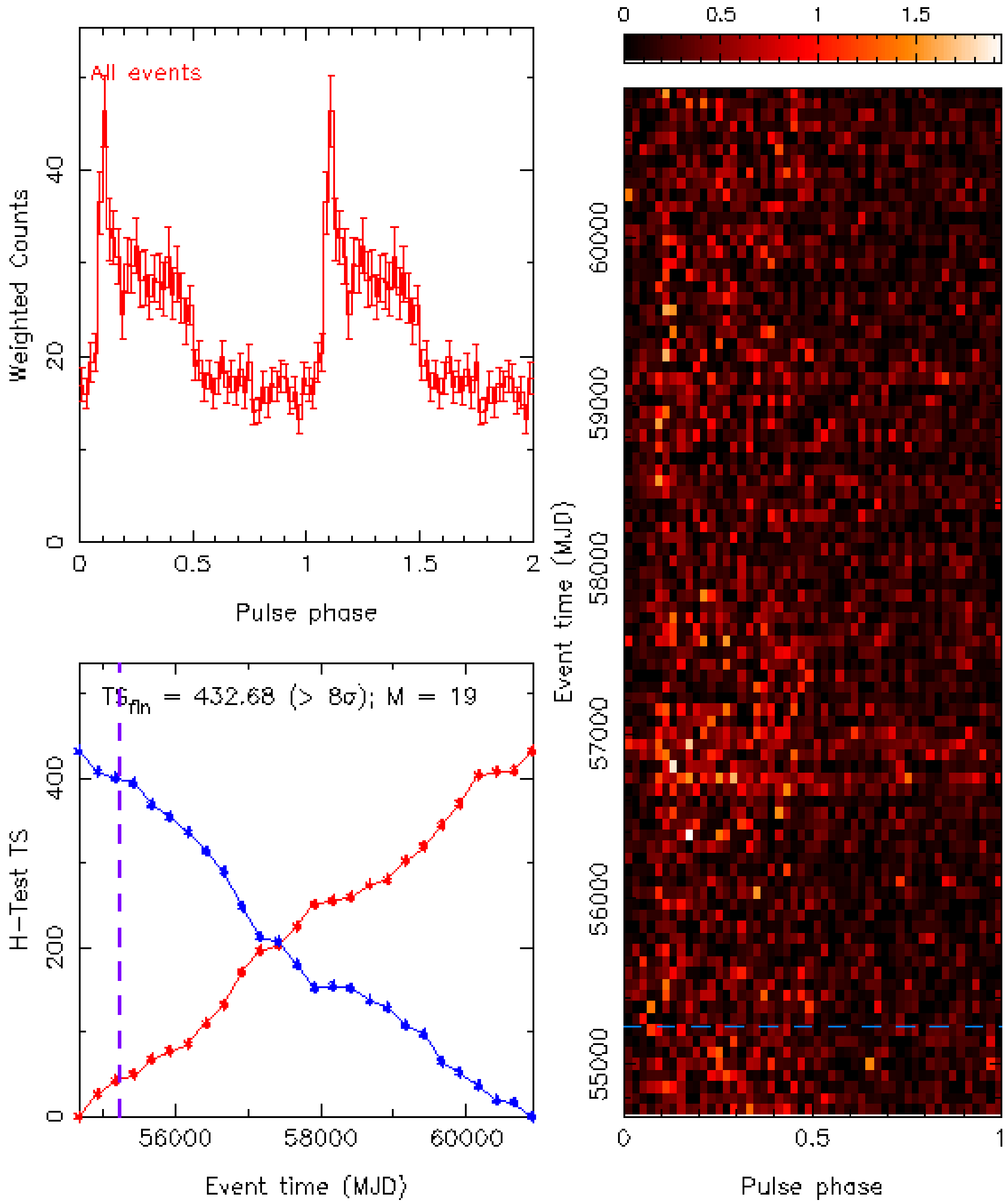

Figure 5.5: Folding of PSR J175+1017 *Fermi-LAT* data using the ephemeris fitted for with MCMC4T2. The dashed lines indicate the beginning of the NRT dataset. In the right plot one can notice that the peak of the profile is slightly visible above the dashes, which shows a detection. In the bottom left panel, red points show the test significance of the gamma-ray detection according to the H-test (de Jager, Raubenheimer, and Swanepoel, 1989; Kerr, 2011), when integrating the signal in time. The blue points show the same information, but integrating the signal backwards in time. We can see that the signal integrated before the dashed line is significant, as the red (resp. blue) line starts increasing (resp. decreasing) before the dashes. This means that the ephemeris is valid even before the fitting period.

beneficial, as all parameters are strongly covariant this would help constraining the rest of the orbital parameters. Moreover the acceleration is maximum at this point so the "signal" is stronger. Adding observations conducted with other telescopes which might have been monitoring PSR J1745+1017 more closely around the periastron passage would allow a better constraint on T_0 which in turn would help constraining the rest of the orbital parameters. The uncertainty on the orbital period is quite large, to the point that is it unsure if a total orbit has already been covered or not. Yet, this solution is currently the best we have, with a better χ^2 than other timing solutions we got not using a two-orbits ephemeris.

To test our solution we tried folding the *Fermi-LAT* data using this ephemeris. Using the ephemeris on totally independent data would give indications on the validity range of the solution. The analysis is similar to those presented in Smith et al., 2023. The folding yields good results, as shown in Figure 5.5, which is not surprising considering that the data span is similar. Nevertheless, the *Fermi-LAT* dataset starts nearly two years before the monitoring of PSR J1745+1017 with the NRT BON backend, hence the fact that the ephemeris is valid for about ~ 600 days before the beginning of the fitting period is quite encouraging.

This pulsar second orbit is relatively close, hence the "signal" is relatively high, and plotting the residuals without accounting for the second orbit gives a very distinctive signature, as can be seen in Figure 5.6.

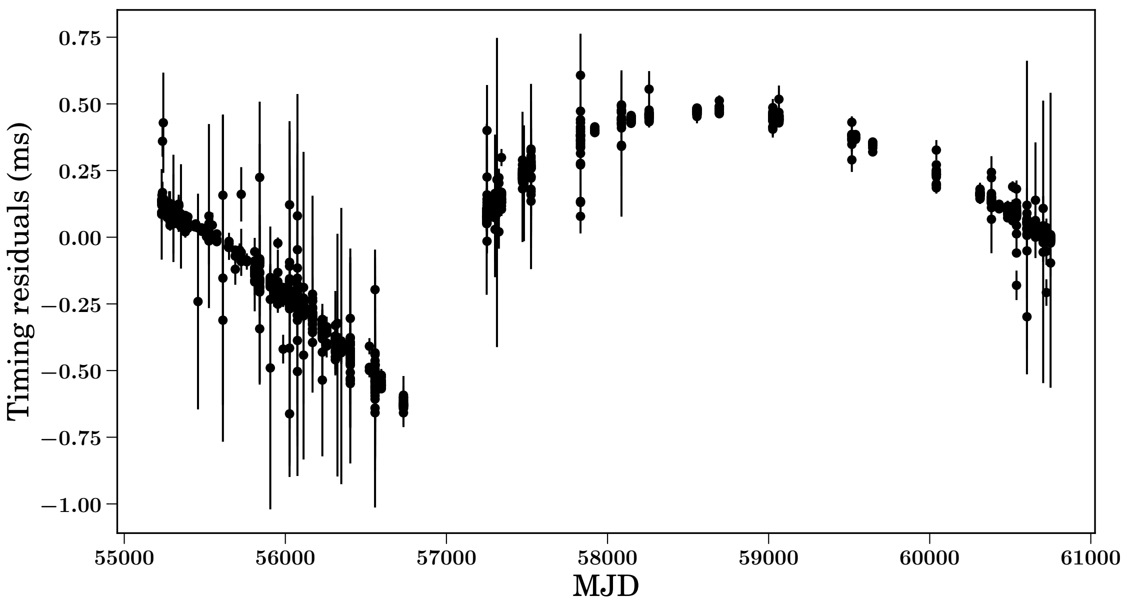

Figure 5.6: Residuals of PSR J1745+1017 using the same ephemeris as for Figure 5.4 but without the second orbit parameters. The shape is very characteristic of a non-fitted orbit. The dip around MJD 57 000 has its lowest point at the periastron passage, but this precise moment is at a period when no observations were conducted.

Keeping all the caveats in mind, we can still consider the results displayed in Table 5.4 as reasonable orders or magnitude to compute the corresponding orbit semi-major axis and companion mass. The mass function gives a companion of mass $M_c = 0.130 \pm 0.013 M_{\oplus}$ (the uncertainty comes from the uncertainties on the parameters as given in Table 5.4). To get a sense of the sensitivity of timing methods, this is slightly above Mars' mass, which is $0.107 M_{\oplus}$, and is smaller than the third smaller exoplanet listed on the Extrasolar Planets Encyclopaedia catalogue[1]. The semi-major axis of the outer orbit is $a_c = (3.35 \pm 0.022) \times 10^3$ light-seconds or 6.7 ± 0.4 astronomical units (AU), but the orbit is very eccentric, and the periastron is actually 0.63 ± 0.08 AU from the pulsar. This

[1] https://exoplanet.eu/catalog/

is relatively small, and "only" 35 times larger than the internal orbit, which has a semi-major axis of ~ 0.02 AU.

5.3.2 J2115+5448

The current best solution for this pulsar is presented in Table 5.5, and the residuals are plotted in Figure 5.7.

Table 5.5: Current best solution from the fitting of the outer orbital parameters of PSR J2115+5448. For comparison, the relevant values for the inner orbit are also in the table.

Parameter	Value	Uncertainty	Inner orbit
P_b, in days	8676	111	0.14
T_0, MJD	56805	13	
a_p, in lt-sec	7.56×10^{-2}	0.14×10^{-2}	4.48×10^{-2}
ω, in degrees	205.1	4.0	
e	0.547	0.013	3×10^{-5}

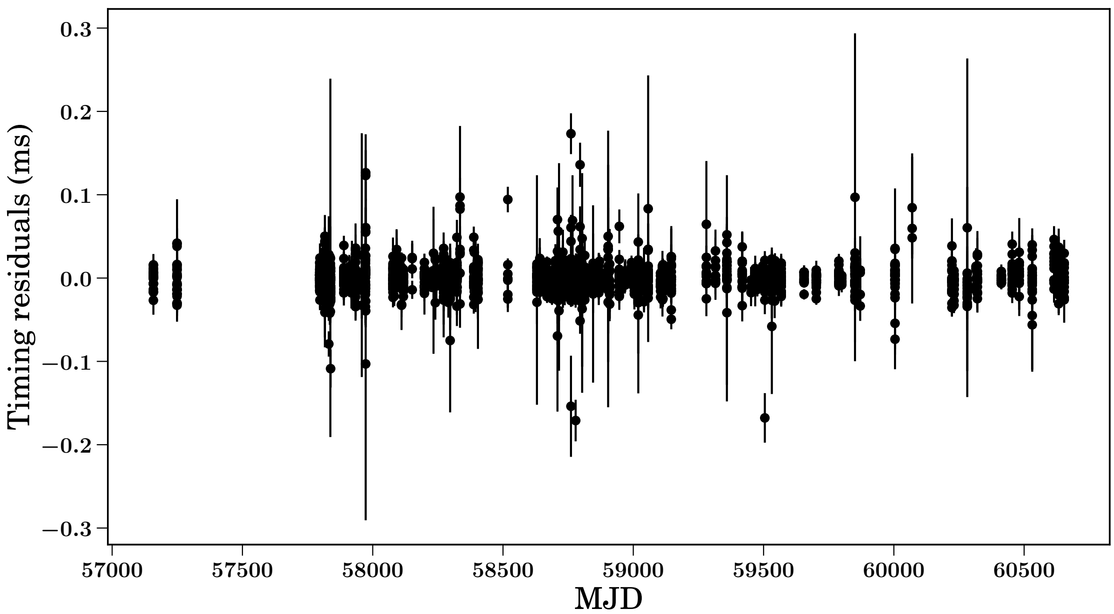

Figure 5.7: Timing residuals of PSR J2115+5448 with the best solution for the second orbit. The residuals have χ^2 = 1.62.

In this case again, the residuals are good, however the data span is much shorter, and the epoch of periastron passage is not included in the data span, although potentially happening just before the beginning of the monitoring. Here the best solution is an orbital period of more than 23 years and a half, which is much longer than the NRT monitoring time, but also much longer than the current *Fermi-LAT* dataset. Contrarily to the previous pulsar, folding the *Fermi-LAT* data using this ephemeris does not yield good results. As can be seen in Figure 5.8, during the last 9.5 years the ephemeris does correctly fold the *Fermi-LAT* data so that the pulsar signal is well detected, however before that the detection is not significant, so the ephemeris is not capable of accounting for the pulsar's rotations.

The fact that the solution is only valid for the duration of the NRT dataset indicates that the solution has no predictive power. In a way, this is not surprising: as presented in the previous

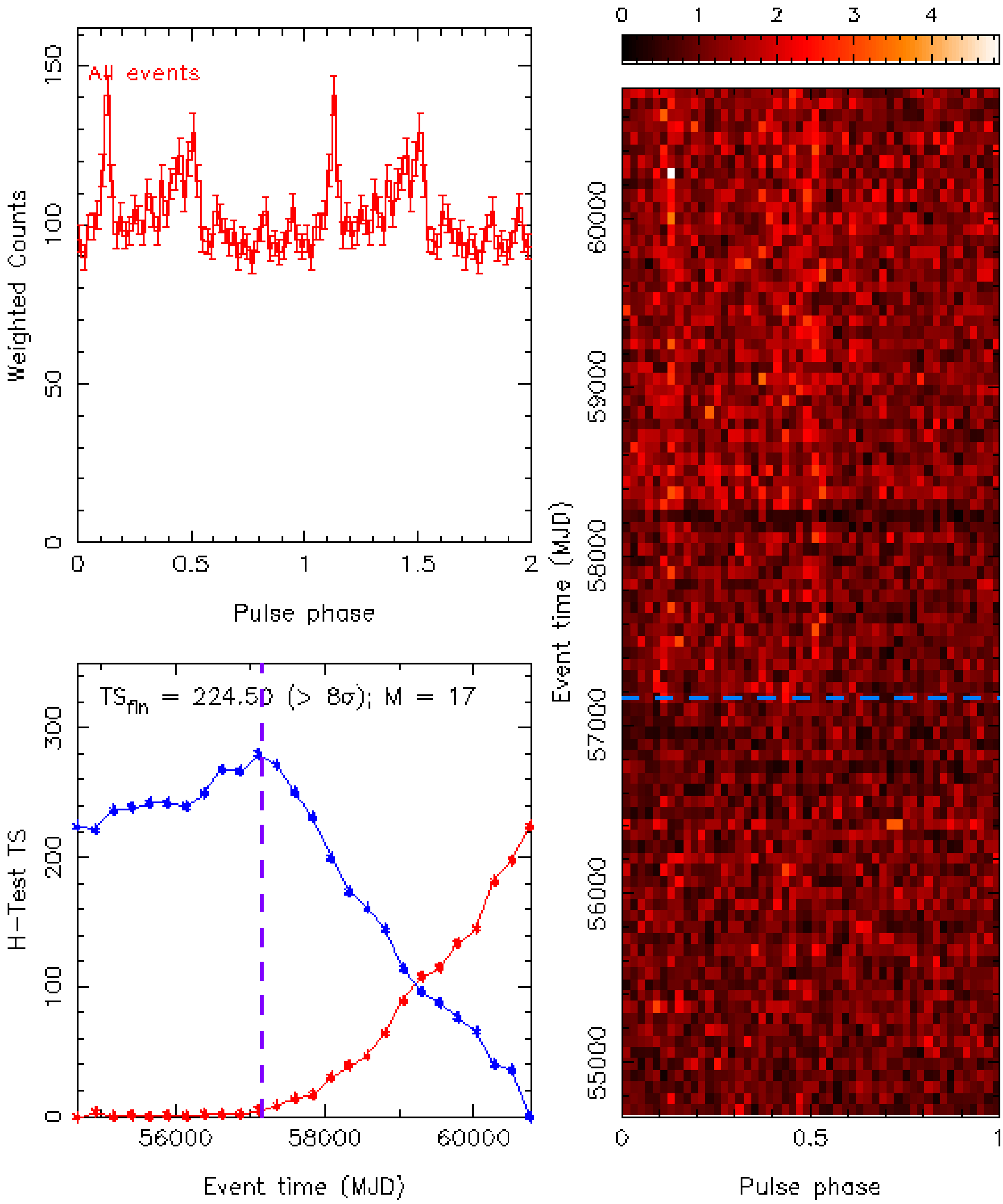

Figure 5.8: Same as Figure5.5 but for PSR J2115+5448. The top left plot shows the profile of the pulsar over two pulse periods. We notice that the profile has two peaks. In the bottom left plot, we can see that the H-test significance of the pulse profile integrated backwards in time (*i.e.*, the blue curve) increases close to linearly until the vertical dashed line, indicating the beginning of the ephemeris' validity interval, and decreases beyond the dashed line. This suggests that the ephemeris does not maintain phase coherence beyond its formal validity interval. Similarly in the right plot, one can see that the profile is slightly visible above the dashes, and not much so below.

Section 5.2, orbital parameters for an incomplete orbit is equivalent to a Taylor expansion of the spin frequency. However it is ordinary to see a Taylor expansion only valid over the fitted timespan, therefore this could indicate that before having nearly a complete orbit, fitting for orbital parameters does not give reliable solutions. This is aggravated by the fact that the residuals are very good: from a radio timing perspective we cannot reasonably hope to get a significantly better result, hence the only possible improvement would be to have a long data span.

One major difficulty we had with this pulsar, that also arose when working on PSR B1620−26, is that the timing usually puts as much weight as possible on the frequency derivatives, rather than on the second orbit. The spin-down is the only derivative for which we expect a measurable value for these MSPs, however even when allowing for a second orbit the model usually produces large values for the higher order derivatives. This meant that to obtain an orbital solution with only f and $\dot{f}$, we had to do the timing taking out higher order derivatives one by one. This was very time consuming and is quite unsatisfying, as the model consistently favoured putting as much weight as possible on a Taylor expansion of the spin frequency.

Nevertheless the current solution seems to account for the pulsar rotations, from a point of view of radio timing. Keeping again all the caveats in mind, the current best solution corresponds to a $8.00 \pm 0.17 M_\oplus$ planet, following a rather eccentric orbit with a semi-major axis of 9.46 ± 0.08 AU. The periastron is 4.29 ± 0.13 AU, a highly hierarchical configuration in which the ~ 0.006 AU internal orbit would have a negligible level of interactions with the outer body.

5.3.3 B1620−26

The peculiarity of B1620−26 lies in its very prominent timing noise. Its unusually large first few spin derivatives for an MSP led to the general conclusion that it is in a triple system. As can be seen on Figure 5.9, even our current best solution, using only one orbit and multiple spin frequency derivatives, still have a lot of structure.

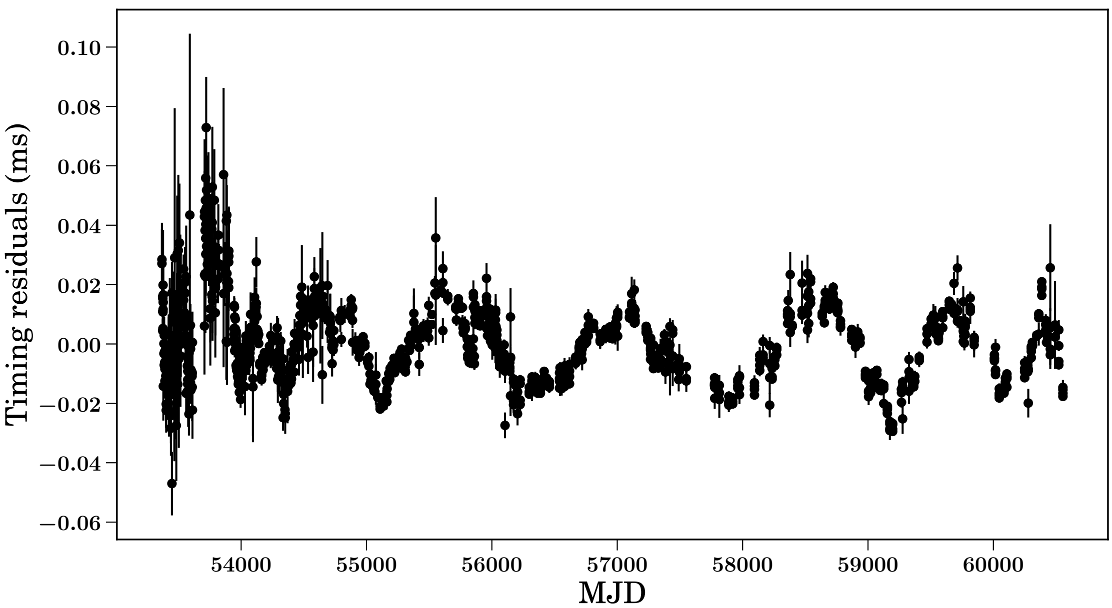

Figure 5.9: Timing residuals of PSR B1620−26 using an ephemeris with one companion and the 12 first spin frequency derivatives. For this solution $\chi^2 = 42.58$.

The current best solution for this pulsar is presented in Table 5.6, and the residuals are plotted in Figure 5.10.

This solution corresponds to a ~ $0.1 M_\odot$ companion on an 335-years orbit with a semi-major

Table 5.6: Current best solution for the fitting of the outer orbital parameters of PSR B1620−26.

Parameter	Value	Uncertainty	Inner orbit
P_b, in days	122411	10	191
T_0, MJD	80841	5	
a_p, in lt-sec	1655	2	0.088
ω, in degrees	215.59	0.08	
e	0.3713	0.0005	0.025

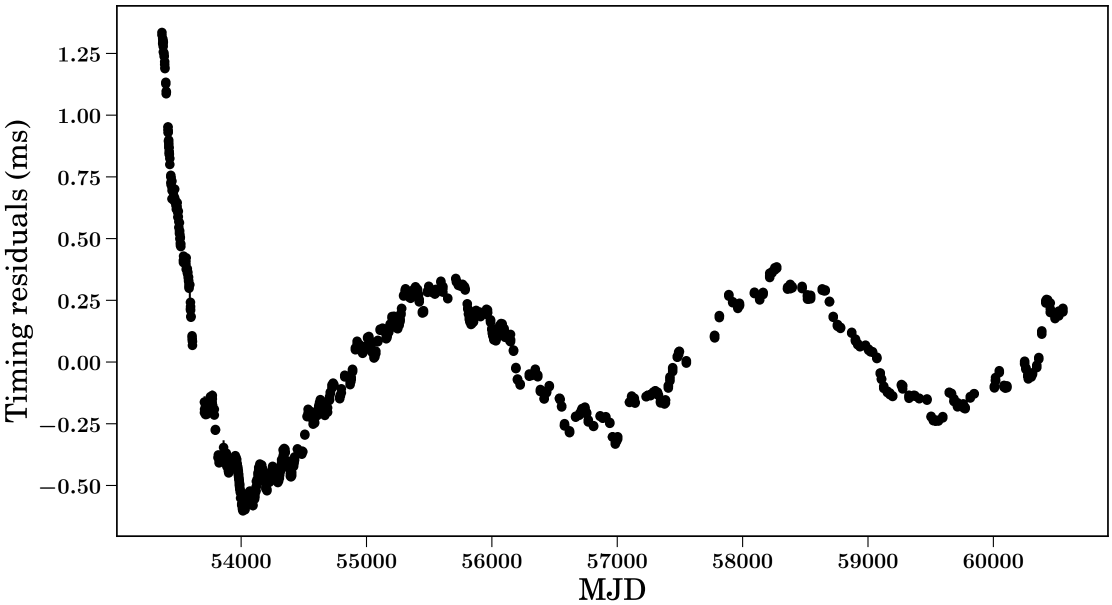

Figure 5.10: Timing residuals of PSR B1620−26 with the best solution for the second orbit. The residuals have $\chi^2 \sim 20000$.

axis of ~ 56 AU. This is clearly not a definitive solution, however it is worth noting that such orders of magnitudes for P_b, a and companion mass were already considered in Thorsett, Arzoumanian, and Taylor, 1993 where it was showed that a $0.8M_\odot$ star in a 250 year, $e = 0.8$, $a = 54$ AU with a certain inclination would account for the measured spin frequency derivatives. Moreover, the results of the direct computation, plotted in Figure 5.2, are also of the same order of magnitude for this eccentricity, yielding $P_b \simeq 335$ years and $m_{comp} \simeq 0.1M_\odot$, which is encouraging.

The residuals in Figure 5.10 still have a lot of structure and it is clear that our model does not manage to account for the timing noise. However, the residuals are contained within less than 20% of the spin period over nearly 20 years of data, which indicates that the 3-body solution is relevant as a timing model for this pulsar.

5.4 Summary and prospects

We have searched for the orbital parameters of the second companions of PSRs B1620−26, J1745+1017, J2115+5448 using both calculations of the parameters from spin frequency derivatives and the direct timing of these pulsars' ToAs. The first method did not yield good results, for multiple reasons. The results of the second method are slightly more promising, although as stated in the beginning of this chapter, everything presented here is very preliminary.

The solution found for PSR J1745+1017 seems slightly more credible than the others, and the current best result is that a ~ $0.13M_\oplus$ planet is orbiting the pulsar in a very eccentric ($e = 0.91$) orbit of semi-major axis of about 6.7 AU. Two improvements can be brought to the solution: the first is simply to wait to accumulate more timing data, the second to gather observations around MJD 57000 from other telescopes. Our best solution suggests that the orbit might already be completely sampled, and waiting for another year or two would confirm this. Having more ToAs around the periastron passage (~ MJD 57000) would constrain this parameter better, and because all orbital parameters are covariant this would help constrain the whole orbit.

The two other cases are quite less encouraging, but both in different ways. It is possible that before covering a significant fraction of the orbit, if not one full orbit, the direct timing cannot get a single solution. The current best solution for PSR J2115+5448 indicates that a ~ $8M_\oplus$ planet is orbiting the pulsar is an eccentric ($e = 0.55$) orbit of semi-major axis of about 9.5 AU. However the example of PSR J2115+5448 clearly shows that having very convincing radio timing residuals does not guarantee that the solution is predictive. A potential way of verifying this would be to create fake ToAs using a fake ephemeris with 3 bodies, and trying to monitor the recovering of the orbital parameters of the outer orbit when varying the orbital coverage.

The case of PSR B1620−26 is different, as the radio timing solution is not satisfactory, yielding a very large χ^2 and still keeping a lot of structure. If the best solution using three orbits is worse than the solution using several spin frequency derivatives, there is no possible scenario other than a second companion that could explain such a large timing noise, which is the reason why the literature consensus is that this system contains three bodies without precise orbital parameters found during the last 30 years or research.

Finally, one major prospect of this study is the possibility for PSR J2055+3829 to also be in a triple system. This pulsar has not been analysed yet. Contrarily to the others, this pulsar is not generally considered as harbouring a second companion, however in our data it displays a level of timing noise similar to that of PSRs J174+1017 and J2115+5448, therefore we plan on analysing it once the method is tested and approved on systems that are more likely to harbour a planet. However we plan on refining the method and understanding as many pitfalls as possible on systems that we know have planets orbiting them before searching on other systems.

A future project about the search or pulsar planet is planned, and includes simulating data of a long period planet orbiting a binary such as those presented earlier, to try to retrieve the correct orbital parameters while gradually shortening the orbital coverage, to get a better idea of the orbital coverage needed to get credible solutions. The inclusion or not of the periastron passage in the data coverage will be under scrutiny, as the constraints coming from the observation of this moment might be crucial to obtain good solutions even with a limited orbital coverage.

Chapter 6

Conclusions and outlook

Banlieue ouest d'Aberlaas, Extrême-Aval, falaise des Confins !

With more than 4000 pulsars in the current version of the ATNF catalogue, 30 galactic redbacks, 50 galactic black widows and nearly 30 spider candidates in the current version of SpiderCat, the pulsar zoo is expanding rapidly, promising many new interesting findings to come. Spider pulsars are fascinating objects, and nearly 40 years after the discovery of the first spider pulsar, many of their properties are still energetically debated in an ever-growing spider pulsar community. Many models are being improved or developed to explain the formation and evolution of such systems, the observed variability in orbital and spin periods, and the eclipses that are displayed by some of the systems. The eclipses are the focus of the first work presented in this thesis, and are observed in many spider systems. They consist in a delay and attenuation of the pulsar beam when it crosses a plasma cloud surrounding the system, constituted of matter blown away from the stellar companion by the pulsar wind.

The works presented in this thesis are based on observations conducted in the radio domain. At these wavelengths the pulsar signal undergoes various natural processes during its travel to Earth that we have to correct for. These processes are frequency dependent, and can be used as probes to study the interstellar medium. The dispersion in particular, adds a delay to the signal which scales with $1/f^2$, delaying low frequencies with respect to higher frequencies, and the pulsar signal needs to be de-dispersed before being further used. Because pulsars are generally weak sources, the de-dispersed data is folded at the spin period to increase the signal. The folded data can then be used for the pulsar timing technique, which consists in the recording of the times of arrival of the pulsars' flashes, and the modelling of said ToAs to account for the pulsar observed cadence. I presented the tools and methods we used, as well as the preparation we applied to the data of our sample.

All data used during my PhD came from the rich dataset built using the Nançay Radio Telescope, an instrument located in central France that has been operating for 60 years and regularly gets updated instrumentations. The NRT is equipped with two receptors, one functioning between 1.1 and 1.8 GHz and the other between 1.7 and 3.5 GHz, the first one being most commonly used for pulsar observations, owing to their spectral properties. The current backend runs on GPUs and coherently de-disperses and folds the data in real time, over a total bandwidth of 512 MHZ. About 80 % of the NRT observation time is dedicated to pulsar monitoring, and the spider pulsars observation program includes 19 systems, more than half of them observed for more than 15 years, with a high observation cadence. The first task of my PhD was to systematically analyse the numerous NRT observations on the monitored spider pulsars and optimise the timing solutions. For each pulsar I produced 2D ToAs and a timing solution that covered the entire dataset in a single ephemeris. In Chapter 3 and Blanchard et al., 2025 I presented this dataset, including polarisation profiles that were previously unpublished, and the characteristics of all 19 systems, alongside with a thorough work of bibliography that highlights the variety of studies of spider systems.

The first work presented has been published in Blanchard et al., 2025. It is the study of the eclipse properties of the 19 spiders in the sample presented previously. The main goal of this study was to properly characterise the orbits and eclipses of the systems, and to explore potential links between the systems' orbital inclinations and the eclipse properties. It has been established (Freire, 2005; Guillemot et al., 2019) that eclipsing systems tend to have higher mass functions than non-eclipsing systems. The mass function can be used as a proxy for the orbital inclination, assuming that the pulsar and companion masses are similar for all systems compared, which is the case for 17 BWs of our sample. We introduced a characterisation of eclipsing systems based on the ToA SNRs around superior conjunction (when the companion is closer to the line-of-sight). Using our definition, 11 systems are considered "eclipsers" in our sample. It is important to note that this number depends on the observing frequency. Because the eclipse comes from the pulsar beam interacting with plasma coming from the companion, the same sample observed at lower frequencies would count under the same definition a higher number of eclipsing systems. We found that for the pulsars in our sample, the mass function distribution of eclipsing and non-eclipsing pulsars are very likely not to come from the same parent distribution, in agreement with previous studies.

For eclipsing systems, eclipses were fitted using a phenomenological model, to derive parameters describing the observed shape of the average eclipse of each system. These parameters were then compared to each other, and to the mass functions of the systems. The fits were also used to classify the different eclipsers into three categories: the "shallow", "progressive" and "abrupt" eclipsers. For systems displaying "shallow" eclipses, the pulsar beam is visible throughout the whole orbital period, but is significantly delayed around the superior conjunction. The "progressive" and "abrupt" eclipsers are on the contrary not visible during the entirety of the eclipse, and are distinguished by the duration of their ingress phase: the "progressive" are visibly delayed before the loss of the pulsar beam, and the "abrupt" do not have a proper ingress before being undetectable.

Comparing several parameters with the mass function, we found that the mass function appears to be correlated with the time during which the pulsar beam is delayed, systems with higher mass functions generally having a longer delay duty cycle. Taking into account the non-eclipsing systems and setting their delay duration to 0 increases the correlation. Ideally we would find the same correlation when comparing the delay duration to the inclination of the systems, however the inclination for these systems is not measurable using radio timing. The go-to method is the modelling of the companion's optical light curve, but this method is very model dependent, might overestimate values and has not been applied to all the systems of our sample. Moreover different articles about the same pulsar can have contradictory results, making the comparison with the eclipse parameters difficult. The main improvement and prospect for this study would be to make the same analysis for a larger sample of pulsars. Another interesting extension to the study would be to include radio data taken at other wavelengths, to study the frequency dependence of the eclipse parameters.

The two "shallow" eclipsers are PSRs J1705−1903 and J2051−0827. PSR J2051−0827 being the second spider system discovered, it has been thoroughly studied, and in particular the variability of its eclipses has been reported at multiple timescales. We showed the variability of the eclipses of the second "shallow" eclipser, PSR J1705−1903, for which we see the maximum delay at superior conjunction to change significantly over the course of months. Multiple investigations can be conducted about these variations: estimating the variation with time of the plasma density and use that to constrain the evaporation rate of the companion, or trying to search for a correlation with a potential variation of the mass function of inclination of the orbital plane to explain the variations observed. Overall, the variations seen in some systems could hint that all spiders have varying evaporation. In this case one could apply the phenomenological fitting to track the variations in time of a pulsar eclipse's shape.

The second main work of my PhD is still in progress. It is the search for planets potentially orbiting pulsars, and more specifically orbiting three binary systems: PSRs B1620−26, J1745+1017 and J2115+5448. The first is a pulsar in a wide binary with a white dwarf, the latter two spider systems are included in the NRT spider sample. All three systems are considered as having a second companion orbiting in a very wide orbit in a hierarchical configuration, meaning that the outer and inner orbits have negligible levels of interactions. This means that the outer orbit is much wider than the inner orbit, thus has a much longer orbital period, and therefore is more difficult to constrain as the timing gets more precise when the orbital coverage increases. In these three cases the outer orbital period is longer than the total monitoring time, or barely contained in it. We tried two different methods to constrain the outer orbit parameters: the direct computation from the measured spin frequency derivatives, following the calculations of Joshi and Rasio, 1997, and the timing technique. The first method did not yield good results. The best solutions depend significantly on the values of the spin frequency derivatives used, however these values themselves depend significantly on the timing solution, and the choice of the timing model is not a straightforward question.

We then tried to do direct timing, using a different timing software than the regular TEMPO2, and got slightly better results. For PSR J1745+1017, the current best solution is a $0.13M_{\oplus}$ (where $M_{\oplus}$ is the Earth's mass) planetary companion in a very eccentric ($e \sim 0.9$) 5200-days orbit. This result means that the NRT monitoring campaign covers the full orbit or most of it. A way of improving and constraining the solution could be to add more data around the periastron passage, which was not covered by the NRT.

For PSR J2115+5448 the current best solution indicates a $\sim 8M_{\oplus}$ companion in a rather eccentric ($e \sim 0.5$) orbit of period > 8000 days. In this case the NRT coverage would be $\lesssim 40\%$, which might not be enough to properly constrain the outer orbit. Using the resulting ephemeris on *Fermi-LAT* data, which is about twice as long as the NRT data for this pulsar, clearly shows that the resulting ephemeris has no predictive power, indicating that our solution can still be improved. Similarly to PSR J1745+1017, the obvious improvement would be to wait and gather more data. Our solution suggests that the periastron passage happened just before the beginning of the NRT monitoring, using data covering this moment can only help constraining the parameters.

The case of PSR B1620−26 is more complicated. This pulsar's outer companion is hunted since the 90s, but the seemingly extremely long orbital period makes the parameters difficult to constrain. Our best solution hints at a period of several centuries, with a sub-stellar mass companion. However in this case, contrarily to the previous two systems the radio timing residuals are not satisfactory. To improve this solution, waiting is not a reasonable option. Understanding the limitations of our methods is key to know if a decent solution could be found with it within the next years. To do so, we can simulate data on a long period planet orbiting a binary, to try to retrieve the injected orbital parameters while gradually shortening the orbital coverage, to get a better idea of the orbital coverage needed to get credible solutions.

Overall, the take home message of this thesis, and one of the reasons why it was advertised in the first place, is that the NRT archival data is a gold mine for whoever wants a long and well-sampled monitoring of a given pulsar, and that the fact that the processing is very homogeneous makes this dataset very fitting to study properties of a group of pulsars, or to compare systems with each other. The NRT spider sample can be used to systematically analyse many properties of this fascinating class of pulsars. With such a dataset many projects are possible: the systematic measure of spider periastron precession, in the same fashion as Voisin et al., 2020b, the modelling of the plasma physics happening in each eclipsing system or the study of the variations of the polarisation properties during the eclipses ingress and egress, using plasma lensing.

Appendices

Appendix A: Polarimetric profiles of the 19 spiders

This appendix refers to Section 3.3.2.

The 1.4 GHz composite profiles shown below were constructed by summing the profiles from individual NUPPI observations conducted after MJD 58800, which are observations that were calibrated using the improved polarisation calibration scheme presented in Guillemot et al. (2023). For polarimetric profiles with SNR values larger than 1000, we kept the original number of phase bins of 2048. We reduced the number of phase bins by a factor of 2 for SNR values under 1000, by a factor of 4 under 300, by a factor of 8 under 100 and by a factor of 16 under 30.

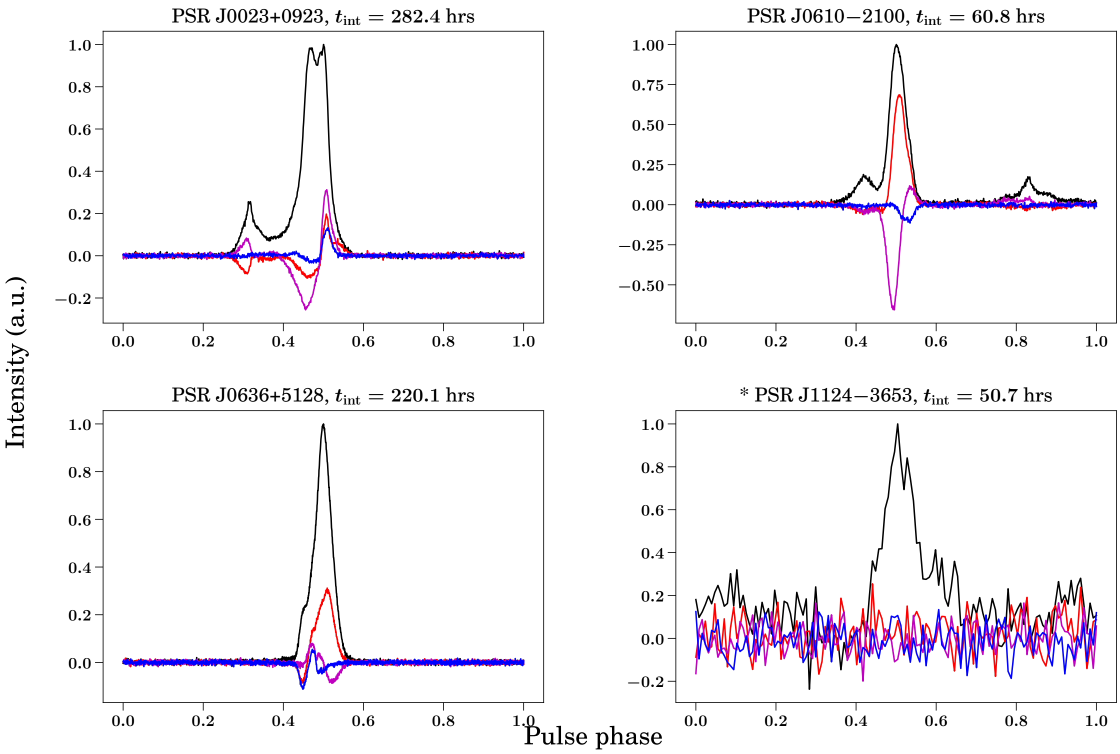

Figure 6.1: Polarimetric profiles for PSRs J0023+0923, J0610–2100, J0636+5128 and J1124–3653. In each panel, the black line represents the total intensity (Stokes parameter I), the red and purple lines correspond to the Stokes parameters Q and U describing the linear polarisation, and the blue line is the circular polarisation (Stokes parameter V). Pulse profiles were rotated in order for the total intensity maxima to be at phase 0.5. For pulsars with no published RM value we did not correct the Stokes parameters Q and U for Faraday rotation. These pulsars are indicated with an asterisk.

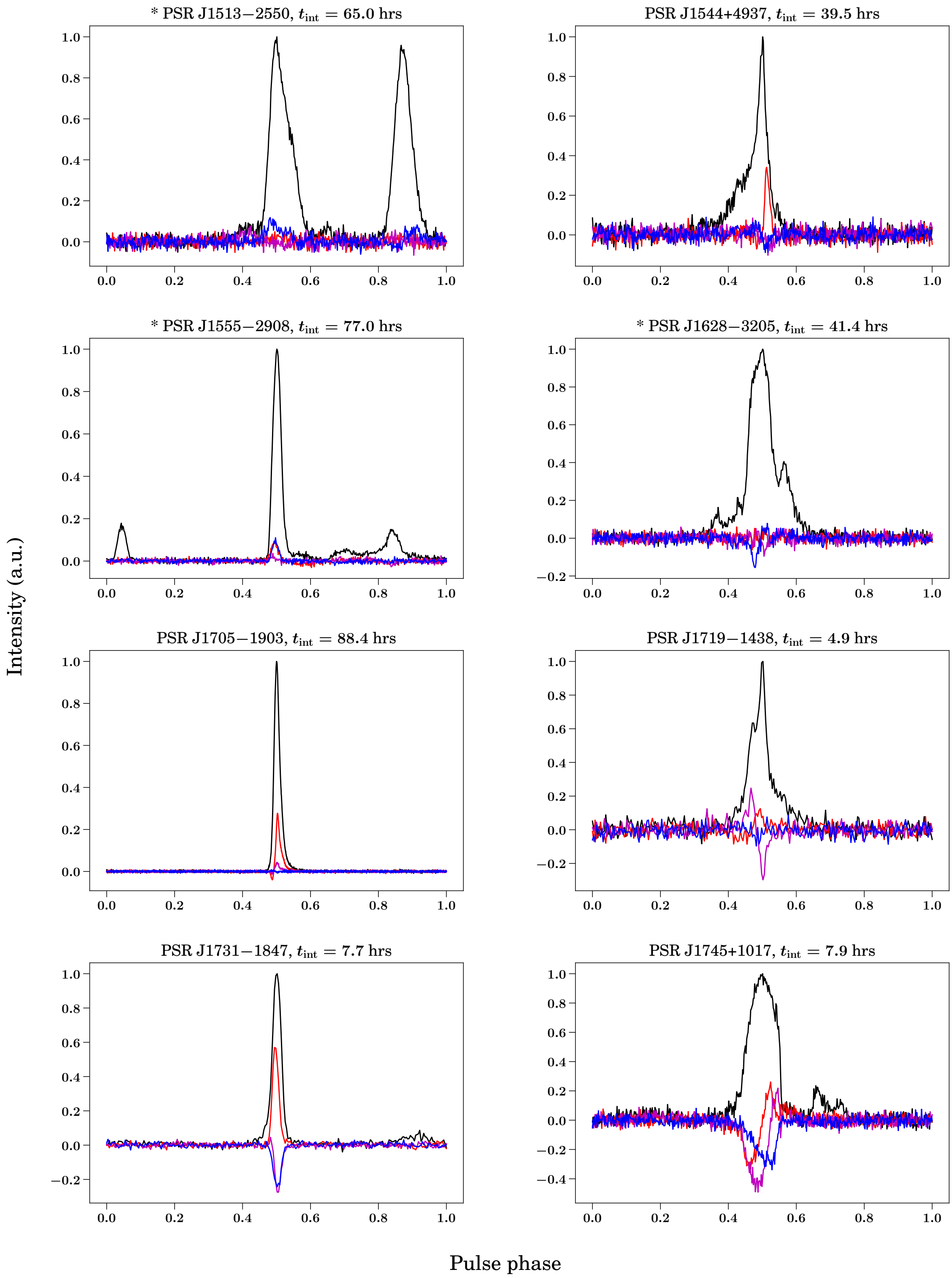

Figure 6.2: Same as Figure 6.1 but for PSRs J1513–2550, J1544+4937, J1555–2908, J1628–3205, J1705–1903, J1719–1438, J1731–1847 and J1745+1017.

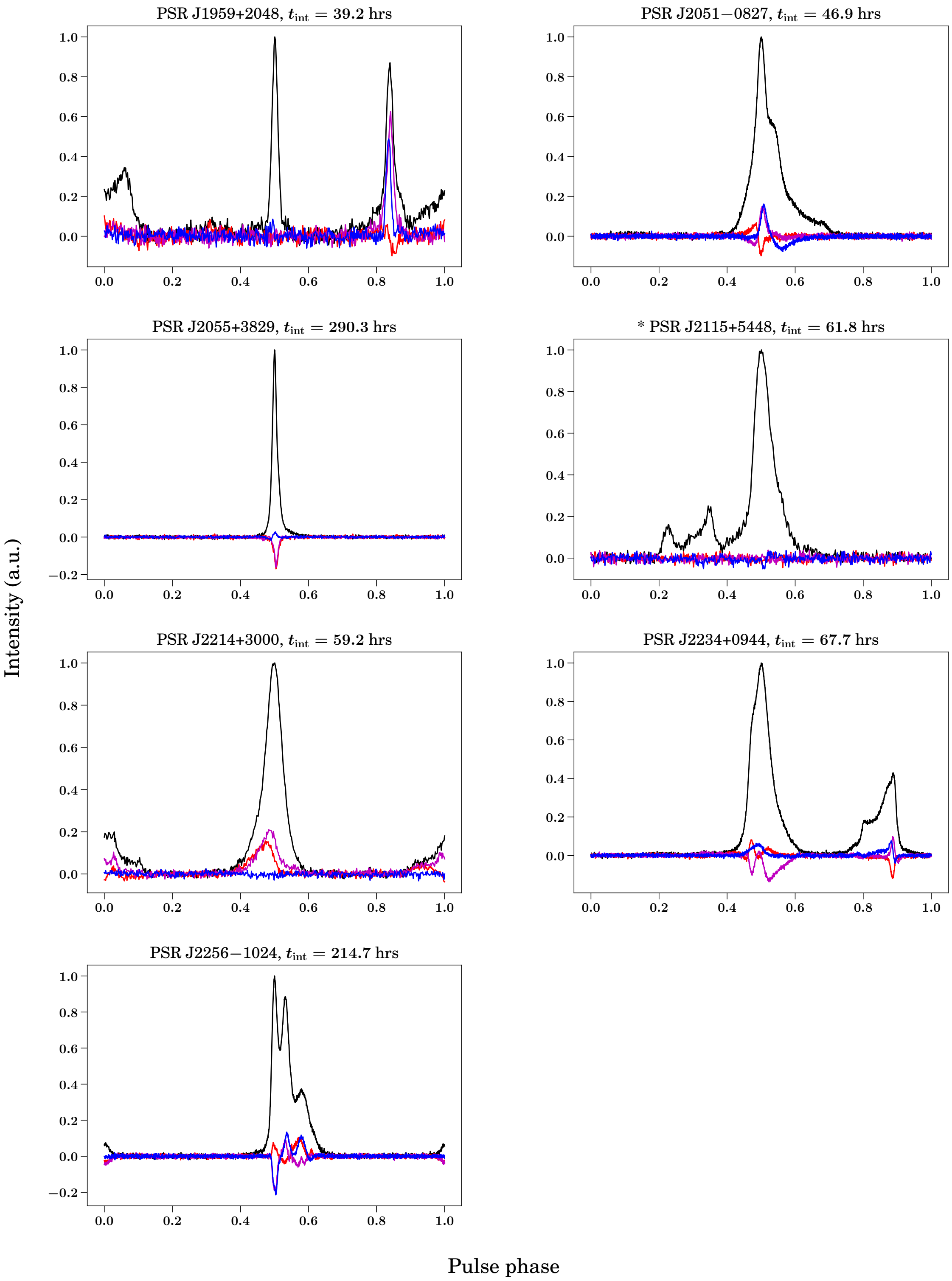

Figure 6.3: Same as Figure 6.1 but for PSRs J1959+2048, J2051−0827, J2055+3829, J2115+5448, J2214+3000, J2234+0944 and J2256−1024.

Appendix B: Timing residuals and SNR plots for the pulsar sample

In Figure 4.2 we show an example of a plot of timing residuals and SNR values as a function of orbital phase for PSR J1731−1847. In Figures 6.4, 6.5 and 6.6 we show the same plots for all the pulsars in our sample.

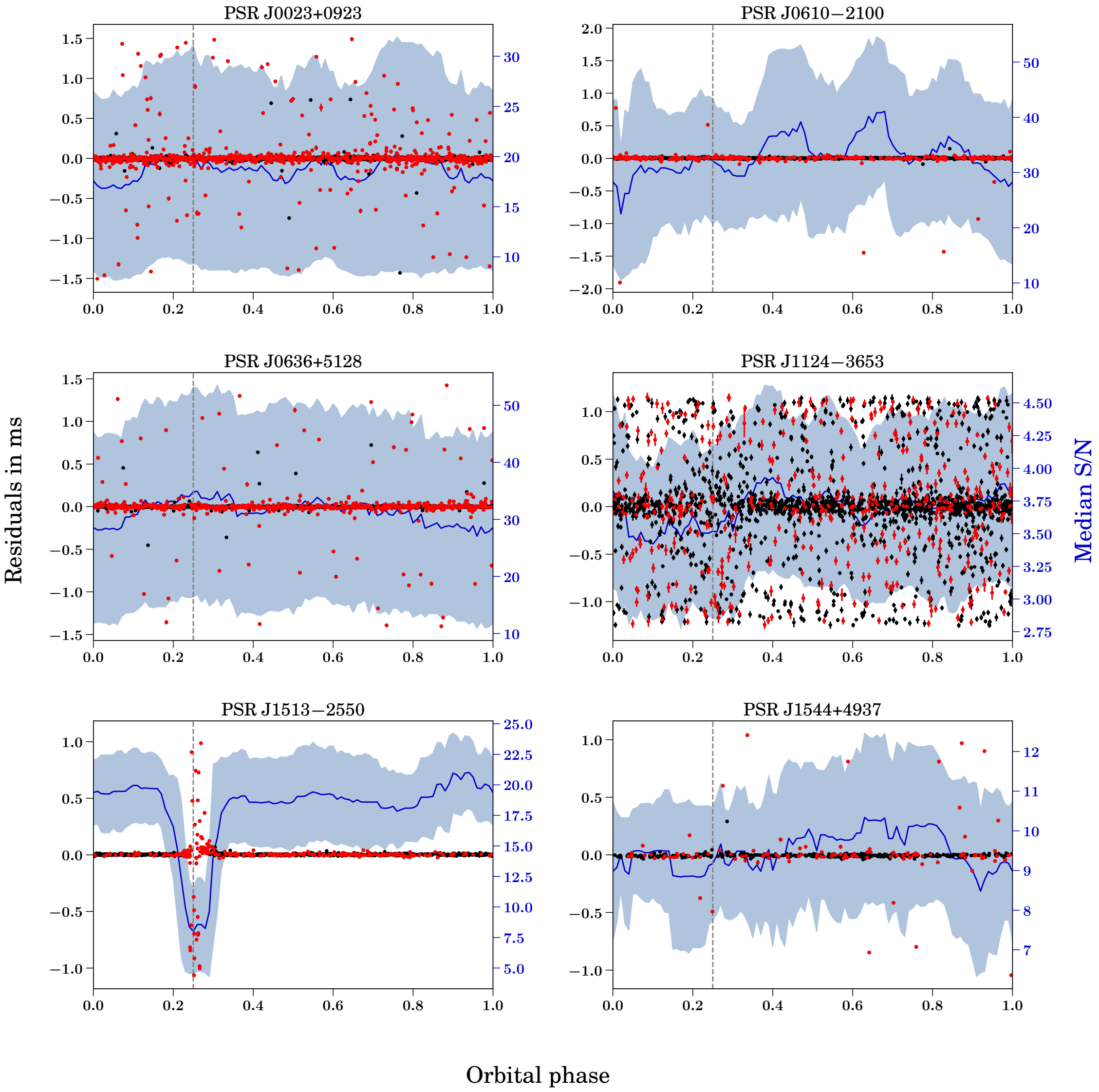

Figure 6.4: Same as Figure 4.2 but for PSRs J0023+0923, J0610−2100, J0636+5128, J1124−3653, J1513−2550 and J1544+4937. We note that in this figure SNR histograms and corresponding axes are shown in blue. TOA residuals are shown as red and black dots. Red dots correspond to observations with SNR values among the 25% lowest. Dashed vertical lines indicate superior conjunction, corresponding to orbital phase 0.25. In some plots the error bars are too small to be apparent.

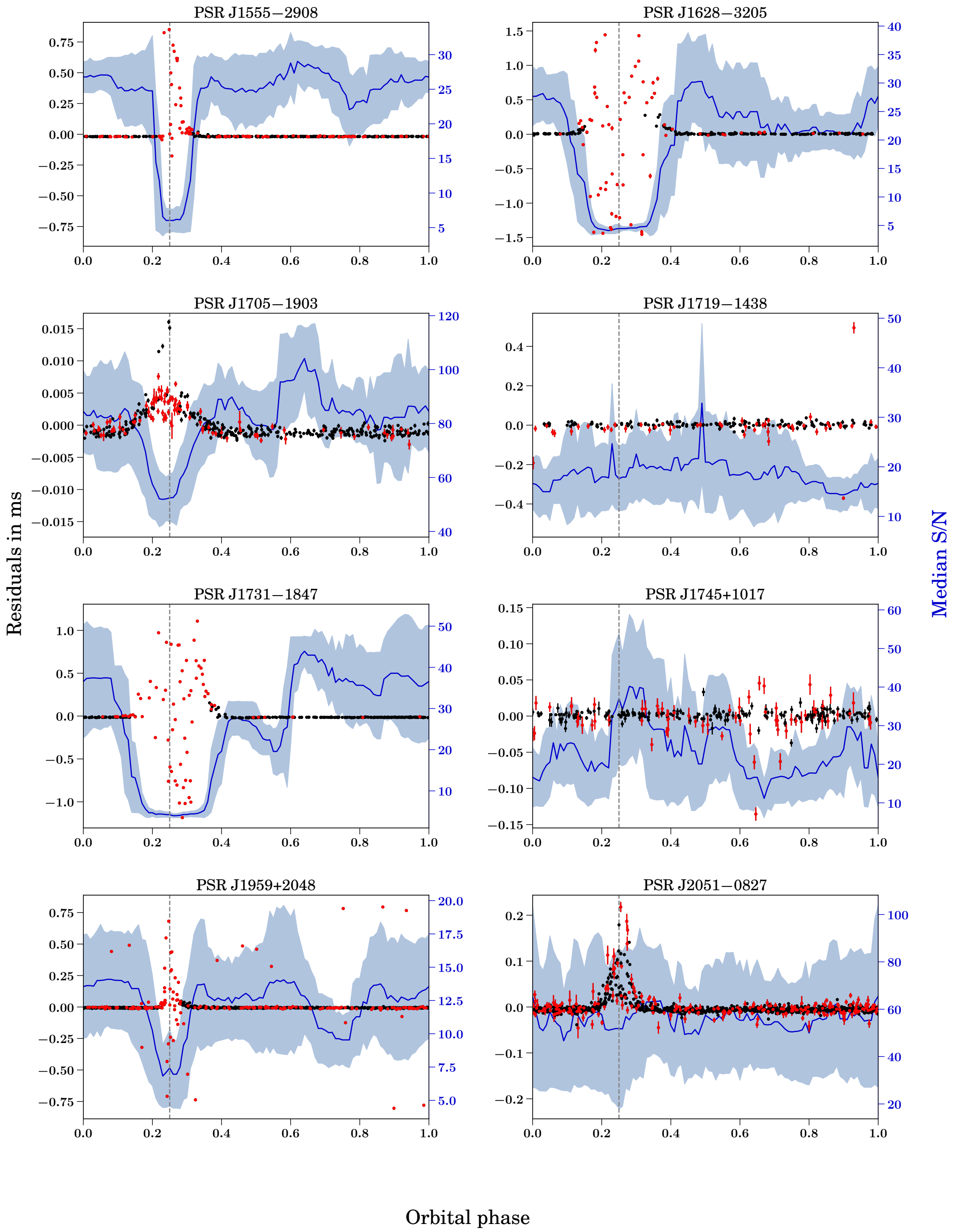

Figure 6.5: Same as Figure 6.4 but for PSRs J1555–2908, J1628–3205, J1705–1903, J1719–1438, J1731–1847, J1745+1017, J1959+2048 and J2051–0827.

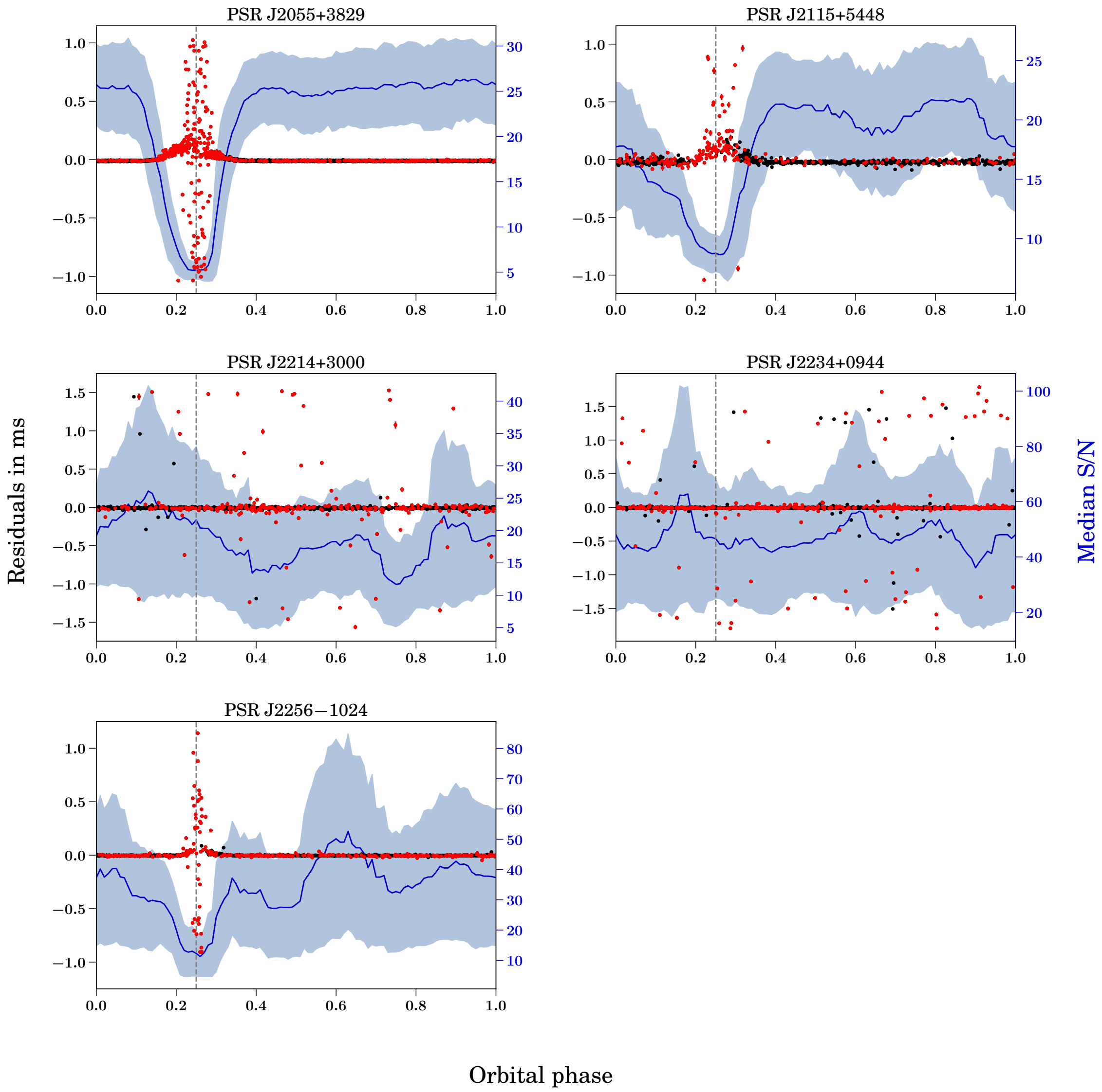

Figure 6.6: Same as Figure 6.4 but for PSRs J2055+3829, J2115+5448, J2214+3000, J2234+0944 and J2256−1024.

Appendix C: Eclipse residuals fits

This appendix refers to Section 4.2.1. In Figures 6.7 and 6.8 we show the same plot for all eclipsing pulsars in our sample. Best-fit parameters from this analysis are listed in Table 4.2.

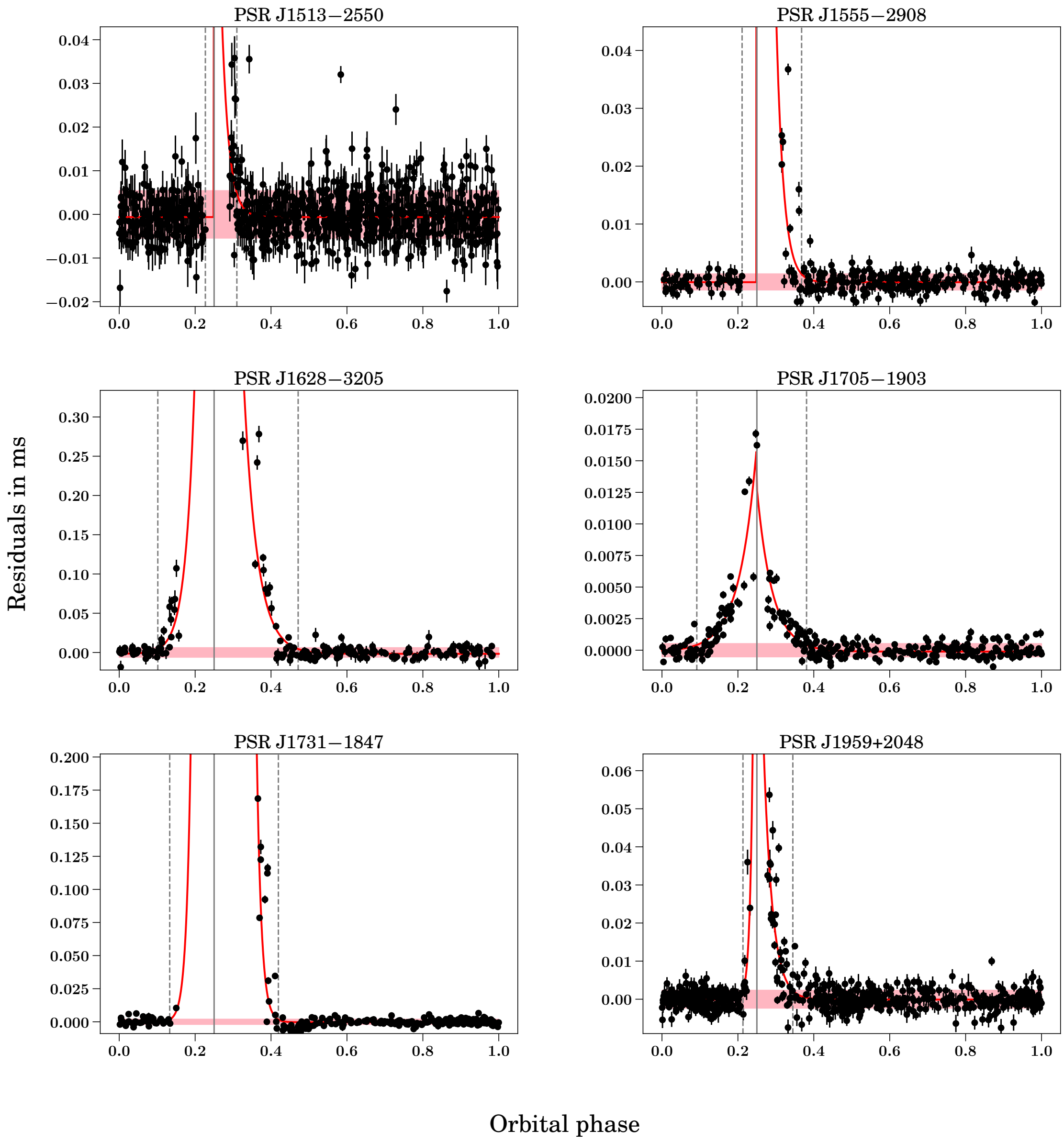

Figure 6.7: Same as Figure 4.4 but for PSRs J1513–2550, J1555–2908, J1628–3205, J1705–1903, J1731–1847 and J1959+2048. The median-fit function obtained from the analysis presented in Section 4.2 is shown in red. The light red zone represents the RMS of the timing residuals for orbital phases $\phi > 0.5$, and the dashed vertical lines correspond to the values of $\Phi_{\rm start}$ and $\Phi_{\rm end}$.

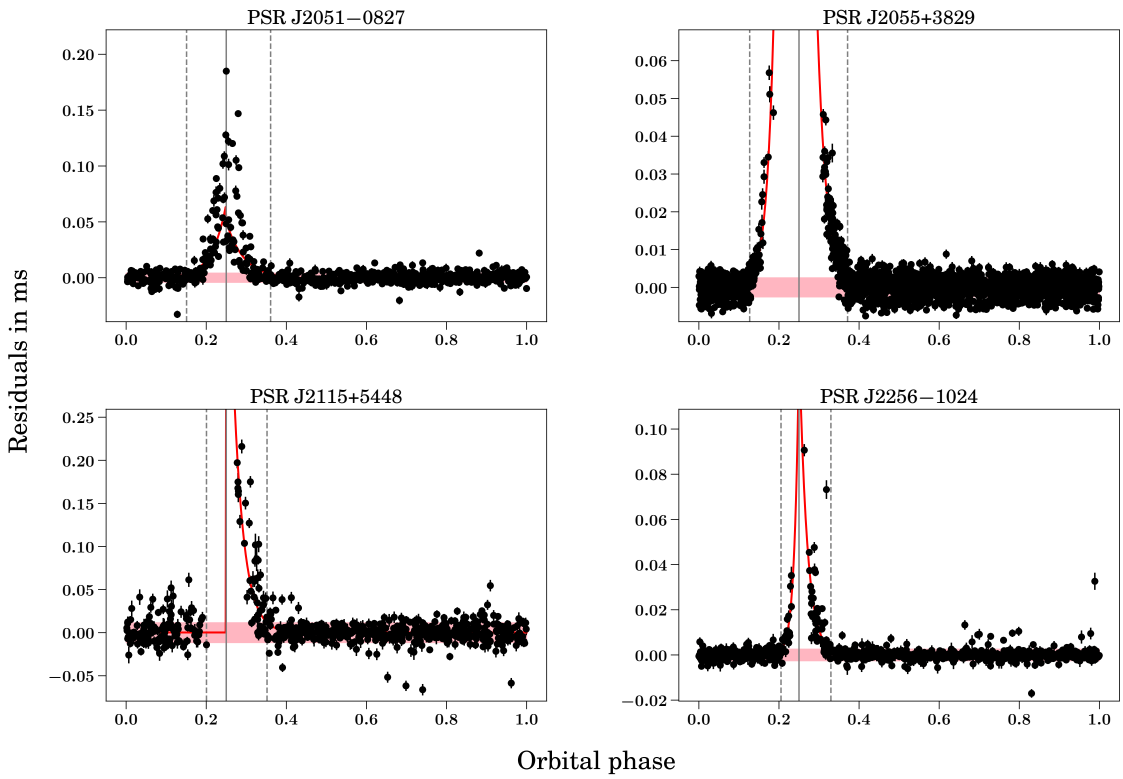

Figure 6.8: Same as Figure 6.7 but for PSRs J2051−0827, J2055+3829, J2115+5448, and J2256−1024.

Appendix D: Relationship between effective and L1 filling factors

This appendix refers to Table 4.1. It is adapted from Appendix D of Blanchard et al., 2025), written by Guillaume Voisin.

Roche-lobe geometry is determined by two parameters: the mass ratio $q = m_p/m_c$ and the binary separation a. The latter acts as a scaling factor. The stellar surface follows an equipotential surface, the largest one being by definition the boundary of the Roche lobe which goes through the L1 Lagrange point.

There is not a unique way of defining the filling factor. The L1 filling factor is defined as

$$f_{\mathrm{L1}} = \frac{r_{\mathrm{s}}}{r_{\mathrm{L1}}}, \tag{6.1}$$

where r_{s} is the distance from the centre to the surface of the star along the line connecting the two components of the binary system (the intrabinary line), and r_{L1} is the distance of the Lagrange L1 point. On the other hand the effective-radius filling factor is defined as

$$f_{\mathrm{eff}} = \frac{\bar{R}_{\mathrm{s}}}{\bar{R}_{\mathrm{L1}}}, \tag{6.2}$$

where $\bar{R}_{\mathrm{s}}$ and $\bar{R}_{\mathrm{L1}}$ are the volume-averaged radii corresponding to the stellar surface and the Roche lobe, that is the radii of spheres with the same volumes as those enclosed in the stellar surface equipotential and Roche lobe, respectively (Paczynski, 1981; Kopal, 1978). The effective Roche lobe radius $\bar{R}_{\mathrm{L1}}$ can be conveniently calculated using an approximation due to Eggleton (1983).

In Table 4.1 we have generated a numerical interpolation of the functions $f_{\mathrm{eff}}(f_{\mathrm{L1}}, q)$, and inversely $f_{\mathrm{L1}}(f_{\mathrm{eff}}, q)$. The separation a does not appear since it cancels out in the definition of the filling factors.

Bibliography

Andrade, Maydianne C. B. (July 2003). “Risky mate search and male self-sacrifice in redback spiders”. In: *Behavioral Ecology* 14.4, pp. 531–538. ISSN: 1045-2249. DOI: 10.1093/beheco/arg015.

Applegate, James H. (Feb. 1992). “A Mechanism for Orbital Period Modulation in Close Binaries”. In: *The Astrophysical Journal* 385, p. 621. DOI: 10.1086/170967.

Applegate, James H. and Jacob Shaham (Nov. 1994). “Orbital Period Variability in the Eclipsing Pulsar Binary PSR B1957+20: Evidence for a Tidally Powered Star”. In: *The Astrophysical Journal* 436, p. 312. DOI: 10.1086/174906.

Archibald, Anne M. et al. (June 2009). “A Radio Pulsar/X-ray Binary Link”. In: *Science* 324.5933, p. 1411. DOI: 10.1126/science.1172740. arXiv: 0905.3397 [astro-ph.HE].

Arons, Jonathan and Marco Tavani (Jan. 1993). “High-Energy Emission from the Eclipsing Millisecond Pulsar PSR 1957+20”. In: *The Astrophysical Journal* 403, p. 249. DOI: 10.1086/172198.

Baade, W. (Sept. 1942). “The Crab Nebula.” In: *The Astrophysical Journal* 96, p. 188. DOI: 10.1086/144446.

Baade, W. and F. Zwicky (May 1934a). “On Super-novae”. In: *Proceedings of the National Academy of Science* 20.5, pp. 254–259. DOI: 10.1073/pnas.20.5.254.

— (July 1934b). “Remarks on Super-Novae and Cosmic Rays”. In: *Physical Review* 46.1, pp. 76–77. DOI: 10.1103/PhysRev.46.76.2.

Bailes, M., A. G. Lyne, and S. L. Shemar (July 1991). “A planet orbiting the neutron star PSR1829-10”. In: 352.6333, pp. 311–313. DOI: 10.1038/352311a0.

Bailes, M. et al. (Sept. 2011). “Transformation of a Star into a Planet in a Millisecond Pulsar Binary”. In: *Science* 333.6050, p. 1717. DOI: 10.1126/science.1208890. arXiv: 1108.5201 [astro-ph.SR].

Ballet, J. et al. (July 2023). “Fermi Large Area Telescope Fourth Source Catalog Data Release 4 (4FGL-DR4)”. In: *arXiv e-prints*, arXiv:2307.12546, arXiv:2307.12546. DOI: 10.48550/arXiv.2307.12546. arXiv: 2307.12546 [astro-ph.HE].

Bangale, P. et al. (May 2024). “A 350 MHz Green Bank Telescope Survey of Unassociated Fermi LAT Sources: Discovery and Timing of 10 Millisecond Pulsars”. In: *apj* 966.2, 161, p. 161. DOI: 10.3847/1538-4357/ad2994. arXiv: 2402.09366 [astro-ph.HE].

Barr, E. D. et al. (Feb. 2013). “Pulsar searches of Fermi unassociated sources with the Effelsberg telescope”. In: *mnras* 429.2, pp. 1633–1642. DOI: 10.1093/mnras/sts449. arXiv: 1301.0359 [astro-ph.HE].

Bassa, C. G. et al. (June 2014). “A state change in the low-mass X-ray binary XSS J12270-4859”. In: *Monthly Notices of the Royal Astronomical Society* 441.2, pp. 1825–1830. DOI: https://doi.org/10.1093/mnras/stu708. arXiv: 1402.0765 [astro-ph.HE].

Bates, S. D., D. R. Lorimer, and J. P. W. Verbiest (May 2013). “The pulsar spectral index distribution”. In: *Monthly Notices of the Royal Astronomical Society* 431.2, pp. 1352–1358. DOI: 10.1093/MonthlyNoticesoftheRoyalAstronomicalSociety/stt257. arXiv: 1302.2053 [astro-ph.SR].

Bates, S. D. et al. (Oct. 2011). “The High Time Resolution Universe Pulsar Survey - II. Discovery of five millisecond pulsars”. In: *mnras* 416.4, pp. 2455–2464. DOI: 10.1111/j.1365-2966.2011.18416.x. arXiv: 1101.4778 [astro-ph.SR].

Bell Burnell, Jocelyn (Dec. 2017). “The past, present and future of pulsars”. In: *Nature Astronomy* 1, pp. 831–834. DOI: 10.1038/s41550-017-0323-x.

Benvenuto, O. G., M. A. De Vito, and J. E. Horvath (May 2014). "Understanding the Evolution of Close Binary Systems with Radio Pulsars". In: *The Astrophysical Journal Letters* 786.1, L7, p. L7. DOI: 10.1088/2041-8205/786/1/L7. arXiv: 1402.7338 [astro-ph.SR].

Berthereau, Anaïs (Mar. 2023). "Méthodes avancées en chronométrie des pulsars : réjection d'interférences radio par apprentissage profond et étude chronométrique du système binaire relativiste J1528-3146". PhD thesis. Université d'Orléans, France.

Bhat, N. D. Ramesh et al. (Apr. 2004). "Multifrequency Observations of Radio Pulse Broadening and Constraints on Interstellar Electron Density Microstructure". In: *The Astrophysical Journal* 605.2, pp. 759–783. DOI: 10.1086/382680. arXiv: astro-ph/0401067 [astro-ph].

Bhattacharya, D. and E. P. J. van den Heuvel (Jan. 1991). "Formation and evolution of binary and millisecond radio pulsars". In: *physrep* 203.1-2, pp. 1–124. DOI: 10.1016/0370-1573(91)90064-S.

Bhattacharya, Dipankar (Mar. 2002). "Evolution of Neutron Star Magnetic Fields". In: *Journal of Astrophysics and Astronomy* 23.1-2, pp. 67–72. DOI: 10.1007/BF02702467.

Bhattacharyya, B. et al. (Aug. 2013). "GMRT Discovery of PSR J1544+4937: An Eclipsing Black-widow Pulsar Identified with a Fermi-LAT Source". In: *The Astrophysical Journal Letters* 773.1, L12, p. L12. DOI: 10.1088/2041-8205/773/1/L12. arXiv: 1304.7101 [astro-ph.HE].

Blanchard, C. et al. (June 2025). "A census of galactic spider binary millisecond pulsars with the Nançay Radio Telescope". In: *aap* 698, A239, A239. DOI: 10.1051/0004-6361/202453499. arXiv: 2504.10037 [astro-ph.HE].

Blandford, R. and S. A. Teukolsky (Apr. 1976). "Arrival-time analysis for a pulsar in a binary system." In: *The Astrophysical Journal* 205, pp. 580–591. DOI: 10.1086/154315.

Bolton, J. G., G. J. Stanley, and O. B. Slee (July 1949). "Positions of Three Discrete Sources of Galactic Radio-Frequency Radiation". In: *Nature* 164.4159, pp. 101–102. DOI: 10.1038/164101b0.

Bowyer, S. et al. (Jan. 1964). "X-Ray Emission from the Direction of Scorpius." In: *aj* 69, p. 135. DOI: 10.1086/109364.

Breton, R. P. et al. (June 2013). "Discovery of the Optical Counterparts to Four Energetic Fermi Millisecond Pulsars". In: *The Astrophysical Journal* 769.2, 108, p. 108. DOI: 10.1088/0004-637X/769/2/108. arXiv: 1302.1790 [astro-ph.HE].

Burgay, M. et al. (Dec. 2003). "An increased estimate of the merger rate of double neutron stars from observations of a highly relativistic system". In: *Nature* 426.6966, pp. 531–533. DOI: 10.1038/nature02124. arXiv: astro-ph/0312071 [astro-ph].

Burgay, M. et al. (May 2006). "The Parkes High-Latitude pulsar survey". In: *Monthly Notices of the Royal Astronomical Society* 368.1, pp. 283–292. DOI: 10.1111/j.1365-2966.2006.10100.x.

Chadwick, James (1932). "The existence of a neutron". In: *Proceedings of the Royal Society of London. Series A, Containing Papers of a Mathematical and Physical Character* 136.830, pp. 692–708. DOI: 10.1098/rspa.1932.0112.

Chandrasekhar, S. (July 1931). "The Maximum Mass of Ideal White Dwarfs". In: *The Astrophysical Journal* 74, p. 81. DOI: 10.1086/143324.

Chen, Hai-Liang et al. (Aug. 2013). "FORMATION OF BLACK WIDOWS AND REDBACKS—TWO DISTINCT POPULATIONS OF ECLIPSING BINARY MILLISECOND PULSARS". In: *The Astrophysical Journal* 775.1, p. 27. DOI: 10.1088/0004-637X/775/1/27. URL: https://dx.doi.org/10.1088/0004-637X/775/1/27.

Cisneros-Parra, J. U. (Jan. 1970). "Apsidal motion in close binaries with and without mass exchange." In: *Astronomy & Astrophysics* 8, p. 141.

Clark, C. J. et al. (Nov. 2016). "THE BRAKING INDEX OF A RADIO-QUIET GAMMA-RAY PULSAR". In: *The Astrophysical Journal Letters* 832.1, p. L15. DOI: 10.3847/2041-8205/832/1/L15. URL: https://dx.doi.org/10.3847/2041-8205/832/1/L15.

Clark, C. J. et al. (Apr. 2023). "Neutron star mass estimates from gamma-ray eclipses in spider millisecond pulsar binaries". In: *Nature Astronomy* 7, pp. 451–462. DOI: 10.1038/s41550-022-01874-x. arXiv: 2301.10995 [astro-ph.HE].

Crowter, Kathryn et al. (July 2020). "The GBT 350-MHz Drift Scan Pulsar Survey - III. Detection of a magnetic field in the eclipsing material of PSR J2256-1024". In: *Monthly Notices of the Royal

Astronomical Society 495.3, pp. 3052–3064. DOI: 10.1093/mnras/staa933. arXiv: 2004.00164 [astro-ph.HE].
Damour, Thibault and Nathalie Deruelle (1986). "General relativistic celestial mechanics of binary systems. II. The post-newtonian timing formula". eng. In: *Annales de l'I.H.P. Physique théorique* 44.3, pp. 263–292. URL: http://eudml.org/doc/76319.
de Jager, O. C., B. C. Raubenheimer, and J. W. H. Swanepoel (Aug. 1989). "A powerful test for weak periodic signals with unknown light curve shape in sparse data." In: 221, pp. 180–190.
Demianski, M. and M. Proszynski (Nov. 1979). "Does PSR0329 + 54 have companions?" In: 282.5737, pp. 383–385. DOI: 10.1038/282383a0.
Demorest, Paul B. (Aug. 2007). "Measuring the gravitational wave background using precision pulsar timing". PhD thesis. University of California, Berkeley.
Dhillon, V. S. et al. (Oct. 2022). "Multicolour optical light curves of the companion star to the millisecond pulsar PSR J2051-0827". In: *Monthly Notices of the Royal Astronomical Society* 516.2, pp. 2792–2800. DOI: 10.1093/mnras/stac2357. arXiv: 2208.09249 [astro-ph.SR].
Draghis, Paul and Roger W. Romani (July 2018). "PSR J0636+5128: A Heated Companion in a Tight Orbit". In: *The Astrophysical Journal Letters* 862.1, L6, p. L6. DOI: 10.3847/2041-8213/aad2db. arXiv: 1807.04249 [astro-ph.HE].
Draghis, Paul et al. (Sept. 2019). "Multiband Optical Light Curves of Black-widow Pulsars". In: *The Astrophysical Journal* 883.1, 108, p. 108. DOI: 10.3847/1538-4357/ab378b. arXiv: 1908.00992 [astro-ph.HE].
Du, Ze-Xin et al. (Dec. 2023). "Constraining the Orbital Inclination and Companion Properties of Three Black Widow Pulsars Detected by FAST". In: *Research in Astronomy and Astrophysics* 23.12, 125024, p. 125024. DOI: 10.1088/1674-4527/ad034b. arXiv: 2310.08197 [astro-ph.HE].
DuPlain, Ron et al. (Aug. 2008). "Launching GUPPI: the Green Bank Ultimate Pulsar Processing Instrument". In: *Advanced Software and Control for Astronomy II*. Ed. by Alan Bridger and Nicole M. Radziwill. Vol. 7019. Society of Photo-Optical Instrumentation Engineers (SPIE) Conference Series, 70191D, p. 70191D. DOI: 10.1117/12.790003.
Dutta, A. et al. (May 2025). "NGC 1851A: Revealing an ongoing three-body encounter in a dense globular cluster". In: 697, A166, A166. DOI: 10.1051/0004-6361/202452433. arXiv: 2503.05466 [astro-ph.HE].
Eggleton, P. P. (1983). "Aproximations to the radii of Roche lobes." In: *The Astrophysical Journal* 268, p. 368. ISSN: 0004-637X. DOI: 10.1086/160960. URL: https://ui.adsabs.harvard.edu/#abs/1983ApJ...268..368E/abstract (visited on 10/29/2018).
EPTA Collaboration (2023). "The second data release from the European Pulsar Timing Array - I. The dataset and timing analysis". In: *A&A* 678, A48. DOI: 10.1051/0004-6361/202346841. URL: https://doi.org/10.1051/0004-6361/202346841.
Espinoza, C. M., A. G. Lyne, and B. W. Stappers (Nov. 2016). "New long-term braking index measurements for glitching pulsars using a glitch-template method". In: *Monthly Notices of the Royal Astronomical Society* 466.1, pp. 147–162. ISSN: 0035-8711. DOI: 10.1093/mnras/stw3081.
Espinoza, C. M. et al. (Jan. 2013). "Six millisecond pulsars detected by the Fermi Large Area Telescope and the radio/gamma-ray connection of millisecond pulsars". In: *Monthly Notices of the Royal Astronomical Society* 430.1, pp. 571–587. ISSN: 0035-8711. DOI: 10.1093/mnras/sts657.
Fairhead, Laurent (Jan. 1989). "Chronométrage du pulsar milliseconde PSR1937+214 : analyse Astrométrique et Observations à Nançay". Theses. Observatoire de Paris.
Faucher-Giguère, Claude-André and Kaspi (May 2006). "Birth and Evolution of Isolated Radio Pulsars". In: *The Astrophysical Journal* 643.1, pp. 332–355. DOI: 10.1086/501516. arXiv: astro-ph/0512585 [astro-ph].
Ferdman, R. D., R. F. Archibald, and V. M. Kaspi (Oct. 2015). "Long-term timing and emission behaviour of the young Crab-like pulsar PSR B0540–69". In: *The Astrophysical Journal* 812.2, p. 95. DOI: 10.1088/0004-637X/812/2/95. URL: https://dx.doi.org/10.1088/0004-637X/812/2/95.

Fonseca, E. et al. (July 2021). "Refined Mass and Geometric Measurements of the High-mass PSR J0740+6620". In: 915.1, L12, p. L12. DOI: 10.3847/2041-8213/ac03b8. arXiv: 2104.00880 [astro-ph.HE].

Fonseca, Emmanuel et al. (Jan. 2015). "Long-term Timing of the Pulsar Triple System in M4". In: *American Astronomical Society Meeting Abstracts #225*. Vol. 225. American Astronomical Society Meeting Abstracts, 346.15, p. 346.15.

Fontaine, G., P. Brassard, and P. Bergeron (Apr. 2001). "The Potential of White Dwarf Cosmochronology". In: *pasp* 113.782, pp. 409–435. DOI: 10.1086/319535.

Foreman-Mackey, Daniel et al. (Mar. 2013). "emcee: The MCMC Hammer". In: *pasp* 125.925, p. 306. DOI: 10.1086/670067. arXiv: 1202.3665 [astro-ph.IM].

Freire, P. C. C. (July 2005). "Eclipsing Binary Pulsars". In: *Binary Radio Pulsars*. Ed. by Fred A. Rasio and Ingrid H. Stairs. Vol. 328. Astronomical Society of the Pacific Conference Series, p. 405. DOI: 10.48550/arXiv.astro-ph/0404105. arXiv: astro-ph/0404105 [astro-ph].

Fruchter, A. S., D. R. Stinebring, and J. H. Taylor (May 1988). "A millisecond pulsar in an eclipsing binary". In: *Nature* 333.6170, pp. 237–239. DOI: 10.1038/333237a0.

Gardner, F. F. and D. K. Milne (Nov. 1965). "The supernova of A.D. 1006". In: *aj* 70, p. 754. DOI: 10.1086/109813.

Gentile, P. A. et al. (Feb. 2014). "X-RAY OBSERVATIONS OF BLACK WIDOW PULSARS". In: *The Astrophysical Journal* 783.2, p. 69. DOI: 10.1088/0004-637X/783/2/69.

Gold, T. (May 1968). "Rotating Neutron Stars as the Origin of the Pulsating Radio Sources". In: *Nature* 218.5143, pp. 731–732. DOI: 10.1038/218731a0.

Goldreich, Peter and William H. Julian (Aug. 1969). "Pulsar Electrodynamics". In: *The Astrophysical Journal* 157, p. 869. DOI: 10.1086/150119.

Guillemot, L. et al. (Jan. 2012). "Pulsed Gamma Rays from the Original Millisecond and Black Widow Pulsars: A Case for Caustic Radio Emission?" In: *apj* 744.1, 33, p. 33. DOI: 10.1088/0004-637X/744/1/33. arXiv: 1110.1271 [astro-ph.HE].

Guillemot, L. et al. (Sept. 2019). "Timing of PSR J2055+3829, an eclipsing black widow pulsar discovered with the Nançay Radio Telescope". In: *aap* 629, A92, A92. DOI: 10.1051/0004-6361/201936015. arXiv: 1907.09778 [astro-ph.HE].

Guillemot, L. et al. (Oct. 2023). "Improving pulsar polarization and timing measurements with the Nançay Radio Telescope". In: *Astronomy & Astrophysics* 678, A79, A79. DOI: 10.1051/0004-6361/202347018. arXiv: 2308.01599 [astro-ph.HE].

Guo, Yunlang, Bo Wang, and Zhanwen Han (Sept. 2022). "Formation of black widows through ultracompact X-ray binaries with He star companions". In: *Monthly Notices of the Royal Astronomical Society* 515.2, pp. 2725–2732. DOI: 10.1093/mnras/stac1917. arXiv: 2204.06132 [astro-ph.HE].

Han, J. L. et al. (Jan. 2018). "Pulsar Rotation Measures and Large-scale Magnetic Field Reversals in the Galactic Disk". In: *The Astrophysical Journal Supplement Series* 234.1, p. 11. DOI: 10.3847/1538-4365/aa9c45. URL: https://dx.doi.org/10.3847/1538-4365/aa9c45.

Hellings, R. W. and G. S. Downs (Feb. 1983). "Upper limits on the isotropic gravitational radiation background from pulsar timing analysis." In: *The Astrophysical Journal Letters* 265, pp. L39–L42. DOI: 10.1086/183954.

Hewish, A. et al. (Feb. 1968). "Observation of a Rapidly Pulsating Radio Source". In: *Nature* 217.5130, pp. 709–713. DOI: 10.1038/217709a0.

Hinkle, Dennis E, William Wiersma, and Stephen G Jurs (1979). *Applied statistics for the behavioral sciences*. English. Includes index. Chicago : Rand McNally College Pub. Co.

Hirai, Ryosuke and Philipp Podsiadlowski (Dec. 2022). "Neutron stars colliding with binary companions: formation of hypervelocity stars, pulsar planets, bumpy superluminous supernovae and Thorne-Żytkow objects". In: 517.3, pp. 4544–4556. DOI: 10.1093/mnras/stac3007. arXiv: 2208.00915 [astro-ph.HE].

Hobbs, G. B., R. T. Edwards, and R. N. Manchester (June 2006). "TEMPO2, a new pulsar-timing package - I. An overview". In: *Monthly Notices of the Royal Astronomical Society* 369.2, pp. 655–672. DOI: 10.1111/j.1365-2966.2006.10302.x. arXiv: astro-ph/0603381 [astro-ph].

Hotan, A. W., W. van Straten, and R. N. Manchester (Jan. 2004). "PSRCHIVE and PSRFITS: An Open Approach to Radio Pulsar Data Storage and Analysis". In: *pasa* 21.3, pp. 302–309. DOI: 10.1071/AS04022. arXiv: astro-ph/0404549 [astro-ph].

Hulse, R. A. and J. H. Taylor (1975). "A Deep Sample of New Pulsars and their Spatial Extent in the Galaxy". In: *The Astrophysical Journal Letters* 201, pp. L55–L59.

Hurley, Jarrod R., Christopher A. Tout, and Onno R. Pols (Feb. 2002). "Evolution of binary stars and the effect of tides on binary populations". In: *Monthly Notices of the Royal Astronomical Society* 329.4, pp. 897–928. DOI: 10.1046/j.1365-8711.2002.05038.x. arXiv: astro-ph/0201220 [astro-ph].

Jansky, Karl G. (July 1933). "Radio Waves from Outside the Solar System". In: *Nature* 132.3323, p. 66. DOI: 10.1038/132066a0.

Jenet, Fredrick A. and Joseph D. Romano (July 2015). "Understanding the gravitational-wave Hellings and Downs curve for pulsar timing arrays in terms of sound and electromagnetic waves". In: *American Journal of Physics* 83.7, pp. 635–645. DOI: 10.1119/1.4916358. arXiv: 1412.1142 [gr-qc].

Jia, Kun and Xiang-Dong Li (Oct. 2016). "EVOLUTION OF LOW-MASS X-RAY BINARIES: THE EFFECT OF DONOR EVAPORATION". In: *The Astrophysical Journal* 830.2, p. 153. DOI: 10.3847/0004-637X/830/2/153. URL: https://dx.doi.org/10.3847/0004-637X/830/2/153.

Joshi, Kriten J. and Frederic A. Rasio (Apr. 1997). "Distant Companions and Planets around Millisecond Pulsars". In: *The Astrophysical Journal* 479.2, p. 948. DOI: 10.1086/303916. URL: https://dx.doi.org/10.1086/303916.

Kaplan, D. L. et al. (Sept. 2018). "A Dense Companion to the Short-period Millisecond Pulsar Binary PSR J0636+5128". In: *The Astrophysical Journal* 864.1, 15, p. 15. DOI: 10.3847/1538-4357/aad54c. arXiv: 1807.04610 [astro-ph.HE].

Keith, M. J. et al. (Dec. 2010). "The High Time Resolution Universe Pulsar Survey - I. System configuration and initial discoveries". In: 409.2, pp. 619–627. DOI: 10.1111/j.1365-2966.2010.17325.x. arXiv: 1006.5744 [astro-ph.HE].

Kennedy, M. R. et al. (May 2022). "Measuring the mass of the black widow PSR J1555-2908". In: *Monthly Notices of the Royal Astronomical Society* 512.2, pp. 3001–3014. DOI: 10.1093/mnras/stac379. arXiv: 2202.05111 [astro-ph.HE].

Kerr, M. (May 2011). "Improving Sensitivity to Weak Pulsations with Photon Probability Weighting". In: 732.1, 38, p. 38. DOI: 10.1088/0004-637X/732/1/38. arXiv: 1103.2128 [astro-ph.IM].

Koljonen and Linares (May 2025). "SpiderCat: A Catalog of Compact Binary Millisecond Pulsars". In: *arXiv e-prints*, arXiv:2505.11691, arXiv:2505.11691. DOI: 10.48550/arXiv.2505.11691. arXiv: 2505.11691 [astro-ph.HE].

Komesaroff, M. M. (Feb. 1970). "Possible Mechanism for the Pulsar Radio Emission". In: *Nature* 225.5233, pp. 612–614. DOI: 10.1038/225612a0.

Kopal, Zdeněk (1978). *Dynamics of Close Binary Systems*. OCLC: 851368874. Dordrecht: Springer Netherlands. ISBN: 978-94-009-9780-6. URL: http://dx.doi.org/10.1007/978-94-009-9780-6 (visited on 10/30/2018).

Kramer, Michael et al. (July 1998). "The Characteristics of Millisecond Pulsar Emission. I. Spectra, Pulse Shapes, and the Beaming Fraction". In: *The Astrophysical Journal* 501.1, pp. 270–285. DOI: 10.1086/305790. arXiv: astro-ph/9801177 [astro-ph].

Kramer et al. (Aug. 2003). "The Proper Motion, Age, and Initial Spin Period of PSR J0538+2817 in S147". In: *The Astrophysical Journal Letters* 593.1, pp. L31–L34. DOI: 10.1086/378082. arXiv: astro-ph/0306628 [astro-ph].

Kraus, John D. (Mar. 1960). "The Ohio State University 360-Foot Radio Telescope." In: *aj* 65, p. 54. DOI: 10.1086/108183.

Kumari, Sangita et al. (Feb. 2024). "First Systematic Study Reporting the Changes in Eclipse Cutoff Frequency for Pulsar J1544+4937". In: *The Astrophysical Journal* 961.2, 155, p. 155. DOI: 10.3847/1538-4357/ad0b83. arXiv: 2311.02071 [astro-ph.HE].

Landau, L. (Feb. 1938). "Origin of Stellar Energy". In: *Nature* 141.3564, pp. 333–334. DOI: 10.1038/141333b0.

Landau, L. D. (Dec. 1932). "To the Stars theory". In: *Phys. Zs. Sowjet* 1, p. 285.

Lange, Ch. et al. (Sept. 2001). "Precision timing measurements of PSR J1012+5307". In: *Monthly Notices of the Royal Astronomical Society* 326.1, pp. 274–282. DOI: 10.1046/j.1365-8711.2001.04606.x. arXiv: astro-ph/0102309 [astro-ph].

Lanza, Antonino F. (Oct. 2006). "On the time dependence of differential rotation in young late-type stars". In: *Monthly Notices of the Royal Astronomical Society* 373.2, pp. 819–826. ISSN: 0035-8711. DOI: 10.1111/j.1365-2966.2006.11085.x.

Laycock, Silas G. T. and Dimitris M. Christodoulou (Mar. 2025). "On the Number of Confirmed Pulsar Planets: The Rule of Six". In: 982.1, 63, p. 63. DOI: 10.3847/1538-4357/adb1a8.

Lazarus, P. et al. (May 2016). "Prospects for high-precision pulsar timing with the new Effelsberg PSRIX backend". In: *Monthly Notices of the Royal Astronomical Society* 458.1, pp. 868–880. DOI: 10.1093/mnras/stw189. arXiv: 1601.06194 [astro-ph.IM].

Lee, K. J. et al. (Aug. 2012). "Application of the Gaussian mixture model in pulsar astronomy - pulsar classification and candidates ranking for the Fermi 2FGL catalogue". In: *Monthly Notices of the Royal Astronomical Society* 424.4, pp. 2832–2840. DOI: 10.1111/j.1365-2966.2012.21413.x. arXiv: 1205.6221 [astro-ph.IM].

Lee, L. C. and J. R. Jokipii (June 1976). "The irregularity spectrum in interstellar space." In: 206, pp. 735–743. DOI: 10.1086/154434.

Lequeux, James, Jean-Louis Steinberg, and Wayne Orchiston (Mar. 2010). "Highlighting the history of French Radio Astronomy. 5: The Nançay Large Radio Telescope". In: *Journal of Astronomical History and Heritage* 13.1, pp. 29–42.

Li, Miao, Jules P. Halpern, and John R. Thorstensen (Nov. 2014). "Optical Counterparts of Two Fermi Millisecond Pulsars: PSR J1301+0833 and PSR J1628-3205". In: *The Astrophysical Journal* 795.2, 115, p. 115. DOI: 10.1088/0004-637X/795/2/115. arXiv: 1409.3877 [astro-ph.HE].

Lin, D. N. C., S. E. Woosley, and P. H. Bodenheimer (Oct. 1991). "Formation of a planet orbiting pulsar 1829-10 from the debris of a supernova explosion". In: 353.6347, pp. 827–829. DOI: 10.1038/353827a0.

Lin, F. X. et al. (Sept. 2021). "Discovery and modelling of broad-scale plasma lensing in black-widow pulsar J2051 - 0827". In: *Monthly Notices of the Royal Astronomical Society* 506.2, pp. 2824–2835. DOI: 10.1093/mnras. eprint: 2106.12359 (astro-ph.HE).

Lin, F. X. et al. (Feb. 2023). "Plasma lensing near the eclipses of the Black Widow pulsar B1957+20". In: *Monthly Notices of the Royal Astronomical Society* 519.1, pp. 121–135. DOI: 10.1093/mnras/stac3456. arXiv: 2208.13868 [astro-ph.HE].

Linares, M. (Dec. 2020). "Super-Massive Neutron Stars and Compact Binary Millisecond Pulsars". In: *Multifrequency Behaviour of High Energy Cosmic Sources - XIII. 3-8 June 2019. Palermo*, 23, p. 23. DOI: 10.22323/1.362.0023. arXiv: 1910.09572 [astro-ph.HE].

Livingstone, Margaret A. and Victoria M. Kaspi (Nov. 2011). "LONG-TERM X-RAY MONITORING OF THE YOUNG PULSAR PSR B1509-58". In: *The Astrophysical Journal* 742.1, p. 31. DOI: 10.1088/0004-637X/742/1/31. URL: https://dx.doi.org/10.1088/0004-637X/742/1/31.

Lorimer, D. R. and M. Kramer (2004). *Handbook of Pulsar Astronomy*. Vol. 4.

Love, A. E. H. (Feb. 1909). "The Yielding of the Earth to Disturbing Forces". In: *Proceedings of the Royal Society of London Series A* 82.551, pp. 73–88. DOI: 10.1098/rspa.1909.0008.

Lyne, A. G. et al. (Mar. 1988). "Discovery of a binary millisecond pulsar in the globular cluster M4". In: 332.6159, pp. 45–47. DOI: 10.1038/332045a0.

Lyne, A. G. et al. (Jan. 2015). "45 years of rotation of the Crab pulsar". In: *Monthly Notices of the Royal Astronomical Society* 446.1, pp. 857–864. DOI: 10.1093/mnras/stu2118. arXiv: 1410.0886 [astro-ph.HE].

Main, Robert et al. (May 2018). "Pulsar emission amplified and resolved by plasma lensing in an eclipsing binary". In: *nat* 557.7706, pp. 522–525. DOI: 10.1038/s41586-018-0133-z. arXiv: 1805.09348 [astro-ph.HE].

Manchester, R. N. et al. (Apr. 2005). "The Australia Telescope National Facility Pulsar Catalogue". In: *aj* 129.4, pp. 1993–2006. DOI: 10.1086/428488. arXiv: astro-ph/0412641 [astro-ph].

Mata Sánchez, D. et al. (Apr. 2023). "A black widow population dissection through HiPERCAM multiband light-curve modelling". In: *Monthly Notices of the Royal Astronomical Society* 520.2, pp. 2217–2244. DOI: 10.1093/mnras/stad203. arXiv: 2301.07132 [astro-ph.HE].

Matthews, Thomas A. and Allan R. Sandage (July 1963). "Optical Identification of 3C 48, 3C 196, and 3C 286 with Stellar Objects." In: *The Astrophysical Journal* 138, p. 30. DOI: 10.1086/147615.

McLaughlin, M. A. et al. (Dec. 2009). "Timing observations of rotating radio transients". In: *Monthly Notices of the Royal Astronomical Society* 400.3, pp. 1431–1438. DOI: 10.1111/j.1365-2966.2009.15584.x. arXiv: 0908.3813 [astro-ph.SR].

Meltzer, David W. and Kip S. Thorne (Aug. 1966). "Normal Modes of Radial Pulsation of Stars at the End Point of Thermonuclear Evolution". In: *The Astrophysical Journal* 145, p. 514. DOI: 10.1086/148792.

Michel, F. C. and H. Li (Sept. 1999). "Electrodynamics of neutron stars". In: *physrep* 318.6, pp. 227–297. DOI: 10.1016/S0370-1573(99)00002-2.

Miret-Roig, Núria et al. (Feb. 2022). "A rich population of free-floating planets in the Upper Scorpius young stellar association". In: *Nature Astronomy* 6, pp. 89–97. DOI: 10.1038/s41550-021-01513-x. arXiv: 2112.11999 [astro-ph.EP].

Morello, V et al. (Dec. 2018). "The High Time Resolution Universe survey – XIV. Discovery of 23 pulsars through GPU-accelerated reprocessing". In: *Monthly Notices of the Royal Astronomical Society* 483.3, pp. 3673–3685. ISSN: 0035-8711. DOI: 10.1093/mnras/sty3328.

Navarrete, Felipe H et al. (Oct. 2019). "Magnetohydrodynamical origin of eclipsing time variations in post-common-envelope binaries for solar mass secondaries". In: *Monthly Notices of the Royal Astronomical Society* 491.1, pp. 1043–1056. ISSN: 0035-8711. DOI: 10.1093/mnras/stz3065.

Ng, Mason et al. (Apr. 2022). "NICER Pulsation Search and Spectroscopy of the Original Black Widow Pulsar, PSR B1957+20". In: *AAS/High Energy Astrophysics Division*. Vol. 54. AAS/High Energy Astrophysics Division, 110.04, p. 110.04.

Nice, D. J. and J. H. Taylor (Mar. 1995). "PSR J2019+2425 and PSR J2322+2057 and the Proper Motions of Millisecond Pulsars". In: *The Astrophysical Journal* 441, p. 429. DOI: 10.1086/175367.

Nieder, L. et al. (May 2022). "Is the Black-widow Pulsar PSR J1555-2908 in a Hierarchical Triple System?" In: 931.1, L3, p. L3. DOI: 10.3847/2041-8213/ac6b35. arXiv: 2202.05482 [astro-ph.HE].

O'Sullivan, S. P. et al. (Mar. 2023). "The Faraday Rotation Measure Grid of the LOFAR Two-metre Sky Survey: Data Release 2". In: *mnras* 519.4, pp. 5723–5742. DOI: 10.1093/mnras/stac3820. arXiv: 2301.07697 [astro-ph.CO].

Ogilvie, Gordon I. (Aug. 2014). "Tidal Dissipation in Stars and Giant Planets". In: *araa* 52, pp. 171–210. DOI: 10.1146/annurev-astro-081913-035941. arXiv: 1406.2207 [astro-ph.SR].

Olausen, S. A. and V. M. Kaspi (May 2014). "The McGill Magnetar Catalog". In: *apjs* 212.1, 6, p. 6. DOI: 10.1088/0067-0049/212/1/6. arXiv: 1309.4167 [astro-ph.HE].

Oppenheimer, J. R. and G. M. Volkoff (Feb. 1939). "On Massive Neutron Cores". In: *Physical Review* 55.4, pp. 374–381. DOI: 10.1103/PhysRev.55.374.

Ostriker, J. P. and J. E. Gunn (Sept. 1969). "On the Nature of Pulsars. I. Theory". In: *The Astrophysical Journal* 157, p. 1395. DOI: 10.1086/150160.

Pacini, F. (Nov. 1967). "Energy Emission from a Neutron Star". In: 216.5115, pp. 567–568. DOI: 10.1038/216567a0.

Paczynski, B. (1981). "Evolution of cataclysmic binaries." In: *Acta Astronomica* 31, p. 1. URL: https://ui.adsabs.harvard.edu/abs/1981AcA....31....1P/abstract (visited on 05/10/2019).

Pallanca, C. et al. (Aug. 2012). "THE IDENTIFICATION OF THE OPTICAL COMPANION TO THE BINARY MILLISECOND PULSAR J0610–2100 IN THE GALACTIC FIELD". In: *The Astrophysical Journal* 755.2, p. 180. DOI: 10.1088/0004-637X/755/2/180.

Papitto, A. et al. (Sept. 2013). "Swings between rotation and accretion power in a binary millisecond pulsar". In: *Nature* 501.7468, pp. 517–520. DOI: 10.1038/nature12470. arXiv: 1305.3884 [astro-ph.HE].

Papitto, Alessandro and Domitilla de Martino (Jan. 2022). "Transitional Millisecond Pulsars". In: *Astrophysics and Space Science Library*. Ed. by Sudip Bhattacharyya, Alessandro Papitto, and

Dipankar Bhattacharya. Vol. 465. Astrophysics and Space Science Library, pp. 157–200. DOI: 10.1007/978-3-030-85198-9_6. arXiv: 2010.09060 [astro-ph.HE].

Park, Ryan S. et al. (Feb. 2021). "The JPL Planetary and Lunar Ephemerides DE440 and DE441". In: *The Astronomical Journal* 161.3, p. 105. DOI: 10.3847/1538-3881/abd414. URL: https://dx.doi.org/10.3847/1538-3881/abd414.

Pennucci, Timothy T., Paul B. Demorest, and Scott M. Ransom (July 2014). "ELEMENTARY WIDE-BAND TIMING OF RADIO PULSARS". In: *The Astrophysical Journal* 790.2, p. 93. DOI: 10.1088/0004-637X/790/2/93.

Perera, B. B. P. et al. (Aug. 2011). "The evolution of PSR J0737-3039B and a model for relativistic spin precession". In: *Radio Pulsars: An Astrophysical Key to Unlock the Secrets of the Universe*. Ed. by Marta Burgay et al. Vol. 1357. American Institute of Physics Conference Series. AIP, pp. 105–108. DOI: 10.1063/1.3615090.

Perera, B. B. P. et al. (Feb. 2017). "Evidence for an intermediate-mass black hole in the globular cluster NGC 6624". In: *Monthly Notices of the Royal Astronomical Society* 468.2, pp. 2114–2127. ISSN: 0035-8711. DOI: 10.1093/mnras/stx501.

Phillips, J. A., Steve E. Thorsett, and Shri R. Kulkarni, eds. (Jan. 1993). *Planets Around Pulsars*. Vol. 36.

Phinney, E. S. (Jan. 1993). "Pulsars as Probes of Globular Cluster Dynamics". In: *Structure and Dynamics of Globular Clusters*. Ed. by S. G. Djorgovski and Georges Meylan. Vol. 50. Astronomical Society of the Pacific Conference Series, p. 141.

Podsiadlowski, Philipp (Jan. 1993). "Planet formation scenarios." In: *Planets Around Pulsars*. Ed. by J. A. Phillips, Steve E. Thorsett, and Shri R. Kulkarni. Vol. 36. Astronomical Society of the Pacific Conference Series, pp. 149–165.

Polzin, E. J. et al. (May 2018). "The low-frequency radio eclipses of the black widow pulsar J1810+1744". In: 476.2, pp. 1968–1981. DOI: 10.1093/mnras/sty349. arXiv: 1802.02594 [astro-ph.HE].

Polzin, E. J. et al. (Nov. 2019). "Long-term variability of a black widow's eclipses - A decade of PSR J2051-0827". In: *Monthly Notices of the Royal Astronomical Society* 490.1, pp. 889–908. DOI: 10.1093/mnras/stz2579. arXiv: 1909.06130 [astro-ph.HE].

Press, William H. et al. (1992). *Numerical recipes in FORTRAN. The art of scientific computing*.

Ransom, S. M. et al. (Jan. 2011). "Three Millisecond Pulsars in Fermi LAT Unassociated Bright Sources". In: *apjl* 727.1, L16, p. L16. DOI: 10.1088/2041-8205/727/1/L16. arXiv: 1012.2862 [astro-ph.HE].

Rappaport, S., F. Verbunt, and P. C. Joss (Dec. 1983). "A new technique for calculations of binary stellar evolution application to magnetic braking." In: *The Astrophysical Journal* 275, pp. 713–731. DOI: 10.1086/161569.

Rasio, Frederic A. (June 1994). "Is There a Planet in the PSR 1620-26 Triple System?" In: 427, p. L107. DOI: 10.1086/187376. arXiv: astro-ph/9402008 [astro-ph].

Ray, P. S. et al. (May 2012). "Radio Searches of Fermi LAT Sources and Blind Search Pulsars: The Fermi Pulsar Search Consortium". In: *arXiv e-prints*, arXiv:1205.3089, arXiv:1205.3089. DOI: 10.48550/arXiv.1205.3089. arXiv: 1205.3089 [astro-ph.HE].

Ray, Paul S. et al. (Mar. 2022). "Discovery, Timing, and Multiwavelength Observations of the Black Widow Millisecond Pulsar PSR J1555-2908". In: *The Astrophysical Journal* 927.2, 216, p. 216. DOI: 10.3847/1538-4357/ac49ef. arXiv: 2202.04783 [astro-ph.HE].

Reardon, Daniel J. et al. (July 2023). "Search for an Isotropic Gravitational-wave Background with the Parkes Pulsar Timing Array". In: 951.1, L6, p. L6. DOI: 10.3847/2041-8213/acdd02. arXiv: 2306.16215 [astro-ph.HE].

Reynolds, M. T. et al. (Aug. 2007). "The light curve of the companion to PSR B1957+20". In: *Monthly Notices of the Royal Astronomical Society* 379.3, pp. 1117–1122. DOI: 10.1111/j.1365-2966.2007.11991.x. arXiv: 0705.2514 [astro-ph].

Rezzolla, Luciano, Elias R. Most, and Lukas R. Weih (Jan. 2018). "Using Gravitational-wave Observations and Quasi-universal Relations to Constrain the Maximum Mass of Neutron Stars". In: *The Astrophysical Journal Letters* 852.2, L25, p. L25. DOI: 10.3847/2041-8213/aaa401. arXiv: 1711.00314 [astro-ph.HE].

Richards, D. W. et al. (Apr. 1970). "Quasi-Sinusoidal Oscillation in Arrival Times of Pulses from NP 0532". In: 160, p. L1. DOI: 10.1086/180511.

Rickett, B. J. (Jan. 1977). "Interstellar scattering and scintillation of radio waves." In: 15, pp. 479–504. DOI: 10.1146/annurev.aa.15.090177.002403.

Roberts, Mallory S. E. (2013). "Surrounded by spiders! New black widows and redbacks in the Galactic field". In: *Proceedings of the International Astronomical Union* 8.S291, pp. 127–132. DOI: 10.1017/S174392131202337X.

Rochberg-Halton, F. (1983). "Stellar Distances in Early Babylonian Astronomy: A New Perspective on the Hilprecht Text (HS 229)". In: *Journal of Near Eastern Studies* 42.3, pp. 209–217. ISSN: 00222968, 15456978.

Rutherford, Ernest (1920). "Nuclear Constitution of Atoms." In: *Proceedings of the Royal Society of London. Series A, Containing Papers of a Mathematical and Physical Character (1905-1934)* 97, pp. 374–400. DOI: http://dx.doi.org/10.1098/rspa.1920.0040.

Sanpa-Arsa, Siraprapa (Jan. 2016). "Searching for new millisecond pulsars with the GBT in Fermi unassociated sources". PhD thesis. University of Virginia.

Schroeder, Joshua and Jules Halpern (Oct. 2014). "Observations and Modeling of the Companions of Short Period Binary Millisecond Pulsars: Evidence for High-mass Neutron Stars". In: *apj* 793.2, 78, p. 78. DOI: 10.1088/0004-637X/793/2/78. arXiv: 1401.7966 [astro-ph.HE].

Shaifullah, G. et al. (Oct. 2016). "21 year timing of the black-widow pulsar J2051-0827". In: *Monthly Notices of the Royal Astronomical Society* 462.1, pp. 1029–1038. DOI: 10.1093/mnras/stw1737. arXiv: 1607.04167 [astro-ph.HE].

Shapiro, Irwin I. (Dec. 1964). "Fourth Test of General Relativity". In: *prl* 13.26, pp. 789–791. DOI: 10.1103/PhysRevLett.13.789.

Sigurdsson, Steinn et al. (July 2003). "A Young White Dwarf Companion to Pulsar B1620-26: Evidence for Early Planet Formation". In: *Science* 301.5630, pp. 193–196. DOI: 10.1126/science.1086326. arXiv: astro-ph/0307339 [astro-ph].

Smith, D. A. et al. (July 2023). "The Third Fermi Large Area Telescope Catalog of Gamma-ray Pulsars". In: *ApJ supplements*. arXiv: 2307.11132 [astro-ph.HE].

Smith, D. A. et al. (Jan. 2019). "Searching a Thousand Radio Pulsars for Gamma-Ray Emission". In: *apj* 871.1, 78, p. 78. DOI: 10.3847/1538-4357/aaf57d. arXiv: 1812.00719 [astro-ph.HE].

Spearman, C. (1904). "The Proof and Measurement of Association between Two Things". In: *The American Journal of Psychology* 15.1, pp. 72–101. ISSN: 00029556.

Spiewak, R. et al. (July 2022). "The MeerTime Pulsar Timing Array: A census of emission properties and timing potential". In: *pasa* 39, e027, e027. DOI: 10.1017/pasa.2022.19. arXiv: 2204.04115 [astro-ph.HE].

Spitkovsky, A. (Jan. 2004). "Electrodynamics of Pulsar Magnetospheres". In: *Young Neutron Stars and Their Environments*. Ed. by Fernando Camilo and Bryan M. Gaensler. Vol. 218. IAU Symposium, p. 357. DOI: 10.48550/arXiv.astro-ph/0310731. arXiv: astro-ph/0310731 [astro-ph].

Staelin, David H. and Edward C. Reifenstein III (Dec. 1968). "Pulsating Radio Sources near the Crab Nebula". In: *Science* 162.3861, pp. 1481–1483. DOI: 10.1126/science.162.3861.1481.

Stappers, B. W. et al. (July 1996). "Probing the Eclipse Region of a Binary Millisecond Pulsar". In: *The Astrophysical Journal* 465.2, p. L119. DOI: 10.1086/310148. URL: https://dx.doi.org/10.1086/310148.

Stappers, B. W. et al. (July 2014). "A State Change in the Missing Link Binary Pulsar System PSR J1023+0038". In: *apj* 790.1, 39, p. 39. DOI: 10.1088/0004-637X/790/1/39. arXiv: 1311.7506 [astro-ph.HE].

Stephenson, F. Richard and David A. Green (Jan. 2002). "Historical supernovae and their remnants". In: *International Series in Astronomy and Astrophysics* 5.

Stovall, K. et al. (Aug. 2014). "The Green Bank Northern Celestial Cap Pulsar Survey. I. Survey Description, Data Analysis, and Initial Results". In: *The Astrophysical Journal* 791.1, 67, p. 67. DOI: 10.1088/0004-637X/791/1/67. arXiv: 1406.5214 [astro-ph.HE].

Strader, Jay et al. (Feb. 2019). "Optical Spectroscopy and Demographics of Redback Millisecond Pulsar Binaries". In: 872.1, 42, p. 42. DOI: 10.3847/1538-4357/aafbaa. arXiv: 1812.04626 [astro-ph.HE].

Tang, Sumin et al. (Aug. 2014). "Identification of the Optical Counterpart of Fermi Black Widow Millisecond Pulsar PSR J1544+4937". In: *The Astrophysical Journal Letters* 791.1, L5, p. L5. DOI: 10.1088/2041-8205/791/1/L5. arXiv: 1407.0081 [astro-ph.HE].

Tauris, Thomas M. (Jan. 2015). "Millisecond Pulsars in Close Binaries". In: *arXiv e-prints*, arXiv:1501.03882, arXiv:1501.03882. DOI: 10.48550/arXiv.1501.03882. arXiv: 1501.03882 [astro-ph.SR].

Taylor, J. H. and J. M. Weisberg (Feb. 1982). "A new test of general relativity - Gravitational radiation and the binary pulsar PSR 1913+16". In: *The Astrophysical Journal* 253, pp. 908–920. DOI: 10.1086/159690.

Thompson, C. et al. (Feb. 1994). "Physical Processes in Eclipsing Pulsars: Eclipse Mechanisms and Diagnostics". In: *The Astrophysical Journal* 422, p. 304. DOI: 10.1086/173728.

Thorsett, S. E., Z. Arzoumanian, and J. H. Taylor (July 1993). "PSR B1620-26: A Binary Radio Pulsar with a Planetary Companion?" In: 412, p. L33. DOI: 10.1086/186933.

Tutukov, A. V. et al. (Feb. 1985). "Evolution of Low-Mass Close Binaries - the Minimum Orbital Period". In: *Soviet Astronomy Letters* 11, pp. 52–56.

van der Wateren, E. et al. (May 2022). "Irradiated but not eclipsed, the case of PSR J0610−2100". In: *Astronomy & Astrophysics* 661, A57, A57. DOI: 10.1051/0004-6361/202142741. arXiv: 2203.05872 [astro-ph.HE].

van Haaften, L. M. et al. (Mar. 2013). "Formation of the planet orbiting the millisecond pulsar J1719-1438". In: *Neutron Stars and Pulsars: Challenges and Opportunities after 80 years*. Ed. by Joeri van Leeuwen. Vol. 291. IAU Symposium, pp. 133–136. DOI: 10.1017/S1743921312023381. arXiv: 1210.6332 [astro-ph.SR].

van Kerkwijk, M. H., R. P. Breton, and S. R. Kulkarni (Feb. 2011). "Evidence for a Massive Neutron Star from a Radial-velocity Study of the Companion to the Black-widow Pulsar PSR B1957+20". In: *The Astrophysical Journal* 728.2, 95, p. 95. DOI: 10.1088/0004-637X/728/2/95. arXiv: 1009.5427 [astro-ph.HE].

Verbunt, F. and C. Zwaan (July 1981). "Magnetic braking in low-mass X-ray binaries." In: *Astronomy & Astrophysics* 100, pp. L7–L9.

Voisin, G. et al. (June 2020a). "An improved test of the strong equivalence principle with the pulsar in a triple star system". In: *aap* 638, A24, A24. DOI: 10.1051/0004-6361/202038104. arXiv: 2005.01388 [gr-qc].

Voisin, Guillaume, René P. Breton, and Charlotte Summers (Feb. 2020). "A spider timing model: accounting for quadrupole deformations and relativity in close pulsar binaries". In: *Monthly Notices of the Royal Astronomical Society* 492.2, pp. 1550–1565. DOI: 10.1093/mnras/stz3430. arXiv: 1912.03935 [astro-ph.HE].

Voisin, Guillaume et al. (Apr. 2020b). "First measurement of the total gravitational quadrupole moment of a black widow companion". In: *Monthly Notices of the Royal Astronomical Society* 494.3, pp. 4448–4453. ISSN: 0035-8711. DOI: 10.1093/mnras/staa953.

Völschow, M. et al. (2016). "Eclipsing time variations in close binary systems: Planetary hypothesis vs. Applegate mechanism". In: *Astronomy & Astrophysics* 587, A34. DOI: 10.1051/0004-6361/201527333. URL: https://doi.org/10.1051/0004-6361/201527333.

Wahl, H. M. et al. (Feb. 2022). "The NANOGrav 12.5 yr Data Set: Polarimetry and Faraday Rotation Measures from Observations of Millisecond Pulsars with the Green Bank Telescope". In: *apj* 926.2, 168, p. 168. DOI: 10.3847/1538-4357/ac4045. arXiv: 2104.05723 [astro-ph.SR].

Wang, P. F. et al. (Oct. 2023a). "FAST Pulsar Database. I. Polarization Profiles of 682 Pulsars". In: *Research in Astronomy and Astrophysics* 23.10, 104002, p. 104002. DOI: 10.1088/1674-4527/acea1f. arXiv: 2307.10340 [astro-ph.HE].

Wang, S. Q. et al. (Sept. 2023b). "Change of Rotation Measure during the Eclipse of a Black Widow PSR J2051-0827". In: *The Astrophysical Journal* 955.1, 36, p. 36. DOI: 10.3847/1538-4357/acea81. arXiv: 2307.13198 [astro-ph.HE].

Warner, B. (Jan. 1978). “Apsidal motion and evolution of cataclysmic variables.” In: *actaa* 28, pp. 303–326.

Weisberg, J. M. et al. (Feb. 2008). “Arecibo H I Absorption Measurements of Pulsars and the Electron Density at Intermediate Longitudes in the First Galactic Quadrant”. In: *apj* 674.1, pp. 286–294. DOI: 10.1086/523345. arXiv: 0709.3854 [astro-ph].

Weltevrede, Patrick, Simon Johnston, and Cristóbal M. Espinoza (Mar. 2011). “The glitch-induced identity changes of PSR J1119-6127”. In: *Monthly Notices of the Royal Astronomical Society* 411.3, pp. 1917–1934. DOI: 10.1111/j.1365-2966.2010.17821.x. arXiv: 1010.0857 [astro-ph.SR].

Witte, M. G. and G. J. Savonije (Oct. 1999). “Tidal evolution of eccentric orbits in massive binary systems. A study of resonance locking”. In: *Astronomy & Astrophysics* 350, pp. 129–147. DOI: 10.48550/arXiv.astro-ph/9909073. arXiv: astro-ph/9909073 [astro-ph].

Wolszczan, A. and D. A. Frail (Jan. 1992). “A planetary system around the millisecond pulsar PSR1257 + 12”. In: *Nature* 355.6356, pp. 145–147. DOI: 10.1038/355145a0.

Wolszczan, Alexander (Apr. 1994). “Confirmation of Earth-Mass Planets Orbiting the Millisecond Pulsar PSR B1257+12”. In: *Science* 264.5158, pp. 538–542. DOI: 10.1126/science.264.5158.538.

Wu, J. H. K. et al. (Apr. 2012). “Discovery of γ-Ray Pulsation and X-Ray Emission from the Black Widow Pulsar PSR J2051-0827”. In: *The Astrophysical Journal* 748.2, 141, p. 141. DOI: 10.1088/0004-637X/748/2/141. arXiv: 1201.5980 [astro-ph.HE].

Xu, Yu-Jing et al. (Mar. 2025). “A New X-Ray Census of Rotation Powered Pulsars”. In: 981.2, 100, p. 100. DOI: 10.3847/1538-4357/adaebc. arXiv: 2501.10999 [astro-ph.HE].

Yao, J. M., R. N. Manchester, and N. Wang (Jan. 2017). “A New Electron-density Model for Estimation of Pulsar and FRB Distances”. In: *The Astrophysical Journal* 835.1, 29, p. 29. DOI: 10.3847/1538-4357/835/1/29. arXiv: 1610.09448 [astro-ph.GA].

Clara BLANCHARD

Caractérisation détaillée des paramètres orbitaux et des éclipses des pulsars « veuves noires » par leur chronométrie radio et utilisation de cette nouvelle population de pulsars rapides pour la détection du fond d'ondes gravitationnelles

Résumé : Le radiotélescope décimétrique de Nançay (NRT) observe régulièrement 19 systèmes «araignées», des systèmes binaires composés d'un pulsar milliseconde et d'une étoile de faible masse, qui gravitent en orbite serrée, entraînant l'évaporation de l'étoile par le vent du pulsar et créant ainsi un nuage de matière capable d'éclipser le pulsar. Le premier travail de cette thèse s'intéresse aux propriétés de groupe des éclipses, afin de mettre en évidence les similitudes ou les disparités entre les systèmes. La forme des éclipses est paramétrisée, et ces paramètres sont comparés à l'inclinaison ou à la fonction de masse. Toutes les araignées ne présentent pas d'éclipse, et une des explications possibles est qu'un élément clé est l'angle de vue. Nous avons constaté que les systèmes ayant une fonction de masse élevée ont tendance à avoir des éclipses plus longues, ce qui semble confirmer un lien entre la géométrie et la présence d'éclipses. Le deuxième travail présenté porte sur la recherche de planètes orbitant autour de binaires, en particulier deux systèmes araignées et une autre binaire situées dans un amas globulaire. Deux méthodes ont été utilisées : la première est le calcul des paramètres orbitaux à partir des dérivées de fréquence de rotation, qui n'a pas donné de résultats satisfaisants. La seconde est la chronométrie directe utilisant une extension au logiciel standard, étude encore en cours mais qui semble plus prometteuse. Les systèmes araignées semblent abriter des compagnons planétaires, et l'autre binaire un compagnon stellaire de masse subsolaire. Nous présentons les solutions actuelles ainsi que les prochaines étapes pour mieux contraindre les paramètres orbitaux.

Mots-clés : Radioastronomie, pulsar, ondes gravitationnelles

Detailed characterisation of the orbital parameters and eclipses of 'black widow' pulsars by radio timing and use of this new population of fast pulsars for the detection of the gravitational wave background

Abstract : The Nançay Radio Telescope (NRT) monitors 19 “spider” systems, binaries composed of a millisecond pulsar and a low-mass star that tightly orbit. This causes the star to be evaporated by the pulsar wind, and the ablated matter creates a cloud of plasma that can eclipse the pulsar beam. The first part of this thesis is about the group properties of the eclipses, to highlight the similarities and differences between systems. The eclipses shapes are parametrized, and the resulting parameters are compared to the inclination and mass function. Not all spiders display eclipses, and one possible explanation is that the viewing angle is key. We have shown that systems with a higher mass function tend to have longer eclipses, suggesting a link between the viewing geometry and the presence of eclipses. The second part is the search for planet orbiting pulsar binaries, specifically two spider systems and one globular cluster binary. Two methods were used: the first is the direct computation of orbital parameters from spin frequency derivatives, which did not yield convincing results, the second is the timing of the pulsars using an extension of the usual timing software. This is still a work in progress but seems more promising. The spider systems seem to harbour planetary companion, and the other binary a subsolar mass stellar companion. We present the current solutions alongside the next steps to better constrain the orbital parameters.

Keywords: Radio astronomy, pulsar, gravitational waves

LPC2E, CNRS
3A avenue de la recherche scientifique
45071 Orléans